Progress in Chemical and Biological Science

Edited by

Hari Shankar Biswas
Dilip Kumar Maiti
Sandeep Poddar
Amiya Bhaumik

Published by:

Lincoln University College, Malaysia

www.lucp.net

Progress in Chemical and Biological Science

Edited by

Dr. Hari Shankar Biswas
Assistant Professor, Department of Chemistry
Surendranath College
Kolkata, West Bengal, India

Dr. Dilip Kumar Maiti
Professor, Department of Chemistry
University of Calcutta
Kolkata, West Bengal, India

Dr. Sandeep Poddar
Deputy Vice Chancellor (Research & Innovation)
Lincoln University College
Malaysia

Dr. Amiya Bhaumik
President
Lincoln University College
Malaysia

Published by:

Lincoln University College, Malaysia

www.lucp.net

Published on: 3rd July, 2023

Published by:

Lincoln University College
Wisma Lincoln
No. 12-18, Off Jalan, Perbandaran SS 6/12
47301 Petaling Jaya
Selangor Darul Ehsan
Malaysia
Tel.: +603-7806 3478
Fax: +603-7806 3479
Toll Free: 1-300-880-111
E-mail: lucp@lincoln.edu.my
Web.: www.lucp.net

ISBN: 978-967-2819-22-6
eISBN: 978-967-2819-23-3

doi: 10.31674/book.2023pcbs

Price: USD 80

Editors

Hari Shankar Biswas

Rtn. Dr. Hari Shankar Biswas, M.Sc. Ph.D.
Assistant Professor (II) and Ex-Head of the Department
Department of Chemistry, Surendranath College, Kolkata, India

Dr. Biswas received his B.Sc. degree in Chemistry Honours (2005) from R.K.M.V.C. College and his M.Sc. (2008) degree from Presidency College, Kolkata. He was awarded a Ph.D. (2015) in Material Science from the Saha Institute of Nuclear Physics, University of Calcutta. From 2008 to 2010 he was a School teacher at Keshub Academy, Kolkata, then he joined assistant professor in Chemistry at Surendranath College. His current research topic is Carbon thin Film, Graphene, Graphene Oxide-based nano Composite, Synthesis Characterization, and Application in the Environmental, Biological, and Technological fields. He is the author of 10 book chapters and has published more than 23 papers in International Journals. He is a life member of the Indian Science Congress Association and the Indian Chemical Society and an affiliated member of the Royal Society of Chemistry. He is a series book Editor and reviewer of reputed international publishers and journals. He is an Editorial board member of the American Journal of Chemical Engineering, Lincoln University College, and a member of Rotary International. He is also an editor of some books namely: Emerging Concepts in Chemical and Biological Science; Modern Approaches in Chemical and Biological Sciences; Advances in Science Education and Modern Approaches in Chemical and Biological Sciences Vol.2

Dilip Kumar Maiti

Professor
Department of Chemistry, University of Calcutta
Kolkata, India

Prof. Maiti completed his graduation in chemistry in 1991 from Ramkrishna Mission Vidyamandir, University of Calcutta. He completed his master's from University College of Science, University of Calcutta in 1993 . In 1998 he received Ph.D. degree from Indian Institute of Chemical Biology, Jadavpur University. Then he joined Jadavpur University for post doctoral studies (Jan 2000-July 2002). He moved to School of Medicine, Wayne State University, Detroit, USA as a post doctoral fellow (July, 2002 - June, 2004). He was appointed as a senior lecturer of Chemistry at Dumkal College Basantapur, Kalyani University. In 2005, he moved to Department of Chemistry, Calcutta University as a full professor. His field of research interest is Organic Synthesis and Material Chemistry.

Editors

Sandeep Poddar

Deputy Vice Chancellor (Research & Innovation)
Lincoln University College, Malaysia

Prof. Dr. Sandeep Poddar, presently the Deputy Vice Chancellor (Research & Innovation) of Lincoln University College, Malaysia. He also served as Senior Research Director and Executive Editor(Publications), Lincoln University College, Adjunct Faculty (Honorary), Bharat Center Canada. He has graduated from University of Calcutta in 1993 with Honours in Zoology, he has obtained Post Graduate Diploma in Dietetics from All India Institute of Hygiene and Public Health 1995, Master of Science in Zoology with specialization in Biochemical Genetics from Dayalbagh Educational Institute 1998 with distinction. In addition to this he also obtained Master of Business Administration (MBA) from Lincoln University College in 2021. He has completed Ph.D. in Zoology from Vivekananda Institute of Medical Sciences on Cytotoxicity in 2004. After completing Ph.D. he pursued Post Doctoral Research in different projects on Hemoglobinopathies and Oral Cancer mutation. He is serving as reviewer of several International Journals. He has published several research papers, organized international conferences, and edited books in Malaysia, Australia and India. Dr. Sandeep is founder Assistant Secretary of Dr. Tarak Nath Podder Memorial Foundation, Kolkata, India.

Amiya Bhaumik

President
Lincoln University College, Malaysia

Prof. Dr. Amiya Bhaumik is the Founder and Former Vice-Chancellor of Lincoln University College. He is purely from the field of education. Dr. Bhaumik is Executive Vice President of the International Education Consulting Group, St. Louis, USA since 1999. Dr. Amiya Bhaumik was Research Fellow of UNESCO, Paris. During this tenure, Dr. Bhaumik has traveled extensively to Europe, Africa, Asia and Latin America. He has served as Professor of Business Administration in University of Lucknow, India and in University of Malaya and many other places. Dr. Amiya Bhaumik is a very dynamic personality. He has authored numerous book chapters and has huge number of publication in many national and international journals. He has also edited several books.

https://doi.org/10.31674/book.2023pcbs

Contents _____ *Pages*

Preface

"Progress in Chemical and Biological Science" takes readers on a captivating journey through the ever-evolving realms of chemical and biological sciences. As the understanding of these fields continues to expand, the potential for groundbreaking discoveries and advancements grows exponentially. This book serves as a comprehensive compilation of cutting-edge research, showcasing remarkable progress made in various sub-disciplines. From innovative synthetic methodologies to the exploration of intricate biological processes, this collection highlights the collective efforts and achievements of scientists worldwide. The aim is to inspire collaboration, ignite fresh ideas, and nurture the spirit of inquiry that propels progress in these fascinating scientific domains.

Ethnobotany explores traditional plant uses and aids in discovering potential medicines. *Aloe barbadensis* is a medicinal plant with diverse therapeutic applications, native to the Darjeeling Himalayas. The study, “An Account on *Aloe barbadensis* with Special Reference to the Phytochemistry and Antibacterial Property of *Aloe barbadensis* from Darjeeling Himalayas”, conducted by Rupam Mandal, aims to investigate the phytochemical properties and antibacterial potential of Aloe barbadensis, a plant found in the Darjeeling Himalayas. The study analyzes various compounds such as alkaloids, tannins, glycosides, steroids, saponins, phenols, flavonoids, quinines, xanthoproteins, coumarins, and anthraquinones in the leaves of the plant. The results of the study provide insights into the phytochemical composition and antibacterial properties of different leaf extracts of *Aloe barbadensis* from the Darjeeling Himalayas.

Long-term ecological monitoring is crucial to understand faunal communities in urban environments. In West Bengal, the Santragachijheel wetland, located near Kolkata city, is a 12.75-hectare habitat by the Hugli River. Sobhana Palit (Paul) conducted a study titled "Study of Migratory Avifauna of Santragachijheel" to inventory the bird diversity in this wetland. The research reveals that birds predominantly utilized the lake from November to February-March, which corresponds to their primary migratory season. Among the recorded species, 44% are residents, while the remainder are either resident migratory or migratory.

This paper entitled “The Synthesis, Spectral and Antimicrobial Study of Heterobinuclear Complexes of Copper (II) Schiff Base with Alkali Metals Salts” by Chandan Kumar explores the synthesis, characterization, and antimicrobial study of heterobinuclear complexes of copper (II) Schiff base with alkali metal salts. The complexes are prepared using a Schiff base derived from salicylaldehyde and propylenediamine, along with various alkali metal salts. The study also reveals non-electrolyte nature and dative bonding between copper (II) metal chelate and alkali metal. The complexes display a square planar structure and demonstrated antimicrobial activity against E. coli, S. aureus, and C. albicans, suggesting their potential as antimicrobial agents.

The significance of developing advanced technologies for efficient wastewater treatment is rapidly growing on a global scale. Photocatalysis emerges as a highly valuable, economical, and easily controllable approach for breaking down and addressing organic pollutants in wastewater treatment. Amit Kumar Dutta in his study, “Waste-Water Treatment: Based on Solar-Light-Driven Photo-Catalysis Using Semiconducting Nano-Materials” depicts the photo-catalytic efficacy of the proposed NPs has been elaborated based on its structural modification, increasing surface area, and controlling size and morphology. On the basis of this developed methodology, the unlimited abundance of solar energy can be used in large scale waste-water treatment.

Diabetes mellitus is a global health concern associated with increased morbidity rates due to changes in quality of life and healthcare negligence. Suvroma Gupta's article, "In Vitro Anti-Amylase Activity of Daidzein & Evaluation of Its Synergistic Role with Acarbose in Combination," explores the inhibitory effects of Daidzein and Eriodyctiol on PPA, with IC50 values of 26 uM and 22 uM, respectively. Daidzein also enhances the inhibitory effects of the commonly used amylase inhibitor acarbose in a synergistic manner, while exhibiting additional inhibition of lipid peroxidation. These findings suggest that Eriodyctiol and Daidzein could serve as suitable alternatives to acarbose in the treatment of Diabetes mellitus.

Pyrroles are versatile compounds with a broad chemistry. Functionalized pyrroles have diverse structures and are essential in modern technology. The paper titled "Recent Advances in the Green Synthesis of Polyfunctionalized Pyrroles" by Harisadhan Ghosh and Anupam Jana summarizes the latest environmentally friendly methods for synthesizing diverse pyrrole derivatives. The authors target synthetic organic chemists interested in applying Green Chemistry principles to pyrrole synthesis.

The paper named “Hydrogen Production from Biomass” focuses on the importance of hydrogen as a fuel and its potential as a future energy source. Currently, a significant amount of hydrogen is produced from non-renewable sources like natural gas. However, the paper highlights the promising route of hydrogen production from biomass, which is abundant, clean, and sustainable. Different thermochemical and biological processes for hydrogen manufacturing from biomass are discussed, along with their advantages. The paper also addresses catalyst effects, reaction conditions, and biomass analysis. Overall, it provides valuable insights into the advancements and potential of sustainable hydrogen production from biomass.

Heteroisobenzofurans, the heteroanalogue of isobenzofurans, are widely used as intermediates in the synthesis of important heterocyclic compounds. Interest in heteroisobenzofuran chemistry has recently increased due to its potential for creating innovative heteroaromatic assemblies with biological significance. In “Applications of Heteroisobenzofurans in Natural and Non-natural Product Synthesis”, Biswajit Panda discusses the application of various heteroisobenzofurans in the synthesis of biologically important natural and non-natural products. It also provides an overview of the synthesis and reactivity of this reactive intermediate, highlighting its significance in the field of natural product synthesis.

Hari Shankar Biswas
Dilip Kumar Maiti
Sandeep Poddar
Amiya Bhaumik

https://doi.org/10.31674/book.2023pcbs001

Account of *Aloe barbadensis*: Emphasizing Phytochemistry and Antibacterial Potential in Darjeeling Himalayas

Rupam Mandal
Department of Botany, Sree Chaitanya College, Habra, West Bengal, India

Corresponding Author's Email: rupam.atom@gmail.com

ABSTRACT

Plants have been widely used throughout human history as a basis for medical treatment. Ethnobotany, the study of traditional human uses of plants, is recognized as an effective way to discover future medicines. The Darjeeling Himalayas are home to a huge number of medicinal plants used by the local people. *Aloe barbadensis* is a plant that grows in this area and has a long history of being used as a medicinal plant with diverse therapeutic applications. The study was conducted to determine the phytochemical properties of the leaves of the plant. Flavonoidsce or absence of alkaloids, tannin, glycosides, steroids, saponins, phenol, flavonoids, quinine, xanthoprotein, coumarin, anthraquinone were tested. The antimicrobial activity of the leaves was also examined against gram negative bacteria (*Klebsiella pneumonia*) and one-gram positive bacteria (*Bacillus subtilis*) by disc diffusion antibiotic sensitivity testing method. Water, ethanol, chloroform and acetone were used to prepare the extract from fresh and dry leaves. The *Aloe barbadensis* shows the maximum inhibition zone in acetone and ethanol extracts against gram positive bacteria (*Bacillus subtilis*). The *Aloe barbadensis* shows the maximum inhibition zone in chloroform extract and acetone extract of dry leaf against gram negative bacteria (*Klebsiella pneumonia*). In a nutshell, this study reveals the different phytochemicals present and antibacterial properties of different leaf extracts of *Aloe barbadensis* from Darjeeling Himalayas

Keywords: *Aloe barbadensis; Anti-bacterial Property; Phytochemicals; Darjeeling Himalayas*

Introduction

Plants have been widely used by man since time immemorial as a basis for medical treatment. Ethnobotany, the study of traditional human uses of plants, is recognized as an effective way to discover future medicines. Reports suggest that the first study of medicinal plants started about 5000 years ago in Sumerians. In India, a great culture of Ayurveda medicine has been found, possibly as early as 1900 BC. Ancient Indian herbalists Charaka and Sushruta during the 1st millennium BC, described different herbs used in Ayurveda. The World Health Organization (WHO) estimates that 80 percent of the population of some 3rd world countries (e.g. Asian and African countries) presently uses

herbal medicine for some aspect of primary health care, as Pharmaceuticals are costly and herbal medicine is very cost-effective.

Aloe vera (*Aloe barbadensis* miller) is a plant of the Asphodelaceae family. The name is derived from the Arabic word ‘alloeh’ which means ‘bitter’, referring to the taste of the liquid contained in the leaves. Aloe is a drought registrant perennial succulent plant. The thick leaves are capable of retaining water. Aloe has been reported to have different types of beneficial effects (Aida *et al*., 2021).

Medicinal Importance of *Aloe barbadensis*

Anti inflammatory action

A number of *in-vitro* and *in-vivo* studies have revealed the anti-inflammatory activity of *Aloe sp*. (Sánchez *et al*., 2020). The sterols in *Aloe* have been reported to reduce croton oil induced oedima in mice. Out of all the sterols found in *Aloe sp.* Lupeol was the most effective and acted in a dose-dependent manner (Haller Jr, 1990). A report suggests that in a rat adjuvant-induced arthritic in- flammatory model, the *Aloe sp*. extracts were really effective (Davis *et al*., 1991). *Aloe* contains bradykinase, which is capable of breaking down bradykinin, a pain causing inflammatory substance (Ito *et al*., 1993). The production of prostaglandin E2 from arachidonic acid is reduced by Aloe extracts through the inhibition of the cyclo-oxygenase pathway (Sahu *et al*., 2013). Anti-inflammatory effects of *Aloe* have been reported in human colorectal mucosa *in vitro*.

Anti-tumor activity

In rat hepatocytes, the binding of benzopyrene to form a cancer-initiating benzopyrene-DNA adduct has been reported to be inhibited by *Aloe* (Sánchez *et al*., 2020). In another study, the authors reported the anticancerous activity of *Aloe* in DMBA/croton oil-induced skin papillomagenesis in Swiss albino mice. The tumor promoting effects of phorbol myristic acetate and glutathione S-transferase induction by *Aloe* gel suggest some role of Aloe in cancer treatment (Kim & Lee, 1997) Apart from these studies, a number of glycoproteins present in *Aloe* have been reported to have antitumor activity (Sánchez *et al*., 2020). Reports suggest that aloe juice have the ability to heal the body from cancer and chemotherapy-induced damage. Emodin, an anthraquinone from *Aloe* can inhibit malignant cancer cell growth (Mathieson & Thomson, 1971). However, it is to be mentioned that statistically significant studies on the efficacy of *Aloe* on human health are limited (Eshun & He, 2004).

Anti diabeic property of *Aloe*

Reports suggest that *Aloe* contains polysaccharides capable of exhibiting hypoglycemic properties. Phytosterols like 24-ethyl-lophenol, 24-methyl- lophenol, 24-methy-lenecycloartanol, cycloartanol and lophenol present in *Aloe* have shown anti diabetic properties in mice models of type 2 diabetes (Aida *et al*., 2021). In a streptozotocin induced rat model of diabetes, Aloe gel has been reported to exhibit a hypoglycemic effect as well as a beneficial effect on the lipid profile (Rajasekaran *et al*., 2004, Rajasekaran *et al*., 2006).

In general, *Aloe* extract reportedly increases glucose tolerance in both normal and diabetic rats (Mathieson & Thomson, 1971).

Anti aging and moisturizing property of *Aloe*

Due to the presence of biogenic materials in *Aloe*, it exhibits gerontology and rejuvenation of aging skin. Mucopolysaccharide which helps in moisture binding to the skin, is present in *Aloe* in high quantities. The formation of collagen and elasin from fibroblast is stimulated by *Aloe*. This, in turn, helps make the skin elastic. *Aloe* gel has reportedly improved the condition of dry skin associated with occupational exposure by having a moisturizing effect. The hardened skin is softened by the amino acids present in *Aloe*. The Zinc present in *Aloe* acts as an astringent and tightens the pores (Lanka, 2018).

Figure:1 Aloe sp.

Antibacterial property of Aloe barbadensis from Darjeeling Himalayas

Darjeeling is a beautiful hill town located in the northern part of West Bengal. It is a Himalayan region that houses different types of medicinal plants (Das, 1995). Many of the plants are used by the locals, however, proper scientific documentation is scanty.

Aloe barbadensis is commonly found in Darjeeling area and is used by the locals. The aim of the present study was to evaluate the phytochemicals present in Aloe and study the antibacterial properties of *Aloe* from Darjeeling Himalayas. *Bacillus subtilis* and *Klebsiella pneumonia* were taken as representative species of gram positive and gram-negative

bacteria, respectively for studying the antibacterial properties of *Aloe. Bacillus subtilis* is a rod shaped, endospore forming free living soil bacteria. *Klebsiella pneumonia* on the other hand, is a nonmotile encapsulated rod-shaped bacteria capable of causing destructive changes to the lungs of humans and animals if inhaled.

Materials and methods

Materials

All the chemicals were purchased from SRL and Glaxo, India. All plastic wares were purchase from Tarsons.

Plant Collection

Leaves of *Aloe barbadensis* were collected from different areas of Darjeeling town mostly near Mall Road, Hooker Road, Lebong Cart Road.

Preparation of Plant Extracts

The leaf extracts were prepared as described earlier (Al-Manhel & Niamah 2015, Harborn, 1998). Briefly, 5gm of dried leaf were mixed with 50ml of the different solvents in a conical flask. The mixture was kept in a shaker for 24 hours. Next, the mixture was centrifuged at 5000 rpm for 10 mins. The supernatant was used for the treatment.

Test for Tannin:

Tanin was detected by diluting the test sample with water and adding 2-3 drops of ferric chloride solution. Presence of tannin was confirmed by appearance of blue or green colour.

Test for Flavonoids:

Test for flavonoids was performed as described earlier (Mandal & Sanphui, 2023). In short, a few drops of Sodium hydroxide was added to the test sample. In presence of flavonoids, an intense yellow colour appears, which turns colourless on adding few drops of dilute sulfuric acid

Test for Alkaloids:

Mayer's test was performed to test the presence of alkaloids as described earlier (Mandal & Sanphui, 2023). In brief 3ml of Ammonium solution was added in1 ml of test sample. After 10 mins 10 ml of chloroform and 2 ml of mayer's reagent was added. Appearance of cream coloured precipitate confirms the presence of alkaloids.

Test for Glycosides:

The test sample was mixed with few drops of ferric chloride solution & glacial acetic acid. Two layers were formed on adding concentrated sulfuric acid. Lower radish brown layer and upper acetic acid layer turns bluish green indicating presence of glycosides.

Test for Saponin:

Presence of Saponin was tested as described earlier (Mandal & Sanphui, 2023). The test sample was diluted with water and shaken for 10-15 minutes. Presence of saponin was confirmed by formation of a foam layer on the top.

Test for Coumarin:

On mixing equal volume of test sample with alcoholic sodium hydroxide, appearance of yellow colour indicates presence of coumarin (Mandal & Sanphui, 2023).

Test for Anthraquinone:

Presence of anthraquinone was tested as described earlier(Mandal & Sanphui, 2023). Briefly, a few drops of magnesium acetate was added to the test sampleand mixed well. Presence of anthraquinone was confirmed by appearance of light pink colour

Test for Quinone:

Presence of Quinone was detected following the method described earlier (Mandal & Sanphui, 2023). Briefly, few drops of concentrated sulfuric acid or aqueous sodium hydroxide solution was added to the test sample. Change of colour confirms the presence of quinine.

Test for Phenol:

Presence of phenol was detected by adding 5% ferric chloride to the test sample. Appearance of dark green colour confirms presence of phenol (Mandal & Sanphui, 2023)

Test for Steroids:

Presence of steroids was tested as described earlier (Mandal & Sanphui, 2023). In short 10 ml chloroform was added to 1ml of the test sample. 1 ml concentrated sulfuric acid was added slowly by the wall. The presence of steroid was confirmed by the appearance of upper red colouredlayer and lower yellow coloured layer with green fluorescence.

Evaluation of Anti-Bacterial Property

The antibacterial activity of the extracts was tested by the disc diffusion method. In brief, a small round piece of Whatman filter paper was made using a punching machine. The paper discs were dipped in plant extract, dried in air and placed on the agar plate containing bacteria. For control, solvent dipped paper discs were used. The plates were incubated at 37^0 C for 24 hours. After 24 hours, the zone of inhibition was measured.

Results

Phytochemical Analysis of the Leaf Extract of *Aloe barbadensis*

The phytochemical analysis of the leaf extracts of *Aloe barbadensis*from Darjeeling Himalayas was performed following the standard methods mentioned in the Materials and

Methods section. Tests were performed to check the presence of different phytochemicals like alkaloids, tannin, glycosides, steroids, saponins, phenol, flavonoids, quinine, xanthoprotein, coumarin, anthraquinone. Test was performed using Aqueous, Ethanolic, Chloroform and acetone extracts of *A. barbadensis* leaf. This study revealed the presence of different types of phytochemicals in the leaf extracts. The result is shown in Table 1. The result indicates the presence of Alkaloids and Saponin in the Aqueous, Chloroform and acetone extracts. Tanin, Flavonoids and coumarin were found to be present in all four extracts tested. On the other hand Glycosides and Anthraquinone were absent in all four extracts tested. Steroids, Phenols and Quinone could be detected only in the Aqueous and Ethanolic extracts. Xanthoprotein was detected only in the Chloroform extract. Therefore, the result of this study indicates that *A. barbadensis* leaf is a rich source of phytochemicals.

Table 1: Phytochemical Analysis of Aloe barbadensis from Darjeeling Himalayas

Phytochemicals	LEAF			
	Aqueous extracts	Ethanol Extract	Chloroform extract	Acetone Extract
Alkaloid	+	-	+	+
Glycosides	-	-	-	-
Saponin	+	-	+	+
Tanin	+	+	+	+
Flavonoids	+	+	+	+
Steroids	-	-	+	+
Phenols	-	-	+	+
Coumarin	+	+	+	+
Quinone	-	-	+	+
Anthraquinone	-	-	-	-
Xanthoprotein	-	-	+	-

Anti Bacterial Property of Leaf Extract of *Aloe barbadensis*

The antibacterial properties of different leaf extracts of *Aloe barbadensis* from Darjeeling Himalayas were tested using the disc diffusion method. Two concentrations of each extract were used. Anti bacterial property was tested against one gram positive and one gram negative bacteria. *Bacillus subtilis* and *Klebsiella pneumonie*was were the gram positive and gram negative bacteria used, respectively. Result clearly indicates the antibacterial property of leaf extracts of *Aloe barbadensis* (Fig. 2). The chloroform and acetone extract exhibits the highest antibacterial effect against gram positive *Bacillus subtilis.* However, the aqueous and acetone extracts were more effective against gram negative *Klebsiella pneumonie.* The aqueous and acetone leaf extracts were more effective against gram

negative bacteria compared to the gram positive bacteria tested. Interestingly, no such preference was seen in the case of ethanolic and chloroform extracts.

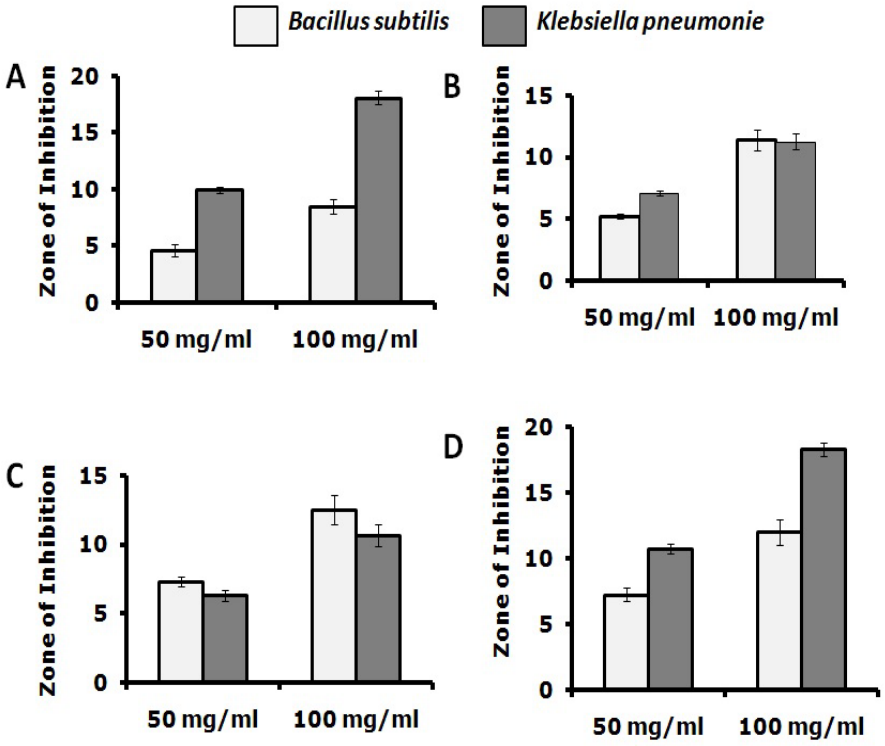

Figure 2: Antibacterial Activity of Leaf Extracts of Aloe barbadensis from Darjeeling Himalayas

The extracts were prepared at a concentration of 50mg/ml and 100 mg/ml. For testing the antibacterial activity, Disc diffusion method was used on Gram positive bacteria *Bacillus subtilis* and Gram-negative bacteria *Klebsiella pneumoniae*. The zone of inhibition (in mm) are represented graphically. Data represented as mean ± SEM of three independent experiments. A: Antibacterial property of Aqueous extract of leaf, B: Antibacterial property of Ethanolic extract of leaf, C: Antibacterial property of chloroform extract of leaf, D: Antibacterial property of Acetone extract of leaf. (Figure 2 graphs were plotted based on the result of experiments performed).

Discussion

The active components present in the leaves of *Aloe* have the power to make human life and health better in a number of ways. Aloe is a wonder plant, exhibiting its antiseptic, anti-inflammatory, anti-cancer, and anti-diabetic properties (Sahu *et al.,* 2013). This study on *Aloe barbadensis* from the Darjeeling Himalayas evaluates the phytochemistry and antibacterial properties of the plant. Results indicate the presence of various phytochemicals in four different solvent extracts of Aloe. The presence of different Phytochemicals contributes to the medicinal properties of the plants. The investigation revealed the antibacterial activity of *Aloe*. As the climatic and spatial conditions contribute to

the variation in the phytochemical property and, accordingly, the medicinal property of a plant, investigation of other medicinal properties of *Aloe barbadensis* from the Darjeeling Himalayas would be interesting.

The antibacterial property of *Aloe barbadensis* was tested on one gram positive bacteria *Bacillus subtilis* and one gram negative bacteria *Klebsiella pneumoniae.* All the extracts showed antibacterial potential against the tested bacteria. The aqueous and acetone extracts showed more antibacterial properties against the gram-negative bacteria *Klebsiella pneumonie* whereas acetone and chloroform extracts were most effective against the gram positive bacteria *Bacillus subtilis.*

Though an impressive number of in vitro and in vivo studies have been conducted on Aloe , the number of clinical trials has been limited. Moreover, all the clinical trials have been conducted with Aloe and not the active compound (Sánchez *et al*., 2020). It would therefore be very interesting to study the clinical effects of the relevant components in different human pathologies and conditions.

Conclusion

In conclusion, it can be said that the study indicates the presence of various phytochemicals in *Aloe barbadensis* from Darjeeling Himalayas and that the plant has antibacterial properties. The active ingredients present in succulent plants like Aloe have the power to benefit human life in a number of ways. The plant is used in everyday life in different ways. Aloe is sometimes referred to as a wonder plant due to its diverse medicinal activity. Though the plant is known for its medicinal values, detailed scientific study and clinical trials are needed to prove its acute efficacy. *Aloe barbadensis* is definitely nature’s gift to mankind and should be exploited scientifically in a more extensive way.

Acknowledgment

The authors are grateful for kind support from Sree Chaitanya College management for supporting and encouragement to complete the present article.

References

Aida, P. U. I. A., Cosmin, P. U. I. A., Emil, M. O. I. Ș., Graur, F., Fetti, A., & Florea, M. (2021). The phytochemical constituents and therapeutic uses of genus Aloe: A review. *Notulae Botanicae Horti Agrobotanici Cluj-Napoca*, *49*(2), 12332-12332. https:// doi.org/ 10.15835/nbha49212332

Al-Manhel, A. J., & Niamah, A. K. (2015). Effect of aqueous and alcoholic plant extracts on inhibition of some types of microbes and causing spoilage of food. *Pakistan Journal of Food Sciences*, *25*(3), 104-109.

Das, A. P. (1995). Diversity of angiospermic flora of Darjeeling hills. *Taxonomy and Biodiversity*, 118-127.

Davis, R. H., Parker, W. L., Samson, R. T., & Murdoch, D. P. (1991). Isolation of a stimulatory system in an aloe extract. *Journal of the American Podiatric Medical Association*, *81*(9), 473-478. https://doi.org/10.7547/87507315-81-9-473

Eshun, K., & He, Q. (2004). Aloe vera: a valuable ingredient for the food, pharmaceutical and cosmetic industries—a review. *Critical Reviews in Food Science and Nutrition*, *44*(2), 91-96. https://doi.org/10.1080/10408690490424694

Haller Jr, J. S. (1990). A drug for all seasons. Medical and pharmacological history of aloe. *Bulletin of the New York Academy of Medicine*, *66*(6), 647.

Harborne, A. J. (1998). *Phytochemical methods a guide to modern techniques of plant analysis*. springer science & business media.

Ito, S., Teradaira, R., Beppu, H., Obata, M., Nagatsu, T., & Fujita, K. (1993). Properties and pharmacological activity of carboxypeptidase in Aloe arborescens Mill var. natalensis Berger. *Phytotherapy Research*, *7*(7), S26-S29.

Kim, H. S., & Lee, B. M. (1997). Inhibition of benzo [a] pyrene-DNA adduct formation by Aloe barbadensis Miller. *Carcinogenesis*, *18*(4), 771-776. https://doi.org/10.1093/carcin/18.4.771

Lanka, S. (2018). A review on Aloe vera-The wonder medicinal plant. *Journal of Drug Delivery and Therapeutics*, *8*(5-s), 94-99. https://doi.org/10.22270/jddt.v8i5-s.1962

Mandal, R., & Sanphui, P. (2023). Study of Phytochemistry, Antibacterial and Anticancer property of Aqueous and Acetone extracts of *Bergenia ciliate* (Haw.) Sternbfrom Darjeeling Himalayas. *Ecology and Environment, 41*(1A), 210-216. https://doc.article-environmentandecology.com/external/file/lt463d9286feaa7924174bcf463f8849747e1

Mathieson, J. W., & Thomson, R. H. (1971). Naturally occurring quinones. Part XVIII. New spinochromes from Diadema antillarum, Spatangus purpureus, and Temnopleurus toreumaticus. *Journal of the Chemical Society C: Organic*, 153-160. https://doi.org/10.1039/J39710000153

Rajasekaran, S., Ravi, K., Sivagnanam, K., & Subramanian, S. (2006). Beneficial effects of Aloe vera leaf gel extract on lipid profile status in rats with streptozotocin diabetes. *Clinical and Experimental Pharmacology and Physiology*, *33*(3), 232-237.

Rajasekaran, S., Sivagnanam, K., Ravi, K., & Subramanian, S. (2004). Hypoglycemic effect of Aloe vera gel on streptozotocin-induced diabetes in experimental rats. *Journal of Medicinal food*, *7*(1), 61-66. https://doi.org/10.1089/10966 2004322984725

Sahu, P. K., Giri, D. D., Singh, R., Pandey, P., Gupta, S., Shrivastava, A. K., ... & Pandey, K. D. (2013). Therapeutic and medicinal uses of Aloe vera: a review. *Pharmacology & Pharmacy*, *4*(08), 599. http://dx.doi.org/10.4236/pp. 2013.48086

Sánchez, M., González-Burgos, E., Iglesias, I., & Gómez-Serranillos, M. P. (2020). Pharmacological update properties of Aloe vera and its major active constituents. *Molecules*, *25*(6), 1324. https://doi.org/10.3390/molecules25061324

https://doi.org/10.31674/book.2023pcbs002

Study of Migratory Avifauna of Santragachi Jheel

Sobhana Palit (Paul)
Department of Zoology, Sree Chaitanya College, West Bengal, India

Corresponding Author's Email: sobhanapaul70@gmail.com

ABSTRACT

Long-term ecological monitoring of urban environments is vital to determining the composition of faunal communities in the surrounding area. In West Bengal, SantragachiJheel, which is a 12.75-hectare wetland situated beside a railway station on the west bank of the river Hugli in the vicinity of Kolkata city, is an abode of various migratory birds. As it is surrounded by dense human habitations, railway yards, etc., the existing biodiversity of the lake is under various levels of anthropogenic pressure. Considering this scenario, an effort has been made to inventory the avifaunal diversity of this wetland. Transect walks, point transect and direct observation methods were deployed for the avifaunal survey. This paper reported that birds used the lake mostly from November of one year to February–March of the following year, which is their main migratory season. The avifauna included both local and winter migrants. The family Anatidae excels all other families put together, having the highest number of species. It was found that 44% of the species are resident, rest are either resident migratory or migratory. Among the birds, the lesser whistling duck was found to be the dominant one, followed by the Gadwall and Northern Pintail. Birds like the common moorhen, little egret, and cattle egret are the resident birds found there, along with many migratory birds. Rare birds like swinhoe's snipe and ferruginous pochard were also spotted there. Some rare birds, which are nearly threatened, were also spotted. Policymakers and planners are required for effective management actions in this lake ecosystem.

Keywords: *Avifauna; Migratory Birds;, SantragachiJheel*

Introduction

Long-term ecological monitoring of urban environments is vital to determining the composition of faunal communities in the surrounding area. In West Bengal, Santragachi Jheel, which is a 12.75-hectare wetland situated beside a railway station on the west bank of the river Hugli in the vicinity of Kolkata city, is an abode of various migratory birds. Wetlands provide food to birds in various forms, such as invertebrates, vertebrates, plants, etc. Avifauna play important roles in pollination and seed dispersal, as well as being scavengers and predators of many insect pests. Wetlands have been extensively investigated for their diversity, ecology, management and conservation (Fraser & Keddy, 2005; Gupta & Palit, 2014; Erard, 2011; Mazumdar, Ghosh & Saha, 2005; Dubey *et al*., 2015; Ganguly, 2015). As this lake is surrounded by dense human habitations, railway yards, etc. the existing biodiversity of the lake is under various levels of anthropogenic pressure. The effects of urbanisation, such as habitat destruction, modification of natural

areas, pollution etc., commonly cause threat to biodiversity. Considering this scenario, an effort has been made to inventory the avifaunal diversity of this wetland.

Methodology

Study Site:

The Santragachi Lake or Jheel, is a roughly rectangular area in Howrah district about 8km from Kolkata, India (220 34’60" N, 88017’60" E). The study of avian fauna was conducted in SantragachiJheel, a half an hour's drive from the main city of Kolkata, during the winter months of November–March.

(Source: google map)

Figure 1: Map of the Study Site (SantragachiJheel)

Study Method:

The study was made in the early hours of the morning. The birds were spotted by binoculars, Spotter and telescopes. Care was taken for their proper identification with the help of ornithologists and various books on birds (Ali, 2003; Grimmett *et al*., 1999).

To determine the seasonal status of different species of birds, they were placed into 3 categories – resident = R, migratory = M and resident migratory = RM. According to the availability, also avifauna was classified as A=abundant, 1997 M = Moderate and R = rare. Each of the four sides of the lake was traversed during each survey time. Shannon Weiner's species diversity index(H’) was also worked out for the four months from November to February. Survey was done from each side by walking along a transect and counting all the birds seen. Transect walks, point transects, and direct observation methods were deployed for the avifaunal survey.

Results and Discussion

This paper reports that birds use the lake mostly from November of one year to the months of February and March of the following year, which is their main migratory season. The avifauna included both local and winter migrants (Table 1). The family Anatidae excels all other families put together, having the highest number of species, as also found in the study of Gayen *et al*. (2022) in a man-made reservoir in West Bengal. It was found that 44% of the species are resident, rest are either resident migratory or migratory. Among the birds – lesser whistling duck was found to be the dominant one, followed by Gadwall and Northern Pintail. Birds like the common moorhen, little egret, and cattle egret are the resident birds found there, along with many migratory birds. Rare birds like Swinhoe's snipe, ferruginous pochard were also spotted there. The Baikal teal, a famous bird species from Siberia, was only spotted once in the last few years. The Swinhoe's snipe is a major attraction for bird watchers. Some rare birds, which are nearly threatened, were also spotted.

Avifaunal diversity acts as an important indicator to evaluate different habitats (Samanta, Das & Mandal, 2022). In the present study, it was also found that the jheel could act as an abode for so many migratory birds (Patode, Salve & Pawar, 2021; Arya *et al*., 2021; Bhagyasree, Rathod & Selvam, 2020)

Table 1: Avifauna at SantragachiJheel

Sl. No.	Name of Birds	Scientific Name	Occurrence	Seasonal status
1.	Lesser Whistling duck	*Dendrocygnajavanica*	A	R
2.	Common Moorhen	*Gallinula chloropus*	M	R
3.	Bronze Winged jacana	*Metopidius indicus*	M	R
4.	Little Cormorant	*Phalacrocorax niger*	M	R
5.	Pond heron	*Ardeolagrayii*	A	R
6.	White breasted kingfisher	*Halcyon smyrnensis*	M	R
7.	Northern Pintail	*Anas acuta*	A	M
8.	Baikal teal	*Anas formosa*	R	M
9.	Gadwall	*Anas strepera*	A	M
10.	Drongo	*Dicrurusmacrocercus*	M	R
11.	Garganey	*Anas querquedula*	A	M
12.	Swinhoe's snipe	*Gallinagomegala*	R	M
13.	Cotton Pygmy goose	*Nettapuscoromandelianus*	A	M
14.	Great cormorant	*Phalacrocorax carbo*	M	R
15.	Little cormorant	*Phalacrocorax niger*	M	R
16.	Purple heron	*Ardea purpurea*	M	R
17.	Median Egret	*Mesophoyx intermedia*	M	R
18.	Ferruginous Pochard	*Aythya nyroca*	R	M
19.	White breasted water hen	*Amaurornisphoenicurus*	M	R
20.	Common kingfisher	*Alcedoatthis*	M	R
21.	Yellow Bittern	*Ixobrychus sinensis*	M	R
22.	Sandpiper	*Tringastagnalis*	M	RM
23.	Common Pochard	*Aythya ferina*	M	R
24.	Common coot	*Fulicaatra*	M	M
25.	Darter or snake bird	*Anhinga melanogaster*	A	RM

The Shannon –Weiner diversity index for the months of November, December, January and February are reflected below graphically. The values indicated that maximum diversity occurred during the months of December –January.

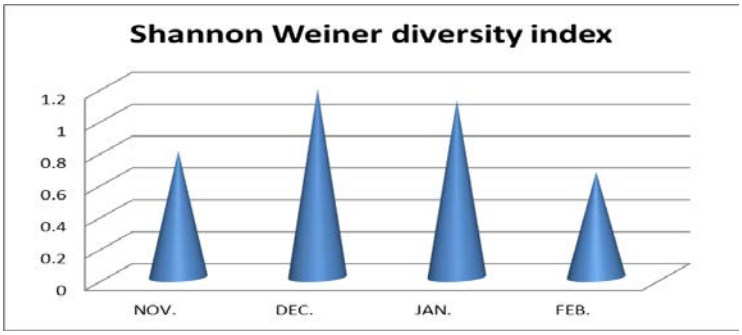

Figure 2: Shannon Weiner Diversity Index During the Period of Major Bird Aggregation

The lake is under the management of the South Eastern Railway and forest Department of West Bengal. But for better management involvement of local people particularly wetland users, people living around the wetlands, are essential to protect the water body. Policy makers and planners are required for effective management actions of this lake ecosystem.

Conclusion

The Santragchi Jheel is the abode of so many migratory birds, including rare species. As the area is jeopardized by threats such as habitat destruction, unscientific cleaning of the lake area, sounds arising from the railway tracks nearby, construction activities, etc., public awareness is also required so that the breeding and feeding grounds of the avifauna are not harmed in order to restore their diversity.

Acknowledgement

The author is thankful to the principal of Sree Chaitanya College and also to the colleagues of the department of zoology for their continuous encouragement and cooperation.

References

Ali, S. (2003). *The book of Indian birds*.13th edition. Oxford University press, New Delhi,1-326.

Arya, A. K., Durgapal, M., Singh, V., & Bisht, M. (2021). Archives of Agriculture and Environmental Science. *Archives of Agriculture and Environmental Science*, *6*(2), 249-256. https://doi.org/10.26832/24566632.2021.0602018

Bhagyasree, V., Rathod, V. N., & Selvam, C. (2020). A checklist of birds from Kondakarla Ava, a freshwater lake in Visakhapatnam, Andhra Pradesh, India. Bird-O-Soar# 59 in: Zoo's Print 35 (11): 6-15.

Dubey, S. K., Chakraborty, D. C., Sandipan, G., Mahashweta, M., Ranita, B., & Neogy, A. B. (2015). Avian diversity in the Jaldapara National Park, West Bengal, India with a

notes on their habitat association and feeding guild. *Indian Forester*, *141*(10), 1092-1101.

Erard, C. (2011). Keddy, PA—Wetland ecology. Principles and conservation. Cambridge University Press, Cambridge & New York. 2010. *Revue d'Écologie (La Terre et La Vie)*, *66*(1), 103-104.

Fraser, L. H., & Keddy, P. A. (Eds.). (2005). *The World's Largest Wetlands: Ecology and Conservation*. Cambridge University Press.

Ganguly, S. (2015). Diversity and temporal variation of migratory water birds of some selected wetlands from eastern India. *Species*, *13*(40), 42-50.

Gayen, D., Mukherjee, B., Sarkar, S., Goswami, B., Adhurya, S., & Chakrabarty, M. (2022). Study of winter avifauna diversity from a man-made reservoir in the West Bengal, India. *Journal of Animal Diversity*, *4*(1), 58-73. https://doi.org/10.52547/JAD.2022.4.1.7

Grimmett, R., Inskipp, C., Inskipp, T., & Byers, C. (1999). Pocket guide to the birds of the Indian subcontinent. *(No Title)*.

Gupta, S., & Palit, D. (2014). Biosurvilance of wetlands in Eastern India (Birbhum, West Bengal) for wise use. *International Journal of Science, Environment and Technology*, *3*(6), 2136-2144.

Mazumdar, S., Ghosh, P., & Saha, G. K. (2005). Diversity and behaviour of waterfowl in Santragachi Jheel, West Bengal, India, during winter season. *Indian Birds*, *1*(3), 68-69.

Patode, P. S., Salve, B. S., & Pawar, R. T. (2021). Avifaunal diversity status and abundance of Siddheshwar Reservoir, district Hingoli, Maharashtra, India. *International Journal of Advanced Research in Biological Sciences*, *8*(12), 47-55.

Samanta, S., Das, D., & Mandal, S. (2022). Diversity, status and guild structure of the avifauna in the Ajodhya Foothills, Baghmundi, Purulia, West Bengal, India. *Tropical Ecology*, 1-13. https://doi.org/10.1007/s42965-022-00265-7

https://doi.org/10.31674/book.2023pcbs003

Role of Paclitaxel and Vinblastine in Modern Cancer Therapy

Suranjana Sarkar
Department of Botany, Surendranath College, Kolkata, West Bengal, India

Corresponding Author's E-mail: drsuranjanasarkar@gmail.com

ABSTRACT

Natural products still account for more than half of all medications in clinical use in the generic age of contemporary biotechnology. According to the World Health Organization, plant extracts are used in 85 percent of out-dated medicine, and around 80 percent of people in underdeveloped nations rely on conventional medicinal substances for their main health care. 62 percent of the 87 anticancer medicines authorised in the last 10 years are natural products. The major drugs among them include paclitaxel and vinblastine, extracted from *Taxus brevifolia* and *Catharanthus roseus* respectively. All of them work by binding to tubulin and altering microtubule dynamics to impede cancer cell proliferation. They trigger apoptosis by causing mitotic arrest. These findings from epidemiological and investigational research emphasise the usefulness of phytochemicals in reducing cancer risk and inhibiting the growth and spread of tumours in investigational animals, which are medically more important. In a range of spontaneous or transplanted lymphocytic leukaemia, paclitaxel and Vinblastine medications have a high inhibitory impact on monozygotic leukaemia, breast cancer, lung cancer, liver cancer, ovarian cancer, solid sarcoma, malignant melanoma, head and neck cancer, and testicular cancer. Anti-tumour effects, on the other hand, still encounter obstacles and have a long way to go. The study and development of these medications will provide more significant results in the future.

Keywords: *Paclitaxel; Vinblastine; Cancer; Taxus Brevifolia; Catharanthus Roseus*

Introduction

Cancer, as a serious public health issue, affects simultaneously both developed and emerging nations globally. In 2018, an estimated 18.1 million new cases of cancer were diagnosed worldwide, with the number expected to rise to 23.6 million new cases per year by 2030 (Bray *et al.,* 2018). Because of this disease's extraordinary notoriety, treating it has been a never-ending battle with mixed results.

Plant phytochemicals and derivatives are promising alternatives to boosting therapeutic efficacy and decreasing unwanted effects in cancer patients. Some of these plant-based, physiologically active substances are naturally occurring. The examination of natural extracts (from dehydrated or wet plant material) is the initial step towards potential biological action against cancer and the creation of effective anticancer therapies based on phytochemicals that have few adverse effects. The effects of the separated active phytochemicals are next examined in vitro and in vivo using bioassay-guided fractionation (Ravina, 2011). Based on their roles, chemotherapeutic drugs that target microtubules are classified into two groups:

Paclitaxel (Taxol) is a microtubule stabiliser that promotes microtubule polymerization, which causes difficulties in chromosomal separation and the cell cycle process. Paclitaxel is commonly used to treat solid tumours such as advanced cases of ovarian and breast cancer, non-small cell lung cancer (NSCLC), and Kaposi's sarcoma (Hennessy, Coleman & Markman, 2009; Takashima *et al.,* 2015). The other is vinblastine, a vinca alkaloid that destabilizes microtubules and prevents cell growth mostly by binding to tubulin and disassembling microtubules. According to Coderch, Morreale and Coderch, Morreale and Gago, (2012) and Koontz *et al*. (2013), vinblastine is frequently used to treat cancers such as choriocarcinoma, Hodgkin's disease, malignant lymphoma, osteosarcoma, breast, ovarian, gastric, and lung cancers. Taxol and Vinblastine consequently interact with tubulin in opposing ways (Shen *et al.,* 2017).

Paclitaxel was found to be a component of the National Cancer Institute screening program launched in 1960 by Dr. Jonathan L. Hartwell, and to have anticancer potential (Wani & Horwitz, 2014). Scientist Wani and his group isolated and identified paclitaxel (which they termed Taxol®) from the bark extract of the Pacific Yew Tree (*Taxus brevifolia*) and conveyed their findings (Wani *et al.,* 1971). Nonetheless, the mechanism of action of paclitaxel as an anticancer medication attracted the interest of cancer pharmacology or pharmaceutical corporations. Dr. Horwitz's laboratory inspected and confirmed that paclitaxel besides having powerful cytotoxic properties capable of inhibiting the developmental development of human cervical cancer cells (HeLa) at nanomolar concentrations, also detained cells in the mitotic (M) phase of the cell cycle while not disrupting the S- phase (Horwitz *et al.,* 1986; Schiff, Fant & Horwitz, 1979). Scientists conducted more biochemical tests and experiments to discover the significant and distinct features of paclitaxel (Rowinsky, Cazenave & Donehower, 1990). Paclitaxel research as an anticancer agent is still ongoing decades later (Barbuti & Chen, 2015).

A vinca alkaloid anti-cancer agent is vinblastine. Vindoline and catharanthine are two multiringed units that make up the structurally related vinca group of alkaloids (Jordan & Kamath, 2007). Since the discovery of the vinca alkaloids' antitumor effects in 1959, they have been effective in clinical settings. The periwinkle plant (*Catharanthus roseus*) extracts were initially looked into for their alleged hypoglycemic characteristics, however it was discovered that they also have antileukemic effects in vitro and marrow suppression in rats. Vinblastine can suppress the immune system in some ways. Cell cycle phase-specificity is thought to apply to vinca alkaloids. The interaction between vinblastine and tubulin, which stops mitosis at metaphase, is considered to be responsible for the majority of the drug's anticancer effects. (Jordan *et al*., 1998; Islam & Iskander, 2004). Vinblastine binds to the proteins in the microtubules of the mitotic spindle, driving the microtubule-crystallisation and causing mitotic arrest or cell death (Gupta & Bhattacharyya, 2003).

Source Plant Material

1. Madagascar periwinkle / Nayantara

   Family: Apocynaceae

Scientific Name: *Catharanthus roseus* (L.) G. Don

Synonym: *Vinca rosea* L.

2. Pacific yew

   Family: Taxaceae

   Scientific Name: *Taxus brevifolia*

Literature Review

Cancer is responsible for approximately 10 million annual deaths worldwide (WHO, 2022). Cancer treatment includes, among other things, surgery, chemotherapeutic treatment, radiation therapy, and medication, all of which not only significantly affect patients' financial situations but also lead to resistance to drugs in patients over time. Implementing evidence-based preventive strategies can prevent or treat a large number of cancer cases. Drugs made from plants have emerged as promising anti-cancer treatments in both developing and developed countries (Garcia-Oliveira *et al.,* 2021). Some alkaloids have already demonstrated efficiency in protecting us against cancer (Dhyani *et al.,* 2022).

***The Pharmacology of Paclitaxel*:**

Microtubules are a dynamic and complex web of tubulin heterodimers comprising and β subunits, participating in many essential cellular activities, including the formation of mitotic spindle fibres required for M-phase cell division (Wilson, 1975). Microtubule-targeting medicines, viz., colchicine and the vinca alkaloids, cause microtubule breakdown. Taxanes, on the other hand, bind to tubulin and prevent microtubule disintegration. Antimicrotubule drugs, whether depolymerizing or stabilising tubulin, alter microtubule dynamics, induce mitotic arrest, and prevent cell division, eventually leading to programmed cell death (Mukhtar, Adhami & Mukhtar, 2014). Paclitaxel, like docetaxel, belongs to the taxane class of anticancer medicines. Though tubulin is the primary target for inducing apoptosis, paclitaxel also targets mitochondria and prevents the apoptosis inhibitor protein B-cell Leukemia 2 (Bcl-2) (Ferlini *et al.,* 2003). Paclitaxel is a very hydrophobic medication that needs appropriate delivery vehicles to properly allocate it into tumour tissues. Paclitaxel is now manufactured and supplied to patients in either polyethoxylated castor oil (Cremophor EL, CrEL) or albumin-bound (nab-paclitaxel, Abraxane®) form for efficient distribution. For many years, intravenous (IV) administration of CrEL-paclitaxel, generally once every three weeks, was a standard method, although it has been linked to hypersensitivity responses and neurotoxicity (Fransson *et al.,* 2011). Fresh paclitaxel preparations incorporating the utilisation of nanoparticles, emulsions, liposomes, and micelles have been investigated to reduce toxicity and improve transport and dispersion (Hennenfent & Govindan, 2006). Because it does not include CrEL, Nab-paclitaxel, a newer albumin-bound paclitaxel nanoparticle version, has been shown to reduce hypersensitivity responses. Indeed, Li et al. revealed variations in the distribution of paclitaxel between CrEL- and nab-paclitaxel. When compared to CrEL-paclitaxel micelles, nab-paclitaxel distribution to peripheral tissue was quicker (4-fold) and more widespread (10-fold) (Li *et al.,* 2015). The study also found that when liberated from the

respective carrier complexes, tissue distribution of free and protein-bound paclitaxel was restricted and sluggish, attesting to the drug's hydrophobic nature.

Taxanes are metabolised by cytochrome P450 enzymes in the liver and removed by biliary excretion (Vaishampayan *et al.,* 1999). Paclitaxel's known metabolites are largely inactive when biotransformed by means of hydroxylation events. These are 6--hydroxypaclitaxel (via CYP2C8), 3′-p-hydroxyphenylpaclitaxel (via CYP3A4), and 6--p-3-dihydroxypaclitaxel (by subsequent CYP3A4 and CYP2C8 metabolism, respectively) (Rowinsky *et al.,* 1993). Paclitaxel's most serious side effects are neutropenia, peripheral neuropathy, and mild cardiotoicity (Vaishampayan *et al.,* 1999). Nonetheless, because paclitaxel is eliminated in the bile, it is frequently the first choice of anticancer treatment in individuals with decreased creatinine clearance or renal illness. The ATP Binding Cassette (ABC) transporter B1 (ABCB1/MDR1/P-gp) has also been discovered to have a function in paclitaxel metabolism (Fransson *et al.,* 2011; Yamaguchi *et al.,* 2006). The involvement of ABCB1 in paclitaxel-treated cells has been linked to drug resistance.

Paclitaxel has been authorised by the FDA to treat AIDS-related Kaposi sarcoma, breast cancer, non-small cell lung cancer (NSCLC), and ovarian cancer, either alone or in combination with other anticancer therapies. It is also being researched for usage in the treatment of various malignancies, including head, neck, esophageal, bladder, endometrial and cervical cancer. Recently, the FDA authorised Abraxane® to treat metastatic pancreatic cancer, non-small cell lung cancer, and breast cancer. The drug management caution that comes with these paclitaxel formulations states that patients' neutrophil counts should be monitored to treat any bone marrow suppression (Barbuti & Chen, 2015). Neutropenia caused by chemotherapy is a typical side effect of numerous anticancer medications.

***Pharmacology of Vinblastin*:**

The natural Vinca alkaloid, Vinblastine, was first discovered in Catharanthus roseus. The plant's potential as a chemotherapeutic agent was initially discovered when the extract was offered to rabbits to investigate the plant's purported anti-diabetic effect. Because the rabbits died of a bacterial infection owing to a huge deficiency of white blood cells in the experiment, Vinblastine was assumed to be useful against white blood cell cancers such as lymphoma (Noble, Beer & Cutts, 1958). It was originally isolated from *Catharanthus roseus* extracts due to its suspected hypoglycemic effects. According to the National Center for Biotechnology Information (2023), it shares structural similarities with two additional multi-ringed compounds, vindoline and catharanthine. It adheres to tubulin and hinders the production of microtubules, disrupting the construction of the mitotic spindle and stopping cancer cells from progressing through the cell cycle's M phase. The metabolism of amino acids, cyclic AMP, glutathione, calmodulin-dependent Ca++-transport, ATPase activity, cellular respiration, and the synthesis of nucleic acids and lipids may all be affected by this molecule. It is used to treat testicular cancer, breast cancer, Kaposi sarcoma, renal cell carcinoma, and Hodgkin's and non-Hodgkin lymphomas. The characteristic side effects, like mucositis, myelosuppression, anaemia, fever, and baldness, are brought on by unfavourable responses.

Vinblastine is rapidly absorbed from the plasma and transported to tissues, notably the lung, liver, spleen, and kidneys (Owellen & Hartke, 1975; Owellen, Hartke & Hains, 1977). Vinblastine, like the other vinca alkaloids, is processed by the hepatic cytochrome P450 3A enzyme. This pathway may be compromised in people with hepatic dysfunction and may be influenced by various medicines that either promote or inhibit cytochrome P450 3A activity. Vinblastine is mostly eliminated in the bile and faeces, with little excretion in the kidney (28).

The pharmacologic behaviour of Vinblastine is similar to that of Vincristine (Owellen, Hartke & Hains, 1977; Zhou *et al.,* 1990). Peak plasma drug concentrations are around 0.4 mol/L following a fast intravenous injection of VBL at normal dosages. Similar to VCR, vinblastine binds extensively to blood components and plasma proteins. Moreover, dispersion is fast, with half-lives of roughly 4 min and 1.6 h for the and β phases, respectively. Similar to VCR, tissue sequestration is significant, with 73% of radioactivity remaining in the body for six days following radiolabelled medication administration (Ratain & Vogelzang, 1986). 20 to 24 hour terminal half-life values have been recorded. Like the VCR, the hepatobiliary system is primarily responsible for vinblastine disposal. Low fecal excretion of the parent substance suggests significant metabolism. Its biotransformation appears to be mostly caused by the cytochrome P450 CYP3A isoform (Zhou *et al.,* 1990; Rowinsky, 2003). The primary metabolite of VINBLASTINE is 4-diacetyl vinblastine, also known as vindesine (VDS), despite the fact that its metabolic destiny has not yet been thoroughly characterized. (Rowinsky & Donehower, 1991; Rowinsky, 2003).

Discussion

Paclitaxel has been used in several anticancer therapy regimens because it is an efficient microtubule stabiliser and radiation sensitizer. However, paclitaxel's therapeutic effectiveness has been proven to promote multidrug resistance (MDR) via numerous cellular contrivances that have yet to be completely comprehended. Resistance to Paclitaxel has been reported to comprise both tubulin mutations, modifications in the binding areas of -tubulin, decreased efficacy of key creator proteins of apoptosis, and variations in cytokine release, in addition to over-expression of the ABCB1 and ABCC10 efflux transporters. Paclitaxel will be delivered to tumour tissue by novel drug delivery technologies such as nanoparticles and targeted drug conjugates, allowing for improved anticancer efficacy and safety. Moreover, novel drugs, as well as already authorised small molecule inhibitors, must be investigated in order to counteract the ABC transport-mediated MDR associated with paclitaxel resistance. Paclitaxel (Taxol®) has been isolated and identified for over 40 years, and its exclusive pharmacokinetic and pharmacodynamic anticancer features continue to support its therapeutic importance. Paclitaxel treatment will continue to transcend the centuries of cancer therapy with additional research focused on identifying the origins of de novo and acquired resistance, together with improved chemotherapy and radiation.

Vinblastine is a mitotic inhibitor used in the treatment of leukaemia, non-lymphoma, Hodgkin's lymphoma, breast malignancies such as breast carcinoma, Wilm's tumour, Ewing's sarcoma, small-cell lung cancer, testicular carcinoma, and germ cell tumours (Dandamudi & Campbell, 2007; Moudi *et al.,* 2013). Vinblastine inhibits not just tumour development but also malignant

angiogenesis and can bind selectively to tubulin, blocking polymerization and following microtubule attachment (Dandamudi & Campbell, 2007; Moudi *et al.,* 2013).

They inhibit microtubule dynamics when administered at very low concentrations and lower microtubule polymer mass when doses are increased. Recent research indicates that they can form microtubule fragments by inducing detachment from microtubule organising centres. These studies show that increased microtubule dissociation from spindle poles correlates best with cytotoxicity (Ganguly *et al.,* 2010). However, research into the process is still ongoing since new findings reveal Vinblastine triggering apoptosis that is phase-independent in some leukemias (Salerni *et al.,* 2010).

In combination with other chemotherapeutic medicines, Vinblastine can treat a wide range of cancers. Vinblastine, cisplatin, and radiation treatment, or VCRT, are used to treat non-small-cell lung cancer stages IIIA and IIIB (Waters *et al.,* 2010). In patients with disseminated non-seminomatous germ-cell cancers, CISCA/VB (cisplatin, doxorubicin, cyclophosphamide, Vinblastine, and bleomycin) is used (Fizazi *et al.,* 2002). As a conventional chemotherapy treatment for Hodgkin's lymphoma it is used along with doxorubicin, bleoycin, and dacarbazine (Schwenkglenks *et al.,* 2010).

Although simple diffusion-like non saturable mechanisms, which are temperature-independent, probably account for the bulk of drug transport (Zhou, Placidi & Rahmani, 1994). This is contrary to the widespread belief that the cellular entry of the Vinca alkaloids occurs through both energy and temperature-dependent transport methods. Drug exposure over a critical threshold concentration is the significant predictor, although drug concentration and treatment time are also significant factors in drug accumulation and cytotoxicity, according to the majority of the evidence now available (Jackson & Bender, 1979). Vinblastine side effects include toxicity to white blood cells, nausea, vomiting, constipation, dyspnea, chest or tumour discomfort, wheezing, fever, and, in rare cases, antidiuretic hormone production (Chen & Zhang, 2004).

Table 1: Comparative Account between Paclitaxel and Vinblastine

	Paclitaxel (Taxol)	**Vinblastine (Velban)**
Chemical Formula:	$C_{47}H_{51}NO_{14}$	$C_{46}H_{58}N_4O_9$
Molecular Weight:	853.9 g/mol (Computed by PubChem, 2019)	811 g/mol (Computed by PubChem, 2019)
Discovery	First isolated in 1971 by Mansukhlal C. Wani, Harold Lawrence Taylor, Monroe E. Wall, Philip Coggon, and Andrew T. McPhail	First isolated in 1958 by Robert Noble, Charles Thomas Beer and Cutts, J.H.
Chemical Nature	Tetracyclic diterpenoid, lipophilic in nature	Natural Vinca Alkaloid comprising of two multiringed units: vindoline and catharanthine
Source Plant Part	Bark of pacific yew tree *Taxus brevifolia*	Mainly obtained from leaves and partly from stems and buds of *Catharanthus roseus*

Physical Nature	This anti-neoplastic drug appears as fine white powder.	White to slightly yellow crystalline solid, melting point is 267˚C
Uses	Ovarian cancer, breast cancer, AIDS related Kaposi's sarcoma cervical cancer, pancreatic cancer and lung cancer.	Hodgkin's lymphoma, non-small cell lung cancer, bladder cancer, brain cancer, melanoma, breast cancer and testicular cancer
Mode of Action	Paclitaxel disrupts the normal function of microtubule development by hyper-stabilizing its structure. This robs the cell of its capacity to employ its cytoskeleton flexibly. Paclitaxel specifically targets the tubulin subunit. Tubulin is the "building block" of mictotubules that holds them together. This has a negative impact on cell function since microtubule shortening and lengthening is required for their function as a transportation highway for the cell. Paclitaxel causes programmed cell death in cancer cells by attaching to an apoptosis-inhibiting protein called Bcl-2 (B-cell leukaemia 2) and therefore terminating its action.	The primary mechanism by which vinblastine suppresses mitosis during metaphase is thought to be its interaction with tubulin. Vinblastine interacts to the microtubular proteins in the mitotic spindle, resulting in crystallisation and mitotic arrest or cell death.

Conclusion

The current review aims to assess the anticancer activity of two distinct phytochemicals - Paclitaxel and Vinblastine. Cancer is a constant threat to mankind. These two natural cancer chemo-preventive substances are capable of preventing or suppressing carcinogenesis. Paclitaxel is a medication that is used exclusively or in combination with other medications to address AIDS-type diseases, Kaposi's sarcoma, advanced ovarian cancer, some forms of breast cancer, and non- small cell lung cancer. To treat various forms of cancer, Paclitaxel is being tested. Paclitaxel inhibits cancer cell growth and division, perhaps killing them. Vinblastine has long been used for several forms of advanced lymphomas, and also as a chemotherapy ingredient for germ cell malignancies. Vinblastine has previously been used wholly or in conjunction with other medications to treat different types of cancer. The process of researching and developing these medications will provide additional significant future revelations.

Acknowledgement

The author would like to thank the Government of India's Department of Biotechnology for funding this review study under the DBT-Star College Grant. The author would like to thank the Principal of Surendranath College and the DBT-STAR Coordinator for their assistance and support in carrying out this review project.

References

Barbuti, A. M., and Z. S. Chen. "Cancers, 2015, 7, 2360–2371." Chapter 11–Triazole CBD analogues and Substituted CPPs–References.

Bray, F., Ferlay, J., Soerjomataram, I., Siegel, R. L., Torre, L. A., & Jemal, A. (2018). Global cancer statistics 2018: GLOBOCAN estimates of incidence and mortality worldwide for 36 cancers in 185 countries. CA: a cancer journal for clinicians, 68(6), 394-424. https://doi.org/10.3322/caac.21492

Chen, W., & Zhang, D. (2004). Kinetochore fibre dynamics outside the context of the spindle during anaphase. *Nature Cell Biology*, *6*(3), 227-231. https://doi.org/10.1038/ncb1104

Coderch, C., Morreale, A., & Gago, F. (2012). Tubulin-based structure-affinity relationships for antimitotic Vinca alkaloids. Anti-Cancer Agents in Medicinal Chemistry (Formerly Current Medicinal Chemistry-Anti-Cancer Agents), 12(3), 219-225. https://doi.org/10.2174/187152012800228841

Dandamudi, S., & Campbell, R. B. (2007). The drug loading, cytotoxicty and tumor vascular targeting characteristics of magnetite in magnetic drug targeting. *Biomaterials*, *28*(31), 4673-4683. https://doi.org/10.1016/j.biomaterials.2007.07.024

Dhyani, P., Quispe, C., Sharma, E., Bahukhandi, A., Sati, P., Attri, D. C., ... & Cho, W. C. (2022). Anticancer potential of alkaloids: a key emphasis to colchicine, vinblastine, vincristine, vindesine, vinorelbine and vincamine. Cancer Cell International, 22(1), 1-20. https://doi.org/10.1186/s12935-022-02624-9

Ferlini, C., Raspaglio, G., Mozzetti, S., Distefano, M., Filippetti, F., Martinelli, E., ... & Scambia, G. (2003). Bcl-2 down-regulation is a novel mechanism of paclitaxel resistance. Molecular pharmacology, 64(1), 51-58. https://doi.org/10.1124/mol.64.1.51

Fizazi, K., Do, K. A., Wang, X., Finn, L., Logothetis, C. J., & Amato, R. J. (2002). A 20% dose reduction of the original CISCA/VB regimen allows better tolerance and similar survival rate in disseminated testicular non-seminomatous germ-cell tumors: final resultsof a phase III randomized trial. *Annals of Oncology*, *13*(1), 125-136. https://doi.org/10.1093/annonc/mdf005

Fransson, M. N., Green, H., Litton, J. E., & Friberg, L. E. (2011). Influence of Cremophor EL and genetic polymorphisms on the pharmacokinetics of paclitaxel and its metabolites using a mechanism-based model. Drug metabolism and disposition, 39(2), 247-255. https://doi.org/10.1124/dmd.110.035394

Ganguly, A., Yang, H., Pedroza, M., Bhattacharya, R., & Cabral, F. (2011). Mitotic centromere-associated kinesin (MCAK) mediates paclitaxel resistance. Journal of Biological Chemistry, 286(42), 36378-36384. https://doi.org/10.1074/jbc.M110.160820

Garcia-Oliveira, P., Otero, P., Pereira, A. G., Chamorro, F., Carpena, M., Echave, J., ... & Prieto, M. A. (2021). Status and challenges of plant-anticancer compounds in cancer treatment. Pharmaceuticals, 14(2), 157. https://doi.org/10.3390/ph14020157

Gupta, S., & Bhattacharyya, B. (2003). Antimicrotubular drugs binding to vinca domain of tubulin. Molecular and cellular biochemistry, 253, 41-47. https://doi.org/10.1023/A:1026045100219

Hennenfent, K., & Govindan, R. (2006). Novel formulations of taxanes: a review. Old wine in a new bottle?. Annals of oncology, 17(5), 735-749. https://doi.org/10.1093/annonc/mdj100

Hennessy, B. T., Coleman, R. L., & Markman, M. (2009). Ovarian cancer. The lancet, 374(9698), 1371-1382. https://doi.org/10.1016/S0140-6736(09)61338-6

Horwitz, S., Lothstein, L., Manfredi, J. J., Mellado, W., Parness, J., Roy, S. N., ... & Zeheb, R. (1986). Taxol: Mechanisms of Action and Resistance a. Annals of the New York Academy of Sciences, 466(1), 733-744. https://doi.org/10.1111/j.1749-6632.1986.tb38455.x

Islam, M., & Iskander, M. N. (2004). Microtubulin binding sites as target for developing anticancer agents. Mini reviews in medicinal chemistry, 4(10), 1077-1104. https://doi.org/10.2174/1389557043402946

Jackson Jr, D. V., & Bender, R. A. (1979). Cytotoxic thresholds of vincristine in a murine and a human leukemia cell line in vitro. Cancer Research, 39(11), 4346-4349.

Jordan, A., Hadfield, J. A., Lawrence, N. J., & McGown, A. T. (1998). Tubulin as a target for anticancer drugs: agents which interact with the mitotic spindle. *Medicinal research reviews*, *18*(4), 259-296. https://doi.org/10.1002/(SICI)1098-1128(199807)18:4%3C259::AID-MED3%3E3.0.CO;2-U

Jordan, M. A., & Kamath, K. (2007). How do microtubule-targeted drugs work? An overview. Current cancer drug targets, 7(8), 730-742. https://doi.org/10.2174/156800907783220417

Koontz, Michael Zach, Sandra J. Horning, Raymond Balise, Peter L. Greenberg, Saul A. Rosenberg, Richard T. Hoppe, and Ranjana H. Advani. "Risk of therapy-related secondary leukemia in Hodgkin lymphoma: the Stanford University experience over three generations of clinical trials." Journal of Clinical Oncology 31, no. 5 (2013): 592. https://doi.org/10.1200%2FJCO.2012.44.5791

Li, B. J., Hao, X. Y., Ren, G. H., & Gong, Y. (2015). Effect of lipoic acid combined with paclitaxel on breast cancer cells. Genet Mol Res, 14(4), 17934-17940.

Moudi, M., Go, R., Yien, C. Y. S., & Nazre, M. (2013). Vinca alkaloids. International journal of preventive medicine, 4(11), 1231.

Mukhtar, E., Adhami, V. M., & Mukhtar, H. (2014). Targeting microtubules by natural agents for cancer therapymicrotubule-targeting agents for cancer chemotherapy. Molecular cancer therapeutics, 13(2), 275-284. https://doi.org/10.1158/1535-7163.MCT-13-0791

National Center for Biotechnology Information. (12th June 2023). *Compound Summary: Vinblastine*. https://pubchem.ncbi.nlm.nih.gov/compound/Vinblastine

Noble, R. L., Beer, C. T., & Cutts, J. H. (1958). Role of chance observations in chemotherapy: Vinca rosea. Annals of the New York Academy of Sciences, 76(3), 882-894. https://doi.org/10.1111/j.1749-6632.1958.tb54906.x

Owellen, R. J., & Hartke, C. A. (1975). The pharmacokinetics of 4-acetyl tritium vinblastine in two patients. Cancer Research, 35(4), 975-980.

Owellen, R. J., Hartke, C. A., & Hains, F. O. (1977). Pharmacokinetics and metabolism of vinblastine in humans. Cancer Research, 37(8_Part_1), 2597-2602.

Ratain, M. J., & Vogelzang, N. J. (1986). Phase I and pharmacological study of vinblastine by prolonged continuous infusion. Cancer research, 46(9), 4827-4830.

Ravina, E. (2011). The evolution of drug discovery: from traditional medicines to modern drugs. John Wiley & Sons. 157–159.

Rowinsky, E. (2003). The vinca alkaloids. *Holland-Frei Cancer Medicine*. 6th edition. Hamilton (ON): BC Decker.

Rowinsky, E. K., & Donehower, R. C. (1991). The clinical pharmacology and use of antimicrotubule agents in cancer chemotherapeutics. Pharmacology & therapeutics, 52(1), 35-84. https://doi.org/10.1016/0163-7258(91)90086-2

Rowinsky, E. K., Cazenave, L. A., & Donehower, R. C. (1990). Taxol: a novel investigational antimicrotubule agent. JNCI: Journal of the National Cancer Institute, 82(15), 1247-1259. https://doi.org/10.1093/jnci/82.15.1247

Rowinsky, E. K., Wright, M., Monsarrat, B., Lesser, G. J., & Donehower, R. C. (1993). Taxol: pharmacology, metabolism and clinical implications. Cancer surveys, 17, 283-304.

Salerni, B. L., Bates, D. J., Albershardt, T. C., Lowrey, C. H., & Eastman, A. (2010). Vinblastine Induces Acute, Cell Cycle Phase–Independent Apoptosis in Some Leukemias and Lymphomas and Can Induce Acute Apoptosis in Others when Mcl-1 Is SuppressedAcute Apoptosis Induced by Vinblastine. Molecular cancer therapeutics, 9(4), 791-802. https://doi.org/10.1158/1535-7163.MCT-10-0028

Schiff, P. B., Fant, J., & Horwitz, S. B. (1979). Promotion of microtubule assembly in vitro by taxol. Nature, 277(5698), 665-667.

Schwenkglenks, M., Pettengell, R., Szucs, T. D., Culakova, E., & Lyman, G. H. (2010). Hodgkin lymphoma treatment with ABVD in the US and the EU: neutropenia occurrence and impaired chemotherapy delivery. Journal of hematology & oncology, 3(1), 1-6. https://doi.org/10.1186/1756-8722-3-27

Shen, F., Long, D., Yu, T., Chen, X., Liao, Y., Wu, Y., & Lin, X. (2017). Vinblastine differs from Taxol as it inhibits the malignant phenotypes of NSCLC cells by increasing the phosphorylation of Op18/stathmin. Oncology Reports, 37(4), 2481-2489. https://doi.org/10.3892/or.2017.5469

Takashima, S., Kiyoto, S., Takahashi, M., Hara, F., Aogi, K., Ohsumi, S., ... & Fujita, Y. (2015). Clinical experience with nanoparticle albumin-bound paclitaxel, a novel taxane anticancer agent, and management of adverse events in females with breast cancer. Oncology Letters, 9(4), 1822-1826. https://doi.org/10.3892/ol.2015.2954

Vaishampayan, U., Parchment, R. E., Jasti, B. R., & Hussain, M. (1999). Taxanes: an overview of the pharmacokinetics and pharmacodynamics. Urology, 54(6), 22-29. https://doi.org/10.1016/S0090-4295(99)00451-3

Wani, M. C., & Horwitz, S. B. (2014). Nature as a Remarkable Chemist: A personal story of the discovery and development of Taxol®. Anti-cancer drugs, 25(5), 482. https://doi.org/10.1097%2FCAD.0000000000000063

Wani, M. C., Taylor, H. L., Wall, M. E., Coggon, P., & McPhail, A. T. (1971). Plant antitumor agents. VI. Isolation and structure of taxol, a novel antileukemic and antitumor agent from

Taxus brevifolia. *Journal of the American Chemical Society*, *93*(9), 2325-2327. https://doi.org/10.1021/ja00738a045

Waters, E., Dingle, B., Rodrigues, G., Vincent, M., Ash, R., Dar, R., ... & Yu, E. (2010). Analysis of a Novel Protocol of Combined Induction Chemotherapy and Concurrent Chemoradiation in Unresected Non–Small-Cell Lung Cancer: A Ten-Year Experience With Vinblastine, Cisplatin, and Radiation Therapy. Clinical Lung Cancer, 11(4), 243-250. https://doi.org/10.3816/CLC.2010.n.031

WHO. (3rd February 2022). Cancer. *World Health Organization.https://www.who.int/news-room/fact-sheets/detail/cancer#:~:text=The%20problem Cancer%20is%20a% 20leading %20cause%20of%20death%20worldwide%2C%20accounting%20for,lung%20(2.21%20 million%20cases)%3B*

Wilson, L. (1975). Microtubules as drug receptors: pharmacological properties of microtubule protein. Annals of the New York Academy of Sciences, 253(1), 213-231. https://doi.org/10.1111/j.1749-6632.1975.tb19201.x

Yamaguchi, H., Hishinuma, T., Endo, N., Tsukamoto, H., Kishikawa, Y., Sato, M., ... & Goto, J. (2006). Genetic variation in ABCB1 influences paclitaxel pharmacokinetics in Japanese patients with ovarian cancer. International Journal of Gynecologic Cancer, 16(3). http://dx.doi.org/10.1136/ijgc-00009577-200605000-00004

Zhou, X. J., Martin, M., Placidi, M., Cano, J. P., & Rahmani, R. (1990). In vivo and in vitro pharmacokinetics and metabolism of vincaalkaloids in rat II. Vinblastine and Vincristine. European journal of drug metabolism and pharmacokinetics, 15, 323-332. https://doi.org/10.1007/BF03190222

Zhou, X. J., Placidi, M., & Rahmani, R. (1994). Uptake and metabolism of vinca alkaloids by freshly isolated human hepatocytes in suspension. Anticancer research, 14(3A), 1017-1022.

https://doi.org/10.31674/book.2023pcbs004

The Synthesis, Spectral and Antimicrobial Study of Heterobinuclear Complexes of Copper (II) Schiff Base with Alkali Metals Salts

Chandan Kumar
Department of Chemistry, Deoghar College, Deoghar, (S.K.M. University), Jharkhand, India

Corresponding Author's Email: chandankumar78@yahoo.com

ABSTRACT

The condensation reaction of a primary amine with carbonyl compounds results in a Schiff base, which is effectively incorporated in the preparation of metal complexes. Herein, a series of hetero binuclear complexes have been synthesized of the general formula CuPS.ML, where PS = Schiff base prepared by condensation of salicylaldehyde and propylene diamine; ML = Li, Na or K salts of 2-nitrophenol; 2,4-dinitrophenol; 2,4,6-trinitrophenol & 1-nitroso-2-naphthol. The compounds are generally soluble in most of the organic solvents but insoluble in water. These complexes have been characterized by elemental analysis, IR spectra, UV-VIS spectra, magnetic measurement and molar conductance results. The low value of molar conductance of the complexes suggested the non-electrolyte nature of the complexes. The spectral analysis suggested that the bonding between copper (II) metal chelate and alkali metal, appeared through the dative bond through the phenolic oxygen atoms. The study also revealed the square planar structure of the complexes. Some of these complexes showed the antimicrobial activity on *E. coli, S. aureus* and *C. albicans* and so, these complexes may be considered as good antimicrobial agents.

Keywords: *Heterobinuclear Complexes; Alkali Metal; Schiff Base; Spectra; Antimicrobial Studies*

Introduction

Schiff bases have capability in the formation of metal complexes (Singh & Chaudhary, 2019) and they also deserve great attention because of their biological properties (Mishra *et al*., 1991). Transition metal complexes of the Schiff base are established to be of great attentiveness in inorganic chemistry and it also, has been considered significantly in the complexes (Ahmed, Dalia & Fatmaa, 2015; Patel *et al*., 2005). The heterobinuclear alkali metal complexes of Cu (II) Schiff base are also biologically active (Zhong *et al.,* 1994) and they exhibit enhanced activities as compared to their parent ligand. They have previously reported the preparation and characterization of number of heterobinuclear complexes derived with Schiff base (Kumar, 2017; Prakash, Kumar & Singh, 2008). In continuation of their earlier works, they have reported here, the study of some novel heterobinuclear alkali metal complexes. The bonding between the metal complex as ligand and the alkali metal is

probably with the two phenolic oxygen atoms of the ligand, this has been assisted by the Infrared, UV-Visible spectra and magnetic properties. The prepared complexes show the antimicrobial effectiveness.

Methodology

The chemicals used were of AR grade. Sigma Aldrich chemicals were used in the synthesis without purification. All the compound synthesis was carried out in the solvent which was purified and dried before use by using standard literature methods. IR spectra were recorded in KBr phase through the FTIR spectrophotometer, Shimadzu model 8201PC. The UV-visible spectra of the complexes were recorded through a Perkin Elmer Lambda 15 UVB VIS spectrophotometer and magnetic measurements were taken from Gouys balance. Systronics digital conductivity meter was used to measure molar conductance. Elemental analysis was carried out by Thermo Fisher Scientific-Flash Smart V. An electrical melting point apparatus was used for melting point measurements.

Synthetic Procedure

The Schiff base was prepared by refluxing salicylaldehyde and 1,2-propylenediamine in ethanol in 2:1 molar proportion. The solution was stirred for 15 minutes at 70^0C. The yellow Schiff base; N,N′-1,2-propylene-bis(salicylaldimine); PS was precipitated after cooling in ice bath. This solid yield was separated from solution, recrystallized with absolute ethanol and then dried in oven. Then a ethanolic solution of copper (II) acetate (2.0g)) was added gradually with continuous stirring to a hot alcoholic solution of the Schiff base (2.82g). The solution for cooling the purple copper (II) complex obtained. It was filtered, washed two times with ethanol and dried.

Synthesis of Heterobinuclear Complexes of Cu(II) Metal and Alkali Metal.

In the alcoholic solution of N,N′-1,2-propylene-bis(salicylideneiminato)copper (II); CuPS, the different alkali metal salts of organic acids o-nitrophenol, dinitrophenol, trinitrophenol or 1-nitroso-2-naphthol were separately added with a 1:1 molar ratio. The mixture was refluxed with stirring at 75–80 ^{0}C for 1-1½ hours. The characteristic color complexes were precipitated, and then it was filtered, washed two times with absolute alcohol and dried.

Results and Discussion

The copper (II) metal chelate and also their alkali metal adducts are colored solid (Table. 1.), non-hygroscopic and stable at room temperature. The complexes are soluble in acetone, methanol, benzene, and DMF but insoluble in water. Most of the complexes were decomposed after melting. The elemental analysis results of the compounds revealed a good consensus with their calculated values. The molar conductivities of complexes were measured in DMF at 30(±0.5) ^{0}C at 10^{-3}M. The compounds show molar conductivity in the range 0.5-8.9 $\Omega^{-1}cm^2mol^{-1}$ shows the non-electrolytic nature (Geary, 1971) of the complexes.

Infrared Spectra:

The IR spectra of the copper metal chelate and it adducts are shown in Table 2. The band at rage 1538-1570 suggests that these bands are due to the C-O stretching of the phenolic group (Sonbati *et al*., 2004). Comparing the C-O infrared bands for both the transition metal complex ligand and their alkali metal binuclear complexes, they arrive at the conclusion that the infrared bands for both are nearly the same. The metal complex as ligand copper exhibits the υ_{C-O} (phenolic) at 1538 cm^{-1}, that shifts to the direction of higher energy side on the complex formation, these shifts indicate the coordination with the phenolic oxygen (Sonbati *et al*., 2012). This shift may be due to the maintenance of a ring current emerging from the electron delocalization in the ring. The υ_{C-O} (phenolic) shifts to higher energy with 12 to 42 cm^{-1} in heterobinuclear complexes of copper is certainly indicating the presence of phenoxo-bridge. It is, therefore, suggesting the phenol C-O link attained a significant amount of partial double bond character in these complexes. In the complexes, the bands are found in the far IR region at ranging to 505-548 cm^{-1} and 461-470 cm^{-1} may be assigned to υ_{M-O} and υ_{M-N} modes respectively (Nakamoto, 2009). It is also observed that there is a positive shift in adducts compared to the metal complex as ligand, suggesting that the formation of adducts is the by the phenolic oxygen. These results are explained on the assumption that the nitrogen atom is less electronegative than the oxygen atom and the M-N band tends to be less ionic than the M-O bond. The above considerations coordinate the coordination of the oxygen atom of the phenolic group and the nitrogen atom of –NO, $-NO_2$ etc. to the alkali metal in all the heterobinuclear complexes.

Table 1: Physical Characteristics, Analytical Results of The Complexes

Complexes (CuPS.ML)	***Colour***	***m.p. (^0C)***	***Mol. Cond. $\Omega^{-1} cm^2 mol^{-1}$***	***Elemental analysis (%) Found (Calculated)***					***Yield (%)***
				C	***H***	***N***	***Cu***	***M***	
CuPS	Purple	255	-	58.91 (59.39)	4.42 (4.66)	7.68 (8.15)	18.21 (18.49)	-	74.62
CuPS.LiONP	Golden brown	228	1.4	56.46 (56.50)	4.01 (4.09)	8.52 (8.60)	12.88 (13.00)	1.37 (1.43)	77.79
CuPS.NaONP	Purple	247	0.5	54.62 (54.71)	3.87 (3.96)	8.22 (8.33)	12.53 (12.59)	4.41 (4.56	72.84
CuPS.KONP	Purple	245	0.6	52.82 (53.03)	3.72 (3.84)	7.88 (8.07)	12.12 (12.20)	7.41 (7.49)	66.76
CuPS.LiDNP	Brownish red	242	3.2	51.55 (51.73)	3.47 (3.56	10.45 (10.51)	11.83 (11.92)	1.21 (1.29)	73.1
CuPS.NaDNP	Brownish yellow	202	3.3	50.18 (50.23)	3.35 (3.46)	10.13 (10.19)	11.49 (11.56)	4.14 (4.19)	75.07
CuPS.KDNP	Teak brown	241	6.1	48.77 (48.81)	3.22 (3.36)	9.81 (9.90)	11.14 (11.23)	6.78 (6.90)	76.04

CuPS.LiTNP	Brownish yellow	218	6.5	47.52 (47.11)	3.02 (3.11)	12.02 (12.11)	10.79 (10.98)	1.11 (1.21)	’6.92
CuPS.NaTNP	Brownish yellow	266	7.2	46.31 (46.43)	2.88 (3.03)	11.62 (11.77)	10.55 (10.68)	3.73 (3.87)	’0.65
CuPS.KTNP	Brownish yellow	278	8.9	45.05 (45.21)	2.82 (2.95)	11.41 (11.47)	10.28 (10.40)	6.31 (6.39	›6.75
CuPS.Li1N2N	Brown	228	0.7	61.83 (62.01)	4.03 (4.21)	7.95 (8.04)	12.05 (12.15)	1.3 (1.34)	’8.95
CuPS.Na1N2N	Light Brown	226	2	60.1 (60.17)	3.91 (4.09)	7.67 (7.80)	11.68 (11.79)	4.18 (4.27)	’0.57
CuPS.K1N2N	Brown	225	2.4	58.38 (58.43)	3.82 (3.97)	7.48 (7.57)	11.31 (11.45)	6.88 (7.03)	’4.39

Table 2: IR and UV-Vis Data of Complexes

Compound	IR spectra (cm^{-1}) υ(C-O)) phenolic/ υ(M-O)/υ(M-N)	UV-Vis spectra Diffuse reflectance (in nm)	Magnetic moment (in BM)
CuPS	1538, 505, 466	219, 242, 352, 652	1.95
CuPS.LiONP	1570, 520, 465	226, 267, 351, 652	1.84
CuMPS.LiDNP	1550, 548, 469	224, 266, 352, 653	1.74
CuPS.NaTNP	1568, 541, 461	224, 266, 351, 652	1.73
CuPS.K1N2N	1565, 516, 470	225, 267, 353, 652	1.94

UV-Vis Spectra and Magnetic Moment:

The UV-visible absorption spectra of the heterobinuclear complexes are shown in Table 2. The absorption bands are found in the range 219–267 nm, suggesting the formation of π-π* transition. The bands observed between 351-653 nm in the complexes show the d-d transition and charge transfer (Condrate & Nakamoto, 1965; Jaffé & Orchin, 1962 & Thirumavalavan *et al.,* 2006). These absorption band of binuclear alkali metal complexes also suggesting the same square planar geometry with coordination number four (Jaffé & Orchin, 1962). The spectra of transition metal complexes as ligands and their oxygen bridge complexes show similar types of bands, these results suggest that there is no change in their stereochemistry of them. The magnetic moment of transition metal complex CuPS has been observed at 1.95 BM and its binuclear complexes varied between 1.73 to 1.94 BM (table 2), strongly indicating the presence of one unpaired electron. These results suggested that the transition metal complex as ligand and its heterobinuclear complexes are in square planar geometry with coordination number four.

Antimicrobial Activity:

The antimicrobial activity of the some of the heterobinuclear complexes was tested on bacteria viz. *Escherichia coli*, *Staphylococcus aureus* and fungus viz. *Candida albicans* by the serial dilution method in DMF in the concentration range 25-200 µg ml^{-1}. From results

(table 3 and figure 1) they found that the complexes show better antimicrobial activity at higher concentrations against the test organism and antimicrobial activity increases gradually as the concentration of these compounds increases (Singh *et al*., 2006). Better activities of the complexes can be explained with chelation theory (Ghosh *et al*., 2012), The decrease in polarizability of the metal cloud increases the lipophilicity of the compound which results to the breakdown of the permeability of the cells. Chelation also reduces the polarity of the metal ion because its positive charge is considerably shared by the donor groups and the p electron delocalizes over the chelate ring. Therefore the chelation could increase the lipophilic character of the metal atoms, which afterwards favors their permeation by the lipid layer of the cell-membranes (Panchal & Patel, 2006).

Table 3: Antimicrobial Result of Compounds

Compound	Conc. (μgml^{-1})	Percentage inhibition		
		E.coli	*S.aureus*	*C.albicans*
CuPS.NaONP	200	100	100	100
	100	100	100	100
	50	100	85-90	100
	25	85-90	85-90	85-90
CuPS.LiDNP	200	85-90	50-55	85-90
	100	85-90	50-55	85-90
	50	85-90	50-55	85-90
	25	50-55	50-55	50-55
CuPS.KTNP	200	100	85-90	85-90
	100	85-90	85-90	85-90
	50	85-90	50-55	50-55
	25	50-55	50-55	50-55
CuPS.K1N2N	200	100	100	100
	100	100	100	100
	50	85-90	85-90	100
	25	85-90	85-90	85-90

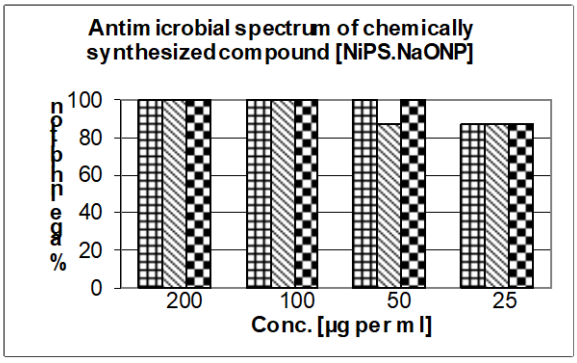

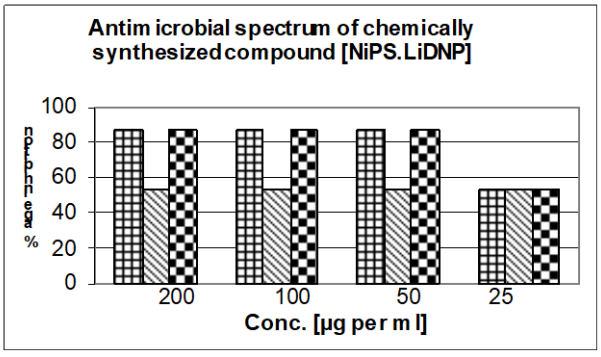

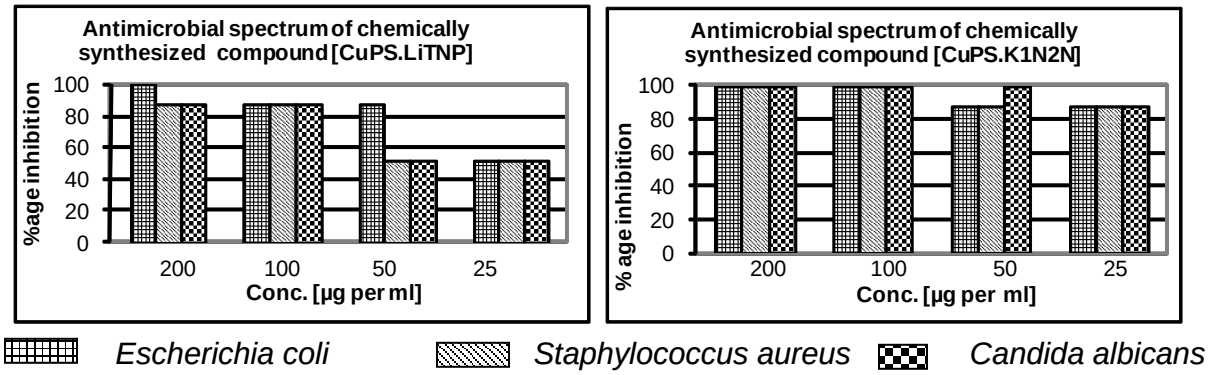

Figure1: Antimicrobial Data of Binuclear Complexes

Conclusion

The bonding of N,N′-1,2-propylene-bis(salicylideneiminato)copper(II) complex (CuPS) and the alkali metal is probably by the dative bonding though the two phenolic oxygen atoms, which is supported by the infrared spectra UV-visible spectra and magnetic results. The stoichiometry and the physico-chemical studies as discussed above suggested the square planar geometry of the complexes with coordination number 4. The proposed structure of the prepared compounds of general formula [CuPSML]; Where, M = Li, Na or K; L = alkali metal salts of 2-nitrophenol; 2,4-ditrophenol, 2,4,6-trinitrophenol or 1-nitroso-2-naphthol may be shown as in [Fig.2]. The compound also show the good results of antimicrobial activity against the bacteria viz. *Escherichia coli*, *Staphylococcus aureus* and fungus viz. *Candida albicans*

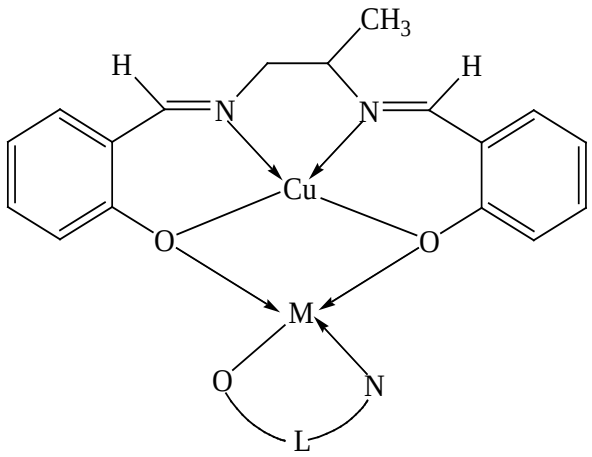

Figure 2: Probable Structure and Bonding of Complex

Acknowledgement

The authors are thankful to the Director, C.D.R.I. Lucknow and Head, Deptt. of Chemistry, BHU for conducting spectral measurement and magnetic measurements.

References

Abu-Dief, A. M., & Mohamed, I. M. (2015). A review on versatile applications of transition metal complexes incorporating Schiff bases. *Beni-suef University Journal of Basic and Applied Sciences*, *4*(2), 119-133.

Ahmed, A., Dalia, M., & Fatmaa, H. (2015). Preparation and Spectral Characterization of Isonazide Ligand with Some Transition Metal Complexes. *Australian Journal of Basic and Applied Sciences*, *9*(31), 42-46.

Condrate, R. A., & Nakamoto, K. (1965). Infrared spectra and normal coordinate analysis of metal glycino complexes. *The Journal of Chemical Physics*, *42*(7), 2590-2598.

El-Sonbati, A. Z., Al-Shihri, A. S., & El-Bindary, A. A. (2004). Stereochemistry of new nitrogen containing heterocyclic aldehyde: Part XI. Novel ligational behaviour of quinoline as chelate ligand toward transition metal ions. *Spectrochimica Acta Part A: Molecular and Biomolecular Spectroscopy*, *60*(8-9), 1763-1768.

El-Sonbati, A. Z., Diab, M. A., & El-Bindary, A. A. (2012). Stoichiometry of polymer complexes. *Stoichiometry and Research—The Importance of Quantity in Biomedicine*.

Geary, W. J. (1971). The use of conductivity measurements in organic solvents for the characterisation of coordination compounds. *Coordination Chemistry Reviews*, *7*(1), 81-122.

Ghosh, S., Malik, S., Jain, B., & Gupta, M. (2012). Synthesis, spectral and pharmacological studies of some transition metal complexes derived from Schiff base of Acetazolamide drug. *Journal of the Indian Chemical Society*, *89*(4), 471.

Golcu, A., Tumer, M., Demirelli, H., & Wheatley, R. A. (2005). Cd (II) and Cu (II) complexes of polydentate Schiff base ligands: synthesis, characterization, properties and biological activity. *Inorganica Chimica Acta*, *358*(6), 1785-1797.

Jaffé, H. H., & Orchin, M. (1962). Theory and applications of ultraviolet spectroscopy. *Wiley*

Kumar, C. (2017). Synthesis, characterization and biological evaluations of heterobinuclear complexes of Cu-II and Ni-II Schiff base of ethylenediamine and o-hydroxyacetophenone with alkali metal salts of o-nitrophenol. *Journal of the Indian Chemical Society*, *94*(8), 857-861.

Mishra, P., Gupta, P. N., & Shakya, A. K. (1991). Synthesis of some Schiff bases of 3-amino-2-methylquinazolin-4 (3H)-ones and their antimicrobial activities. *Journal of the Indian Chemical Society*, *68*(11), 618-619.

Nakamoto, K. (2009). *Infrared and Raman spectra of inorganic and coordination compounds, part B: applications in coordination, organometallic, and bioinorganic chemistry*. John Wiley & Sons.

Panchal, P. K., & Patel, M. N. (2006). Synthesis, spectroscopy, and antibacterial activity of some transition metal complexes with tridentate (ONS) and bidentate (NN) donor Schiff bases. *Pharmaceutical Chemistry Journal*, *40*(10), 544-548.

Patel, N. H., Parekh, H. M., & Patel, M. N. (2005). Synthesis, characterization and biological evaluation of manganese (II), cobalt (II), nickel (II), copper (II), and cadmium (II) complexes with monobasic (NO) and neutral (NN) Schiff bases. *Transition Metal Chemistry*, *30*, 13-17.

Prakash, D., Kumar, C., & Singh, K. R. R. P. (2008). Binuclear complexes of CuII and NiII Schiff base of 2-hydroxy-1-naphthaldehyde and o-phenylenediamine with alkali metal salts of oxygen and nitrogen containing organic acids. *Journal of the Indian Chemical Society*, *85*(4), 371-375.

Singh, A., & Chaudhary, A. (2019). Synthesis, Spectral Characterization and Biological Study of Heterobinuclear Complexes of Cu (II) with Si (IV). *Silicon*, *11*, 1107-1118.

Singh, K., Barwa, M. S., & Tyagi, P. (2006). Synthesis, characterization and biological studies of Co (II), Ni (II), Cu (II) and Zn (II) complexes with bidentate Schiff bases derived by heterocyclic ketone. *European Journal of Medicinal Chemistry*, *41*(1), 147-153.

Thirumavalavan, M., Akilan, P., & Kandaswamy, M. (2006). Synthesis of heterobinuclear Cu (II) Zn (II) complexes derived from lateral macrobicyclic tricompartmental ligands: Spectral, electrochemical and kinetic studies. *Polyhedron*, *25*(13), 2623-2628.

Zhong, W., Zishen, W., Zhenhuan, Y., & Qinghua, H. (1994). Synthesis, characterization and antifungal activities of copper (II), zinc (II), cobalt (II) and nickel (II) complexes with the Schiff base derived from 3-chlorobenzaldehyde and glycine. *Transition Metal Chemistry*, *19*, 235-236.

https://doi.org/10.31674/book.2023pcbs005

Waste-Water Treatment: Based on Solar-Light-Driven Photo-Catalysis using Semiconducting Nano-Materials

Amit Kumar Dutta
Department of Chemistry, Bangabasi Morning College, Kolkata, West Bengal, India

Corresponding Author's Email: akdutta84@gmail.com

Abstract

The development of innovative technologies for effective waste-water treatment is gaining extraordinary importance worldwide. Photocatalysis is one of the most useful, cost-effective and easily manageable methods for decomposition and remediation of organic pollutants in waste-water treatment. In this sense, several semiconducting nano-scaled materials, such as iron sulfide (FeS), CdS, ZnS, CuS, iron oxide (Fe_2O_3) nanoparticles (NPs) etc., have been established as effective catalysts for conducting such types of photochemical reactions. When the nano-materials have the ability to absorb solar light energy, i.e., to utilise the most of the solar spectrum, the performance of photo-degradation reactions has increased much more. In this chapter, the photo-catalytic efficacy of the proposed NPs has been elaborated based on its structural modification, increasing surface area, and controlling size and morphology. The possible mechanism of this photo-catalytic procedure has also been deliberated through the recognition of hydroxyl radical (OH•). On the basis of this developed methodology, the unlimited abundance of solar energy can be used in large scale waste-water treatment.

Keywords: *Photocatalysis; Semiconducting Nano-Materials; Solar-Light-Driven Reaction Kinetics; Nonlinear Least Square Fitting; Waste-Water Treatment; Hydroxyl Radical (OH•)*

Introduction

Because of the gradual increase in water pollution, the demand for remediation and restoration of this contaminated water is increasing day by day. Several organic pollutants, such as pesticide products, pharmaceutical products, textile effluents, and supplementary organic products (Hasija *et al.*, 2019), which have poisonous effects and prolonged persistence in water bodies, have severe adverse impacts on life and the environment of the planet. Considering their high solubility in water and low-biodegradability, complete removal from polluted water is vital and treatment of that waste-water is often difficult by conventional methods.

Several analytical techniques have been developed for the elimination of contaminants, including bio-degradation, adsorption, sedimentation, membrane filtering, and coagulation

(Ge *et al.*, 2018). The photocatalytic degradation process is the more efficient and acceptable method, which involves photochemical reactions in the presence of catalysts under light illumination (Dutta *et al*., 2012). As a catalyst material, semiconducting nano-scaled materials, which have suitable band-gap energy, have been often used to absorb light energy and accelerate the photo-chemical reaction rate (Hoffmann *et al.*, 1995). As a result, it can decompose numerous environmental pollutants completely within a few hours at room temperature (Rafiq *et al.*, 2021). TiO_2-based resources are well known catalysts and have been widely used for photo-decomposition of pollutants over the past decade; however, it is catalytically active only under UV radiation ($\lambda < 400$ nm) as it has widespread band gap energy ($Eg \approx 3.2$ eV) (Nakata & Fujishima, 2012). Of late, several non-titania-based materials such as CuO, ZnO, FeS, ZnS etc. (Sun *et al*., 2008) and even doped hetero-nanostructures Bi_2S_3/BiOCl, Eu-doped Bi_2S_3 (Sarkar *et al*., 2015) have been found to show visible-light-driven catalytic efficiency. Recently, considerable attention has been paid to narrow band-gapped (1.0-2.0 eV but not over 3.0 eV) semiconducting nanomaterials having absorption matches with the solar spectrum exhibit enhanced photocatalytic activity under solar light illumination. So, focus needs to be put on improving environmentally friendly, low-energy, and cost-effective technologies for solar-light-driven photo-catalysis.

Keeping this in mind, in the following chapter, details have been elaborated on about the photo-catalytic activities of the proposed semiconducting nano-materials and their use as effective photo-active devices for decomposition and remediation of organic pollutants in waste-water treatment. At last, the possible mechanism of the photo-catalytic procedure has also been deliberated through the recognition of hydroxyl radical (OH•).

Nano-Scaled Semiconducting Materials

As effective heterogeneous photo-catalysts, the most widely studied nano-scaled semiconducting materials include transition metal sulfides, oxides such as iron sulfide (FeS), CdS, ZnS, CuS and iron oxide (Fe_2O_3) nanoparticles (NPs). Different synthesis methods are available to prepare different shapes, sizes, morphologies, and even different forms such as nano-spheres, nano-tubes etc., which are important factors that affect their photo-catalytic performances.

Iron sulfide (FeS) NPs with different morphologies, i.e., nanospheres and nanorods, have been manufactured from a precursor complex [$Fe(ACDA)_3$] [where the ligand is 2-aminocyclopentene-1-dithiocarboxylic acid (HACDA)] through a solvothermal way at 120 °C (Maji *et al.*, 2012a) using different nucleophilic solvents: Ethylene glycol (EG), Ethylene diamine (EN) or Ammonia (NH_3). To improve photo-catalytic performance, the shape, size, and morphology have been controlled during the crystal growing progression, where crystal nuclei favourably grow along a unique route to produce nano-rods in the presence of EN or are combined into quasi sphere-shaped assemblies to produce nano-spheres in the presence of EG and NH_3. As a result, the band gap energy of different FeS NPs has been automatically

tuned between 2.75 to 3.13 eV which has been measured through UV-Vis absorption spectroscopy (Figure 1).

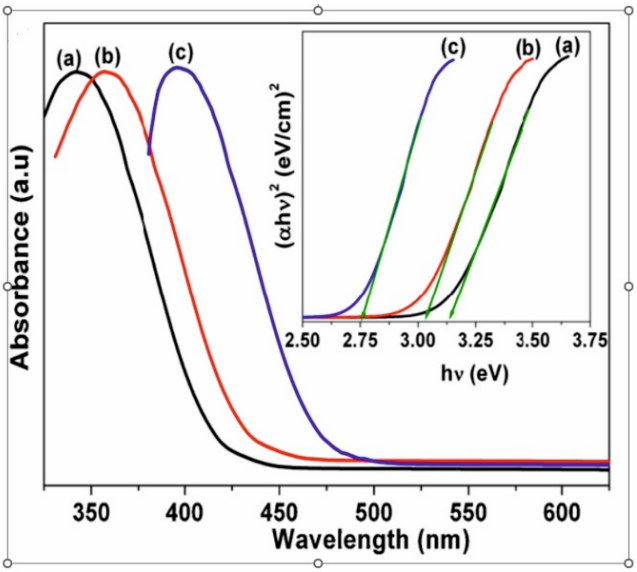

Figure 1: UV–vis Absorbance Spectra (inset: corresponding Tauc's plots) of FeS NPs, Manufactured in Solvent (a) EG, (b) EN and (c) NH_3 (S.K. Maji, 2012a)

The crystalline nature has been examined through powder X-Ray diffraction (XRD) pattern where low crystal defect has been indicated by fairly intense peaks. The diffraction patterns confirmed the formation of hexagonal FeS (JCPDS: 370477) (Figure 2).

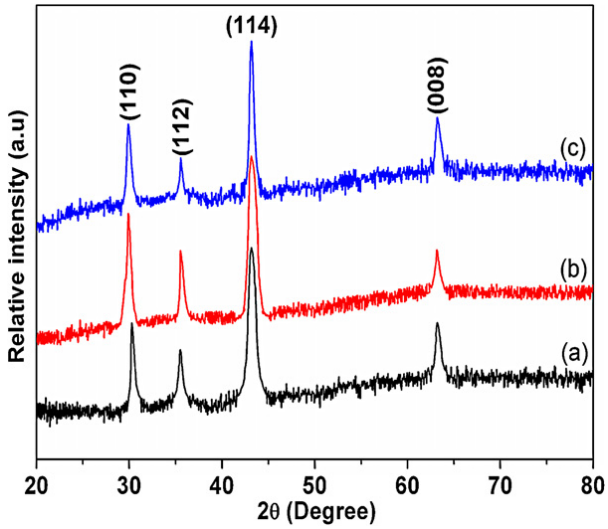

Figure 2: XRD Pattern of FeS Nanoparticles, Manufactured in Presence of (a) EG, (b) EN and (c) NH_3 (Maji et al., 2012a)

[$Cd(ACDA)_2$] has been used as a precursor material for the manufacturing of CdS NPs with dissimilar morphologies through the same solvothermal route at 120 °C using different nucleophilic solvents EN or hexadecyl-amine (HDA) or dimethyl-sulfoxide (DMSO) (Maji *et al.*, 2012b). The effect of solvents on the morphologies of CdS NPs has been investigated using transmission electron microscopy (TEM), which confirms the presence of rod-like structures with average length and diameter of 70 and 5 nm, respectively (Figure 3a) and spherical structures with average diameters of 4 and 6 nm, (Figure 3b, 3c), respectively. Also, the second important factor to increase the catalytic efficiency, i.e., highly crystalline nature, is indicated by the magnified image of lattice fringes in the live-Fast-Fourier Transform (FFT) (inset Figure 3). Moreover, all CdS NPs possess a high specific surface area (32.1-81.9 m^2g^{-1}) and a mesoporous nature, which are also responsible for high catalyst loading capacity and enhancing the rate of photo-degradation reactions.

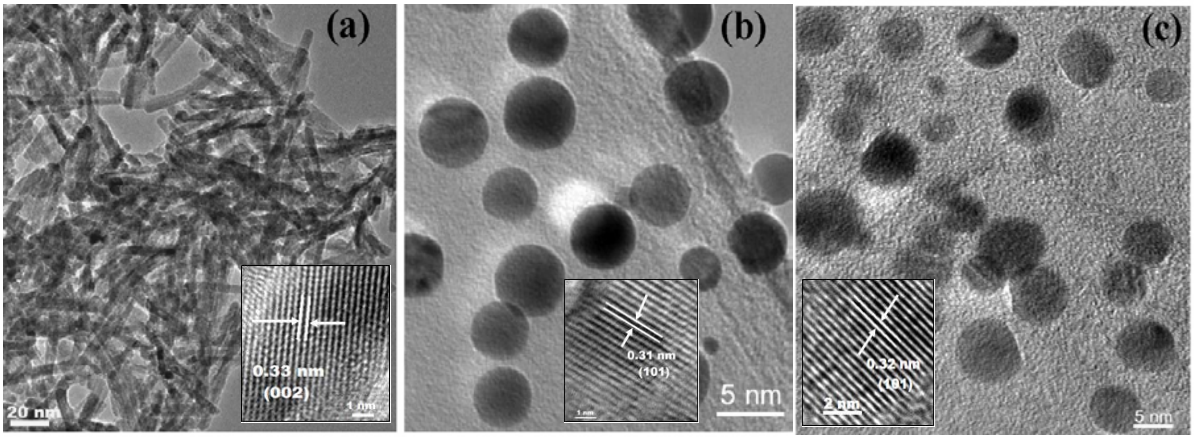

Figure 3: TEM and Inset Magnified Image of Lattice Fringes of CdS NPs, Manufactured in Presence of (a) EN, (b) HDA and (c) DMSO (Maji et al., 2012b)

To prepare another semiconducting nano-materials, ZnS NPs, an important II–VI semiconductor, Maji *et al.* (2011) has chosen the same solvothermal decomposition of precursor [$Zn(ACDA)_2$] using different nucleophilic solvents. Nanorods (diameter ~6 nm and length ~50 nm) and Nano-sphere (~5 nm) have been deposited in presence of EN (20 ml) and [HDA (15 ml) + TOP (5 ml)], respectively.

γ–Fe_2O_3 NPs (Dutta, Maji & Adhikary, 2014) has been prepared from a Fe(III) starting material, where the complex in solid state just burned inside a quartz tube of a horizontal tubular furnace at 670°C for 1 h.

Recently, Eu-doped Bi_2S_3 hetero-nanostructures (1.8 %, 2.3 % and 4.3 % Eu-doped) (Sarkar *et al*., 2015) have been synthesized through the same solvothermal process but a mixture of precursor materials [$Bi(ACDA)_3$] and [$Eu(ACDA)_3{\cdot}H_2O$] in different ratios have been decomposed at 140 °C for 5 h.

Photo-Catalytic Action Measurements

To measure the photo-catalytic performances of the proposed nano-scaled materials, water-soluble and non-biodegradable organic pollutants, such as rose bengal (RB), methylene blue (MB) dyes, and phenol-based pollutants, have been chosen as examples because they are commonly used in industries. The catalytic performances have been investigated spectro-photometrically through the degradation of RB in the wavelength range 400–600 nm under visible light illumination. The UV–vis absorption curves decrease rapidly with the irradiation time (Figure 4A), catalysed by γ–Fe_2O_3 NPs and the corresponding solution becomes colorless (Figure 4A inset) within a few hours. A comparative performance has been illustrated in Figure 4B with γ–Fe_2O_3 NPs and commercial TiO_2 or commercial tungsten (VI) oxide (WO_3) as an example.

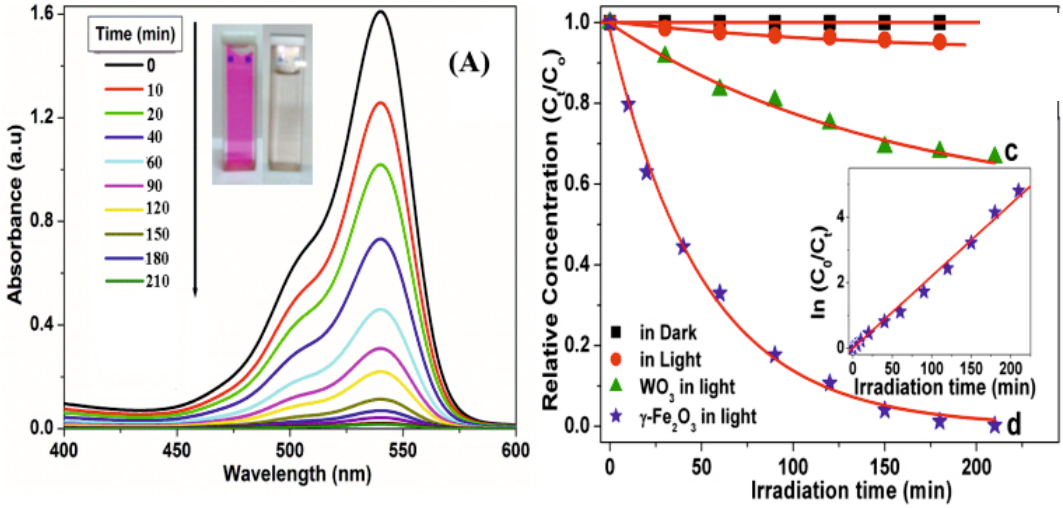

Figure 4:(A) Spectro-photometric Variations of RB with Time in Presence of γ–Fe_2O_3 Nano-catalyst under Light Illumination. Inset: Photography of Corresponding Colour Changes Before and After Decomposition Process, (B) Corresponding Reaction Profile with Pseudo–First Order Kinetics Fitting (Dutta, Maji & Adhikary, 2014)

To investigate the kinetics of the above photo-chemical reactions, the decomposition processes have been modelled as a pseudo–first order reaction kinetics expressed by the equation (1)

$$\ln(C_0/C_t) = k\,t \qquad (1)$$

C_0 = initial concentration, C_t = concentration at a reaction time '*t*', and k = reaction rate constant. The data have been fitted to the above model using a nonlinear least square fitting method, and the corresponding rate constant values have been summarized in Table 1. By comparison with commercial photo-catalyst, TiO_2 (Degussa P-25) and WO_3, it has been recognised that pollutant decomposition happens in a quicker way in the presence of the proposed NPs. It has also been established that, photocatalytic activities of the different CdS NPs increase with the order of CdS NPs manufactured in solvents from NH_3 < DMSO < EN < HT based on the increase in specific surface area and crystallinity of the NPs.

In another study, the photo–degradation of phenol-based compounds was carried out using another photo-catalyst, Eu-doped Bi_2S_3 hetero-nanostructure (Figure 5).

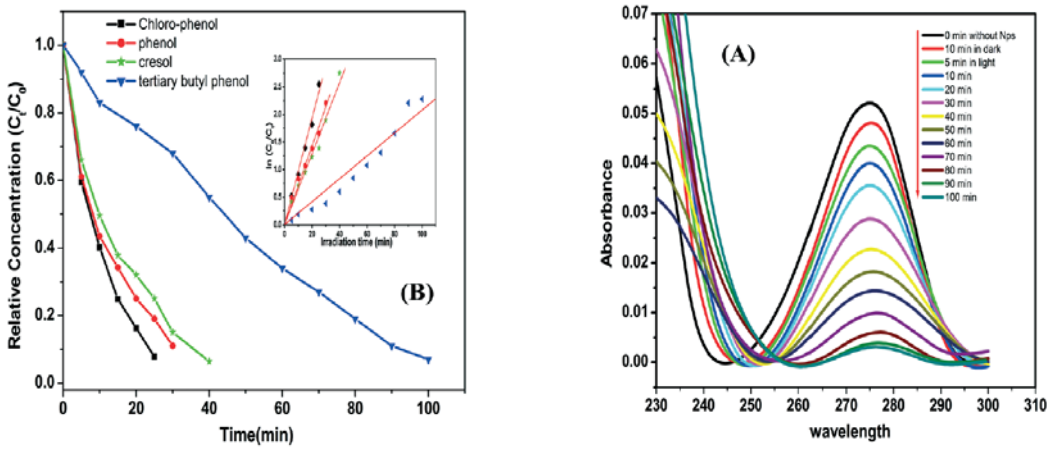

Figure 5: (A) UV–Vis Spectral Changes of 4-tert-butylphenol with Time in Absence and Presence of 4.26% Eu-doped Bi_2S_3 NPs, (B) Corresponding Reaction Profile with Kinetics Fitting (Sarkar et al., 2015)

Table 1: Comparison of the Kinetic Parameters for the Photo-Catalytic Activity of the Proposed Nano-Scaled Materials

Nano–catalyst	**Rate constant (min^{-1}) for RB degradation**	**Rate constant (min^{-1}) for MB degradation**	**Reference**
γ–Fe_2O_3	2.15×10^{-2}	8.80×10^{-2}	Dutta, Maji & Adhikary, 2014
WO_3	3.3×10^{-3}	4.5×10^{-3}	Dutta, Maji & Adhikary, 2014
TiO_2 (Degussa P-25)	1.7×10^{-3}	1.16×10^{-3}	Maji *et al.*, 2012b
CdS (from HDA)	2.2×10^{-2}	–	Maji *et al.*, 2012b
ZnS (from HDA)	2.17×10^{-2}	–	Maji *et al.*, 2011
FeS (from EG)	–	2.71×10^{-2}	Maji *et al.*, 2012a
FeS	6.02×10^{-2}	5.73×10^{-2}	Dutta *et al.*, 2012
FeSe	3.39×10^{-2}	2.32×10^{-2}	Dutta *et al.*, 2012

Photo–Catalytic Mechanism

To understand the mechanism of the photo–catalytic activity of the proposed semiconducting nano-materials, it has been established that during light irradiation, the nano-materials use the light energy to excite electrons from their valance band (VB) to the conduction band (CB), thus leaving behind holes (Figure 6). This hole can capture electrons from water bodies to generate hydroxyl radical (OH•) (Al–Ekabi, 1989). These radicals actually oxidize or decompose the pollutants.

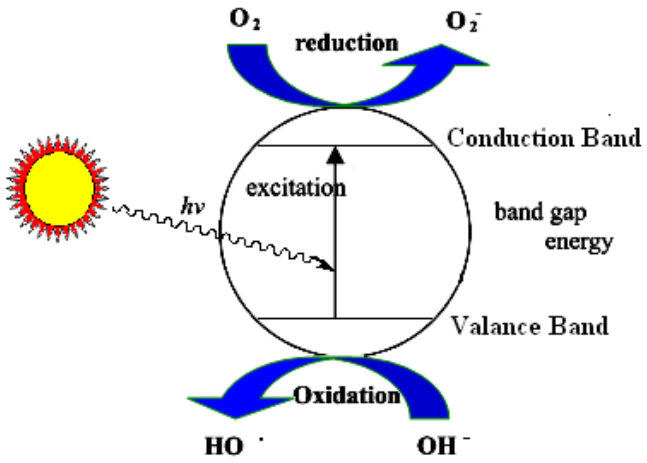

Figure 6: Illustration of Photo-Catalytic Mechanism (Dutta, Maji & Adhikary, 2014)

If that band gap energy becomes tremendously short, the lifetime of the produced electrons and holes on its surface also becomes short, there is a possibility of recombination of electron-hole pairs, and hence the photocatalytic activity is decreased. In that case, doped hetero-nanostructures have been used, where the dopant operates as an electron scavenger on the surface of the nano-structures, defeating the recombination of electron-hole pairs and enhancing their lifetime.

The overall reactions are presented in equations (2)–(5).

$$\gamma\text{-}Fe_2O_3 + h\nu \longrightarrow \gamma\text{-}Fe_2O_3\,(e^-_{CB} + h^+_{VB}) \quad (2)$$

$$H_2O \longrightarrow H^+ + OH^- \quad (3)$$

$$OH^- + h^+_{VB} \longrightarrow OH^{\cdot} \quad (4)$$

$$RB/MB + OH^{\cdot} \longrightarrow \text{Products} \quad (5)$$

The aromatic dyes have been further degraded by O_2^- active species, which was generated on the surface of the proposed NPs according to following equations.

$$O_2 + e \longrightarrow O_2^- \quad (6)$$

$$O_2^- + 2H^+ + 2e \longrightarrow H_2O_2 \quad (7)$$

$$H_2O_2 + e \longrightarrow OH^- + \cdot OH \quad (8)$$

$$RB/MB + \cdot OH \longrightarrow \text{Products} \quad (9)$$

The final product after the photo–catalytic decomposition process has been investigated through LC–MS spectrum, where a significant peak at m/z = 113.1 corresponds to the chloro-benzene group, indicating the total breakage of the RB molecule into very small fragments. In the case of phenol-based pollutants, the decomposition process occurs through the formation of a hydroxy-phenyl radical (HPR) and various intermediates like dihydroxy-biphenyl (DHB) or catechol (CC) or hydroquinone (HQ) followed by photo-catalytic oxidation and ring cleavage to yield carboxylic acids or aldehydes, which are further degraded to CO_2 and H_2O (Figure 7) (Sarkar *et al*., 2015).

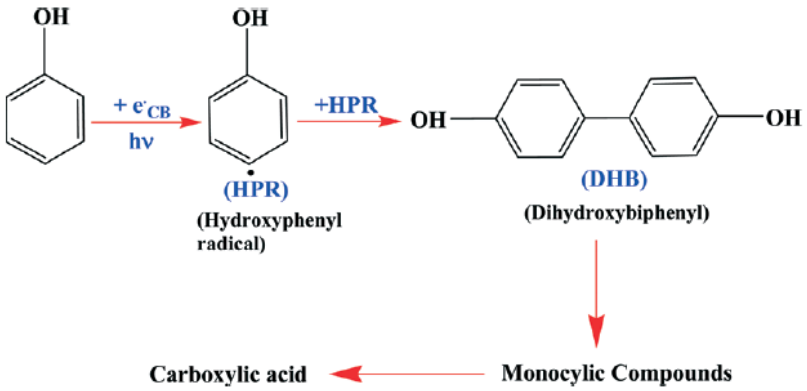

Figure 7: Representation of Degradation Mechanism of Phenol-Based Pollutants (Sarkar et al., 2015)

The generation of OH· has been recognised by terephthalic acid (TA) photoluminescence analytical systems (Barreto *et al*., 1994), where TA combined with hydroxyl radicals and formed highly fluorescent 2–hydroxy terephthalic acid (HTA) (Figure 8 inset) as stated by the following equation.

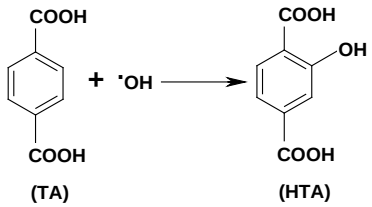

(7)

The corresponding photo-luminescence spectral study of NPs/TA system under light irradiation, indicates the increase in luminescence intensity of the solution with irradiation time (Figure 8), which is responsible for formation of more and more HTA and OH•.

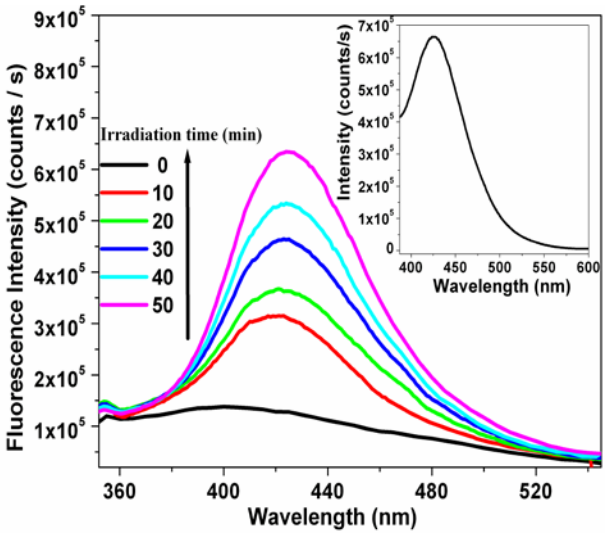

Figure 8: Fluorescence Spectro-Metric Variations of Terephthalic Acid (TA) in Presence of γ–Fe_2O_3 Nano-Catalyst under Light Irradiation. Inset: Fluorescence Spectrum of the Commercial HTA (Sigma–Aldrich) (Dutta, Maji & Adhikary, 2014)

Conclusion

In summary, the proposed nano-scaled materials are widely explored as an efficient photo-catalyst for the degradation of various organic pollutants under solar and visible light illumination. They exhibit different catalytic efficiencies based on different size, shape and morphology. The catalytic performances have also been improved by tuning band-gap energy and surface area during the synthesis process. Finally, an environmentally friendly, cost-effective technology has been developed for solar-light-driven photo-catalysis so that most of the solar spectrum and light energies can be utilized for large-scale waste-water treatment processes.

Acknowledgment

The author is grateful to Prof. Bibhutosh Adhikary, Department of Chemistry, Indian Institute of Engineering Science and Technology (IIEST), Shibpur, for helpful discussions. The author is indebted to UGC, India, for financial support through the MRP [PSW–066/15–16 (ERO)]. The author also acknowledges the RUSA Scheme of the Ministry of Education, Government of India, for providing instrumental facilities to the Department of Chemistry, Bangabasi Morning College, Kolkata.

References

Al-Ekabi, H., Serpone, N., Pelizzetti, E., Minero, C., Fox, M. A., & Draper, R. B. (1989). Kinetic studies in heterogeneous photocatalysis. 2. Titania-mediated degradation of 4-chlorophenol alone and in a three-component mixture of 4-chlorophenol, 2, 4-dichlorophenol, and 2, 4, 5-trichlorophenol in air-equilibrated aqueous media. *Langmuir*, *5* (1), 250-255. https://doi.org/10.1021/la00085a048

Barreto, J. C., Smith, G. S., Strobel, N. H., McQuillin, P. A., & Miller, T. A. (1994). Terephthalic acid: a dosimeter for the detection of hydroxyl radicals in vitro. *Life sciences*, *56*(4), 89–96. https://doi.org/10.1016/0024-3205(94)00925-2

Dutta, A. K., Maji, S. K., & Adhikary, B. (2014). γ-Fe2O3 nanoparticles: an easily recoverable effective photo-catalyst for the degradation of rose bengal and methylene blue dyes in the waste-water treatment plant. *Materials Research Bulletin*, *49*, 28-34. https:// doi.org/ 10.1016/j.materresbull.2013.08.024

Dutta, A. K., Maji, S. K., Srivastava, D. N., Mondal, A., Biswas, P., Paul, P., & Adhikary, B. (2012). Synthesis of FeS and FeSe nanoparticles from a single source precursor: a study of their photocatalytic activity, peroxidase-like behavior, and electrochemical sensing of H2O2. *ACS applied materials & interfaces*, *4*(4), 1919-1927. https://doi.org/10.1021/ am300408r

Ge, L., Peng, Z., Wang, W., Tan, F., Wang, X., Su, B., ... & Wong, P. K. (2018). gC 3 N 4/MgO nanosheets: light-independent, metal-poisoning-free catalysts for the activation of hydrogen peroxide to degrade organics. *Journal of Materials Chemistry A*, *6*(34), 16421-16429. https://doi.org/10.1039/C8TA05488F

Hasija, V., Raizada, P., Sudhaik, A., Sharma, K., Kumar, A., Singh, P., ... & Thakur, V. K. (2019). Recent advances in noble metal free doped graphitic carbon nitride based nanohybrids for photocatalysis of organic contaminants in water: a review. *Applied Materials Today*, *15*, 494-524. https://doi.org/10.1016/j.apmt.2019.04.003

Hoffmann, M. R., Martin, S. T., Choi, W., & Bahnemann, D. W. (1995). Environmental applications of semiconductor photocatalysis. *Chemical Reviews*, *95*(1), 69-96. https://doi.org/10.1021/cr00033a004

Maji, S. K., Dutta, A. K., Biswas, P., Srivastava, D. N., Paul, P., Mondal, A., & Adhikary, B. (2012a). Synthesis and characterization of FeS nanoparticles obtained from a dithiocarboxylate precursor complex and their photocatalytic, electrocatalytic and biomimic peroxidase behavior. *Applied Catalysis A: General*, *419*, 170-177. https://doi. org/10.1016/j.apcata.2012.01.025

Maji, S. K., Dutta, A. K., Srivastava, D. N., Paul, P., Mondal, A., & Adhikary, B. (2011). Effective photocatalytic degradation of organic pollutant by ZnS nanocrystals synthesized via thermal decomposition of single-source precursor. *Polyhedron*, *30*(15), 2493-2498. https://doi.org/10.1016/j.poly.2011.06.029

Maji, S. K., Dutta, A. K., Srivastava, D. N., Paul, P., Mondal, A., & Adhikary, B. (2012b). Peroxidase-like behavior, amperometric biosensing of hydrogen peroxide and photocatalytic activity by cadmium sulfide nanoparticles. *Journal of Molecular Catalysis A: Chemical*, *358*, 1-9. https://doi.org/10.1016/j.molcata.2012.03.007

Nakata, K., & Fujishima, A. (2012). TiO2 photocatalysis: Design and applications. *Journal of Photochemistry and Photobiology C: Photochemistry Reviews*, *13*(3), 169-189. https:// doi. org/10.1016/j.jphotochemrev.2012.06.001

Rafiq, A., Ikram, M., Ali, S., Niaz, F., Khan, M., Khan, Q., & Maqbool, M. (2021). Photocatalytic degradation of dyes using semiconductor photocatalysts to clean industrial water pollution. *Journal of Industrial and Engineering Chemistry*, *97*, 111-128. https://doi.org/10.1016/j.jiec.2021.02.017

Sarkar, A., Ghosh, A. B., Saha, N., Dutta, A. K., Srivastava, D. N., Paul, P., & Adhikary, B. (2015). Enhanced photocatalytic activity of Eu-doped Bi 2 S 3 nanoflowers for degradation of organic pollutants under visible light illumination. *Catalysis Science & Technology*, *5*(8), 4055-4063. https://doi.org/10.1039/C5CY00473J

Sun, M., Li, D., Li, W., Chen, Y., Chen, Z., He, Y., & Fu, X. (2008). New photocatalyst, Sb2S3, for degradation of methyl orange under visible-light irradiation. *The Journal of Physical Chemistry C*, *112*(46), 18076-18081. https://doi.org/10.1021/jp806496d

https://doi.org/10.31674/book.2023pcbs006

In Vitro Anti-Amylase Activity of Diadzein and Evaluation of its Synergistic Role with Acarbose in Combination

Suvroma Gupta

Department of Biotechnology, Haldia Institute of Technology, Haldia, West Bengal, India

Corresponding Author's Email: suvroma.gupta@gmail.com

ABSTRACT

Diabetes mellitus is a worldwide health issue and one of the leading causes of morbidity. The mortality creates a pandemic situation in developing nations. The changes in quality of life and negligence in health care statistics are responsible for increasing the chances of developing diabetes mellitus. Accordingly, there is an upward trend in its occurrence, particularly in industrialized urban zones. Type 2 diabetes mellitus (DM) is characterised by debilitated insulin hormone secretion and increased insulin obstruction. The utilization of therapeutic plants and their phytochemicals for curing diabetes isn't only a quest for more secure options in contrast to pharmaceuticals, which temporarily bring down the blood glucose, forestall coronary illness and hypertension, and enhance the antioxidant system, insulin activity, and discharge. Flavonoids are very useful for their multi-directional activities including therapeutic approaches for diabetes. Numerous studies have been carried out to explore their potential role in the treatment of diabetes. Flavonoids from the biggest family of polyphenolic herbal compounds have many functions to manage diabetes such as proliferating the *β* cell of the pancreas, regulating the insulin signaling pathway, progression of glucose metabolism, etc. With *in vitro* experiments, it has further been established that Daidzein and Eriodyctiol (Abbreviation) inhibit PPA with IC_{50} values of 26 and 22 uM respectively. Their interaction with PPA has also been established by docking studies. Diadzein exhibits noncompetitive kinetics during interaction with PPA with a K_M value of 0.49 mM in contrast to the competitive mode of inhibition of PPA by Eriodyctiol. Moreover, Daidzein augments the inhibitory potential of commonly used amylase inhibitor acarbose in a synergistic way. It inhibits lipid peroxidation, which remains unaffected by the presence of acarbose. So Eriodyctiol and Daidzein (Abbreviation) can be considered suitable alternatives to acarbose in the treatment of Diabetes mellitus.

Keywords: *Flavonoids; Hyperglycemia; Acarbose; Amylase; Combination Therapy; Hyperglycemia*

Introduction

Diabetes: A Global Concern

Diabetes is sure to be among the most crucial medical issues in the 21st century (Chakrabarti & Rajagopalan, 2002). Diabetes mellitus is a heterogeneous disease and has become a curse for the entire world, of which already 100 million people have become victims (Balaji *et al.,* 2019; American Diabetes Organization, 2003). This disease adversely affects other crucial

cellular functions namely the cardiovascular system, increasing the risk of heart attack, neuropathy, and retinopathy (Inzucchi, 2002; Boivin *et al.,* 1988; Eyre *et al.,* 2004; Schreiber *et al.,* 2015). Type 2 Diabetes comprises 90% of the diabetic population and is expanding rapidly. At the point when the way of life is gradually becoming too complex, due to poor control of blood glucose, the administration of accurate medicine and proper treatment choices are crucial for type 2 diabetes (Breuer, 2003; DiNicolantonio *et al.,* 2015). To prevent postprandial hyperglycemia which is an outcome of type II diabetes originates from insulin resistance and inadequate insulin secretion from the beta cells of the pancreas. Although several lines of therapies are already in progress, one effective therapy is to reduce the activity of starch degrading enzymes like α amylase to keep control over the amount of free glucose in the system, thereby reducing the glycemic index. Flavonoids have attracted much attention in the past few years for their amylase inhibition potential. Another significant treatment alternative is the use of alpha-glucosidase inhibitor like acarbose, an authorized drug entity for the treatment of prediabetes in numerous nations (Eyre *et al.,* 2004). It has been utilized worldwide for over 20 years for the treatment of type 2 diabetes (Schreiber *et al.,* 2015). Several studies have surveyed the role of acarbose in combating these conditions.

Mode of Function of Alpha Glucosidase Inhibitor

Alpha-glucosidase inhibitors act as competitive or noncompetitive inhibitors of enzymes needed to digest carbohydrates: specifically alpha-glucosidase enzymes in the brush border of the small intestines (Phan *et al.,* 2013; Hung *et al.,* 2012). This group of enzymes hydrolyzes oligosaccharides into simpler form of sugars in the small intestine.

Currently prescribed alpha-glucosidase inhibitor drugs like acarbose, miglitol (synthetic derivative of 1-deoxynojirimycin), metmorfin and voglibose (from microbial origin) are often associated with some undesirable adverse effects such as bloating, diarrhea and abdominal pain if the drugs are prescribed for long term administration to subdue DM (Anisimov *et al.,* 2003; Bolen *et al.,* 2007) (Table 1). These drugs are inhibitory against amylase and drive starch digestion into the colon, followed by fermentation using bacterial enzymes (Lankisch *et al.,* 1998). The production of gases and bloating resulting from the bacterial fermentation of starch causes the unpleasant gastrointestinal side effects typical for this class of anti-diabetic drugs. Metmorfin, another antidiabetic drug, interferes with renal dysfunction and cannot be administered to patients with renal impairment (Inzucchi *et al.,* 2014).

Table 1: Structure of Different Flavonoids and Antidiabetic Drugs

Name of the Drug	Structure of Flavonoids
Daidzein	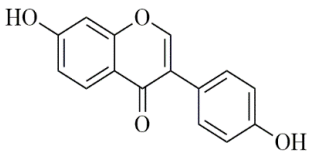
Eriodyctiol	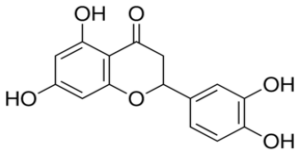
Metformin	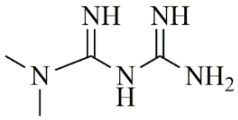
Acarbose	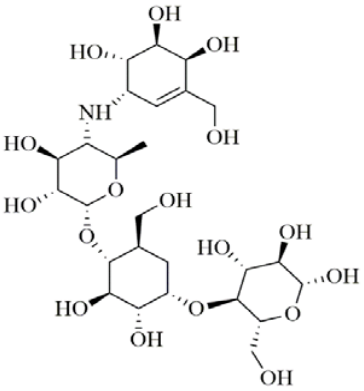
Sulfamethoxazole (SMX)	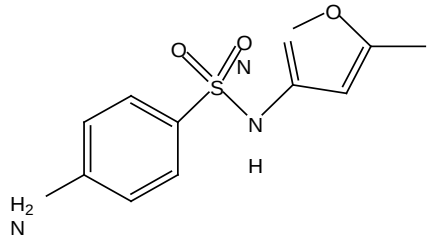
Sulfamerazine (SMZ)	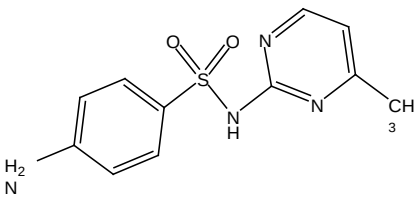

Drug-Target Relationships: From the Magic Bullet to the Multi-Target Paradigm

The idea of “magic bullets” proposed by Paul Erlich is applicable to the drugs that have been used as single disease target is reoriented to drug repurposing concept (Strebhardt & Ullrich, 2008). The earlier ‘one-drug one-target one disease” technique has driven drug discovery a lot in the late twentieth century and has been successfully established as a targeted therapeutic approach. Repurposing of drug entities bearing broad polypharmacologies, may contribute due to their clinical viability and provides knowledge into the development of new repositioning chances (Talevi & Bellera, 2020; Dudley *et al.,* 2011; Turner *et al.,* 2016). In this regard, the mention of sulfamethoxazole (SMX) (Abbreviation) and sulfamerazine (SMZ) (Abbreviation) with their amylase inhibitory potency is noteworthy in the context of amylase inhibition (Maity *et al.,* 2016; Malla *et al.,* 2021) (Table 1). SMX and SMZ repress porcine pancreatic amylase (PPA) (Abbreviation) in a non-competitive mode with a normal IC_{50} range of 0.94 mM and 0.96 mM individually. Interaction of SMX and SMZ with PPA showed progressive extinguishing of tryptophan fluorescence with shift in lambda max emission (λmax). The reaction of SMX and SMZ with PPA is accompanied by the entropy-driven factor (24.8 cal mol^{-1} K^{-1} and 22.8 cal mol^{-1} K^{-1} respectively) with negative commitment from enthalpy change factor. SMX and SMZ meddle with the action of acarbose in a synergistic mode to decrease the usually prescribed dosage of acarbose as obvious from the *in vitro* PPA hindrance study. In synopsis, loss of PPA action in the presence of SMX and SMZ is characteristic of auxiliary conformational changes of PPA. This is additionally sustained from the schematic model as well as from the docking study performed with the sulfur drug and PPA (Maity *et al.,* 2016; Malla *et al.,* 2021). Several classes of medicines for type 2 diabetes are available in the market including acarbose, metmorfin, voglibose etc. Each class of medicine targets to neutralize the blood glucose level. Additionally medicinal plants are also included as a useful resource of ingredients namely isoflavonoids that can be a boon for the arena of drug development in the cure of wide variety of diseases (Phan *et al.,* 2013; Hung *et al.,* 2012; Formica & Regelson, 1995). Diadzein, a plant estrogen, derived from soya products is effective against diseases like cardiovascular, breast cancer and diabetes. However whether diadzein targets amylase and can serve as an antidiabetic drug with amylase inhibitory potential is not known (Table 1). Earlier studies depicted that diadzein is neither associated with improved insulin sensitivity nor regulatory role on the control of glycemic (Gobert *et al.,* 2010; Ye *et al.,* 2015). At this point, it is crucial to check the role of diadzein as an amylase inhibitor, the type of inhibition by this molecule is required in order to use this molecule for therapeutic purpose. Flavonoids like diadzein and eriodyctiol either work exclusively or in combination with other conventional drug molecule, to produce satisfactory pharmacological effect. This might nullify the discomfort associated with the administration of antidiabtic drugs like acarbose. This may offer a new approach to the diabetic patient care.

Materials and method

Molecular Docking: The procedure of assessing binding energy and the chemistry of protein-ligand binding is carried out by docking ligands to proteins and analyzing the three-

dimensional structure of the molecule using different software. The various steps that need to be conducted are mentioned as follows:

Ligand Screening

The initial screening of the Ligands calls for the use of the SwissADME program available on the web (https: //www.swiss adme.ch/) that helps for the assessment of selected compounds (Daina *et al.,* 2017).

Protein Preparation and Active Site Determination

The protein of interest for the study is amylase (PDB ID- 2QMK). The protein structures are retrieved from the website rcsb.org, commonly known as the Protein Data Bank (Berman *et al.,* 2000) in .pdb format. To carry out protein-ligand docking, the protein needs to be prepared by conducting several edits of the structure. The modifications include the elimination of water molecules (since water molecules can interrupt the binding site of the protein) and attached ligands from the protein using Auto Dock Tools (Version 1.5.6) (Trott & Olson, 2009; Formica & Regelson, 1995) software. Further modifications include the addition of partial charges and polar hydrogen atoms. 3D conformations of the ligand molecules were downloaded from the web-based site called PubChem. The .sdf files of the ligands were converted using PyMOL (4.6.0) (Schrödinger, 2015; Balaji *et al.,* 2019). Ligand preparation was carried out with the help of AutoDock Tools (1.5.6) wherein Gasteiger charges were attached to the ligand and the hydrogens of non-polar nature were unified. The ligand molecule was then saved in the. pdbqt format.

Molecular Docking Using Auto Dock Vina (4.2.6)

The initial step that is to be followed to dock protein and ligand structures is grid preparation. It was done for the protein using AutoDock Tools (1.5.6) (Trott & Olson, 2009). The grid box is an indicator of the region where the docking will take place. The grid dimensions were obtained for the amylase molecule. It acts as a prerequisite for conducting docking in the software. Finally, in-silico docking was done using AutoDock Vina (4.2.6) (Trott & Olson, 2009). The docking results were calculated by Auto dock vina using its Scoring function and results were displayed in the form of Scores and RMSD values.

Residue Analysis

PyMOL (4.6.0) and Discovery Studio 2021 were used for visualization of interactions of the docked structure at the ligand sites and Discovery Studio was used to study the interactions between the enzyme and the ligands (Biovia, 2015).

Amylase Assay

All the reagents including Daidzein, Eriodictyol and Porcine pancreatic α-amylase were purchased from Sigma (St. Louis, MO, USA). Acarbose was procured from Bayer (Leverkusen, Germany). All are of analytical grade.

Porcine pancreatic α-amylase was taken in 50 mM phosphate buffer saline, pH 7.0. The flavonoids in different concentrations were dissolved in DMSO. The assay was conducted following standard protocol using the following formula (Maity *et al.,* 2016).

% Inhibition = [ΔAbs_{540} control - ΔAbs_{540} sample] x 100

The extent of PPA inhibition had been calculated as IC_{50} values (Inhibitory concentration of the flavonoid required for 50% inhibition of the test samples).

Determination of the PPA Inhibitory Mode of Action of Flavonoids

The kinetics of inhibition of flavonoids against PPA have been determined with diadzein and eriodictyol for a range of substrate concentrations in the absence or presence of different concentrations of ligands. The mode of inhibition had been determined from the nature of the curve using the Lineweaver-Burk plot. Respective Km (dissociation constant) and V_{max} (maximum reaction velocity) values for each of the flavonoid had been estimated from the slope and intercept of the curve by plotting the inverse of PPA reaction velocity (V) versus 1/ [substrate (starch) concentration] (Johnson, 2013).

Effect of Daidzein *in Vitro* PPA Inhibition in Combination with Acarbose

To judge the effect of Diadzein to inhibit PPA action, daidzein was applied alone at the respective half inhibitory concentrations (IC_{50}) in presence of acarbose (3 µM and 6 µM). % of PPA inhibition had been estimated by the usual DNS assay as described earlier.

In Vitro Anti-Lipid Peroxidation Assay in Presence of Flavonoids

Lipid peroxide formation has been measured by standard protocol (Malla *et al.,* 2021). The reaction is monitored after the addition of FeSO4 followed by an incubation of 20 minutes at 37°C temperature in the presence of diadzein. The intensity of the pink colour developed was measured at 535 nm. The percentage of inhibition by flavonoids had been calculated as stated above.

Results

Molecular Docking Study of Daidzein, Eriodyctiol and Metformin with Amylase

Screening of Ligands

The SwissADME online tool was used to assess the properties of different ligands namely Daidzein and Eriodyctiol in comparison to Metformin. The results have been summarized in Table 3. The analysis shows high bioavailability scores in the case of all the ligands used. Bioavailability can be defined as the drug or molecule that is available in the blood circulation and is responsible for carrying out the intended functions. Daidzein and Eriodyctiol show no violation of the Lipinski Rule which asserts their potential use as viable drugs Also, Metformin shows viable bioavailability scores coupled with zero violations of the Lipinski rules.

Table 2: Bioavailability Score and Radar Charts of Selected Ligands

Ligand	Bioavailability Score	Lipinski Rule	Radar
Eriodyctiol	0.55	Yes; 0 violation	

Daidzein	0.55	Yes; 0 violation	
Metformin	0.55	Yes; 0 violation	

Table 3: Average Docking Score of Ligands with the Confidence Interval (The Docking Scores Were Obtained Upon Running the Program)

Compound name	Average Binding Energy (Kcal/mol)	Std Deviation	Average Sample Size
Diadzein	-8.08	0.495	5
Eriodyctiol	-8.62	0.370	5
Metformin	-5.14	0.149	5

Interactions of the Ligands and Amylase Using Molecular Docking:

Daidzein shows mostly Pi-Pi stacked interaction with aromatic amino acid residues along with a single hydrogen bond with Aspartic acid. Eriodyctiol interaction with amylase is dominated by hydrogen bonds with polar amino acid residues. Metformin accounts for five hydrogen bonds, Vander Waals interaction, and unfavourable donor-donor interaction.

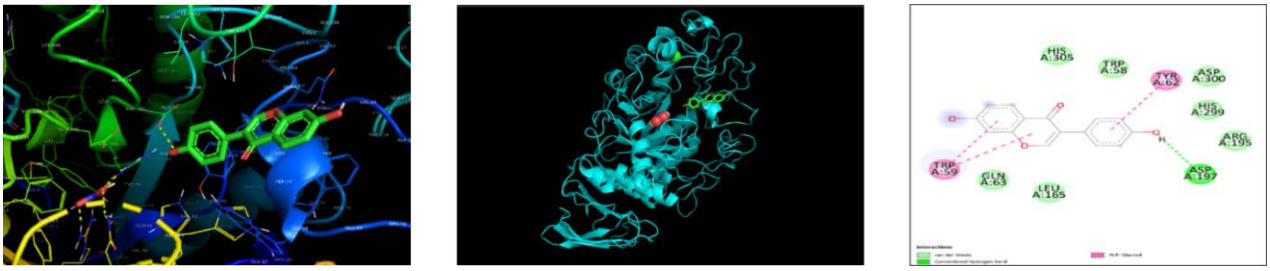

Figure 1A: Interaction between Daidzein and Porcine Pancreatic Amylase Amino Acid Residues B. Interaction between Daidzein and Amylase; C. 2-D Interaction between Daidzein and Amylase

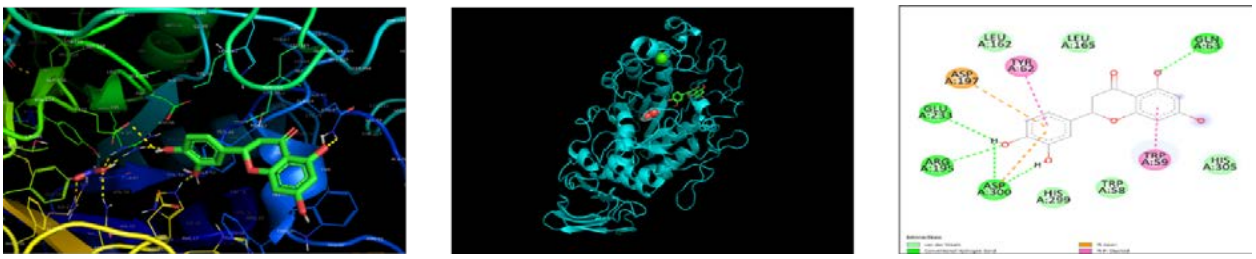

Figure 1B: Interaction between Eriodyctiol and Amylase Amino Acid Residues B. Interaction between Eriodictyol and Amylase; C. 2-D Interaction between Eriodyctiol and Amylase

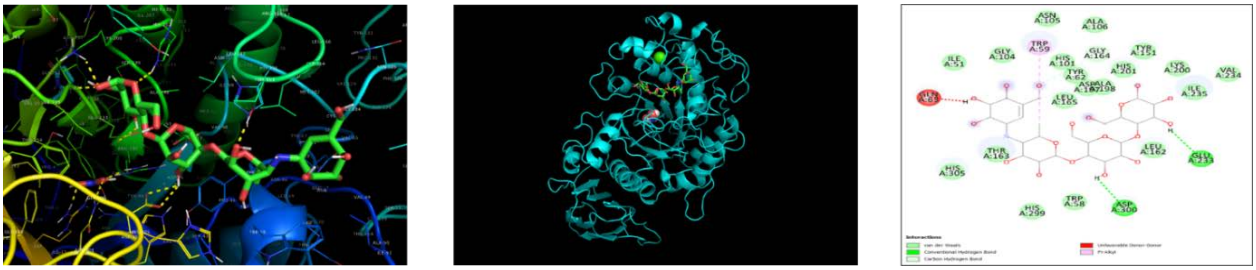

Figure 1C: Interaction between Metformin and Amylase Amino Acid Residues B. Interaction between Metformin and Amylase; C. 2-D Interaction between Metformin and Amylas

Inhibition of PPA Activity by Flavonoids:

Starch digestion by alpha-amylase is mediated through the formation of β-glycosyl enzyme intermediate involving acidic carboxylic acids namely, Asp197, Glu233, and Asp300 present in the catalytic cleft followed by its hydrolysis. From a recent in silico study, involvement of residues of the enzyme including Phe178, Phe303, His280, His351, Arg315, Arg442 and Tyr158 are evident during interaction with the inhibitors (Ernawati *et al.,* 2018). Polyphenolic compounds like flavonoids are implicated as one of the important groups of amylase inhibitors (Lo Piparo *et al.,* 2008; Islam *et al.,* 2020). Interaction between flavonoids and α amylase is facilitated by the presence of several hydroxyl groups on the B ring of the flavonoid skeleton. Hydrogen bonding between the hydroxyl groups in position R6 or R7 of the ring A and position R4/ or R5/ of the ring B of the flavonoids and the catalytic triad (Asp197, Glu233, and Asp300 present in active cleft) is further stabilized through conjugated π-system of the flavonoids (Lo Piparo *et al.,* 2008).

Daidzein is an isoflavone with a B ring attached at 3 positions of the pyrene C ring. The richest sources of this flavonoid are soybeans and soy products. Eriodictyol is a flavanone, bitter in taste, and extracted from a plant, Yerba Santa (Eriodictyon californicum) (Deng *et al.,* 2020). It is also abundant in citrus fruit. This flavanone is of immense health importance protecting against diabetes, cancer, neuro diseases and hepatic insult. Eriodictyol enhances insulin productivity thereby stimulating glucose-utilization aiding cAMP/PKA signaling pathway (Hameed *et al.,* 2018). However, their anti-amylase activity is not explored so far. In the present study, all the flavonoids suppress PPA activity in a dose dependent manner with respective IC_{50} values in the range of 20-26 µM Figure 2, Table 4.

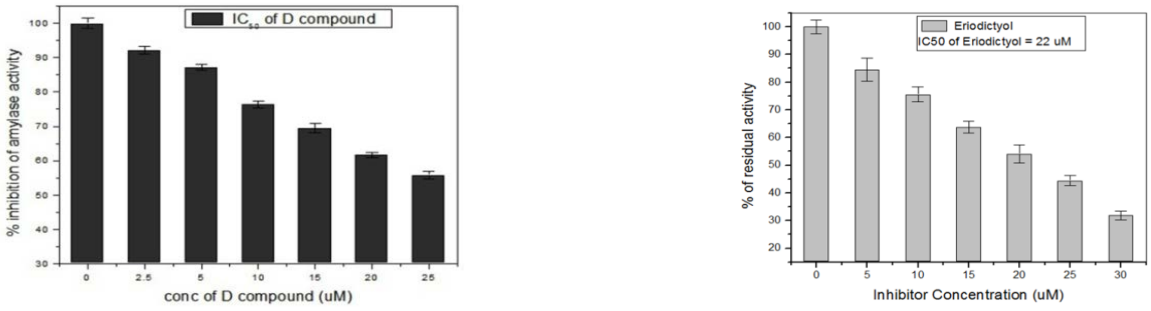

Figure 2: Inhibition of PPA Activities by Flavonoids (A. Diadzein; B. Eriodictoyl)

Estimation of PPA inhibitory action of flavonoids: To further explore the kinetics as well as the nature of inhibition of PPA by the flavonoids, a double reciprocal plot has been plotted for Diadzein and Eriodictyol. Km and V_{max} values derived from each of the kinetic studies have been presented in Table 4. From the result, it is evident that eriodyctiol competitively inhibits PPA whereas daidzein executes noncompetitive mode of inhibition on PPA action.

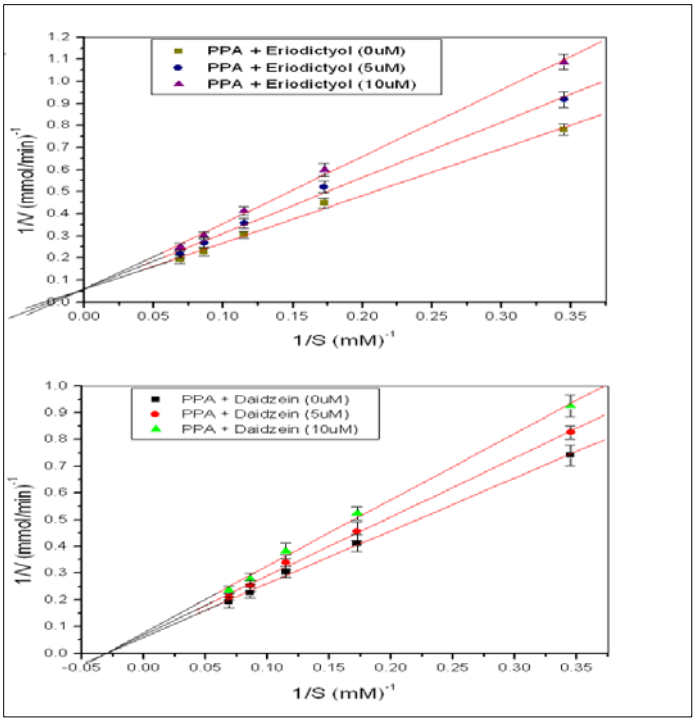

Figure 3: Kinetics of PPA Inhibitions by Flavonoids (A. Eriodictyol, B. Daidzein) by Lineweaver-Burk Plot

Table 4: Kinetic Parameters of PPA Inhibition by Flavonoids

Flavonoids	**K_M (mM)**	**Nature of inhibition**	**IC_{50}**
Diadzein	0.49	Diadzein	26 uM
Eriodictyol	0.41	Competitive	22 uM

Lipid Peroxidation Inhibition and Acarbose in Combination with Diadzein:

There are various reports that indicate reactive oxygen species (ROS) (Abbreviation) has played a crucial role in maintaining cellular homeostasis. Any alteration of the ROS level leads to cell death. ROS are very transient, reactive and unstable in nature. There are varieties of polyunsaturated fatty acids (PUFA) in the cell membrane that help to maintain membrane integrity. There are various reports states that reactive oxygen species (ROS) sometimes target these polyunsaturated fatty acids and peroxidises and as a result cell membrane loses its integrity. ROS is having short half-life, albeit their oxidation products are relatively stable. So they are good indicator of oxidative stress. When ROS attack polyunsaturated fatty acids (PUFAs) of the membranes, they give rise to highly reactive aldehydes. These lipid peroxidation products covalently bind to specific amino acids, commonly histidine, cysteine, or lysine following Michael addition. The resulting modification generates alteration in protein structure with functional impairment. The role of lipid peroxidation affects pathophysiology and aggravates chronic diseases namely Alzheimer's disease, diabetes mellitus, hypertension, and cancers in affected populations (Erejuwa *et al.,* 2012; Butterfield *et al.,* 2010; Zanini *et al.*, 2013). Plethora of information being available deciphering the protective role of diadzein to decline the oxidative stress, lowering of serum triglyceride level and reduced inflammation prompted to evaluate its anti-amylase inhibitory role (Zanini *et al.,* 2013). However, it is ineffective to reduce the glycemic index as reported by (Gobert *et al.,* 2010) mentioned earlier. In order to maintain the protective role of diadzein, any possible interference by acarbose is conducted on the anti-amylase activity of daidzein during lipid peroxidation.

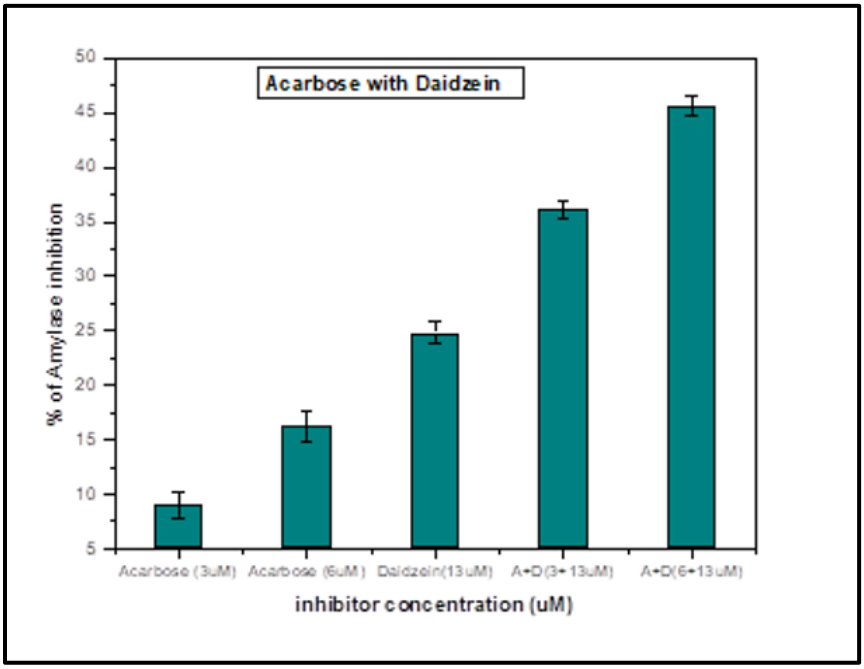

Figure 4: Synergistic Inhibitory Action of Diadzein towards PPA Activity in Presence of a Reduced Dose of Acarbose

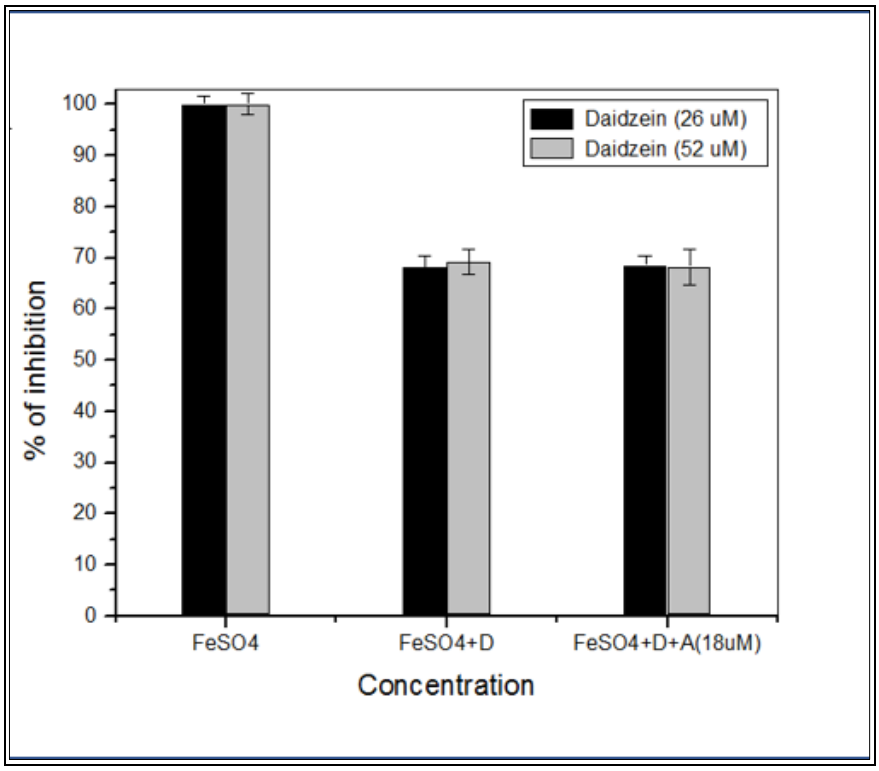

Figure 5: Inhibition of Lipid Peroxidation by Daidzein in Absence and Presence of Acarbose

Lipid peroxidation assay has been performed in the presence of diadzein at its respective IC_{50} values (26 µM respectively) as deduced from Table 4. No remarkable reduction in the inhibition of lipid peroxidation by D has been manifested when carried out in presence of acarbose (18 µM = 1/2 of the IC_{50} value of acarbose for PPA inhibition). The extent of lipid peroxidation induced by FeSO4 has been taken as 100% which has been diminished to 68.1% in the presence of 26 µM Diadzein (IC_{50} for PPA inhibition). As lipid peroxidation is not influenced by the presence of acarbose, so *in vitro* combination study with diadzein and acarbose can be considered together might produce encouraging results during PPA inhibition (Figure 5).

Conclusion

This *in vitro* report of PPA inhibition by deidzein is to be extrapolated to in vivo studies with several diabetic volunteers and should be judged in detail in various combinations of other flavonoids with well-known diabetic drugs like acarbose and metmorfin or with other amylase inhibitors. Flavonoids occupy a key position in the management of critical diseases like diabetes and cancer, with minimal side effects as referred to by several earlier reports. Since they are embedded with several health-promoting activities like antimicrobial, anticancer, antidiabetic, and anti-lipid peroxidation potential, their inclusion in day-to-day life proves to be very much beneficial. They can be considered as natural repurposed natural medicine for the treatment of Diabetes, the deadly one especially in post covid tough situation.

Acknowledgment

The author is grateful to the Department of Biotechnology, Haldia Institute of Technology for providing the experimental space and support.

References

American Diabetes Organization. (2003). Peripheral Arterial Disease in People With Diabetes. *Diabetes Care*, *26*(12), 3333–3341. https://doi.org/10.2337/diacare.26.12.3333

Anisimov, V. N., Semenchenko, A. V., & Yashin, A. I. (2003). Insulin and longevity: antidiabetic biguanides as geroprotectors. *Biogerontology*, *4*(5), 297–307. https://doi.org/10.1023/a:1026299318315

Balaji, R., Duraisamy, R., & Kumar, M. P. S. (2019). Complications of diabetes mellitus: A review. *Drug Invention Today*, *12*(1).

Berman, H. M., Westbrook, J., Feng, Z., Gilliland, G., Bhat, T. N., Weissig, H., ... & Bourne, P. E. (2000). The protein data bank. *Nucleic acids research*, *28*(1), 235-242. https://doi.org/10.1093/nar/28.1.235

Biovia. (2015). *Discovery Studio Modelling Environment* (4.5) [Software].

Boivin, M., Flourié, B., Rizza, R. A., Go, V. L. W., & DiMagno, E. P. (1988). Gastrointestinal and metabolic effects of amylase inhibition in diabetics. *Gastroenterology*, *94*(2), 387–394. https://doi.org/10.1016/0016-5085(88)90426-x

Bolen, S., Feldman, L., Vassy, J., Wilson, L., Yeh, H. C., Marinopoulos, S., ... & Brancati, F. L. (2007). Systematic review: comparative effectiveness and safety of oral medications for type 2 diabetes mellitus. *Annals of internal medicine*, *147*(6), 386-399. https://doi.org/10.7326/0003-4819-147-6-200709180-00178

Breuer, H. M. (2003). Review of acarbose therapeutic strategies in the long-term treatment and in the prevention of type 2 diabetes. *International Journal of Clinical Pharmacology and Therapeutics*, *41*(10), 421–440. https://doi.org/10.5414/cpp41421

Butterfield, D. A., Galvan, V., Lange, M. B., Tang, H., Sowell, R. A., Spilman, P., ... & Bredesen, D. E. (2010). In vivo oxidative stress in brain of Alzheimer disease transgenic mice: requirement for methionine 35 in amyloid β-peptide of APP. *Free Radical Biology and Medicine*, *48*(1), 136-144. https://doi.org/10.1016/j.freeradbiomed.2009.10.035

Chakrabarti, R., & Rajagopalan, R. (2002). Diabetes and insulin resistance associated disorders: Disease and the therapy. *Current science*, 1533-1538.

Daina, A., Michielin, O., & Zoete, V. (2017). SwissADME: a free web tool to evaluate pharmacokinetics, drug-likeness and medicinal chemistry friendliness of small molecules. *Scientific Reports*, *7*(1), 42717. https://doi.org/10.1038/srep42717

Deng, Z., Hassan, S., Rafiq, M., Li, H., He, Y., Cai, Y., ... & Yan, T. (2020). Pharmacological activity of eriodictyol: the major natural polyphenolic flavanone. *Evidence-based complementary and alternative medicine*, *2020*. https://doi.org/10.1155/2020/6681352

DiNicolantonio, J. J., Bhutani, J., & O'Keefe, J. H. (2015). Acarbose: safe and effective for lowering postprandial hyperglycaemia and improving cardiovascular outcomes. *Open Heart*, *2*(1), e000327. https://doi.org/10.1136/openhrt-2015-000327

Dudley, J. T., Deshpande, T., & Butte, A. J. (2011). Exploiting drug-disease relationships for computational drug repositioning. *Briefings in Bioinformatics*, *12*(4), 303–311. https://doi.org/10.1093/bib/bbr013

Erejuwa, O. O., Sulaiman, S. A., Ab Wahab, M. S., Sirajudeen, K. N., Salleh, S., & Gurtu, S. (2012). Honey supplementation in spontaneously hypertensive rats elicits antihypertensive effect via amelioration of renal oxidative stress. *Oxidative Medicine and Cellular Longevity*, *2012*. https://doi.org/10.1155/2012/374037

Ernawati, T. (2018). In silico evaluation of molecular interactions between known α-glucosidase inhibitors and homologous α-glucosidase enzymes from Saccharomyces cerevisiae, Rattus norvegicus, and GANC-human. *Thai Journal of Pharmaceutical Sciences (TJPS)*, *42*(1).

Eyre, H., Kahn, R., Robertson, R. M., ACS/ADA/AHA Collaborative Writing Committee, ACS/ADA/AHA Collaborative Writing Committee Members, Clark, N. G., ... & Thun, M. J. (2004). Preventing cancer, cardiovascular disease, and diabetes: a common agenda for the American Cancer Society, the American Diabetes Association, and the American Heart Association. *Circulation*, *109*(25), 3244-3255. https://doi.org/10.1161/01.CIR. 00001333 21.00456.00

Formica, J., & Regelson, W. (1995). Review of the biology of quercetin and related bioflavonoids. *Food and Chemical Toxicology*, *33*(12), 1061–1080. https://doi.org/ 10.1016/0278-6915(95)00077-1

Gobert, C. P., Pipe, E. A., Capes, S. E., Darlington, G., Lampe, J. W., & Duncan, A. (2010). Soya protein does not affect glycaemic control in adults with type 2 diabetes. *British Journal of Nutrition*, *103*(3), 412–421. https://doi.org/10.1017/s0007114509991802

Hameed, A., Hafizur, R. M., Hussain, N., Raza, S. H. A., Rehman, M. U., Ashraf, S., Ul-Haq, Z., Khan, F., Abbas, G., & Choudhary, M. I. (2018). Eriodictyol stimulates insulin secretion through cAMP/PKA signaling pathway in mice islets. *European Journal of Pharmacology*, *820*, 245–255. https://doi.org/10.1016/j.ejphar.2017.12.015

Hung, H. Y., Qian, K., Morris-Natschke, S. L., Hsu, C. S., & Lee, K. H. (2012). Recent discovery of plant-derived anti-diabetic natural products. *Natural product reports*, *29*(5), 580-606. https://doi.org/10.1039/c2np00074a

Inzucchi, S. E. (2002). Oral antihyperglycemic therapy for type 2 diabetes: scientific review. *Jama*, *287*(3), 360-372. https://doi.org/10.1001/jama.287.3.360

Inzucchi, S. E., Lipska, K. J., Mayo, H., Bailey, C. J., & McGuire, D. K. (2014). Metformin in patients with type 2 diabetes and kidney disease: a systematic review. *Jama*, *312*(24), 2668-2675. https://doi.org/10.1001/jama.2014.15298

Islam, A., Islam, S., Rahman, M. K., Uddin, N., & Akanda, R. (2020). The pharmacological and biological roles of eriodictyol. *Archives of Pharmacal Research*, *43*(6), 582–592. https://doi.org/10.1007/s12272-020-01243-0

Johnson, K. A. (2013). A century of enzyme kinetic analysis, 1913 to 2013. *FEBS Letters*, *587*(17), 2753–2766. https://doi.org/10.1016/j.febslet.2013.07.012

Lankisch, M., Layer, P., Rizza, R. A., & DiMagno, E. P. (1998). Acute Postprandial Gastrointestinal and Metabolic Effects of Wheat Amylase Inhibitor (WAI) in Normal, Obese, and Diabetic Humans. *Pancreas*, *17*(2), 176–181. https://doi.org/10.1097/ 00006676-199808000-00011

Lo Piparo, E., Scheib, H., Frei, N., Williamson, G., Grigorov, M., & Chou, C. J. (2008). Flavonoids for Controlling Starch Digestion: Structural Requirements for Inhibiting Human α-Amylase. *Journal of Medicinal Chemistry*, *51*(12), 3555–3561. https:// doi.org/10.1021/jm800115x

Maity, S., Mukherjee, K., Banerjee, A., Mukherjee, S., Dasgupta, D., & Gupta, S. (2016). Inhibition of Porcine Pancreatic Amylase Activity by Sulfamethoxazole: Structural and Functional Aspect. *Protein Journal*, *35*(3), 237–246. https://doi.org/10.1007/s10930-016-9668-8

Malla, A., Mukherjee, K., Mandal, M., Mukherjee, A., Sur, R., & Gupta, S. (2021). An Insight to the Toxic Effect of Sulfamerazine on Porcine Pancreatic Amylase and Lactate Dehydrogenase Activity: An *In Vitro* Study. *Current Chemical Biology*, *15*(2), 171-181. https://doi.org/10.2174/2212796815666210216101221

Phan, M. Q., Wang, J., Tang, J., Lee, Y., & Ng, K. (2013). Evaluation of α-glucosidase inhibition potential of some flavonoids from Epimedium brevicornum. *Lebensmittel-Wissenschaft & Technologie*, *53*(2), 492–498. https://doi.org/10.1016/j.lwt.2013. 04.002

Schreiber, A., Nones, C. F. M., Reis, R. K., Chichorro, J. G., & Da Cunha, J. M. (2015). Diabetic neuropathic pain: Physiopathology and treatment. *World Journal of Diabetes*, *6*(3), 432-444. https://doi.org/10.4239/wjd.v6.i3.432

Schrodinger, L. L. C. (2015). The PyMOL molecular graphics system. *Version*, *1*, 8.

Strebhardt, K., & Ullrich, A. (2008). Paul Ehrlich's magic bullet concept: 100 years of progress. *Nature Reviews Cancer*, *8*(6), 473–480. https://doi.org/10.1038/nrc2394

Talevi, A., & Bellera, C. L. (2020). Challenges and opportunities with drug repurposing: finding strategies to find alternative uses of therapeutics. *Expert Opinion on Drug Discovery*, *15*(4), 397–401. https://doi.org/10.1080/17460441.2020.1704729

Trott, O., & Olson, A. J. (2009). AutoDock Vina: Improving the speed and accuracy of docking with a new scoring function, efficient optimization, and multithreading. *Journal of Computational Chemistry*, *2*(31), 455-461. https://doi.org/10.1002/jcc.21334

Turner, N., Zeng, X., Osborne, B., Rogers, S. M., & Ye, J. (2016). Repurposing Drugs to Target the Diabetes Epidemic. *Trends in Pharmacological Sciences*, *37*(5), 379–389. https://doi.org/10.1016/j.tips.2016.01.007

Ye, Y. B., Chen, A. L., Lu, W., Zhuo, S. Y., Liu, J., Guan, J. H., ... & Chen, Y. M. (2015). Daidzein and genistein fail to improve glycemic control and insulin sensitivity in Chinese women with impaired glucose regulation: a double-blind, randomized, placebo-controlled trial. *Molecular Nutrition & Food Research*, *59*(2), 240-249. https://doi.org/ 10.1002/mnfr. 201400390

Zanini, D., Schmatz, R., Pelinson, L. P., Pimentel, V. C., Da Costa, P., Cardoso, A. M., ... & Schetinger, M. R. C. (2013). Ectoenzymes and cholinesterase activity and biomarkers of oxidative stress in patients with lung cancer. *Molecular and Cellular Biochemistry*, *374*, 137-148. https://doi.org/10.1007/s11010-012-1513-6

https://doi.org/10.31674/book.2023pcbs007

Recent Advances in the Green Synthesis of Poly Functionalized Pyrroles

Harisadhan Ghosh[1]*, Anupam Jana[2]*
[1]Department of Chemistry, Surendranath College, Kolkata, West Bengal, India
[2]Department of Pharmaceutical Analysis, National Institute of Pharmaceutical Education and Research (NIPER) Hajipur, Bihar, India

*Corresponding Author's Email: ghosh.harisadhan@gmail.com, anupamjana2@gmail.com

ABSTRACT

Pyrroles are five-membered heterocyclic organic compounds with a broad and attractive chemistry. Functionalized pyrroles have a diverse structural variation, and they are important scaffolds in modern technological advancement. Pyrrole derivatives have been widely used as drugs, dyes, catalysts, pesticides etc. Therefore, the synthesis of these heterocyclic skeletons using robust and green methodologies is a great challenge in modern synthetic organic chemistry. In the present literature review, the currently developed green methodologies have been summarized in the synthesis of pyrrole derivatives. The reported methods, which are environmentally benign synthetic procedures as well as highly efficient techniques for the production of pyrrole derivatives, have been scrutinized. So, the present review article will be attractive for synthetic organic chemists who are interested in the application of Green Chemistry principles in the synthesis of pyrrole derivatives.

Keywords*: Pyrroles; Heterocyclic Compounds; Biological Activity; Green Chemistry; Green Synthesis; Paal-Knorr Synthesis*

Introduction

Pyrrole is a nitrogen containing five membered- aromatic, heterocyclic organic compound. Pyrrole is a weak base due to the contribution of lone pair of electrons on the nitrogen to the aromaticity in the ring structure (Figure-1).

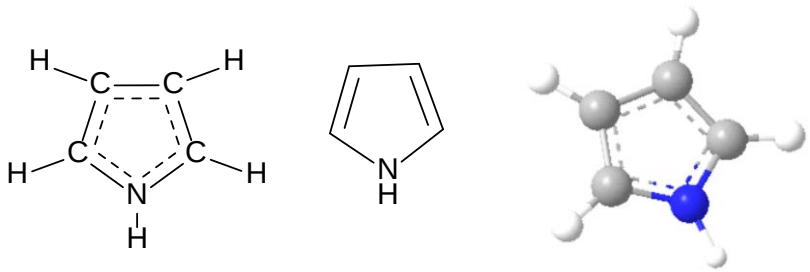

Figure 1: Structure of Pyrrole

Pyrrole was first detected by F.F. Runge in 1834 from coal tar and subsequently, the structure was determined by Baeyer and Emmerling in 1870. Although the Pyrrole molecules are not as such naturally abundant, the various derivatives of these scaffolds are observed in a series of natural products and cofactors. Here are some examples of naturally occurring molecules that contain pyrrole scaffold as one of their main

constituents: vitamin B_{12}, bile pigments *e.g* bilirubin, biliverdin and the porphyrins of heme, chlorophyll, chlorins, bacteriochlorin, porphyrinogens etc. It is also found in the secondary metabolites (Young, Thornton & Thompson 2010) (Figure-2).

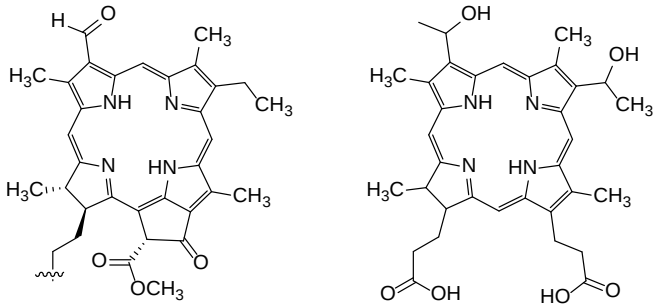

Figure 2: Structure of Some Important Natural Molecule Containing Pyrrole Ring

The derivatives of pyrrole are considered an important class of biologically active molecules with diverse types of activities and they also act as different pharmacophores (Jacobi *et al*., 2000). These types of compounds exhibit anti-bacterial activities that have been extensively investigated during the last few decades, particularly tested on drug-resistant Gram-positive and Gram-negative pathogens (Yamada *et al*., 2017). Another important application of pyrrole derivatives is that they can be used for the production of anti-tumour agents that can act on gene modulation or suppression and conjugate antibodies. They are also employed as coating agents for medical implants (Dadas *et al.,* 2015).

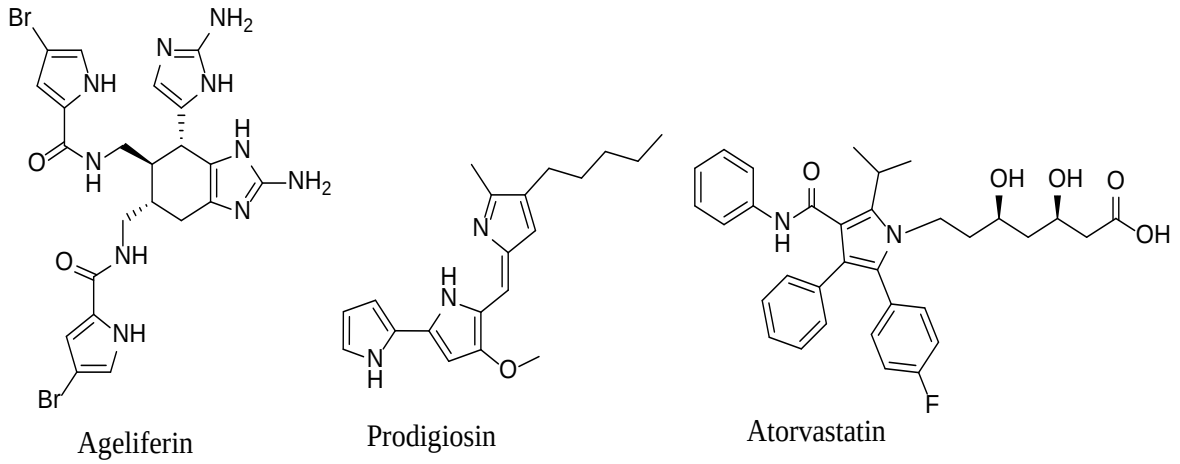

Figure 3: Structure of Few Important Synthetic Molecules that Contain Pyrrole Scaffold

Literature Review

Due to their huge importance, pyrrole scaffolds have attracted the great attention of synthetic organic chemists and it has been an important research area to develop newer methodologies for the synthesis of these compounds. So, several classic named reactions have been developed by various organic chemists to produce these moieties (Ferreira *et al.,* 2001). Here are some classic examples of synthetic procedures that are developed for the synthesis of pyrroles-

(i) Hantzsch synthesis (Trautwein, Süßmuth & Jung, 1998), which furnishes pyrroles through the reaction of α-halo ketones with β–ketoesters and ammonia or primary amines.

(ii) Knorr synthesis (Alberola *et al.*, 1999), which is used to construct the pyrroles scaffold by reacting α–amino-ketones derived from α–haloketones, ammonia and β–ketoesters.

(iii) Paal-Knorr condensation reaction (Pak-Kan & Sannes, 1990), it is one of the most common approaches which uses the primary amines or ammonia and various promoting agents (Figure 4 and Figure 5).

(iv) Buchwald-Hartwig coupling reaction (Bonnaterre, Bois-Choussy & Zhu, 2006).

Several other methods were also demonstrated for the production of specific pyrrole skeletons, such as multi-component reactions (Balme, 2004), addition reaction, Wittig reaction etc. arylglyoxal, which is actually an organic compound with carbonyl functionality adjacent to the aldehydes group, is a quite reactive precursor for the synthesis of different heterocyclic compounds (Eftekhari-Sis, Zirak & Akbari, 2013). Multi-component reactions of arylglyoxals have been utilized for the synthesis of a variety of poly-functionalized pyrrole derivatives (Wang *et al.,* 2013, Ambethkar, Padmini & Bhuvanesh, 2016 & Mishra *et al.,* 2017).

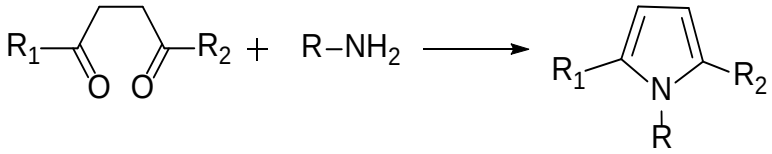

Figure 4: General Paal-Knorr Synthesis of Pyrrole

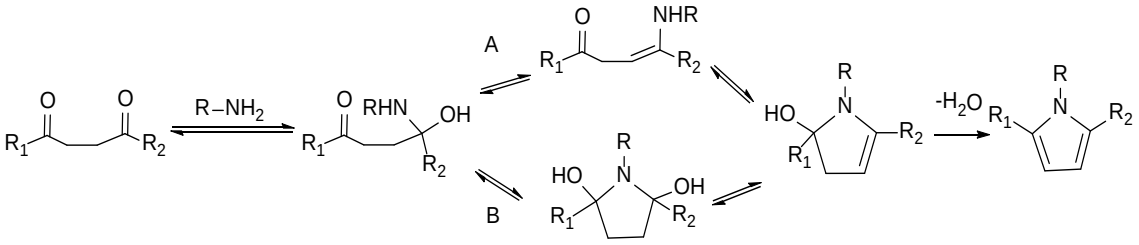

Figure 5: Proposed Pathway for the Paal-Knorr Synthesis of Pyrroles-(A) the Enamine Pathway and (B) the Hemi-aminal Pathway

However, in the above-mentioned methods, some sort of problems are encountered that are not environment friendly, such as extended reaction times, the use of toxic and low boiling solvents, diminished yields, tedious purification methods, the need for high reaction temperature etc.

Discussion

To resolve these eco-unfriendly problems, chemists are in search of novel technologies that follow the principles of Green Chemistry. One of the most important goals of green chemistry is the replacement of hazardous/toxic organic solvents with environmentally benign green solvents. On the other hand, synthetic and industrial chemists are always trying to design suitable solvents or solvent systems as reaction media to improve the efficiency of an organic transformation (Reinhardt *et al.,* 2008). In this context, a wide range of synthetic methodologies have been discovered such as –(i) use of microwave, ultrasound and visible light techniques, (ii) use of Green Solvents (water, ethanol) over

conventional solvents, (iii) reaction by mechanical activation (ball milling), (iv) reaction using Nano and Green Catalyst.

This review article summarizes the latest developments in pyrrole synthesis and gives an emphasis on designing the targeted reactions more eco-friendly using green methodologies for the production of functionalised pyrrole compounds.

Use of Ball Milling Method

Mechanochemistry is the process where grinding the solid reactants increases the surface area, which helps intimate mixing and increases contact among different reactants. The grinding process generates heat, which sometimes melts the reactants and reactions can proceed in a molten state. It is also believed that mechanical energy is directly absorbed by the molecule and undergoes bond rupture to produce reactive species like radicals, which help propagate the reaction. There are a few typical methods, such as shearing, stretching and grinding, that are followed to create reactive species. Mechano-chemical reactors are used for those reactions where high energy and longer reaction times are required.

Prof. Akelis *et al.* (2016) demonstrated the synthesis of *N*-substituted pyrrole derivatives through mechano-chemical activation (ball milling). Bio sourced organic green acids such as citric acid, pyroglutamic acid, succinic acid, ascorbic acid, camphor-sulfonic acid, and oxalic acid have been used as catalysts for this transformation (Figure 6).

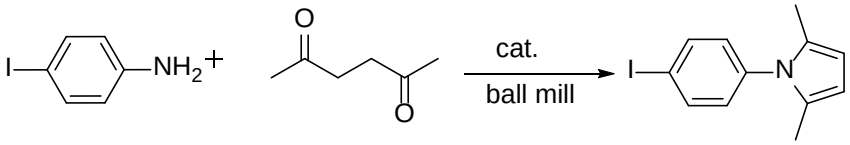

Figure 6: Paal-Knorr Pyrrole Synthesis with 4-Iodoaniline and 2,5-Hexanedione under Ball Milling

After investigating various solid organic acids as catalyst, it is found out that citric acid gives the best result. It was observed that good conversion was seen by using 1 mol (catalyst amount) citric acid at 30 Hz (frequency of ball milling) (Figure 7).

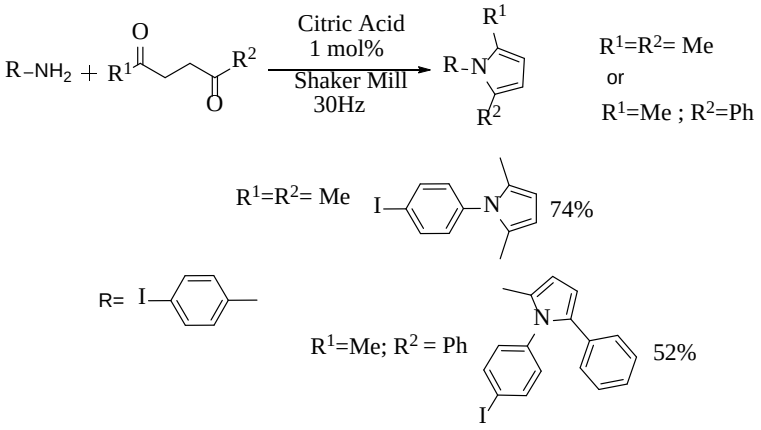

Figure 7: Citric acid Catalysed Pyrrole Synthesis in a Ball Milling

This method is efficient for preparing N-substituted pyrroles in very short times at room temperature rather than the traditional Paal-Knorr method. The main advantages of the

present procedure are –(1) it is a solventless methodology (2) use of a “green” organic acid that is non-toxic and generated from biomass.

Use of Ultrasound

Sonochemistry is a branch of chemistry that deals with the effects of ultrasound on chemical reactions. Ultrasonic sound (US) acts as a non-conventional energy source. Generally, ultrasounds with frequencies 20KHz to 1 MHz are used in sonochemistry. Electromagnetic waves travel in a vacuum, but mechanical waves require an elastic medium to propagate. Ultra sound (US) can be focused, reflected or refracted in an elastic medium. It propagates in a medium like sound waves. Ultrasound also causes compression and rarefaction which create alternative zones of high pressure and low pressure. The low-pressure zones create cavities or bubbles, which suddenly collapse in the compression zone and generate a shock wave. This phenomenon of bubble or cavity formation and collapse is referred to as 'cavitation'. Direct interaction between waves and reactants to induce a chemical reaction is not possible, an indirect phenomenon known as cavitation acts as a relay to induce a chemical reaction. Sonochemical reactions are beneficial to conventional heating because of the following reasons: (1) Ultrasonic sound can conduct a reaction at an ambient temperature without warming the air in close vicinity of the reaction systems. (2) Most of the heat energy is lost to the environment. A small part of the total heat produced is utilized for the actual purpose for which it is generated. (3) It has been observed that in many cases, the use of ultrasound reduces the reaction time and temperature and increases efficiency and selectivity.

Dr. Eftekhari-Sis research group has demonstrated a novel synthesis of pyrrole *via* three component reaction of aryl glyoxal hydrates, β-di carbonyl compound and ammonium acetate in aqueous medium under ultrasonic irradiation (Eftekhari-Sis & Vahdati-Khajeh, 2013) (Figure 8).

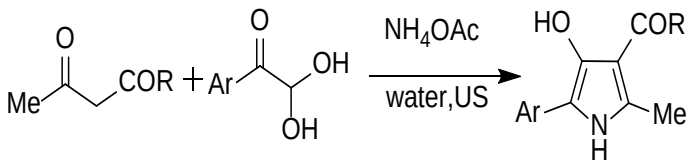

Figure 8: Ultra-sound Promoted Synthesis of Pyrroles

The main advantages of the present methodology are high yield, short reaction time, mild reaction condition. This reaction is the simplest and useful process (according to environmental and economical points) which is the most important advantage (Figure 9).

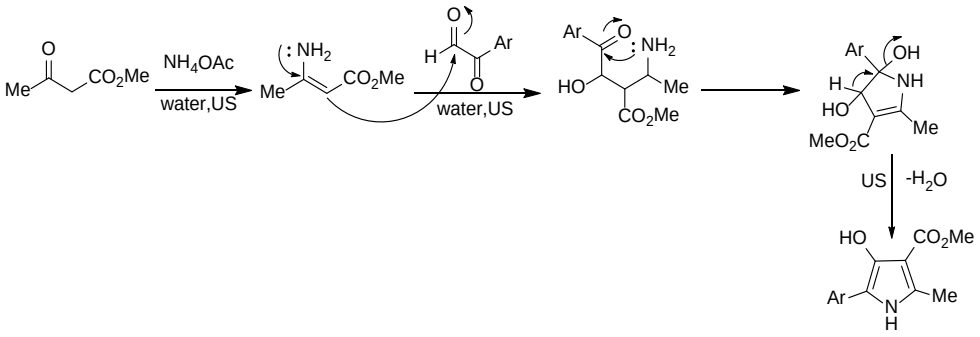

Figure 9: The Plausible Reaction Mechanism of Pyrrole Synthesis

Using Green Solvents

Solvent is the major constituent of a reaction mixture and becomes the prime source of waste mass in the synthetic process. Most organic solvents suffer from their toxicities, hazards, flammability and explosive nature. Nowadays, solvent-free reactions are promoted to overcome this problem. Still, the choice of solvent has a great role in controlling the rate, selectivity and equilibrium position of a chemical reaction. Among all the environmentally benign solvents, water is the most innocuous solvent and it has environmental and economic benefits. Sometimes, the solvent mixture, such as water and ethanol, possesses many interesting inherent properties that make it a unique reaction medium.

In a recent report, the research group of Anary-Abbasinejada disclosed the synthesis of tetrone derivatives through a three-component reaction between arylglyoxal, acetylacetone and enaminoketone. These poly-functionalized intermediates are easily converted to poly-functionalized pyrrole derivatives (Anary-Abbasinejada, Nezhad-Shshrokhabadi & Mohammadi, 2020) (Figure 10).

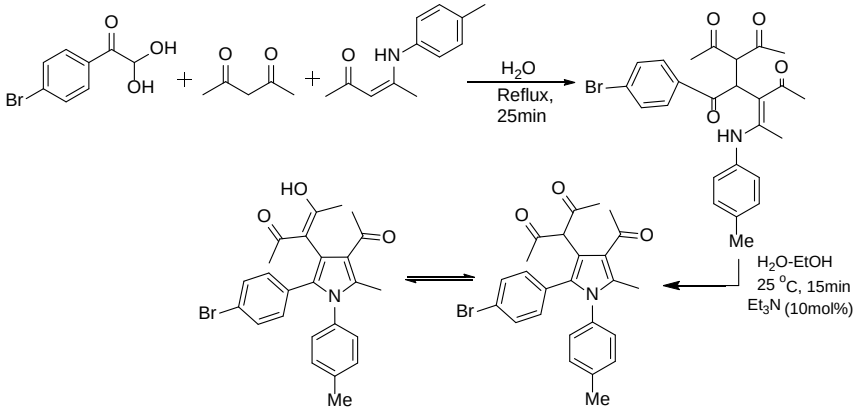

Figure 10: Synthesis of 3-acetayl-4-(4-bromobenzoyl)-5-(p-tolylamino)ethylidene)heptan-2, 6-dione

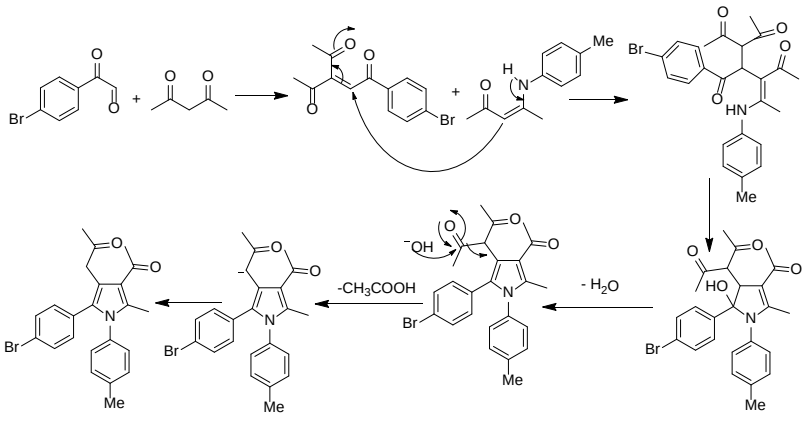

Figure 11: Proposed Mechanism for Formation of Pyrroles Derivatives

The attractive improvements of this method are the convenient workup method and the use of water or a water-ethanol mixture as an environmentally benign solvent. The authors have reported that all the desired products are easily separated and purified by

a simple filtration method, followed by washing with diethyl ether. So, they have avoided the tedious chromatographic purification techniques.

Using Nano-catalyst

Prof. Yousif research group has disclosed a facile and effective methodology for the environmentally benign and speedy production of biologically active poly-substituted pyrroles through Cu@imine/Fe_3O_4 MNPs catalysed reaction under solventless conditions. This catalytic system has been proven to be excellent in terms of high reactivity for the generation of poly-substituted pyrroles in short reaction times. The reactivity of this catalyst greatly depends on the catalyst loading factor and reaction temperature. The most interesting fact is that the catalyst is recyclable and it was reused six times without significant loss of reactivity. The other advantages of this methodology are short reaction times, easy workup procedure (Thwin *et al*., 2019) (Figure 13).

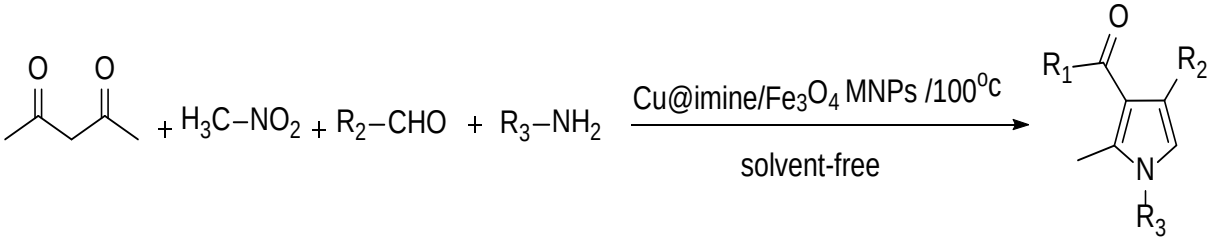

Figure 12: Preparation of Poly-substituted Pyrroles Derivative using Nano catalyst

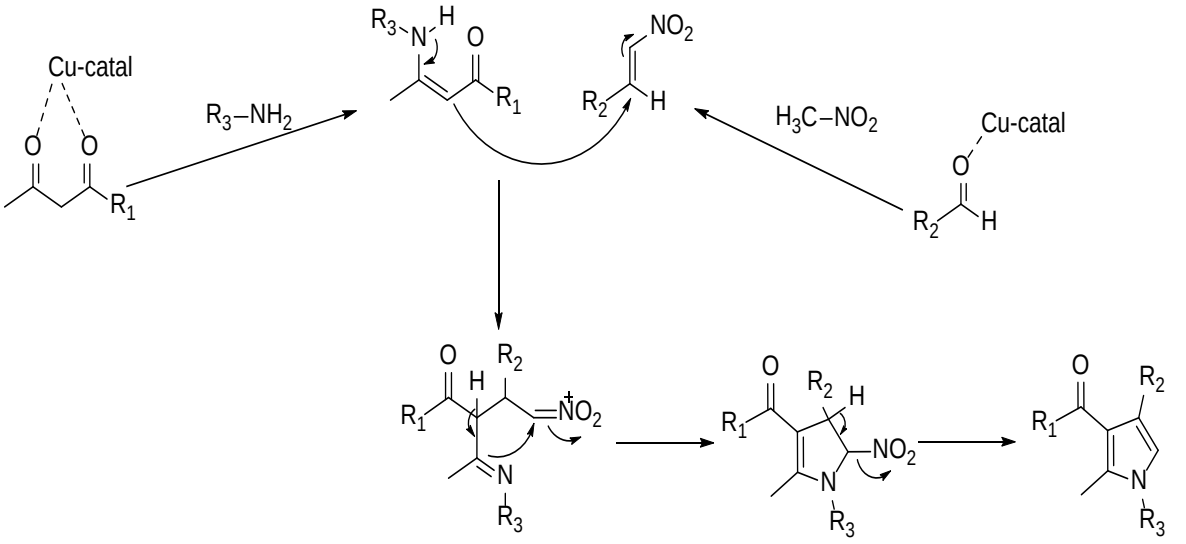

Figure 13: Plausible Mechanism for the Synthesis of Poly-substituted Pyrrole Derivative 3.5

Use of Visible Light

Prof. Wen-Jing Xiao *et al.* have reported an organic dye photocatalyst mediated synthesis of tetra substituted pyrrole derivatives through the formal [3+2] cycloaddition reaction of 2H azirines with alkynes under irradiation by visible light (Figure 14, 15). This synthetic method furnishes efficient access to highly functionalized pyrroles in good yields (Xuan *et al*., 2014).

Figure 14: Preparation of Pyrroles Derivative using Visible Light

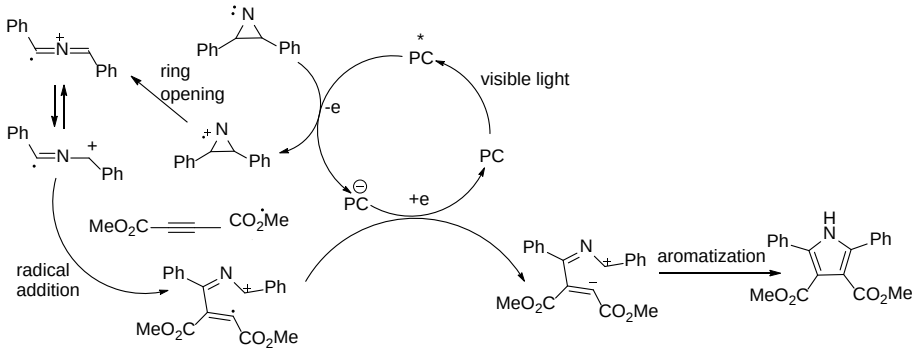

Figure 15: Plausible Reaction Mechanism of Pyrroles Derivative using Photocatalyst

Use of Green Catalyst

A green method for the synthesis of poly-substituted pyrroles in good yield has been achieved very recently (Louroubi *et al.,* 2021). It is a four component reaction of 1,3-dicarbonyl compound, amines, aldehydes, and nitro-alkanes (Figure 16). The natural **hydroxyapatite (HAP**) has been used as an efficient green catalyst in a *one-pot* methodology (Figure 17).

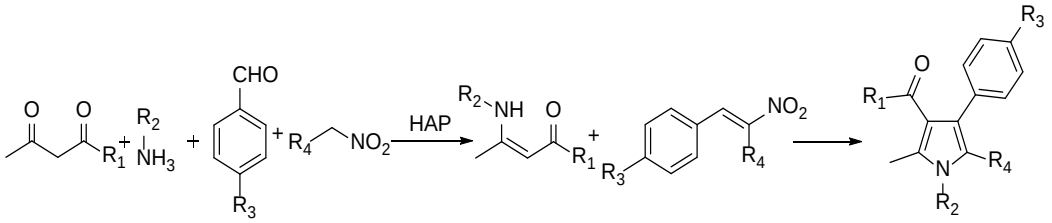

Figure 16: Synthesis of Pyrrole Using Green Catalyst

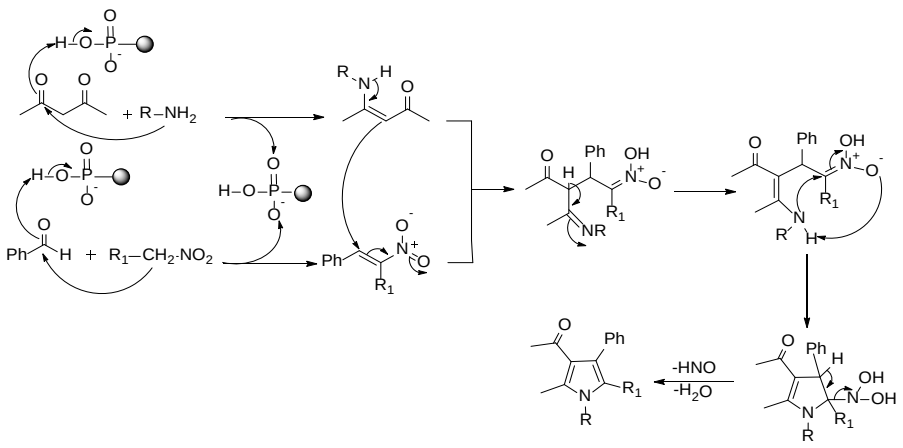

Figure 17: Plausible Mechanism for the Formation of Pyrrole Derivative

The above developed method is an environment friendly, operationally simple, cost-effective and efficient pathway for the synthesis of pyrroles derivative through the four component domino reaction strategy in *one-pot*. This green protocol leads to the generation of densely functionalized pyrroles. The most interesting benefit of this methodology is the use of hydroxyapatite as a cost-effective, natural and safe catalyst.

Use of Microwave

Microwave (MW) is an electromagnetic radiation with wave length ranging from 1mm to 1m. The frequencies and energies of the microwave region are 300 GHz to 300 MHz and 1.24×10^{-3} to 1.24×10^{-6} Ev respectively. In the electromagnetic spectrum, the microwave region is placed between the infrared and radio wave frequencies. Microwave radiation is not as energetic, so it cannot ionize an atom or molecule or break a chemical bond to initiate a chemical transformation. But surprisingly, MW-irradiated chemical reactions are often faster than those operated by conventional heating. Microwave radiations have been used as a non-conventional energy source in the field of synthetic organic chemistry for the following reasons- (a) reaction time is dramatically shortened compared to classical procedure, (b) reaction efficiency is increased, (c) improved yield with less side product, (d) sometimes organic solvents can be replaced by innocuous solvent water, (e) solvent-free reactions can be performed, (f) reactions under MW-irradiations are cleaner with easy workup. Originally, domestic MW ovens were used to carry out organic reactions in an open pot or in a sealed tube, but later MW reactors were modified to carry out reactions in solution under refluxing conditions. Now, microwave reactors are available to carry out a reaction at a particular pressure or temperature in the presence or absence of a solvent.

Microwave assisted Paal-Knorr reactions have been demonstrated by Prof Taddei Research Group (Minetto *et al.,* 2005). They were successful in reacting various well accessible β-keto esters with Et_2Zn/CH_2Cl_2 and aldehydes. The resultant reaction mixture on subsequent oxidation with pyridinium chlorochromate (PCC) furnishes poly-substituted 1,4-dicarbonyl compounds in two steps. In the final step, the authors have demonstrated that microwave irradiation is an excellent energy source for Paal-Knorr cyclisation to afford the pyrroles in good yield (Figure 18).

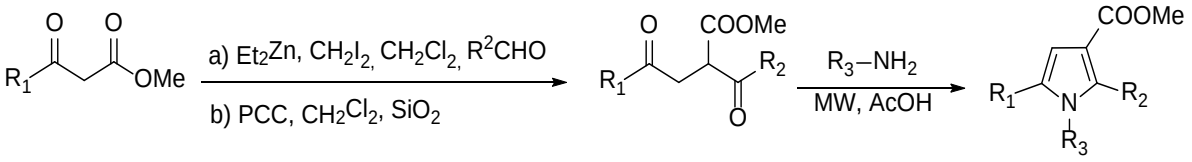

Figure 18: Microwave-assisted Synthesis of Pyrroles

In this transformation, the optimized result was obtained, when the reaction mixture was placed in an open vessel at 120-150^{o}C only for 2-10 min under MW.

Conclusion

One of the main targets of Green Chemistry is to wisely eliminate the production of hazardous or harmful materials or replace them with less harmful and safer ones. Pyrroles derivatives are important materials due to their diverse biological activities and huge demand in the pharmaceutical industry. So, the application of Green Chemistry

principles in the synthesis of these heterocyclic compounds involves multiple economic and social developments. That is why the chemists have developed newer and novel methodologies of green activation, such as microwaves, ultrasound, and continuous flow processes at room temperature, which have resulted in cost and waste reduction and greater efficiency for the production of pyrrole derivatives. In the present review article, the green synthetic techniques that have been used to synthesize pyrrole derivatives in recent years have been documented. The future direction of this study should result in many newer Green protocols for the synthesis of functionalized pyrroles and related heterocycles such as furans and thiophenes in a cost effective way to meet industrial demand.

Acknowledgement

Dr. Ghosh sincerely acknowledges the Principal of Surendranath College and all the faculties of Department of Chemistry for extending their valuable help whenever needed. Dr. Jana greatly acknowledges generous financial support from the National Institute of Pharmaceutical Education and Research (NIPER)-Hajipur, Department of Pharmaceuticals, Ministry of Chemicals and Fertilizers, Govt. of India.

References

Akelis, L., Rousseau, J., Juskenas, R., Dodonova, J., Rousseau, C., Menuel, S., ... & Hapiot, F. (2016). Greener Paal–Knorr pyrrole synthesis by mechanical activation. *European Journal of Organic Chemistry* (1), 31–35, https://doi.org/10.1002/ejoc.201501223

Alberola, A., Ortega, A. G., Sádaba, M. L., & Sañudo, C. (1999). Versatility of Weinreb amides in the Knorr pyrrole synthesis. *Tetrahedron*, *55*(21), 6555-6566. https://doi.org/10.1016/S0040-4020(99)00289-6

Ambethkar, S., Padmini, V., & Bhuvanesh, N. (2016). A one-pot sequential five-component domino reaction for the expedient synthesis of polysubstituted pyrroles. *New Journal of Chemistry*, *40*(5), 4705-4709. https://doi.org/10.1039/C5NJ03444B

Anary-Abbasinejada, M., Nezhad-Shshrokhabadi, F., & Mohammadi, M. (2020). A green method for the synthesis of pyrrole derivatives using arylglyoxals, 1, 3-diketones and enaminoketones in water or water–ethanol mixture as solvent. *Molecular Diversity*, *24*, 1205-1222. https://doi.org/10. 1007/s11030-019-09984-x

Baeyer, A. V., & Emmerling, A. (1870). Reduction des Isatins zu Indigblau. *Berichte der deutschen chemischen Gesellschaft*, *3*(1), 514-517. https://doi.org/10.1002/cber.18700030 1169

Balme, G. (2004). Pyrrole syntheses by multicomponent coupling reactions. *Angewandte Chemie International Edition*, *43*(46), 6238-6241. https://doi.org/10.1002/anie.200461073

Bonnaterre, F., Bois-Choussy, M., & Zhu, J. (2006). Rapid access to oxindoles by the combined use of an Ugi four-component reaction and a microwave-assisted intramolecular buchwald− hartwig amidation reaction. *Organic Letters*, *8*(19), 4351-4354. https://doi.org/10.1021/ ol061755z

Dadaş, Y., Coşkun, G., Bingöl-Özakpınar, Ö., Özsavcı, D., & Küçükgüzel, Ş. (2015). Synthesis and anticancer activity of tolmetin thiosemicarbazides. *Marmara Pharmaceutical Journal*, *19*(3), 259-267. https://doi.org/10.12991/mpj.201519328306

Eftekhari-Sis, B., & Vahdati-Khajeh, S. (2013). Ultrasound-assisted green synthesis of pyrroles and pyridazines in water via three-component condensation reactions of arylglyoxals. *Current Chemistry Letters*, *2*(2), 85-92. http://dx.doi.org/10.5267/j.ccl. 2013.02.002

Eftekhari-Sis, B., Zirak, M., & Akbari, A. (2013). Arylglyoxals in synthesis of heterocyclic compounds. *Chemical Reviews*, *113*(5), 2958-3043. https://doi.org/10.1021/ cr300176g

Ferreira, V. F., de Souza, M. C. B., Cunha, A. C., Pereira, L. O., & Ferreira, M. L. (2001). Recent advances in the synthesis of pyrroles. *Organic Preparations and Procedures International*, *33*(5), 411-454. https://doi.org/10.1080/00304940109356613

Jacobi, P. A., Coutts, L. D., Guo, J., Hauck, S. I., & Leung, S. H. (2000). New strategies for the synthesis of biologically important tetrapyrroles. The “B, C+ D+ A” approach to linear tetrapyrroles. *The Journal of Organic Chemistry*, *65*(1), 205-213. https://doi.org/10.1021/jo 991503u

Louroubi, A., Nayad, A., Hasnaoui, A., Idouhli, R., Abouelfida, A., El Firdoussi, L., & Ait Ali, M. (2021). Natural hydroxyapatite: green catalyst for the synthesis of pyrroles, inhibitors of corrosion. *Journal of Chemistry*, *2021*, 1-11. https://doi.org/10.1155/ 2021/ 6613243

Minetto, G., Raveglia, L. F., Sega, A., & Taddei, M. (2005). Microwave-Assisted Paal–Knorr Reaction–Three-Step Regiocontrolled Synthesis of Polysubstituted Furans, Pyrroles and Thiophenes. *European Journal of Organic Chemistry, 2005*(24), 5277–5288. https://doi.org/ 10.1002/ejoc.200500387

Mishra, R., Panday, A. K., Choudhury, L. H., Pal, J., Subramanian, R., & Verma, A. (2017). Multicomponent Reactions of Arylglyoxal, 4-Hydroxycoumarin, and Cyclic 1, 3-C, N-Binucleophiles: Binucleophile-Directed Synthesis of Fused Five-and Six-Membered N-Heterocycles. *European Journal of Organic Chemistry*, *2017*(19), 2789-2800. https://doi.org/10. 1002/ejoc.201700115

Pak-Kan, C., & Sannes, M. P. (1990). The synthesis and chemistry of azolenines. Part 18. Preparation of 3-ethoxycarbonyl-3h-pyrroles via the paal-knorr reaction, and sigmatropic rearrangements involving competitive ester migrations to c-2, c-4 and n. *Tetrahedron*, *46*(10), 3439-3456. https://doi.org/10.1016/S0040-4020(01)81514-3

Reinhardt, D., Ilgen, F., Kralisch, D., König, B., & Kreisel, G. (2008). Evaluating the greenness of alternative reaction media. *Green Chemistry*, *10*(11), 1170-1181. https://doi.org/10.1039/ B807379A

Thwin, M., Mahmoudi, B., Ivaschuk, O. A., & Yousif, Q. A. (2019). An efficient and recyclable nanocatalyst for the green and rapid synthesis of biologically active polysubstituted pyrroles and 1, 2, 4, 5-tetrasubstituted imidazole derivatives. *RSC advances*, *9*(28), 15966-15975. https://doi.org/10.1039/C9RA02325A

Trautwein, A. W., Süßmuth, R. D., & Jung, G. (1998). Hantzsch pyrrole synthesis on solid support. *Bioorganic & Medicinal Chemistry Letters*, *8*(17), 2381-2384. https://doi.org/10.1016/ S0960-894X(98)00430-2

Wang, H., Liu, X., Feng, X., Huang, Z., & Shi, D. (2013). GAP chemistry for pyrrolyl coumarin derivatives: a highly efficient one-pot synthesis under catalyst-free conditions. *Green chemistry*, *15*(12), 3307-3311. https://doi.org/10.1039/C3GC41799A

Xuan, J., Xia, X. D., Zeng, T. T., Feng, Z. J., Chen, J. R., Lu, L. Q., & Xiao, W. J. (2014). Visible-light-induced formal [3+ 2] cycloaddition for pyrrole synthesis under metal-free conditions. *Angewandte Chemie International Edition*, *53*(22), 5653-5656. https://doi.org/ 10. 1002/anie.201400602

Yamada, Y., Takeuchi, S., Yoneda, M., Ito, S., Sano, Y., Nagasawa, K., ... & Nagata, K. (2017). Atorvastatin reduces cardiac and adipose tissue inflammation in rats with metabolic syndrome. *International Journal of Cardiology*, *240*, 332-338. https://doi.org/ 10.1016/j. ijcard.2017.04.103

Young, I. S., Thornton, P. D., & Thompson, A. (2010). Synthesis of natural products containing the pyrrolic ring. *Natural product reports*, *27*(12), 1801-1839. https://doi.org/10.1039/C0N P00014K

https://doi.org/10.31674/book.2023pcbs008

Heterogeneous Catalysis over Porous Materials: A Critical Review

Najirul Haque[1], Usha Mandi[2], Sk. Manirul Islam[1]*, Noor Salam[3]*
[1]Department of Chemistry, University of Kalyani, Kalyani, West Bengal, India
[2]Department of Chemistry, Jogamaya Devi College, Kolkata, West Bengal, India
[3]Department of Chemistry, Surendranath College, Kolkata, West Bengal, India

*Corresponding Author's Email: noor.salam8@gmail.com, manir65@rediffmail.com

ABSTRACT

The strategy and building of porous constructions in synthesized materials that imitate structures seen natural, macro to the micro- and nanoscale ranges, has long been a vital scientific issue. Porous materials, in particular, have sparked considerable study attention due to their ability to combine the features of porous materials with polymers. To begin with, porous polymers can be engineered to have a larger surface area as well as well-constructed porosity. Second, polymeric porous materials are easily processed. They can, for example, be manufactured in moulded monolithic form or as thin films, which provides considerable benefits in many practical applications. Furthermore, unlike other forms of porous materials, such as porous organic polymers, some of them may be solved and then treated basically utilising solvent-related procedures without losing the porosity. Thirdly, the variety of polymer synthetic pathways makes it easier to design and build various porous materials capable of combining several chemical functions within the polymeric porous frameworks or at the tunable porosity over surface. This book chapter demonstrates the various applications of porous materials as heterogeneous catalyst. It also addressed current breakthroughs in their respective application areas, as well as the numerous hurdles that must be faced.

Keywords: *Heterogeneous Catalyst; Porous Materials; Catalysis*

Introduction

Physical reaction stages such as diffusion, adsorption, and desorption are as important as the chemical reaction itself in heterogeneous catalysed reactions since the starting materials must be delivered to the catalyst for the catalytic process to occur (Chongdar *et al*., 2022). Because of the benefits of facile catalyst separation from the reaction mixture, easy catalyst regeneration after the reactions, and non-corrosive to the reactor system, heterogeneous catalysts are currently more commonly utilised in industry than homogeneous catalysts. The market share of heterogeneous catalysts is now projected to be over 90%. Heterogeneous catalysis involving liquid-solid and gas-solid phases is of special interest, in part because it allows a catalytic material to be deposited and immobilized on the surface of a solid. Surfaces represent a distinct interface between a

material's bulk structure and its external environment. Unlike atoms in the bulk, surface atoms have an asymmetric environment, with their bonds pointing inward. This arrangement exposes free bonds on the surface, making it more reactive compared to the interior of the material. Surface atoms are highly reactive and can readily engage in chemical reactions with neighboring atoms or foreign species to satisfy their bonding needs. This reactivity plays a crucial role in surface-related phenomena and interactions in various fields of science and technology (Kolasinski, 2012).

The reactivity of surface atoms is indeed vital in catalytic reactions that take place on solid surfaces. Catalysis involves the interaction of reactant molecules with the catalyst's surface, where the surface atoms facilitate the conversion of reactants into desired products. The reactivity of surface atoms is influenced by various factors such as their coordination environment, electronic structure, and accessibility of active sites. By providing an active surface with appropriate bonding characteristics, catalysts can enhance the reaction rates and selectivity, enabling more efficient and effective transformation of reactants into desired products.

Literature Review

Porous Materials in Catalysis

High BET surface area porous nanostructured materials are excellent for catalytic processes, and the main active component for catalytic system (e.g., metals, organic functional groups, etc.) in heterogeneous catalysts is most significant. As a result, researchers are currently particularly interested in designing porous nanomaterials with catalytically active centres on their surfaces. In recent times, a number of reviews by (Pérez-Ramírez *et al*., 2008; Lopez-Orozco *et al*., 2011) and others are reported on the synthesis and applications over porous materials. Microporous materials, such as zeolites, have caused a massive economic and environmental revolution (Li *et al.*, 2014) in the industrial production process. These microporous materials are significant in industrial-scale shape-selective catalysis. The small pore openings of microporous materials have prompted researchers to concentrate their efforts on developing materials having pores of even bigger diameters in the nanoscale realm. Through supramolecular templating routes, this leads to the discovery of ordered mesoporous silicas. Mesoporous supports, such as mesoporous oxides, phosphates, carbons, and others, play an important part in the industrial production process for fine compounds that were created subsequently. Liquid phase catalytic reactions in heterogeneous fluids over mesoporous solids result in less diffusion than other porous materials. Other mesoporous materials used in industrial catalysis include carbons, phosphates, oxides, organic-inorganic hybrid periodic mesoporous organosilicas (Fujita & Inagaki, 2008), and polymers. In this study, we focus on heterogeneous catalytic processes mediated by a wide spectrum of mesoporous materials, as well as their chemical production using a clean and green technique.

Application of Porous Materials

Oxidation Reactions over Mesoporous Materials

One of the most pressing issues confronting the chemical business today is the need for cleaner, safer, and more environmentally friendly alternative manufacturing processes. Processes must be efficient in terms of both economics and energy use. In general, catalytic oxidation of hydrocarbons is used in the production of fine compounds. The selective catalytic oxidation of organic molecules employing ecologically safe and inexpensive oxidants such molecular oxygen and aqueous H2O2, as well as a heterogeneous, readily reusable catalyst, is a difficult aim for the fine chemical industry. By avoiding oligomerization of the active monomeric species, site isolation of discrete redox metal centres in inorganic matrices can provide oxidation catalysts with distinct activity and selectivities. Incorporating redox metal ions or complexes into the framework or cavities of these molecular sieves is one method of creating stable, solid catalysts with distinct activity. When oxidising organic compounds with large molecular sizes with a bulky oxidant such as tert-butyl hydroperoxide (TBHP), the use of mesoporous materials is strongly suggested by several researchers, (Delgado *et al*., 2023).

Various inorganic solid supports, such as silica, carbon, clay, zeolite, metal oxide polymers, and mesoporous materials, are utilized in catalytic processes. These supports offer advantages due to their high surface area, porous structure, tunable properties, thermal and chemical stability, and compatibility with different catalysts. Immobilizing or anchoring catalysts onto these solid supports enhances catalytic performance, enables catalyst recyclability, and provides control over reaction conditions (Corma, Garcia & Llabrés i Xamena, 2010). Through the process of heterogenization, it is possible to generate supported materials consisting of transition metals and Schiff base ligands in complex form. This approach allows for the immobilization of the catalytic species on solid supports, providing enhanced stability, recyclability, and control over the catalytic system. Supported polymers have become increasingly popular in catalytic oxidation due to their advantageous characteristics such as inertness, non-toxicity, non-volatility, and recyclability. These properties make them highly desirable for catalytic applications, allowing for efficient and environmentally friendly oxidation processes. Mesoporous materials have emerged as ideal catalyst supports among various inorganic supports due to their unique features. These materials possess a three-dimensional open pore network structure, high surface area, and porosity, allowing for efficient deposition of dynamic components. The uniform interconnected pores create an effective environment for interactions between the catalysts and reactants, enhancing catalytic performance. Furthermore, mesoporous materials exhibit high reusability and heat stability, making them highly suitable for catalytic applications (Kumar, *et al*, 2014). Heterogeneous catalysts facilitate oxidation reactions by attracting oxygen from oxidants, such as TBHP (tert-Butyl hydroperoxide) and HP (Hydrogen peroxide) (Biradar & Asefa, 2012). TBHP has been utilised as an oxidant in a variety of oxidation processes throughout the last decade, including alkyl benzene and benzyl alcohol

oxidation. We have discussed heterogeneous catalysts, their production techniques on diverse substrates, and applications in specific oxidation processes in this chapter.

Oxidation of Hydrocarbons

Homogeneous transition metal complexes such as Mn, Cr, V and also Ti, have been - impregnated into a various of inorganic silica frameworks, and these catalysts have been widely explored for the various hydrocarbons oxidation via liquid phase transformation such as alkenes, cycloalkenes, alkanes, as well as arenes. But, epoxidation of olefin compounds is particularly significant in organic conversion because epoxy compounds are used to make a variety of highly value-added fine chemicals such as unsaturated resins, polyurethanes, as well as glycols. The synthesis and separation of epoxides from alkene sources is similarly problematic, because subsequent oxidation to other yields often reduces the desired one (Nandi *et al*., 2011). As demonstrated in Figure 1, Cu- and Ni-incorporated mesoporous organosilica shows also an effective oxidising catalyst for the different olefins partial oxidation such as cyclohexene, norbornene, styrene, and stilbene under moderate circumstances (Nandi *et al*., 2011). The reaction proceeds by forming a metal a hydroperoxo active intermediate that, upon contact by the olefinic double bond, produces the matching high yield of epoxide.

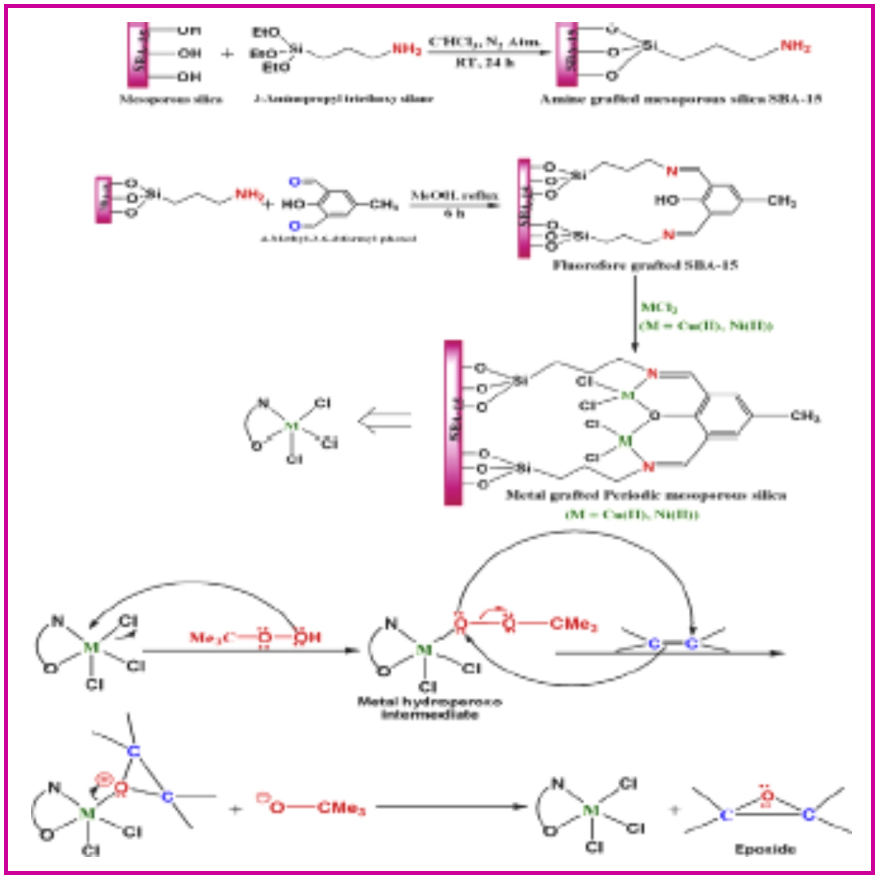

Figure 1: Different olefins Epoxidation Catalyzedny Cu- and Ni-grafted Porous Organosilica (Nandi et al., 2011)

Singh and colleagues (2009) provided a description of Cr-based silica, which has demonstrated effective catalytic properties in the oxidation of aromatic compounds like ethylbenzene and typical alkanes for example cyclohexane. When ethylbenzene is oxidized, the main product obtained is acetophenone, accompanied by a certain amount of benzaldehyde. On the other hand, the cyclohexane oxidized and give the yields as cyclohexanol, cyclohexanone, and a small quantity of benzoic acid (Singh *et al*., 2009 and Zhang *et al*., 2023). When hydrocarbons, specifically methane, undergo high-temperature oxidation in a fixed-bed down-flow reactor utilizing a Mo-SBA-15 material and molecular O_2 gas as an environmentally friendly oxidant, a noteworthy quantity of formaldehyde is generated (Lou *et al.*, 2008).

In contrast, the partial oxidation of various unsaturated alkenes and alkynes in the liquid phase has commonly utilized hydrogen peroxide as a mild and non-toxic oxidant. An example of this is the work conducted by Vasylyev and Neumann (2004) who successfully developed a newly mesoporous material composed of a zinc-based polyoxometalate. This innovative material demonstrated efficient catalytic activity in the epoxidation reactions of allylic alcohols, employing hydrogen peroxide (H_2O_2) as the oxidant. Different metal-based polyoxometalate supported hexagonal mesoporous silicas (Cu, Co, Ni) show great promise in the propylene oxidation to acetone under molecular oxygen (Liu *et al*., 2005). Table 1 provides a detailed summary of the many types of products produced by hydrocarbon oxidation.

Table 1: Various Oxidation Yields Generated by Various Hydrocarbon Compounds

Oxidant reagent	**Hydrocarbons**	**Various Oxidation yields**		**References**
		Examples of Reactants	**Possible Products Formed**	
Hydrogen peroxide (H_2O_2), aerial oxygen, TBHP, air, ozone, etc.	Saturated (alkanes)	Methane, butane, isobutane	Formaldehyde, maleic anhydride, methacrolein	Lou *et al.*, 2008
	Unsaturated (alkenes, allyl and alkynes)	Propylene	Acetone, propylene oxide, allyl alcohol	Liu *et al*., 2005
		Acetylene	Ethanol, glyoxal	Alzueta *et al*., 2008
		Allyl alcohol	Glycidol, glycerine	Vasylyev, & Neumann 2004
	Cycloalkanes and Cycloalkenes	Cyclohexane	Cyclohexanol, cyclohexanone, adipic acid	Singh *et al*., 2009

		Cyclohexene, cyclooctene	Cyclohexene oxide, cyclohexene-1-one, cyclohexene-1-ol, adipic acid, cyclooctene oxide, etc.	Nandi *et al*., 2011
	Aromatic hydrocarbons or arenes	Toluene, ethylbenzene, styrene, etc.	Acetophenone, benzaldehyde, benzoic acid, styrene oxide	Zhang *et al*., 2023

Oxidation of Alcohols

Mesoporous organic-inorganic hybrid solids incorporating transition metals have demonstrated their effectiveness in selectively oxidizing primary and secondary alcohols. The resulting aldehydes and ketones from the oxidation process hold significant value as intermediate compounds in various domains such as organic synthesis, pharmaceuticals, agricultural chemicals, and more. Traditional approaches utilizing stoichiometric quantities of transition metals like chromium (Cr), ruthenium (Ru), manganese (Mn), and others often generate substantial volumes of hazardous waste, rendering them environmentally unfriendly and non-reusable (Verma *et al*., 2011).

As a result, there is a strong demand for metal-based heterogeneous supports to promote environmentally friendly and sustainable advancements in the selectivity of alcoholic oxidation. This process utilizes non-polluting and harmless oxidants such as molecular oxygen and hydrogen peroxide (H_2O_2). Verma *et al*. (2011) have made noteworthy progress in this field, reporting high yields of ketones from secondary alcohols, diols, and α-hydroxy ketones under mild conditions. They achieved this by utilizing a silica-supported oxo-vanadium Schiff base complex, which proved to be an effective and recyclable catalyst for the desired oxidation reactions (Verma *et al*., 2011).

In their research, these scientists employed tert-butyl hydroperoxide (TBHP) for the oxidation process, which can generate toxic by-products. However, they also explored an alternative approach by utilizing molecular oxygen over a cobalt Schiff base complex grafted on SBA-15 through a 'click reaction.' This novel catalyst demonstrated exceptional catalytic activity in converting secondary alcohols into ketones, even at relatively lower temperatures. This advancement holds promise for a greener and more sustainable oxidation process. In a recent development, the conversion of primary alcohols to aldehydes has been successfully achieved using a catalyst known as Au@PMO (gold nanoparticles supported on periodic mesoporous organosilica) at room temperature. Remarkably, this transformation occurs by utilizing molecular oxygen (O_2) as the oxidant. This advancement represents a significant breakthrough in the field, offering a mild and efficient method for the selective oxidation of primary alcohols without the need for high temperatures or toxic reagents. The PMO material has been demonstrated to be an excellent support for gold nanoparticles (Au), as shown in Figure 2. It exhibits high reusability with minimal metal leaching, making it an environmentally friendly option for the

selective oxidation of C_6H_5OH to C_6H_5CHO under liquid-phase conditions. This finding highlights the potential of PMO as a stable and efficient catalyst for various oxidation reactions, providing a sustainable and eco-friendly alternative to chemical transformations (Karimi & Esfahani, 2012).

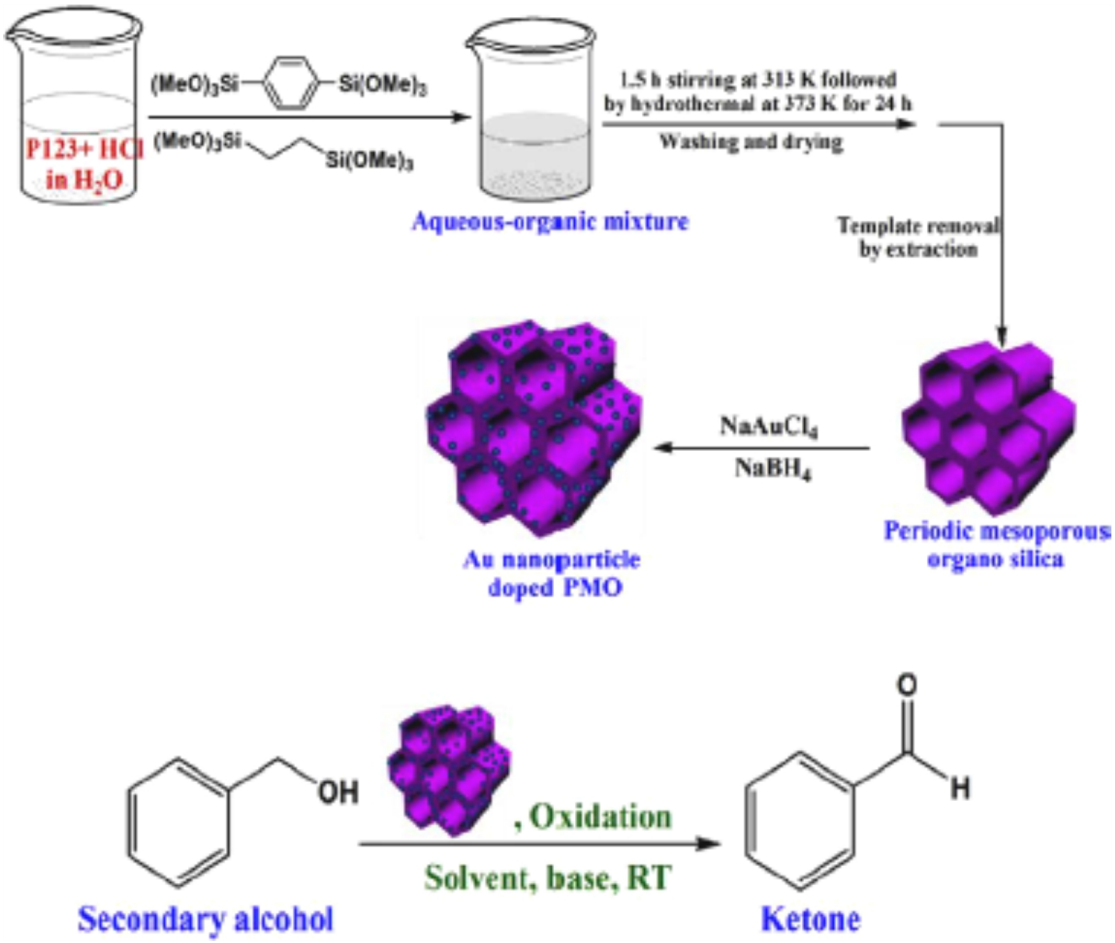

***Figure 2: Schematic Illustration for The Oxidation of Alcohol Catalyzed by The Au-Supported PMO Material* (Karimi & Esfahani, 2012)**

The Reaction of Hydrogenation

The process of hydrogenation, developed by scientist P. Sabatier in 1897, is a chemical reduction method widely utilized in various industrial sectors such as the food, pharmaceutical, agricultural, and petrochemical industries.his method has been universally developed to reduce or saturate organic compounds (Song, *et. al*., 2022) In this reaction, the typical procedure involves the addition of a pair of hydrogen atoms to unsaturated substrates that contain a double or triple bond. This results in the formation of saturated hydrocarbons or their derivatives. In some cases, hydrogenation can also be applied to saturated compounds, leading to ring-opening reactions (Kuhn *et.al.,* 2008). Due to the challenges associated with handling hydrogen gas, substitute hydrogen sources like

hydrazine and alcohols can be utilized as hydrogen donors in a process known as transfer hydrogenation. This technique is particularly valuable in organic synthesis for the asymmetric reduction of polar unsaturated substrates, including aldehydes, ketones, and imines. By using transfer hydrogenation, the selective and controlled reduction of these compounds can be achieved, offering a versatile approach to the synthesis of complex organic molecules (Paul, Pal & Bhaumik, 20 10).

The non-catalytic reaction-way for reduction reactions typically demanded extremely high temperatures and pressures, making it impractical for most applications. In contrast, catalyst-mediated procedures, whether homogeneous or heterogeneous, are more enviable and cost-effective. All of them facilitate reduction reactions at lower temperatures and pressures, enhancing reaction efficiency and selectivity. Additionally, catalysts can be recycled and reused, making them economically viable for large-scale industrial processes. Overall, catalyst-mediated reduction processes offer significant advantages over non-catalytic approaches in terms of feasibility, cost, and environmental impact (Kuhn *et al*., 2008). Indeed, catalysts play a crucial role in enabling enantioselective hydrogenation, which leads to the production of optically active products from prochiral compounds. In this context, two widely recognized homogeneous catalysts are Rh-based Wilkinson's catalyst and Ir-based Crabtree's catalyst. These catalysts have gained popularity for their ability to promote enantioselective hydrogenation reactions, allowing for the controlled synthesis of chiral compounds with specific optical properties. The development and utilization of such catalysts have significantly advanced the field of asymmetric synthesis, opening up new avenues for the production of pharmaceuticals, fine chemicals, and other important organic compounds. For industrial purposes, numerous heterogeneous catalysts have been developed specifically for asymmetric hydrogenation reactions. These catalysts enable the selective reduction of prochiral compounds to produce optically active products. The key strategy involves modifying the metal support of the catalyst with a chiral center, which imparts chirality to the catalyst and allows for enantioselective hydrogenation. By utilizing heterogeneous catalysts with chiral modifications, it becomes feasible to perform large-scale asymmetric hydrogenation reactions, offering a more practical and cost-effective approach for the industrial production of chiral compounds. Precious heavy metals such as palladium (Pd), platinum (Pt), and rhodium (Rh) are widely recognized as highly active catalysts for hydrogenation reactions. These metals exhibit excellent catalytic properties due to their ability to readily adsorb and activate hydrogen molecules. They are commonly used in various hydrogenation processes, ranging from the pharmaceutical industry to petrochemical applications.

Additionally, non-precious metals like nickel (Raney nickel) also serve as active catalysts for hydrogenation reactions. Raney nickel, a porous form of nickel, has exceptional hydrogenation activity and is often employed in industrial-scale hydrogenation processes due to its cost-effectiveness. Hydrogenation products of different substrates are given in Table 2.

Table 2: Hydrogenation Products of Different Substrates

Hydrogenating Agents	**Substrates**	**Possible Products Formed**	**References**
Gaseous H_2, hydrogen donor (cyclohexadiene, 2-propanol, hydrazine, etc.)	Alkene, $R_2C=CR'_2$ Alkyne, $RC\equiv CR'$ Aldehyde, RCHO Ketone, $R_2C=O$ Ester, RCO_2R' Imine, $RR'C\equiv NR''$ Amide, $RC(O)NR'_2$ Nitrile, RCN Nitro, RNO_2	Alkane, $R_2CH–CHR'_2$ Alkene, cis-RHC=CHR´ Primary alcohol, RCH_2OH Secondary alcohol, R_2CH-OH Two alcohols, RCH_2OH + R´OH Secondary amine, RR´CHNHR Tertiary amine, $RCH_2NR'_2$ Primary amine, RCH_2NH_2 Amine, RNH_2	W. Huang, *et. al.,* 2008 J.N. Kuhn, *et. al*, 2008 Tang *et al.,* 2010 S, Parambadath *et al*. 2009, H. Song, *et. al*, 2022

In the catalytic hydrogenation of aromatic nitro compounds, mesoporous oxides or mixed oxides supported with nanoparticles of gold (Au), nickel (Ni), platinum (Pt), and palladium (Pd) thioether have been found to be effective catalysts. These catalysts demonstrate the capability to promote the selective synthesis of aniline from nitrobenzene, employing hydrazine hydrate as the hydrogenating agent. Importantly, these hydrogenation reactions can be carried out under mild conditions.

To enhance the catalytic performance, mesoporous oxides such as TiO_2, Al_2O_3, SiO_2, and ZrO_2 are used as supports for the nanoparticles. The synthesis of these catalysts involves a surfactant-assisted route, which enables the creation of mesoporous structures with confined thioether nanoparticles of PtPd, AuPd, or AuPt. This synthesis method enhances the dispersion and stability of the nanoparticles, leading to improved catalytic activity and selectivity in the hydrogenation of nitrobenzene to aniline.

In contrast to the previous approach, it has been found that the conversion of nitrobenzene and its derivatives to anilines can be achieved using mesostructured nickel-aluminium mixed oxides as catalysts in the presence of 2-propanol as the solvent (Paul, Pal & Bhaumik, 2010). In this system, the catalyst itself is sufficient for the reduction process, and no additional hydrogenating agent is required.

The mesostructure of the catalyst is obtained through the use of lauric acid as a structure-directing agent, which helps in the formation of the desired nickel-aluminium mixed oxide with a mesoporous architecture. This mesoporous structure enhances the accessibility of the reactants to the active sites of the catalyst, thereby promoting the reduction of nitrobenzene and its derivatives to anilines.

An established catalyst with optical activity for the hydrogenation of a-(acetylamino)-cinnamic acid and its methyl ester is a mesoporous silica organic-inorganic hybrid matrix incorporating an anchored Rh complex.

A fascinating one-step hydrogenation/esterification reaction, that plays a vital role in the upgrading of bio-oil obtained from fast pyrolysis of biomass, has been effectively conducted using acetaldehyde and acetic acid on a mesoporous organosilica catalyst modified with metallic Pt. (Tang *et al.,* 2010). In contrast, a true heterogeneous catalyst has been demonstrated for the hydrogenation of nitrobenzene to aminobenzene at a temperature of 323 K under a 20 cm3/min H_2 flow. This catalyst consists of bimetal Pd-Ni nanoparticles deposited on Ti-doped hexagonal mesoporous silica, and its deposition is achieved using a simple photo-assisted deposition method (Schranck, Tlili & Beller, 2013). Conversely, a novel material for the asymmetric hydrogenation of ketones at room temperature, utilizing low to moderate H_2 pressure (<10-40 atm), is an organometallic Ir complex supported on SBA-15 with a chiral ligand. This catalyst has demonstrated good yield and enantioselectivity, reaching near about 93% enantiomeric excess (Liu *et al*, 2010). Parambadath *et al.,* 2010 conducted an investigation on the enantioselective transfer hydrogenation of prochiral ketones using an immobilized Ru(II)-Chiral (1R,2S)-(þ)-cis-1-amino-2-indanol catalyst supported on SBA-15. This catalytic system demonstrated excellent performance under mild reaction conditions, with 2-propanol acting as the hydrogen donor. Currently, this type of asymmetric transfer hydrogenation is recognized as an efficient method for synthesizing chiral molecules. It offers advantages such as low yields of side products, high productive yields, and a high enantiomeric purity. Huang *et al.,* (2008) reported the synthesis of Rh and Pt nanoparticles with a size of approximately 1 nm, which were incorporated within a fourth-generation polyaminoamide (PAMAM) dendrimer. These nanoparticles were subsequently loaded onto an SBA-15 support. The catalysts prepared in this manner were found to be effective for the hydrogenation reactions of pyrrole and ethylene. Specifically, pyrrole was converted to ethane, while ethylene was transformed into n-butylamine (Huang *et al.*, 2008). Figure 3 illustrates the schematic representation of the catalyst preparation process and the subsequent hydrogenation reaction carried out using the catalyst. Additionally, mesoporous polymers have been identified as effective supports for catalytic hydrogenation reactions (Salam *et al.,*2014) In a recent development, a ruthenium embedded over porous cross-linked polymer functionalized with a chiral ligand has demonstrated exceptional performance in terms of both high enantioselective conversion and remarkable reusability. This catalyst has been successfully applied to the asymmetric hydrogenation of a β-keto ester, conducted in methanol at a temperature of 323 K.

The majority of hydrogenation reactions follow a straightforward mechanistic pathway that involves several key steps. Initially, the hydrogen gas and the substrate bind to the surface of a solid catalyst. Subsequently, the hydrogen molecules dissociate into atomic hydrogen species. These atomic hydrogen species then add one by one to the substrate, resulting in

the stepwise addition of hydrogen atoms. Finally, the hydrogenated product desorbs from the surface of catalyst, completing the hydrogenation process.

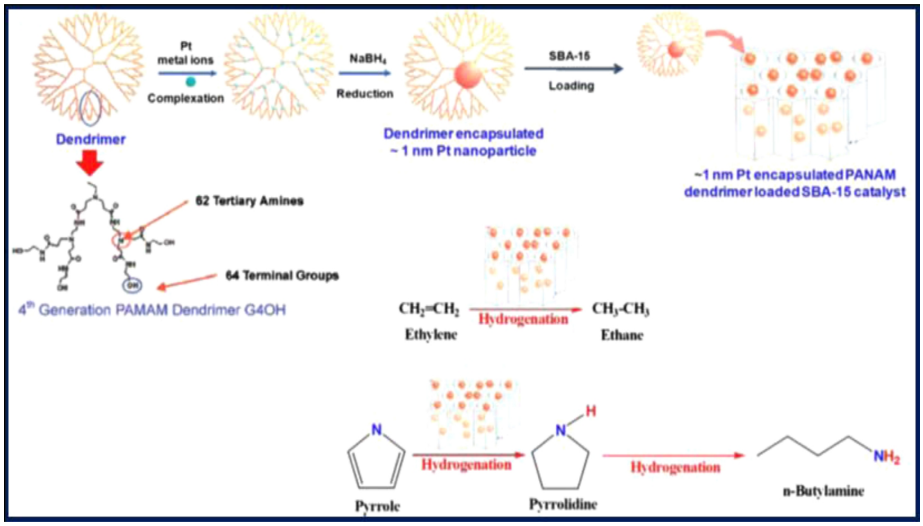

Figure 3: The Hydrogenation Reactions of Ethylene and Pyrrole Catalyzed by PANAM Dendrimer-Grafed Pt Nanoparticles Embedded Over SBA-15 Can Be Represented Schematically (Huang et al., 2008)

N-alkylation reactions

The formation of carbon-nitrogen bonds is a crucial and highly significant process in organic chemistry. It holds great importance in the development and composition of both chemical and biological systems. The N-alkylation of amines holds basic significance in organic synthesis due to the significant role of the resulting higher amines as versatile synthetic intermediates. These higher amines find extensive applications in the production of pharmaceuticals, agrochemicals, fine chemicals, dyes, surfactants, and functionalized materials. Some researchers conducted pioneering research in which alcohols were employed as direct alkylating agents for the N-alkylation of amines, utilizing transition metal catalysts. This represented the first instance of alcohol substitution by N-nucleophiles. Subsequently, significant efforts have been dedicated to the N-alkylation of amines and related reactions, focusing on the activation of alcohols through strategies such as borrowing hydrogen (BH) and hydrogen autotransfer (HA). These approaches have been extensively explored in the literature with the aim of achieving efficient and selective N-alkylation reactions. A variety of catalytic systems have been reported for N-alkylation reactions using alcohols as the alkylating agents (Pera-Titus *et al.,* 2014). The borrowing hydrogen (or hydrogen auto transfer) process involves the alcohol substitution in the presence of an amine or the N-alkylation of an amine with an alcohol, as shown in Figure 4. Mesoporous aluminosilicate nanoparticles have been found to possess unique catalytic properties for the solvent-free N-alkylation of aniline with benzyl alcohol. Under mild reaction conditions, this catalytic system enables the selective production of N-Benzylidenaniline with 100% selectivity (Sreenivasulu, Viswanadham & Saxena, 2014).

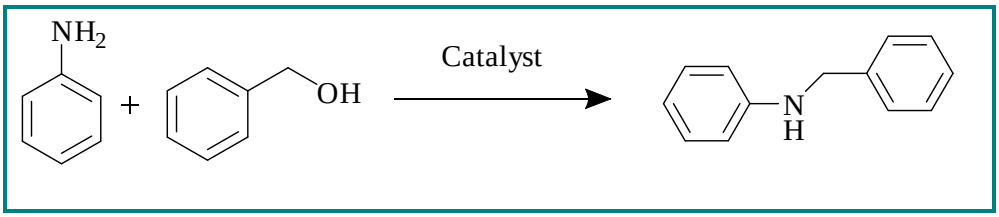

Figure 4: N-Alkylation Reaction Between Amine and Alcohol (Sreenivasulu, Viswanadham & Saxena, 2014)

A catalyst composed of a pyrimidine-substituted N-heterocyclic carbene-iridium complex supported on mesoporous silica (SBA-15) was employed for the environmentally friendly substitution reaction of primary alcohols with amines. This catalytic system facilitated the conversion of primary alcohols into secondary amine products, achieving yields ranging from 52% to 99%. (Wang *et al*., 2013). The catalyst demonstrated remarkable recyclability, maintaining its catalytic efficiency even after being reused for more than nine cycles. Another effective catalyst employed in the substitution of alcohols with amines was a bifunctional Ir-Zr metal-organic framework (MOF) (Rasero-Almansa *et al*., 2014). This catalyst exhibited excellent performance even in the presence of air and without the need for a base. Additionally, a cobalt nanoparticle catalyst supported on N-doped mesoporous carbon (Co/mCN-900) facilitated the reductive N-alkylation of nitroarenes with carbonyl compounds, resulting in the formation of aromatic secondary amines. Notably, this catalytic reaction proceeded under mild reaction conditions. In 2010, Luque and colleagues were the pioneers in reporting the microwave-assisted N-alkylation of amines with benzylic alcohols, utilizing nano-Fe-HMS (HMS referring to hexagonal mesoporous silica) as the catalyst. In a recent study by Paul *et al.,* 2017 a new catalyst called mesoporous silver nanoparticle-supported alumina ($Ag@Al_2O_3$) was synthesized. This innovative nanocatalyst exhibited exceptional catalytic activity in the N-alkylation of hetero (aromatic) amines and aromatic amines using alcohols as the alkylating agent. The catalytic process demonstrated green characteristics, being atom-economical and environmentally friendly. Additionally, the catalyst displayed air stability, and the active sites remained intact within the porous material without decomposition or leaching. These findings indicate that the catalyst is robust and exhibits heterogeneous behavior. (Paul *et al*., 2017).

Acylation Reactions

The acylation of amines, alcohols, and phenols is a widely used and cost-effective method for protecting, identifying, and characterizing these functional groups in multi-step synthetic processes.

Typically, acetic anhydride and acetyl chloride are employed in the presence of acidic or basic catalysts within an organic solvent for the acylation reactions. Acetyl chloride is widely used as an acylating agent due to its availability and affordability. However, it exhibits high reactivity and instability in aqueous environments. Therefore, numerous homogeneous and heterogeneous catalysts have been documented for this organic transformation. These catalysts assist in facilitating the acylation reaction and improving its efficiency. However,

the catalysts that have been reported so far have certain limitations. These include long reaction times, harsh reaction conditions, complicated workup procedures, and in some cases, the catalysts are sensitive to moisture or expensive. These drawbacks hinder their practical application and highlight the need for alternative catalysts that can overcome these challenges. The utilization of acetic acid instead of acetic anhydride or acetyl chloride offers both economic and environmental benefits. This is because substances employed in chemical synthesis can potentially be incorporated into the desired end product or become waste by-products. As the chemical industry strives for high yield and minimal waste, there is a growing emphasis on developing processes that align with these goals. By opting for acetic acid as a reagent, it contributes to the objective of reducing waste and achieving a more sustainable and efficient production process. The concept of "atom economy" has been introduced to assess the efficiency of a reaction by considering the fate of the reactants. In the context of acylation reactions, various greener catalytic methods have been developed. These methods include the acylation of amines using organic acids, the utilization of solid-supported reagents such as polymer-bound acylating agents, arylboronic or boronic acid derivatives, and the application of microwave irradiation. A wide range of catalysts has been reported for the acylation of amines, including transition metal salts, immobilized ionic liquids on mesoporous materials, and solid acid catalyst. These advancements in catalysis contribute to the development of more sustainable and environmentally friendly acylation processes.

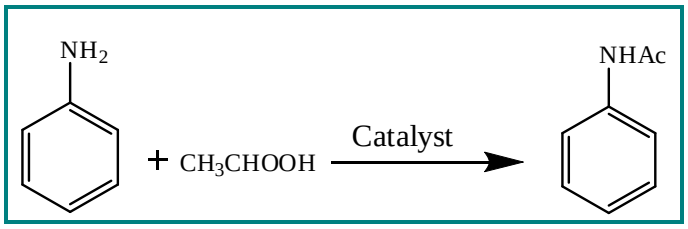

Figure 5: Acylation of Amines with Acetic Acid (Sharley & Jonathan, 2017)

Polysaccharide-derived mesoporous materials, specifically Starbon® acids, have been utilized for the efficient synthesis of various amides through acylation reactions. These reactions involve the combination of amines and acids in a 1:1 ratio. Starbon® acid, derived from renewable biomass sources, serves as a catalyst in these reactions and offers both high activity and selectivity. Moreover, the catalyst demonstrates excellent reusability, making it a sustainable and environmentally compatible option for the acylation of amines using acetic acid under microwave irradiation. The use of Starbon® acid contributes to the advancement of greener and more efficient synthetic methodologies.

A recent study by Shyamaprasad and colleagues described the acylation reactions of alcohols, phenols, and amines using mesoporous aluminophosphate solid acids as catalysts. The remarkable catalytic activity of aluminophosphate was attributed to its high surface area, surface acidity, and mesoporous structure. Notably, the reactions were carried out under solvent-free conditions, making the method environmentally friendly and suitable for industrial applications. The absence of solvents reduces the environmental impact and

improves the overall sustainability of the process. This research contributes to the development of greener and more efficient catalytic systems for acylation reactions. The acylation of various alcohols using acetic acid as the acylating agent has been investigated in the presence of sulfonic acid functionalized periodic mesoporous organosilicas (PMOs). The study demonstrates that the catalysts with high surface hydrophilicity exhibit a high selectivity for the formation of mono-acylated products. In contrast, catalysts with relatively higher hydrophobic characteristics exhibit enhanced selectivity towards the formation of di-acylated products. This observation indicates that the surface properties of the catalysts play a crucial role in determining the selectivity of the acylation reaction. The findings provide valuable insights for the design and optimization of catalysts for selective acylation reactions (Karimi *et al*., 2015).

Sustainable Production of Biodiesel

The utilization of lignocellulosic biomass for the production of chemicals, fuels, and energy has gained significant attention due to the increasing global energy consumption and the gradual depletion of fossil fuel resources. Lignocellulosic biomass, which includes plant materials such as agricultural residues, forestry residues, and dedicated energy crops, offers a renewable and abundant source of carbon that can be converted into valuable products. By efficiently converting lignocellulosic biomass, it is possible to reduce reliance on fossil fuels, mitigate greenhouse gas emissions, and promote a more sustainable and environmentally friendly approach to energy and chemical production. The development of technologies for the efficient conversion of lignocellulosic biomass holds great promise for achieving a more sustainable and diversified energy future. The utilization of lignocellulosic biomass and its derivatives for the production of chemicals, fuels, and energy has gained significant attention due to the increasing global energy demand and the depletion of fossil fuel resources. Various conversion methods, such as gasification, fermentation, hydrogenolysis, and chemical transformation, can be employed to extract value-added platform molecules and biofuels from lignocellulosic biomass and its derivatives. Levulinic acid (LA) and its esters have emerged as highly promising platform chemicals with diverse applications in the biofuel, solvent, polymer, and specialty chemicals industries (Figure 6). LA is typically produced through acid-catalyzed hydrolysis of lignocellulosic biomass, including cellulose, glucose, and fructose. It can be further upgraded catalytically into levulinate esters, γ-valerolactone (GVL), α-methylene-γ-valerolactone, olefins (via ring-opening and decarboxylation of GVL), 2-methyl tetrahydrofuran (via 1,4-pentanediol), 5-nonanone (via pentanoic acid), and diphenolic acid. These derivatives serve as important intermediates for the synthesis of various products such as biofuels, solvents, epoxy resins, polycarbonates, and more. Levulinate esters have proven to be valuable in applications such as plasticizers and solvents, and they have also been proposed as fuel additives. One specific example is ethyl levulinate, which can be utilized as a diesel miscible biofuel in regular diesel car engines at concentrations of up to 5 wt.%. This is possible due to its physicochemical properties, which are comparable to those of biodiesel fatty acid methyl esters (FAME). The use of ethyl levulinate as a biofuel additive offers a potential alternative

to conventional diesel fuels, contributing to the development of more sustainable and environmentally friendly transportation options.

The production of levulinate esters from cellulosic biomass not only provides a cost-effective alternative method for their synthesis but also offers the potential to decrease reliance on petroleum-derived fossil fuels. In acid-catalyzed esterification reactions, various heterogeneous acid catalysts have been identified as effective. These catalysts include acid resins, heteropolyacids, zeolites, metal oxides, and metal salts, among others. These catalysts play a crucial role in promoting the esterification reaction, facilitating the conversion of levulinic acid or its derivatives with alcohols to form the desired levulinate esters. The utilization of such heterogeneous acid catalysts enables sustainable and environmentally friendly production of levulinate esters from cellulosic biomass, contributing to the overall goal of reducing dependence on fossil fuels.

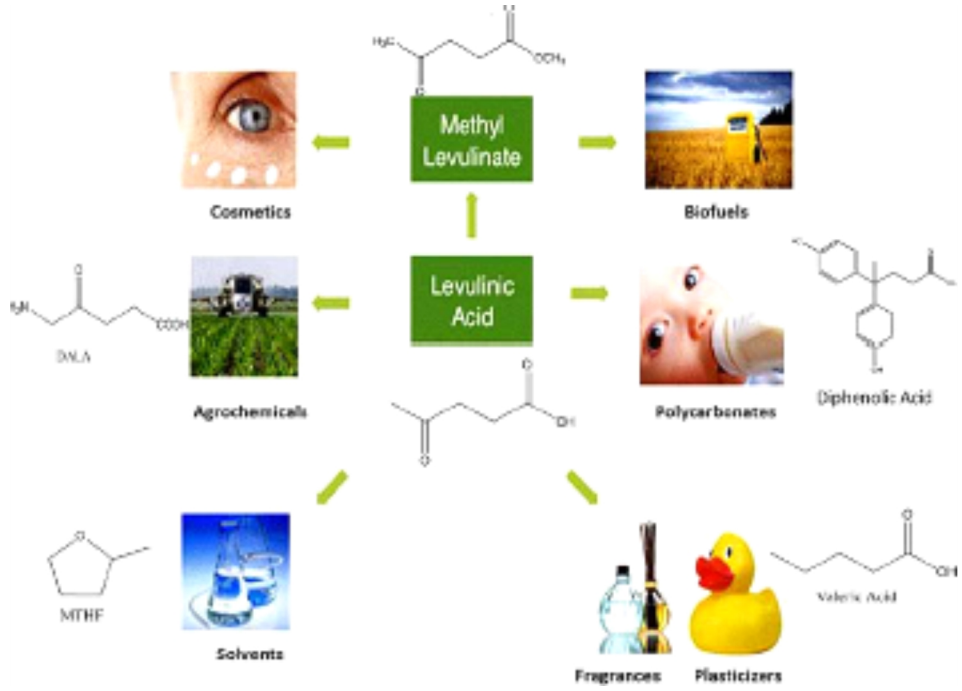

Figure 6: Levulinic Acid Derivatives and their Applications (Pileidis & Titirici 2016)

The esterification reaction by levulinic acid (LA) with alcohols, such as ethanol or 1-butanol, can occur at room temperature, but it proceeds slowly and requires acceleration either through elevated temperatures (70–100 °C) or the use of a catalyst to achieve a desirable conversion rate within a reasonable timeframe. By applying higher temperatures, the reaction kinetics are enhanced, leading to increased reaction rates and improved conversion. Alternatively, the addition of a catalyst can facilitate the esterification process by lowering the activation energy, allowing the reaction to proceed more rapidly even at lower temperatures. These strategies ensure efficient and timely conversion of LA and alcohols to the desired ester products.

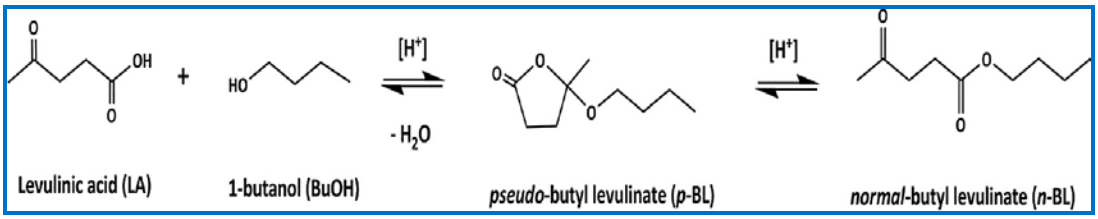

Figure 7: Levulinic acid Esterification with BuOH to n-butyl Levulinate (Kuwahara, Fujitani & Yamashita, 2014)

Solid acids, such as zeolites and sulfated mixed oxides, have been employed in the esterification reaction between levulinic acid and alcohols. Examples of these solid acids include sulfated zirconia (SO_4^{2-}/ZrO_2), titania (SO_4^{2-}/TiO_2), niobia (SO_4^{2-}/Nb_2O_5), and stannia (SO_4^{2-}/SnO_2). These solid acid catalysts exhibit strong acidity, which promotes the esterification reaction by facilitating the protonation of levulinic acid and alcohol molecules, leading to the formation of ester bonds. The presence of sulfated species enhances the catalytic activity of these solid acids, making them effective in promoting the esterification reaction and achieving high conversion of levulinic acid with alcohols.

The sulfated mixed oxides, which possess highly acidic sites, have emerged as the most talented materials for the esterification reaction caused by levulinic acid with alcohols. These catalysts demonstrate excellent catalytic activity, ensuring efficient conversion of levulinic acid to esters within an appropriate reaction time. The presence of robust acid sites on the sulfated mixed oxides facilitates the protonation of levulinic acid and alcohols, thereby promoting the esterification reaction and enhancing overall catalytic performance. Consequently, these sulfated mixed oxides are highly regarded as effective catalysts for the esterification process.

The activity of the sulfated mixed oxides is influenced by the quantity and strength of acid sites as well as the preparation conditions. Enhancements in catalyst activity can be achieved by optimizing the synthesis conditions, increasing the density of acid sites, and improving the dispersion of sulfate species. To this end, the introduction of mesopores in the mixed oxides using a surfactant-induced self-assembly approach represents a potential strategy. This approach allows for the controlled creation of mesopores, which can facilitate improved accessibility of reactants to the active acid sites, leading to enhanced catalytic activity. An alternative approach involves achieving a fine dispersion of the active oxide phase on a suitable neutral support with a larger surface area, such as mesoporous silica materials. By dispersing the active oxide phase evenly on the support material, the catalyst's efficiency can be improved. This strategy allows for better interaction between the active sites and the reactants, leading to enhanced catalytic performance. The high surface area and structural characteristics of mesoporous silica materials make them well-suited for supporting and stabilizing the active oxide phase, thereby promoting effective catalytic reactions. Both methods, namely the introduction of mesopores and the diffusion of the active oxide

phase on a larger surface area support, contribute to enhancing the catalytic activity of these materials in liquid-phase reactions. The resulting high surface area allows for higher dispersion of the active species and an increased density of acid sites, which are crucial for catalytic activity. Additionally, these methods facilitate improved mass transport of reactant and product molecules, leading to enhanced reaction rates. Overall, these approaches improve the accessibility of the active sites and promote efficient molecular interactions, thereby enhancing the catalytic performance of liquid-phase reactions. W. Ciptonugroho *et al.,* 2016 reported the synthesis of WOx/mesoporous-ZrO_2 catalysts via evaporation induced self-assembly (Ciptonugroho *et al*., 2016**)**. The catalysts were evaluated for the esterification of levulinic acid with 1-butanol. Catalysts containing 20–25 wt.% WO_3 demonstrated the formation of WO3 nanoparticles along with polytungstic species and tetragonal ZrO_2. These catalyst materials displayed a significantly high concentration of surface acid centers, ranging from 0.10 to 0.11 mmol/g, with a predominance of Brnsted acidity. Notably, this led to a remarkable enhancement in catalytic activity for the esterification reaction, with turnover frequencies (TOFs) reaching up to 0.16 s-1. Cheng *et al.*, 2016 investigated the esterification of levulinic acid with *n*-hexanol using mesoporous HSiW/MCM-41 as a catalyst (Cheng *et al*., 2016).

Conclusion

Porous materials are required to possess two fundamental characteristics: a significant pore volume and a well-defined pore structure tailored to achieve the desired performance of the material. The pores within the material can be considered functional phases that designers and users aim to optimize for the material's performance. These pores play a crucial role in enhancing the material's properties and functionalities by providing an optimized environment for specific applications. This chapter highlights the significance of porous polymeric materials in advancing future research in chemistry. Mesoporous materials, in particular, offer unique properties that make them valuable in this field. These materials possess a high surface area, a uniform pore size distribution, abundant, well-distributed active sites, and facilitate the easy diffusion of large molecules through their channels. These characteristics make mesoporous materials highly desirable for various applications, as they provide an ideal platform for carrying out chemical reactions and promoting efficient molecular interactions. The use of functionalized porous solids as heterogeneous catalysts offers numerous advantages. These materials enable the development of interactive materials where multiple physical properties can interact at the nanoscale. Additionally, functionalized porous solids are environmentally friendly as they are non-corrosive and non-hazardous. They also facilitate easy recovery and reusability of catalysts, making them highly attractive for sustainable and efficient catalytic processes. By leveraging the unique properties of functionalized porous solids, researchers can explore new avenues in catalysis and advance green chemistry practices.

The use of transition metal-grafted mesoporous polymeric materials as catalysts has shown remarkable advancements in various organic reactions. This thesis discussion highlights the significant progress made in the development of supported reusable catalysts and their

application in different reactions. The incorporation of porous materials as catalyst supports has proven to be highly beneficial, enabling enhanced recyclability of the catalysts and achieving higher catalytic activity compared to their unsupported counterparts. This emphasizes the potential of porous material-supported catalysts to improve the efficiency and sustainability of catalytic processes. Overall, the findings presented in the thesis underscore the importance and effectiveness of transition metal-grafted mesoporous polymeric materials as highly active and reusable catalysts in organic chemistry.

Acknowledgment

NS acknowledges the Department of Chemistry, Surendranath College, Kolkata, West Bengal, for their support and encouragement in implementing this book chapter. NS is also grateful to DBT-Star for providing college grants to the Department of Chemistry, Government of India. UM also acknowledges the Department of Chemistry, Jogamaya Devi College, Kolkata, 700026, W.B., India.

Reference

Alzueta, M. U., Borruey, M., Callejas, A., Millera, A., & Bilbao, R. (2008). An Experimental and Modeling Study of The Oxidation of Acetylene in A Flow Reactor. *Combustion and flame*, *152*(3), 377-386. https://doi.org/10.1016/j.combustflame.2007.10.011

Biradar, A. V., & Asefa, T. (2012). Nanosized Gold-Catalyzed Selective Oxidation of Alkyl-Substituted Benzenes and N-Alkanes. *Applied Catalysis A: General*, *435*, 19-26. https://doi.org/10.1016/j.apcata.2012.05.029

Cheng, C., Liu, H., Dai, P., Shen, X., Zhang, J., Zhao, T., & Zhu, Z. (2016). Microwave-Assisted Preparation and Characterization of Mesoporous Activated Carbon from Mushroom Roots by Phytic Acid (C6H18O24P6) Activation. *Journal of the Taiwan Institute of Chemical Engineers*, *67*, 532-537.

Chongdar, S., Bhattacharjee, S., Bhanja, P., & Bhaumik, A. (2022). Porous Organic–Inorganic Hybrid Materials for Catalysis, Energy and Environmental Applications. *Chemical Communications*, *58*(21), 3429-3460.

Ciptonugroho, W., Al-Shaal, M. G., Mensah, J. B., & Palkovits, R. (2016). One Pot Synthesis of Wox/Mesoporous-Zro2 Catalysts for The Production of Levulinic-Acid Esters. *Journal of Catalysis*, *340*, 17-29.

Corma, A., Garcia, H. I., & Llabrés i Xamena, F. X. (2010). Engineering Metal Organic Frameworks for Heterogeneous Catalysis. *Chemical Reviews*, *110*(8), 4606-4655.

Delgado, R., Márquez-Álvarez, C., Mayoral, Á., de la Serna, R., Agúndez, J., & Pérez-Pariente, J. (2023). Gold Clusters Immobilized by Post-Synthesis Methods on Thiol-Containing SBA-15 Mesoporous Materials for The Aerobic Oxidation of Cyclohexene: Influence of Light and Hydroperoxide. *Chemistry*, *5*(1), 526-543.

Fujita, S., & Inagaki, S. (2008). Self-Organization of Organosilica Solids with Molecular-Scale and Mesoscale Periodicities. *Chemistry of Materials*, *20*(3), 891-908.

Huang, W., Kuhn, J. N., Tsung, C. K., Zhang, Y., Habas, S. E., Yang, P., & Somorjai, G. A. (2008). Dendrimer Templated Synthesis of One Nanometer Rh and Pt Particles Supported on Mesoporous Silica: Catalytic Activity for Ethylene and Pyrrole Hydrogenation. *Nano Letters*, *8*(7), 2027-2034.

Karimi, B., & Esfahani, F. K. (2012). Gold nanoparticles supported on the periodic mesoporous organosilicas as efficient and reusable catalyst for room temperature aerobic oxidation of alcohols. *Advanced Synthesis & Catalysis*, *354*(7), 1319-1326.

Karimi, B., Mirzaei, H. M., Mobaraki, A., & Vali, H. (2015). Sulfonic Acid-Functionalized Periodic Mesoporous Organosilicas in Esterification and Selective Acylation Reactions. *Catalysis Science & Technology*, *5*(7), 3624-3631.

Kolasinski, K. W. (2012). *Surface Science: Foundations of Catalysis and Nanoscience*. John Wiley & Sons.

Kuhn, J. N., Huang, W., Tsung, C. K., Zhang, Y., & Somorjai, G. A. (2008). Structure Sensitivity of Carbon− Nitrogen Ring Opening: Impact of Platinum Particle Size from Below 1 To 5 Nm Upon Pyrrole Hydrogenation Product Selectivity Over Monodisperse Platinum Nanoparticles Loaded onto Mesoporous Silica. *Journal of the American Chemical Society*, *130*(43), 14026-14027.

Kumar, A., Kumar, V. P., Kumar, B. P., Vishwanathan, V., & Chary, K. V. (2014). Vapor Phase Oxidation of Benzyl Alcohol Over Gold Nanoparticles Supported on Mesoporous Tio 2. *Catalysis letters*, *144*, 1450-1459.

Kuwahara, Y., Fujitani, T., & Yamashita, H. (2014). Esterification Of Levulinic Acid With Ethanol Over Sulfated Mesoporous Zirconosilicates: Influences of The Preparation Conditions On The Structural Properties And Catalytic Performances. Catalysis Today, 237, 18-28.

Li, Z. M., Zhou, Y., Tao, D. J., Huang, W., Chen, X. S., & Yang, Z. (2014). MOR Zeolite Supported Brønsted Acidic Ionic Liquid: An Efficient and Recyclable Heterogeneous Catalyst for Ketalization. *RSC Advances*, *4*(24), 12160-12167. https://doi.org/10.1039/C4RA00092G

Liu, G., Wang, J., Huang, T., Liang, X., Zhang, Y., & Li, H. (2010). Mesoporous Silica-Supported Iridium Catalysts for Asymmetric Hydrogenation Reactions. *Journal of Materials Chemistry*, *20*(10), 1970-1975.

Liu, Y., Murata, K., Inaba, M., & Mimura, N. (2005). Design heteropolyacid catalyst for selective vapor-oxidation of propylene to acetone by molecular oxygen. *Leading Edge Catalyis Research*, 41.

Lopez-Orozco, S., Inayat, A., Schwab, A., Selvam, T., & Schwieger, W. (2011). Zeolitic Materials with Hierarchical Porous Structures. *Advanced Materials*, *23*(22-23), 2602-2615.

Lou, Y., Tang, Q., Wang, H., Chia, B., Wang, Y., & Yang, Y. (2008). Selective oxidation of methane to formaldehyde by oxygen over SBA-15-supported molybdenum oxides. *Applied Catalysis A: General*, *350*(1), 118-125.

Nandi, M., Roy, P., Uyama, H., & Bhaumik, A. (2011). Functionalized Mesoporous Silica Supported Copper (II) And Nickel (II) Catalysts for Liquid Phase Oxidation of Olefins. *Dalton Transactions*, *40*(46), 12510-12518.

Parambadath, S., & Singh, A. P. (2009). Ru (II)-Chiral (1R, 2S) -(+)-Cis-1-Amino-2-Indanol Immobilized Over SBA-15 For Asymmetric Transfer Hydrogenation Reaction of Prochiral Ketones. *Catalysis Today*, *141*(1-2), 161-167.

Paul, M., Pal, N., & Bhaumik, A. (2010). Mesoporous Nickel–Aluminum Mixed Oxide: A Promising Catalyst in Hydride-Transfer Reactions.

Paul, P., Bhanja, P., Salam, N., Mandi, U., Bhaumik, A., Alam, S. M., & Islam, S. M. (2017). Silver Nanoparticles Supported Over Mesoporous Alumina as An Efficient Nanocatalyst For N-Alkylation of Hetero (Aromatic) Amines and Aromatic Amines Using Alcohols as Alkylating Agent. *Journal of colloid and interface science*, *493*, 206-217.

Pera-Titus, M., & Shi, F. (2014). Catalytic Amination of Biomass-Based Alcohols. *ChemSusChem*, *7*(3), 720-722.

Pérez-Ramírez, J., Christensen, C. H., Egeblad, K., Christensen, C. H., & Groen, J. C. (2008). Hierarchical Zeolites: Enhanced Utilisation of Microporous Crystals In Catalysis By Advances In Materials Design. *Chemical Society Reviews*, *37*(11), 2530-2542.

Pileidis, F. D., & Titirici, M. M. (2016). Levulinic Acid Biorefineries: New Challenges for Efficient Utilization of Biomass. *ChemSusChem*, *9*(6), 562-582.

Rasero-Almansa, A. M., Corma, A., Iglesias, M., & Sánchez, F. (2014). Design Of a Bifunctional Ir–Zr Based Metal–Organic Framework Heterogeneous Catalyst for the N-Alkylation of Amines with Alcohols. *ChemCatChem*, *6*(6), 1794-1800.

Salam, N., Banerjee, B., Roy, A. S., Mondal, P., Roy, S., Bhaumik, A., & Islam, S. M. (2014). Silver Nanoparticles Embedded Over Mesoporous Organic Polymer as Highly Efficient and Reusable Nanocatalyst for The Reduction of Nitroarenes and Aerobic Oxidative Esterification of Alcohols. *Applied Catalysis A: General*, *477*, 184-194.

Schranck, J., Tlili, A., & Beller, M. (2013). More Sustainable Formation of CN And CC Bonds for The Synthesis Of N-Heterocycles. *Angewandte Chemie (International ed. in English)*, *52*(30), 7642-7644.

Sharley, D. D. S., & Williams, J. M. (2017). Acetic Acid as A Catalyst for the N-Acylation of Amines Using Esters as The Acyl Source. *Chemical Communications*, *53*(12), 2020-2023.

Singh, A. P., Torita, N., Shylesh, S., Iwasa, N., & Arai, M. (2009). Catalytic Aerobic Oxidation of Cyclohexane and Ethyl Benzene Over Chromium-Containing Mesoporous Organosilicas. *Catalysis letters*, *132*, 492-499.

Song, H., Xiao, Y., Zhang, Z., Xiong, W., Wang, R., Guo, L., & Zhou, T. (2021). Switching Selectivity in Copper-Catalyzed Transfer Hydrogenation of Nitriles to Primary Amine-Boranes and Secondary Amines Under Mild Conditions. *The Journal of Organic Chemistry*, *87*(1), 790-800.

Sreenivasulu, P., Viswanadham, N., & Saxena, S. K. (2014). Facile Synthesis of Mesoporous Aluminosilicate Nanoparticles for The Selective Production Of N-Benzylidenaniline in A Solvent-Free Reaction of Aniline with Benzyl Alcohol. *Journal of Materials Chemistry A*, *2*(20), 7354-7359.

Tang, Y., Miao, S., Shanks, B. H., & Zheng, X. (2010). Bifunctional mesoporous organic–inorganic hybrid silica for combined one-step hydrogenation/esterification. *Applied Catalysis A: General*, *375*(2), 310-317.

Vasylyev, M. V., & Neumann, R. (2004). New Heterogeneous Polyoxometalate Based Mesoporous Catalysts for Hydrogen Peroxide Mediated Oxidation Reactions. *Journal of the American Chemical Society*, *126*(3), 884-890.

Verma, S., Nandi, M., Modak, A., Jain, S. L., & Bhaumik, A. (2011). Novel Organic-Inorganic Hybrid Mesoporous Silica Supported Oxo-Vanadium Schiff Base for Selective Oxidation of Alcohols. *Advanced Synthesis & Catalysis*, *353*(11-12), 1897-1902. https://doi.org/10.1002/adsc.201100018

Wang, D., Guo, X. Q., Wang, C. X., Wang, Y. N., Zhong, R., Zhu, X. H., ... & Hou, X. F. (2013). An Efficient and Recyclable Catalyst For N-Alkylation of Amines And B-Alkylation of Secondary Alcohols with Primary Alcohols: SBA-15 Supported N-Heterocyclic Carbene Iridium Complex. *Advanced Synthesis & Catalysis*, *355*(6), 1117-1125.

Zhang, C., Luo, J., Xie, B., Liu, W., & Zhang, J. (2023). Green and Continuous Aerobic Oxidation of Ethylbenzene Over Homogeneous and Heterogeneous NHPI In a Micro-Packed Bed Reactor. *Chemical Engineering Journal*, 143674.

https://doi.org/10.31674/book.2023pcbs009

Hydrogen Production from Biomass

Pradipta Pal, Indrajit Saha, Susmita Jana, Lalita Das*
Department of Chemistry, Surendranath College, Kolkata, West Bengal, India

*Corresponding Author's Email: das.lalita1@gmail.com

ABSTRACT

Nowadays, hydrogen plays a major role as a fuel and in future energy infrastructure for producing heat and power. Hydrogen is used as an energy source. Currently, about 50% of hydrogen is produced through thermo-catalytic and gasification processes using natural gas, heavy oils, naphtha, etc. Recently, much research has focused on sustainable energy production from biomass to replace non-renewable sources. For this purpose, H_2 production from biomass and biomass derivatives is a promising route. Biomass is an abundant, clean, and sustainable source and consumes atmospheric carbon dioxide during its growth. Biomass produces less CO_2 compared to fossil fuels during hydrogen production. Various processes are used for hydrogen manufacturing from biomass. Generally, H_2 is produced through thermochemical and biological methods. Thermochemical processes include pyrolysis, gasification, and supercritical water gasification, and they are widely popular for their high efficiency and low production cost. Biological processes are more environment friendly and less energy intensive than thermochemical processes. Biological processes mainly include Biophotolysis, Fermentation, Biological water gas shift, and Hybrid reactor systems. These H_2 production techniques, their future aspects, and their developments are mainly highlighted in this paper. The effect of the catalyst, different reaction conditions, and the analysis of different types of biomass are mentioned in this paper.

Keywords: *Biomass; Hydrogen; Gasification; Pyrolysis; Biophotolysis; Fermentation*

Introduction

Nowadays, the whole world is completely dependent on non-renewable energy sources. In the 20th century, petroleum has become the primary source of energy for transportation. The increasing cost of petroleum, the limited source of fossil fuels, and concerns regarding the greenhouse effect, health hazards, and safety precautions are forcing us to search for new energy sources. For this purpose, continuous efforts have been made to find renewable energy sources. Increasing energy demand reduced the amount of fossil fuel.

For this purpose, hydrogen is a significant candidate. Hydrogen generates electrical power in a fuel cell, emitting only water vapor and warm air and nearing zero percent greenhouse gas emissions. H_2 has a higher energy yield (122 Kj/g) than hydrocarbon fuels. H_2 is a secondary energy source that has to be generated like electricity.

Research on biomass has recently received increasing attention because of the probable waste-to-energy application. Using biomass instead of fossil fuels to produce H_2 is a better

approach to reducing the net amount of CO_2 in the environment. H_2 is used as a fuel in electric vehicles and in many other applications. It holds promise as a dream fuel of the future with many social, economic, and environmental benefits.

Literature Review

Various Type of Biomass Sources for Energy Production:

Various types of biomasses can be used for producing energy. They can be divided into some general categories.

1. Energy Crops: Energy crops are low cost and low maintenance crops. They are grown only for renewable bio-energy production (not edible). Wood, sugar and starch crops, hydrocarbon producing crops are called energy crops.

2. **Agricultural Waste:** which are mostly left on the fields after harvesting such as rice straw, wheat straw, rice husk, crop waste and animal waste.

3. Forest Residues: These residues include mill wood waste, bark, logging residues, trees and shrub residues.

4. Industrial and Municipal Wastes: These are mainly including municipal solid waste (MSW), sewage sludge and waste materials of several industries.

Component of Biomass:

Biomass components have an important role in Bio-fuels production. Mainly, biomass consists of lignocellulose and a trace amount of minerals. Lignocellulose is composed of cellulose, hemicelluloses, lignin, and extractives. Cellulose [$(C_6H_{10}O_5)n$], hemicellulose ($(C_5H_8O_4)n$) and lignin have high molecular weights and contribute much mass, while extractives have small molecular sizes. Cellulose, hemicellulose, and extractives are more abundant in hardwoods (78.8%) than softwoods (70.3%), while lignin is more abundant in softwoods (29.2%) than hardwoods (21.7%). Generally, hardwoods consist of about 43% cellulose, 35% hemicellulose, and 22% lignin, while softwoods contain about 43% cellulose, 28% hemicellulose and 29% lignin (on an extractive-free basis) (Balat, 2008; Demirbas *et al.,* 2009a).

Cellulose is more abundant in the cell walls of plants. Cellulose is a high-molecular-weight (106 or more) linear polymer of *β*-1,4-linked D-glucose units in the 4C1 conformation. Glucose anhydride is formed by removing water from the glucose molecule. Glucose anhydrate units are linked through *β*-1,4 glycosidic bond. Cellulose contains nearly 5000-10,000 cellobiose units (glucose anhydride).

Hemicellulose is a heteropolymer consisting of various monoccharides such as glucose, mannose, galactose, xylose, arabinose, 4-O-methyl glucuronic acid, and galacturonic acid residues. Among these, Xylose is the major one. The number of repeating saccharide monomers is less in hemicellulose (~150) compared to the number in cellulose (5000-10,000).

Lignin is an aromatic polymer synthesized from phenylpropanoid precursors (Lignols). The lignin fraction consists of non-sugar molecules that are bonded via C-O and C-C bonds. It contains a variety of functional groups, such as hydroxyl, methoxyl, and carbonyl, which give a high polarity to the lignin polymer.

Hydrogen Production Routes from Biomass:

H_2 is mainly produced from biomass through Thermochemical and Biological methods. Thermochemical process further divided into some subdivision: pyrolysis, gasification and super critical water gasification and also biological process has four subdivisions: Bio photolysis, fermentation, biological water gas shift and hybrid reactor system. Hydrogen production from biomass by using thermochemical route has been considered as most promising route.

Basically, thermochemical routes have higher hydrogen production rate than biological process. In presence of heat, biomass molecules break down and produce Bio-H2.

Biological production of hydrogen from biomass is a new section of biotechnology that offers effective production of usable hydrogen. The biological process started receiving attention when the oil crisis broken out in 1970s. Most of the biological techniques are controlled by the hydrogen-producing enzymes such as hydrogenase and nitrogenase. Bio-hydrogen provides low pollution and high working efficiency. Currently, most of the hydrogen is produced through pyrolysis and gasification processes.

Thermochemical Process

Pyrolysis

The pyrolysis process is the thermal breakdown of substances at high temperatures in an inert atmosphere. In pyrolysis, solid (char), liquid (tar and other organic compounds), and gaseous (syngas) products are formed, which are used as alternative sources of energy. In biomass pyrolysis, approximately 650 -800 K is required. A hydrogen production strategy is shown in Figure 1.

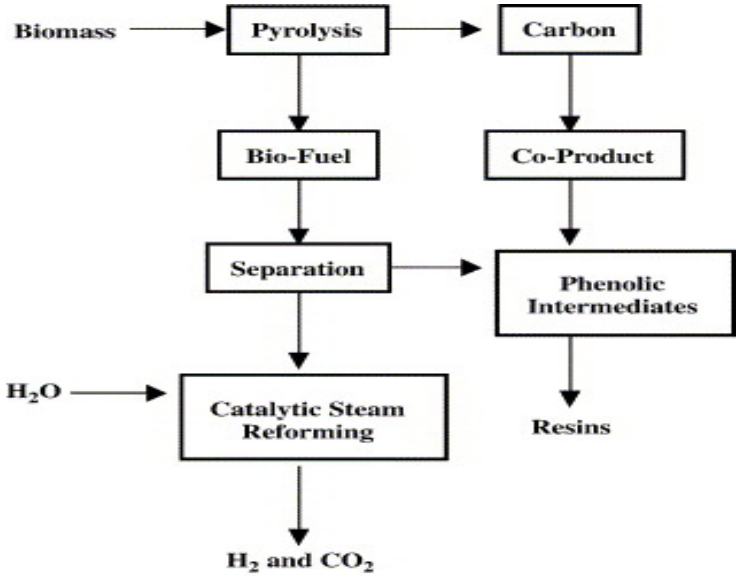

Figure 1: Hydrogen Production Strategy from Biomass Pyrolysis (Ni et al., 2006)

conventional (slow) pyrolysis, fast pyrolysis and flash pyrolysis are the subdivisions of pyrolysis process which are categorized based on working conditions.

In Slow pyrolysis heating rate is lower and charcoal is formed as major product. In the fast pyrolysis requires much faster heating rates (about 10-200°Cs^{-1}), it is associated with tar at low temperature (675-775K) and gas at high temperature. Fast pyrolysis is better than slow pyrolysis. Flash pyrolysis is an improved version of fast pyrolysis where the heating rate is very high (near about >1000°Cs^{-1}) and the reaction is complete within few seconds.

currently fast or flash pyrolysis is widely used. The thermal break down of biomass species is represented by following reaction:

Biomass + Heat → H_2 + CO + CH_4 + other products

Steam reforming process is carried out on CH_4 and other hydrocarbon vapors to form CO and H_2.

$CH_4 + H_2O \rightarrow CO + 3H_2$

Water-gas shift reaction is applied as follows to increase the production of H_2:

$CO + H_2O \rightarrow CO_2 + H_2$

The pyrolysis of biomass is not an easy task. Some factors (types of biomass species, chemical and structural composition of biomass, particle size, temperature, heating rate, atmospheric conditions, etc.) affect the yield and the composition of the products. High temperatures and a high heating rate are required in hydrogen manufacturing. An experiment showed that the gaseous yield increases to around 40–50% at 1023 K, while the yield increases 30–35% at 773K based on dry biomass feedstock. Demirbas *et al.* (2009b) investigated the yield of H_2 rich gases obtained from biomass pyrolysis at different temperature ranges. He found that as the temperature increased, the gaseous yield also increased. Agricultural residues, peanut shell, post-consumer wastes such as plastics, trap grease, mixed biomass, and synthetic polymers have been widely tested for hydrogen production through pyrolysis. Pyrolysis of hazelnut shell, tea waste, and spruce wood showed that the percent of H_2 in gaseous products increased from 36.8% to 43.5%, 41.0% to 53.9%, and 40.0% to 51.5%, respectively, while the reaction temperature increased from 700-950K. Demirbas (2002) pyrolysed the olive husk, cotton cocoon shell, and tea waste at about 775-1025K temperature in the presence of $Zncl_2$. The highest yield of hydrogen rich gas has been obtained from olive husk by using about 13% $ZnCl_2$ at 1025K temperature. This study also examined how K_2CO_3 and Na_2CO_3 affect the yield of gaseous products obtained from different biomass species. In the experimental studies of Çağlar and Demirbas (2002), it was observed that Na_2CO_3 has greater catalytic power than $CaCO_3$ for the pyrolysis of rice straw.

On the other hand, it is also possible to get H_2 from various types of oily products by applying a catalytic steam reforming reaction. The pyrolysis of oil is classified into two sections based on water solubility. The water-soluble fraction can be used for hydrogen production. Hydrogen production from bio-oil is shown by the following reactions:

Bio-oil + H_2O → CO + H_2

CO + H_2O → CO_2 + H_2

Chlorides, carbonates, and chromate salts have an advantageous effect on the pyrolysis reaction rate. Many other catalysts, such as Ni-based catalysts, Y-type zeolite, K_2CO_3, Na_2CO_3, $CaCO_3$, and various metal oxides, have also been explored, and it was found that the catalytic power of different catalysts was different based on feedstocks. Compared to other metal oxides, Al_2O_3 and Cr_2O_3 exhibit better catalytic action than others. Na_2CO_3 shows better catalytic action than K_2CO_3 and $CaCO_3$. Especially noble metals Ru and Rh are far more effective than Ni catalysts as they are less capable of forming carbon. These are more expensive than other catalysts; for this reason, they are not commonly used but are used in some special cases.

Duman and Yanik (2017) tested different char-based catalysts to evaluate the enhancement of hydrogen production from steam pyrolysis of olive pomace in a two-stage fixed-bed reactor system. Biomass char, nickel-loaded biomass char, coal char, nickel- or iron-loaded coal chars, and acid-washed biomass char were tested. The result showed that, in the absence of a catalyst, steam had no effect on hydrogen production. Increasing the catalyst bed temperature (500oC-700oC) increases hydrogen production in the presence of Ni-impregnated and non-impregnated biomass char. Ni-based biomass char exhibits the highest catalytic activity in hydrogen production.

Gasification

Gasification is a thermochemical process where organic matter or fossil fuel-based carbonaceous materials thermally decompose under certain reaction conditions and form gases. Gasification is a thermal treatment that produces gaseous products (producer gas) and small quantities of char, tar, and ash. Gasification is a form of pyrolysis that is carried out at high temperatures with a controlled oxygen supply that restricts the combustion of biomass. In general, gasification is carried out at a higher temperature range than pyrolysis, and the yield of hydrogen in gasification is also higher than that in pyrolysis.

The following reaction takes place in biomass gasification:

Biomass + O_2 (or H_2O) → CO, CO_2, H_2, H_2O, CH_4 + other CHs + tar + char + ash

Biomass is gasified at a higher temperature and produces a gaseous mixture that contains CO, CO_2, CH_4 and 6-6.5% H_2. This gaseous mixture is called producer gas. The biomass particle undergoes partial oxidation and, as a result, produces gases, charcoal, and tar. The steam reforming process was conducted on the produced gases to produce hydrogen, and the process was further improved by the water-gas shift reaction to increase the yield of H_2. When biomass tar and synthetic gas are formed together, it becomes difficult to separate them and remove the tar using a simple physical dust removal method. The following techniques can be utilized to minimize tar formation:

(i) proper design of the gasifier; (ii) proper control and operation; and (iii) use of additives.

Some factors, such as gasification temperature, reactor type, etc., affect the product distribution and gas composition. Some well-known gasifiers are fixed beds (updraft, downdraft, and cross-draft fixed beds), fluidized beds (bubbling, circulating), and entrained flow gasifiers. The design of a gasifier depends on the type of fuel. Synthetic gas is a mixture of carbon monoxide and hydrogen (CO + H_2), which is also called as bio-syngas. Hydrogen can be easily produced using bio-syngas by non-catalytic, catalytic, and steam gasification processes. The steam reforming process which is also known as dry or CO_2 reforming occurs according to the following reactions, and specific catalysts are also used.

$$\mathbf{C_nH_m + nH_2O \leftrightarrow nCO + (n + m/2)\ H_2}$$

$$\mathbf{C_nH_m + nCO_2 \leftrightarrow (2n)\ CO + (m/2)\ H_2}$$

Syngas as well as H_2 production from biomass by steam gasification is not very easy because of the variability of raw materials. Biomasses have different compositions, structures, reactivity rates, physical properties, etc., and they also react under some severe conditions (temperature, residence time, heating rate, etc.). The yield of H_2 from steam gasification increases with an increasing water-to-sample (W/S) ratio.

Researchers tested different biomass under different operating conditions to improve the hydrogen production technology. Using a fluidized bed gasifier along with a suitable catalyst, hydrogen production can be achieved at about 60% volume. Gasification has become an attractive and impressive H_2 production alternative because of its high conversion efficiency.

The effect of catalysts on gasification products is very important. When some catalyst is used in the water-gas shift reaction, the H_2 yield is increased. Dolomite, Ni-based catalysts, and alkaline metal oxides are mostly used as gasification catalysts (Ni *et al.,* 2006). Lv *et al*. (2004) gasified the biomass in a fluidized-bed gasifier using dolomite and in a fixed-bed reactor downstream using nickel-based catalysts and noted the yield of hydrogen for both cases. They obtained a maximum hydrogen yield (130.28 g H_2/Kg biomass) over the temperature range 925-1125K. Xiao and Liu (2009) studied the effect of particle size on the gasification performance at different bed temperatures by the catalytic steam gasification of biomass. The analysis showed that with decreasing particle size, the dry gas yield, carbon conversion efficiency, and Hydrogen yield increased, while the content of char and tar decreased.

Hydrogen production from biomass is a major challenge because there is no proper technology demonstration. A novel gasification method was proposed by Lin *et al*. (2005). The name of the process is hydrogen production by reaction-integrated novel gasification (HyPr-RING). The HyPr-RING method is an integration of the water-hydrocarbon reaction, the water-gas shift reaction, and the absorption of CO_2 and other pollutants in a single reactor under both sub-critical and supercritical water conditions.

This reaction is exothermic and high yield of hydrogen can be obtained at relatively low temperature (923-973 K). The reaction of HyPr-RING method can be expressed as:

$$\mathbf{C + 2H_2O + CaO \rightarrow CaCO_3 + 2H_2 \quad \Delta H^0_{298} = -88\ KJ/mol}$$

As compared with conventional gasification, the HyPr-RING process can be conducted in a much simpler manner as the reactions for hydrogen production and gas separation are carried out in one single reactor at a lower temperature. A comparison between conventional gasification and Hy-Pr-RING is shown in Figure 2.

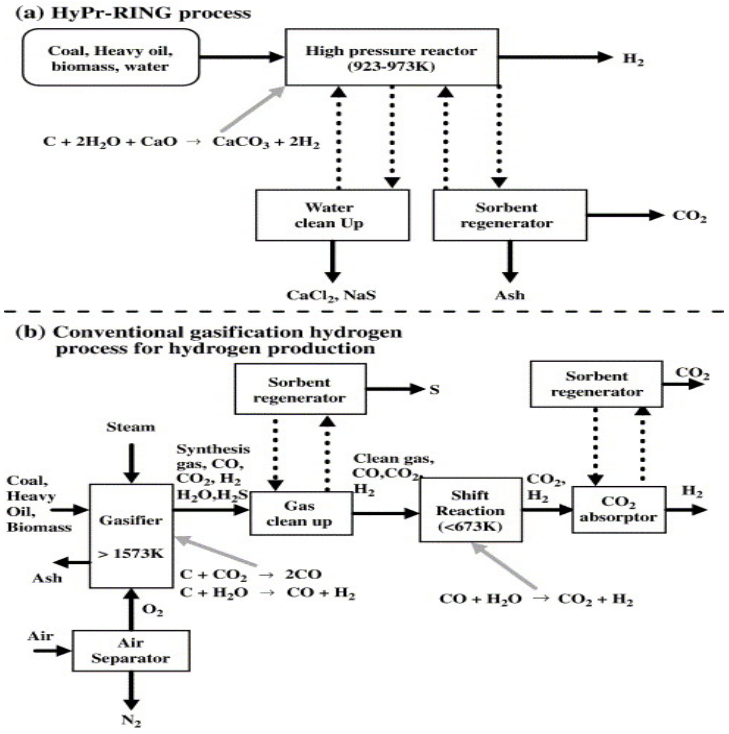

Figure 2: Comparison of HyPr-RING and Conventional Gasification Process of Hydrogen Production (Ni et al., 2006)

This innovative gasification technique has been examined theoretically and demonstrated experimentally in a very efficient way. Biomass gasification will become a dominant technology in future, it is the earliest and most favorable route for the renewable hydrogen production.

Supercritical Water Gasification:

When biomass has a high moisture content above 35%, it is likely to gasify in supercritical water conditions. SFE (supercritical fluid extraction) is a separation method that separates one component from another using a supercritical fluid solvent. Water is a supercritical fluid above 647.2K and 22.1 Mpa (Demirbas, 2004; 2009c). The dielectric constant and the number of hydrogen bonds are much lower in SCW, and their strength is weaker. As a result, at high temperatures, water behaves like organic solvents, so organic compounds are completely miscible with SCW, and gases are also miscible with SCW. Reactions under supercritical water conditions occur in a single phase, while in conventional methods they proceed via a multi-phase system.

The biomass gasification in SCW is a complex process, but the overall chemical conversion can be represented by the following reaction:

$CHxOy + (2-y)\ H2O \rightarrow CO2 + (2-y+x/2)\ H2$

This reaction shows that H_2O is not only a solvent but also a reactant, and H_2 in the water is released by the gasification reaction. The Efficiency and final gas composition depend on the heating rate. The formation of dangerous chemicals such as tars, phenol, and furfural is prevented by a higher heating rate at a temperature over 500°C. Biomass gasification in supercritical water is useful because it reduces several processing steps needed by other thermochemical hydrogen formation methods. Hydrogen was formed by Alvarez et al. through the supercritical conversion of substrate (sawdust). 80 mole H_2/kg biomass were manufactured at 25 MPa and 600 °C, and this amount of H_2 was the maximum condition. H_2 production from cellulose through gasification in SCW using Ni catalysts was also investigated. 95% water-containing bio-fuel gives the most effective results in this process; 90 mole H_2/kg biomass (containing 95% water) produced at 25 MPa and 900 °C was studied by Lu *et al.* (2007). The yield of hydrogen decreased when the substrate contained a very low water content. A hydrogen yield of 12 mol/kg substrate was obtained during gasification of corncob, amended with sodium salt, in the presence of carboxyl methyl cellulose in a fluidized-bed reactor reported by Lu *et al.* (2008). When the raw material contained 3% corncob and 2% salt, it gave the highest H_2 yield at 60 seconds of reaction time. 32 to 36% H_2 was contained in the resultant gas while the reaction conditions were 25MPa pressure and 650°C temperature (Lu *et al.,* 2008).

Comparison between Several Chemical Processes:

Normally, gasification occurs at a higher temperature in the presence of a controlled amount of O_2 and pyrolysis occurs at a lower temperature in the absence of oxygen supply. The yield of H_2 is higher in gasification than in the pyrolysis method. Generally, pyrolysis produces heat, combustible liquids, and gases, while gasification produces heat and combustible gases only. In gasification, there is a major problem with tar (hazardous) formation that occurs during the process. Another problem with gasification is ash formation, which is fixed by fractionation and leaching. Demirbas (2006) studied the yield of H_2 through supercritical fluid extraction, pyrolysis, and steam gasification of wheat straw and olive waste at different temperatures. When pyrolysis and steam gasification occur on wheat straw, it gives the highest H_2 yield, while olive waste gives the lowest H_2 yield. SCW gasification has high efficiency at lower temperatures and can directly deal with wet biomass (Demirbas, 2006). Hydrogen production through SCW gasification reduces the feedstock drying cost and is a promising technology for making use of high moisture content biomass. Another advantage of this method is that the hydrogen produced at a higher pressure can be stored directly.

Biological process:

Fermentation:

There are several H_2 formation methods that use organic raw materials coming from organic effluent, such as farming effluent, food, paper industries, manure, and effluent. Most important is the bacterial fermentation described by many authors (Giang *et al.,* 2019; Zieliński *et al*., 2017), and the other processes that play important roles in H_2 formation. These processes

are butanol fermentation, Bacillus sp., mixed acid fermentation, one kind of the genus Clostridium sp., and the family Enterobacteriaceae (Kapdan & Kargi, 2006).

Kumar and Das (2000) give a vast amount of information about the mechanism of H_2 formation through fermentation by Enterobacter cloacae at IIT-BT 08 using various organic raw materials, and sucrose and cellobiose used as raw materials gave a rate of H_2 formation of about 35.6 mmol H_2 /dm³.h. This formation rate was crossed by using various raw materials known from various studies with a formation rate 75.6mmol H_2 /dm³.h. In this case, the reactor was packed with lignocellulosic materials such as coconut coir, bagasse, and rice straw to create anaerobic bacteria, and the enhanced rate of this bacteria became highest in coconut coir. A coconut coir-based reactor forms more bacteria among those because the coir contains a higher cell density, leading to the greatest active surface area of the cells. Fermentation of swime manure containing glucose gave an H_2 formation rate of 2.25 dm³ /dm³.d and Wu, Yao and Zhu (2010) exanimated this. The optimum pH for fermentation, which is 5.0, leading to the highest performance, was investigated by the authors. That confirmed the stable hydrogen formation and density throughout the experiment (22d) using an ASBR system having a 98.5 to 99.6% $C_6H_{12}O_6$ humiliation capability range.

(a) Dark fermentation

H_2 formation is done, especially under dark conditions. Here, the fermentation is carried out by a few microalgae and anaerobic bacteria on carbohydrate-containing substrates at 30 to 80°C. The biophotolysis method only forms H_2 but H_2 and carbon dioxide merged with other gases such as H_2S and methane can be formed by dark fermentation. The ratio of gases except H_2 and CO_2 can be controlled by the reaction method and substrate. 4 mol H_2/mol glucose (used as the model substrate) is manufactured, leading to the maximum amount of H2 formation with the end of the acetic acid. The dark H_2 fermentation process was tested by Fang and Liu (2002) in a 3L reactor at a pH range 4.0-7.0A synthetic medium containing 7.0g/dm³ C6H12O6 was provided to a digester and the method achieved stability after 14 days by producing 90% degraded glucose. The amount of formed H_2 reached 2.1mol H_2 /mol glucose at optimum pH (5.5) containing 64% hydrogen content in the biogas (Fang & Lui, 2002). 128 cm³ hydrogen/ g COD remove was obtained by Kim *et al.* (2008). At pH 5.5and 40°C, fermentation of food waste was done by Clostridium beijerinckii KCTC 1785 (Kim *et al.,* 2008). Dark fermentation method was also done by taking cow dung compost to form 290.8 cm³ H_2/dm³ culture and the overall method was conducted by Song *et al.* (2012). At initial pH 7.0, the raw material provided into a system having the density of 10g/dm³ and the most useful hydrogen creator were Clostridium sp. and Enterobacter sp. (Song *et al.,* 2012). The reduction of protons is done by hydrogenase utilizing the donated electron of ferredoxin (donated electrons are transferred by ferredoxin) under anaerobic methods and the this is the biohydrogen formation mechanism. On going the degradation of glucose to pyruvate, electrons become free, and pyruvate is further oxidized to acetyl -CO A and CO_2. By following Figure 3 it becomes easy to understand. Types of ingredients and criteria such as substrate density, hydrolytic retention time (HRT), pH, temperature, microbial strain control the formation of H_2 under dark fermentation conditions.

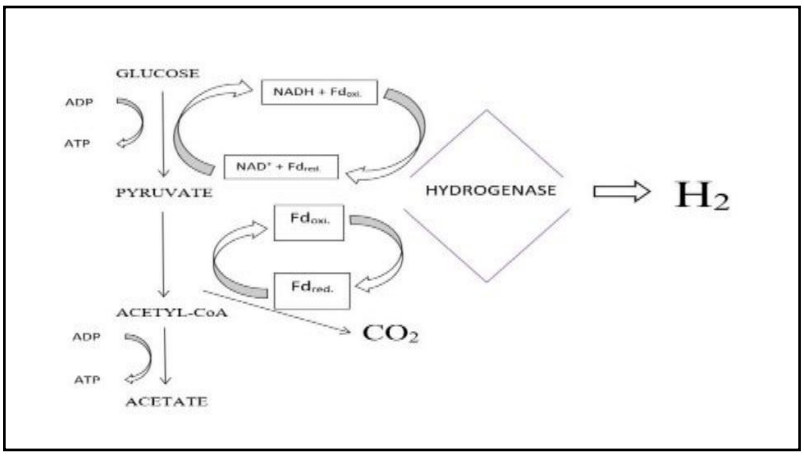

(Source: Dębowski *et al., 2021)*

Figure 3: H_2 formation Using Clostridium sp.

Facultative anaerobes having better capacity to tolerate oxygen, including common Clostridium sp. and Enterobacter sp., are a suitable choice compared to restraint anaerobes because the activity of hydrogenase is hindered by the presence of a small amount of oxygen in the bioreactors. Lower pH has an effect on microbial metabolism, which shifts toward the chemical process. The optimum pH for hydrogen production is the pH range 5.0-6.0 and pH below 4.0 prevents microbial growth (Wu, Yao & Zhu, 2010). Methanogenic bacteria become active at high pH and with the help of this condition, they take hydrogen to produce methane. To remove the Methanogenic bacteria from the communities in anaerobic sludge, heat treatment at 80 to 104°C is used. This heat treatment gives the benefit of surviving the hydrogenous spores, creating microbes such as Clostridium sp. and Bacillus sp. Hydrogen producing microbes get competition from bacteria whose growth limits are fixed by short hydraulic retention times. Undissociated volatile fatty acids produced in the reactor disturb the H_2 fermentation efficiency. Gathered CH_3CH_2COOH and $CH_3CH_2CH_2COOH$ by the presence of excess hydrogen levels in the system reduce the hydrogen production together with a decrease in the partial pressure of hydrogen (Kisielewska, Dębowski & Zieliński, 2015). As a result, the performance of H_2 fermentation is enhanced by the increased concentration of hydrogen. At this time, other parameters, such as iron level and nitrogen level, are kept in a suitable amount.

(b) Photofermentation:

Green or purple Sulphur and non-Sulphur anaerobic bacteria are able to transform the organic acids into H_2 and carbon dioxide. These anaerobic bacteria take part in Photofermentationc. The primary fermentative enzyme that is able to catalyze its reaction in either direction is nitrogenase. Ammonia is formed by the reduction of N_2. Microbes that take electrons from ferredoxin in the presence of inhibitory N_2 use the electron to reduce N_2. Electrons can be transferred by nitrogenase in nitrogen-deficient environments, and oxygen, ammonia, and excess C or N decrease the activity of nitrogenase. The electrons that are transferred by ferredoxin are created during the degradation of organic substrates by ferredoxin, and the

electrons are taken by nitrogenase from ferredoxin to be utilized to reduce the protons into normal H_2. The required energy taken from the light source is used for the protein-mediated electron transfer and is realizable Figure 4 is given below.

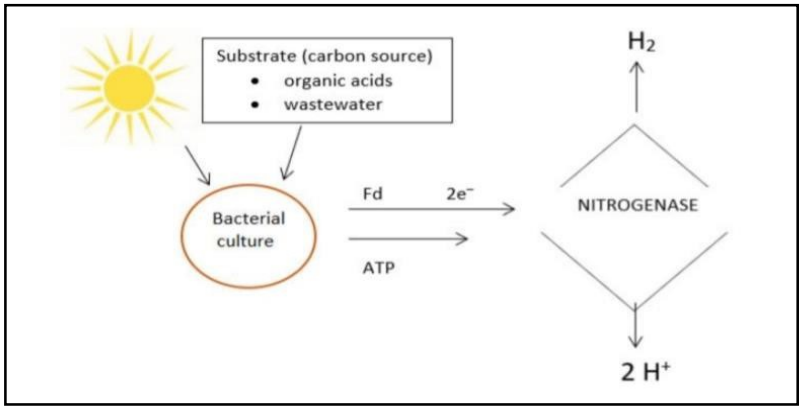

(Source: Dębowski *et al., 2021)*

Figure 4: H_2 Formation under Photo Fermentation Using Microbes

A source of bright light (400–1000 nm), a temperature between 30 and 36 °C, and a near neutral pH (6.8-7.5) must be satisfied to acquire suitable conditions for photo fermentation (Kim, Beak & Lee, 2006). Yields and H_2 formation rates are increased by optical illumination intensity. Alternating light-dark cycles are generally utilized instead to reduce the high running cost of such a solution. The amount of H_2 formed via photofermentation directly depends on various types and designs of bioreactors, and the most common are the tubular column and flat plate. To hinder staining, oxygen enterence, and the formation of competing microbial species, the units are compactly sealed and closed. Recently used bioreactors for photofermentation are very similar in design to microalgae production bioreactors. Rhodobactor sphaeroids O.U.001 utilizing sugar refinery wastewater as raw material gave 3.8cm³/dm³.h H_2 via photo fermentation H_2 formation method. Again, Rhodobactor sphaeroides O.U.001 with dilution of olive mill wastewater, produced hydrogen at about 13.9dm³ H_2/dm³.This was studied by Eroğlu *et al.* (2004). Rhodopseudomonas palustris P4 produced 2.4-2.8 mol H_2/mol CH3COOH under photofermentation, and that was studied by Oh *et al.* (2004). Photofermentation H_2 formation by Rhodobactor spaeroides-RV depends on different light sources and intensities. That was examined by Argun and Kargi (2010). H_2 formation efficacy was 781cm³ H_2/fatty acid. H_2 formation was done by using halogen lamps, where the raw material of fatty acid was used and the fatty acid was collected from ground wheat. The formation of 1037 cm^3 H_2/g fatty acid was done by using high-intensity light of about 5klux expressing the highest performance (Argun & Kargi, 2010). Photofermentative was also done by using Rhodobactor sphaeroides KKU-PS5. The operational parameters that were used in photofermentation were 30°C temperature, 6 klux light intensity, and 7.0 initial pH. Microorganisms used malic acid as a primary feedstock with a concentration of about 30 mmol/dm³. 1330 cm³ H_2/dm³, 3.80 mol H_2/mol malate, and11.08 cm³ H_2 /dm³·h were the yields and rate of H_2 formation.

Biophotolysis:

(a) Direct Biophotolysis:

Chemical energy in the form of H_2 comes from sun radiation by microphytes photosynthetic systems, and this direct biophotolysis method is useful for H_2 formation. The photosynthesis method involves two kinds of photosynthetic systems. The first system, or photosystem I (PSI), involves the formation of a reductant that is utilized to reduce carbon dioxide. Photosystemll (PSll) also involves cleaving water and releasing oxygen. Two photons from water, which are generated in the biophotolysis method, are used by PSl to reduce carbon dioxide, or they are also used to form H_2 in the presence of hydrogenase. The green plant can only reduce carbon dioxide due to the absence of hydrogenase. Microalgae with hydrogenase, like green algae and cyanobacteria, can produce H_2. PSll, consuming solar radiation energy, forms electrons that are introduced at ferredoxin with the help of solar energy that is consumed by PSl. H_2 formation by hydrogenase that takes the electron from Fd is shown below in Figure 5.

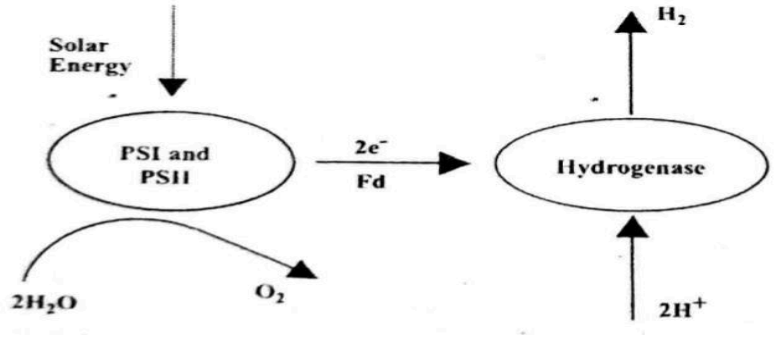

Figure 5: H_2 Formation Via Direct Biophotolysis (Ni et al., 2006)

The working ability of hydrogenase is reduced by the presence of oxygen. That's why oxygen content stays at a very low level, about 0.1%. This situation is created by Chlamydomonas reinhardtii, which can destroy the oxygen content during oxidative respiration. Working ability is lower because, during this process, a sufficient amount of substrate is absorbed and breathed in. Mutants that can be produced from microphytes involve higher H_2 formation and a higher production rate. US$60/m² is the capital cost for an overall solar transformation efficiency of 10%, and that was assumed by Benemann after expressing a hydrogen formation value of $20GJ by himself. The capital cost of US$100/$m^2$ was assumed by Benemann and Hallenbeck with a similar estimation. They avoided gas isolation and maintenance.

(b) Indirect Biophotolysis:

This process contains four steps for H_2 formation. The steps are (l)photosynthesis production of biomass, (ll)biomass density, (lll)formation of 4mol H_2/mol glucose, along with 2mol acetate by aerobic dark fermentation in an algae cell,(IV) transformation of acetate to H_2. In the following reaction, Cyanobacteria involves to the hydrogen formation.

$$12H_2O + 6CO_2 \longrightarrow C_6H_{12}O_6 + 6O_2$$

$$C_6H_{12}O_6 + 12H_2O \longrightarrow 12H_2 + 6CO_2$$

In the first and second stages, at light intensities of 95–55 micromol-1 m2 and 170-180 micro mol-1 m-2 indirect biophotolysis was investigated. During this process, Cyanobacterium anabaena variables manifested at the above-mentioned light intensities. 12.5 mL/g cdw (cell dry weight) was the H_2 formation rate. Optimal H_2 was produced at a pH between 6.8 and 8.3. That was studied by Troshina *et al*. (2002) in the presence of Cyanobacterium gloeocapsa alpicola in indirect biophotolysis. H_2 formation increases twice with an increase in temperature from 30°C to 40ºC. The H_2 formation rate by hydrogenase is comparable with the H_2 formation rate via indirect biophotolysis. Technological advancement can make a comfortable transformation to the estimated cost. Nowadays, the indirect biophotolysis method is under active research and enhancement. The above-mentioned four steps are below Figure 6.

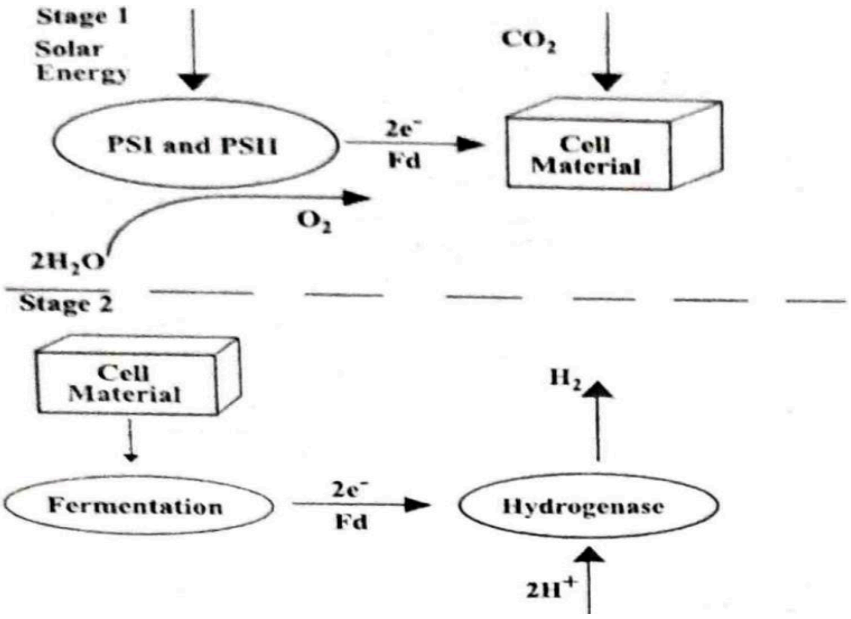

Figure 6: H_2 Formation Via Indirect Biophotolysi (Ni et al., 2006)

Water Gas-shift Reaction:

WSG is the most valuable industrial mechanism for manufacturing of NH_3, hydrocarbon, methanol and mainly hydrogen. It is most important method to producing hydrogen gas from CO or another hydrocarbon. It also become an important source of fuel for current hydrogen economy. If H_2 is produced at low cost, then it would be significant step towards the sustainable energy. This reaction classified in two categories –

Conventional WGS Reaction

Biological WGS Reaction

(a) Conventional WGS Raction:

Mechanism: After long and extensive study, this reaction becomes simple but remains controversial and complicated because of the sensitivity of the catalyst for a very minor change.

The WGS reaction is mainly synthesized by two processes. 1. Redox pathway 2. Associative (Langmuir-Hinshelwoodmen).

The redox mechanism is an endothermic reaction where the adsorption of CO on the surface of the catalyst occurs and takes O_2 from metal oxide. As a result, a vacancy of O_2 is produced, and the vacancy is filled by the dissociation of H_2O molecules and the production of H and O atoms. Then H atoms combine to form hydrogen gas, and O_2 is captured by metal oxide, which is O_2 deficient in nature (Kim *et al.,* 2020).

The associative reaction happens at low temperatures. This reaction also occurs by adsorption of CO and H_2O on the surface of the catalyst to produce an intermediate that is reactive in nature and decomposes to form CO_2 and H_2 (Tenca *et al.,* 2011). Many catalysts are used in this reaction, such as Cu/ ZnO/Al_2O_3, Ru/C, transitional metal catalysts, graphitic oxides, PT nano particles with TiO_2, gold nano particles and Nobel gas.

Theoretically, it is proven from combined DFT calculations that the redox mechanism was the most appropriate mechanism for WGS from combined DFT calculation (micro-kinetic process on Au/TiO_2 catalyst) (Sun *et al.,* 2017). Ammal and Hayden (2017) also got the same result from their reaction on Pt/TiO_2.In this reaction, pt follow the redox mechanism. Hydrogen production by conventional water gas shift reactions is given below in Figure 7.

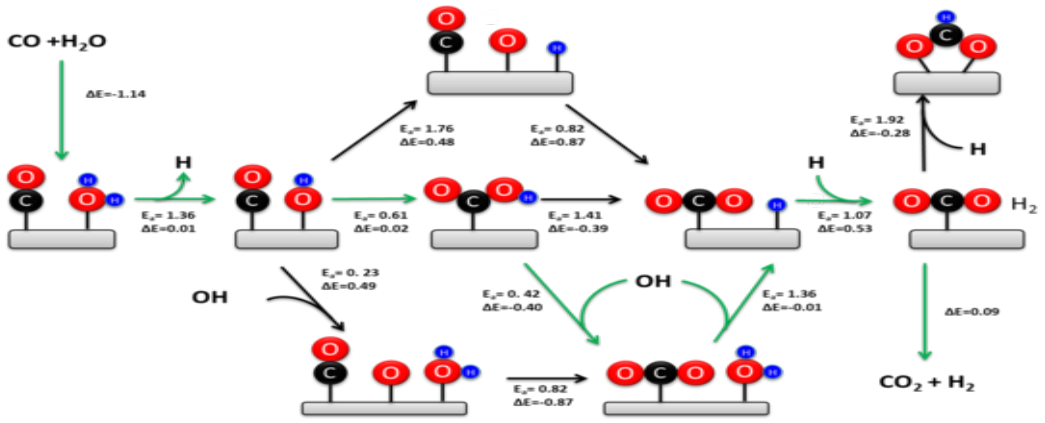

Figure 7: Associative and Redox Mechanism of the Water Gas Shift Reaction (Gokhale, Dumesic & Mavrikakis, 2008)

(b) Biological WGS Reaction:

It is an example of chemically synthesized procedure. Reaction is given below

$CO(g) + H_2O(v) \rightarrow CO_2(g) + H_2(g)$

This reaction is an important industrial reaction. This reaction is used for the production of high-purity H_2. It is a very cost-effective technology.

For this reaction, photosynthetic bacteria are used.

In this reaction, CO is oxidized to CO_2 and H_2O is reduced to hydrogen. Rubrivivax gelatinosus is a purple photosynthetic bacteria that is mainly used in WGS reactions under an anaerobic pathway. This bacterium is a non-sulfate bacteria. The reaction also proceeds under atmospheric pressure and room temperature (25 degrees Celsius). Wolfrum *et al.* (2003) proved that the organism can proceed with reactions at pressures up to 4 atm. The organism obtains energy from the biological water-gas shift reaction to maintain metabolic processes for growth. Alternatively, the biological WSG reaction occurs in an anaerobic dark phase. This mechanism produces less energy than the photosynthetic or aerobic pathways for metabolism. As a result, the production of energy is lower, so the cellular growth rate is very slow. It reduces the production of waste cells, which are produced by the biological water gas shift reaction. In this case no expensive photobioreactor is required. In the biological water gas shift reaction, energy is obtained by giving electrons to CO and H_2O. The reaction is given below.

$CO + H_2O \rightarrow CO_2 + 2e + 2H^+$

$H^+ + 2e \rightarrow H_2$

$CO + H_2O \rightarrow CO_2 + H_2$

This reaction is exothermic in nature. It releases 4.46 kcal/mol. schemetic representation of hydrogen production is given below (Figure 8):

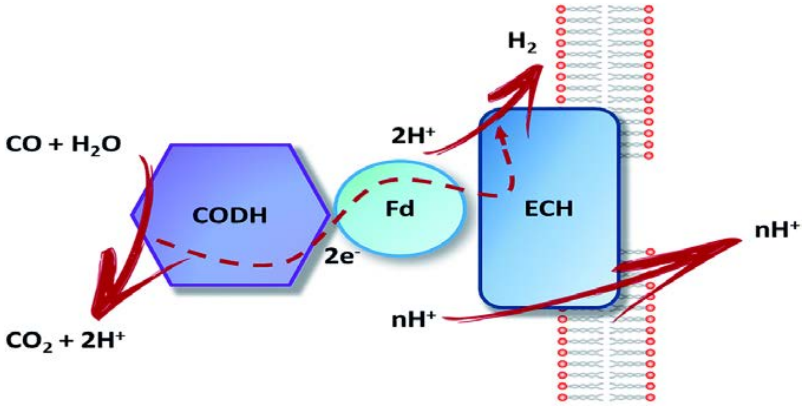

***Figure 8: Schematic Representation of Hydrogen Production by Biological WGS* (Alfano & Cavazza, 2018)**

In this pathway, corpuscles growth is very important to proceed with this reaction. Most of the cells are used to convert the CO to H_2. Sometimes the cell is inoculated for higher growth.

Sometimes the food is provided to Rx. Gelatinous CBs form acetate, malate, or a low-cost sugar source, and well as oxygen to boost energy production.

But sometimes there are some drawbacks. If there are many organisms in the reactor, they use acetate and oxygen for their growing processes. If the growing process of another organism is faster than that of Rx. Gelatinous CBs then no H_2 is produced.

At the time of boosting cell growth, if there are many organisms and if they use acetate and O_2, As a result, other cells growth will be faster than Rx. Gelatinosus CBS, then no hydrogen would be produced. In this situation, the first step should be sterilization and re-inoculation to proceed with the reaction. In this case, a safer solution is to have the reaction proceed only in the presence of CO. Although it is a very time-consuming process, It is also proven that if the reactor has no problem, then the reaction will proceed continuously without any break.

Bio Energetics of the Biological WGS Reaction:

The appropriate metabolic pathway and enzymes that are involved in biological WGS reactions are not well known. The overall free energy helps determine the highest amount of energy the Rx gelatinosus could get from biological WGS performance. Approximately 60% energy is assumed for the biological process, and we came to know that cell production per gram of co-fed bacteria Rx gelatinosus produces 1.4 g of cells per 1 mol of CO. But when it is growing aerobically in O_2 and acetate, the cell production would be 2 g per mol of acetate.

From bioenergetic calculations, one can obtain information about the reaction environment, such as pH, temperature, and feed concentration, and come to know whether the reaction is more favorable or less favorable. When a reaction becomes more favorable, the production of energy is high for the organism. If a reaction is thermodynamically unfavorable, the reaction may shut down completely. Calculations of the effect of co concentration and pH, and concentration of H_2 were done by bio energetics of the biological WGS reaction.

Hydrogen Production by WGS Reaction (Packed Bed Reactor):

In this process, Rhodospirillum rubrum is used for the WGS reaction. In this pathway, scientists observed that high recirculation rates increase the rate of mass transfer in packed bubble columns. Kareem, Al-Obaidi and Mohammed (2013) used a triculture of R. rubrum, M. barkeri, and Methanobacterium formicicum to produce CH_4. Among these, R rubrum performed WGS to produce H_2 and CO. The reaction also proceeds at ambient temperature.

In this reaction, circulation rates are most important. When H_2O circulation rates are checked among 200, 400, 600, and 800 ml/min, In this pathway, the reaction rate increases with increasing water circulation. But it increases at certain times; it reaches up to 67% at a circulation rate of 800. This is the major drawback.

Comparison between Conventional and Biological Water Gas Shift Reaction:

Between two types of reactions conventional WGS reaction is less expensive than biological. So the process is more favorable. In the aspect of thermodynamics biological process is

favored than conventional WGS but kinetically less favored. Biological process is more expensive.

Most important advantage of using bacteria for biological process is that the reaction proceed at room or laboratory temperature and there is no equilibrium limitation. (25 degree centigrade ~ 5×10^{4}).

Hybrid Reactor System:

Hybrid reactor system is two stage process. These two processes are.

First one is dark fermentation in which light independent bacteria is used to produce hydrogen yield. In this reaction anaerobic fermentation of carbohydrate occurs. As a result, an intermediate is formed like as lower weighted molecular acid which transformed into hydrogen by photo fermentation using photosynthetic bacteria in second stage in a photo bio reactor.

The reaction is given below (Figure 9)

First step:

In this reaction (facultative anaerobes)

$$\mathbf{C_6H_{12}O_6 + 2H_2O \rightarrow 2CH_3COOH + 2CO_2 + 4H_2}$$

Second step:

Photo fermentation (photo -synthetic bacteria)

$$\mathbf{2CH_3COOH + 4H_2O \rightarrow 8H_2 + 4CO_2}$$

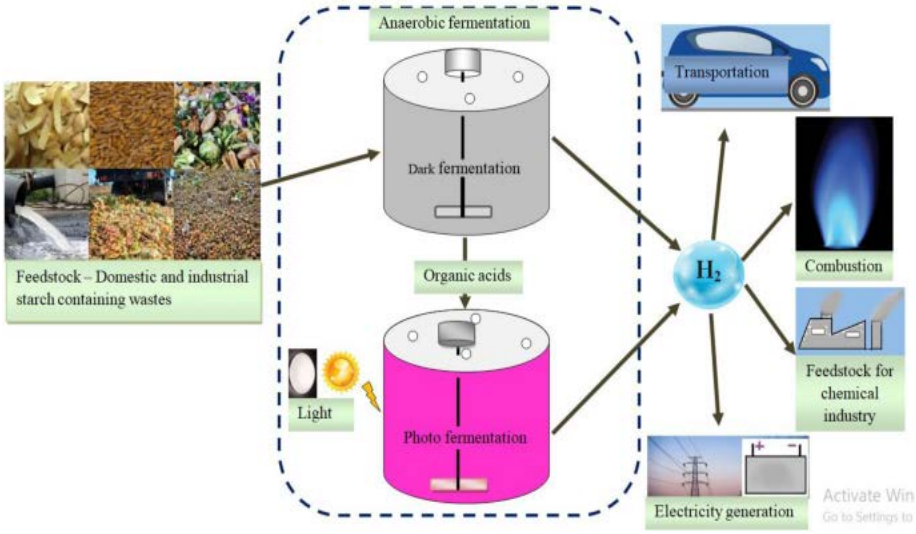

Figure 9: Hybrid Reactor System **(Das & Basak, 2021)**

In anaerobic fermentation (dark condition) reaction acetic acid is main product and assumed that twelve hydrogens are produced from 1 mole of $C_6H_{12}O_6$. Lee *et al*. (2002) analyses that the combination of purple non-sulfur bacteria (photosynthetic) anaerobic bacteria is used to produce hydrogen from waste water. In this reaction three reactors of carbohydrate have

been used. In another case Kim *et al*. (2001) studied the combined procedure of dark and photo fermentation process to synthesis hydrogen from water which is full of waste and drainage water. Nath, Kumar and Das (2005) used glucose in dark fermentation. The result is same but he used anoxygenic phototrophic PNS bacteria to produce hydrogen.

Present Scenario and Future Prospectus:

H_2 can be a most useful alternative source of energy. Now a days H_2 is used in many states as a significant energy source which gives us a sustainable future in purpose of energy Hydrogen is not an original source of energy, it is unavailable in nature.

Hydrogen can be the product of many original energy sources by different technologies. Production of hydrogen is very costly. In this case of hydrogen gas, the most significant problem is that it is not available easily in nature. Now a days mostly used, and less expensive process is steam methane reforming process.

Presently nonrenewable sources like oil, natural gas and coal are involved to produce H_2. Also, thermocatalytic and gasification processes are also used for the half manufacture of H_2. For this pathway the starting materials can be heavy oils and naphtha the percentage ratio of H_2 production from H_2O using electricity and biomass respectively is 4%,1% and 95% H_2 is manufactured from fossil which is one type of fuel.

But fossil fuel is not eco-friendly in nature because of the production of CO_2 as a side product which is responsible for 'greenhouse effect'. As time passes returnable primary energy (wind, biomass and energy) becomes the source of H_2. For H_2 production biomass is used to reduce the releasing of CO_2.

Currently the range of total hydrogen consumption is about 400-500 billion Nm^3. But only 3% is used for energy consumption and it will grow up to 5-10% per year. At present hydrogen is accepted as a (chemical feedstock) for petrochemical, food, electronics and metallurgical industries. The global market of hydrogen is about US$40 billion per year. Mainly H_2 is used to produce NH_3, refine Petroleum and also produce methanol.

H_2 is only fuel (pollution free) which can be used as transportation. It can be used in automobiles also for a pollution free environment. It has a special property to use as transport fuel and it has also an effective octane number. It is nontoxic in nature. It has no sufficient properties to form ozone. From this it has greater flammability range in air than methane and gasoline.

Future of Hydrogen Gas:

In every country, mostly developing countries, the demand for energy has increased significantly, and in the future, the demand will increase continuously. Utilization of energy becomes the main reason for the sustainable development of developed or developing countries (Marechal, Favrat & Jochem, 2005). It is expected that energy demand will be in the range of 600-1000 EJ in 2050 (Miyake, Matsunaga & San Pietro, 2001). But in the present situation, 80% of sources of energy are fossil fuels, such as crude oil, natural gas, and coal (Evans, 2007).

Non-renewable energy sources are limited and reserved for specific places in the world, and the use of non-returnable energy sources reaches its peak. So that condition is very dangerous to us. It also increases the "greenhouse effect". For that, an alternative returnable energy source is required to minimize CO_2 in the environment (Lovley, 2006). Consequently, renewable energies play a major role in innovation in energy.

The main reason for the greenhouse gas effect as well as global warming is increasing CO_2. Most of the CO_2 is produced by commercial processes such as the cement industry and the disposal of natural gas. Globally, one fifth of CO_2 comes from transportation. As a result, other energy sources like ethanol, biodiesel, and H_2 are needed at a time when a great future is in sight.

According to many national environmental agencies around the world, H_2 is selected as a fuel for a feasible future.

Conclusion

Developed human living practices brought a dangerous situation to earth. Due to the sufficient use of fossil fuels or non-returnable energy, pollution and climate change occur. Excessive use of disposable products. Waste increases rapidly, and COVID-19 becomes a favorable condition. This condition has forced us to think about new, returnable energy. In that case, H_2 draws special attention. Biomass can be the source of H_2 production.

This project introduces all the processes for hydrogen production from biomass. This also introduced multiple pathways, such as thermochemical and biological technologies. Pyrolysis and gasification pathways are the most popular for their highest production yields and low costs. The biological process is eco-friendly, so its application has significantly increased.

In the present situation, natural gas produced via steam methane reforming produces H_2. But it is not sustainable. H_2 production from returnable primary energy sources such as solar, wind, and biomass gradually increases, while production of hydrogen from fossil fuels gradually decreases. Biomass is a major raw material for producing H_2 and that has drawn special attention in recent years. But the production technology is not sufficiently developed at present. The manufacture of H_2 from biomass becomes very costly. The process of hydrogen production is much more eco-friendly. So, the innovative thinking about the (automobile's fuel) fuel of vehicles will be advanced gradually.

Recently, gasification of biomass has been introduced to produce renewable H_2 in a beneficial manner. Through this process, biomass resources are successfully utilized. It helps to make an evaluation of the process of H_2 production. It helps to reduce dependence on non-returnable energy sources like fossil fuels and also to create a pollution-free world.

Acknowledgment

The authors express their sincere thanks to the Department of Chemistry, Surendranath College and also grateful to the Principal, Surendranath college, for their support and encouragement in implementing this review project at undergraduate level.

References

Alfano, M., & Cavazza, C. (2018). The biologically mediated water–gas shift reaction: structure, function and biosynthesis of monofunctional [NiFe]-carbon monoxide dehydrogenases. *Sustainable Energy and Fuels, 2(8),* 1653–1670. https://doi.org/10.1039/c8se00085a

Ammal, S. C., & Heyden, A. (2017). Water-gas shift activity of atomically dispersed cationic platinum versus metallic platinum clusters on titania supports. *ACS Catalysis*, *7*(1), 301-309. https://doi.org/10.1021/acscatal.6b02764

Argun, H., & Kargi, F. (2010). Photo-fermentative hydrogen gas production from dark fermentation effluent of ground wheat solution: effects of light source and light intensity. *International Journal of Hydrogen Energy*, *35*(4), 1595-1603. https://doi.org/10.1016/j.ijhydene.2009.12.040

Balat, M. (2008). Mechanisms of thermochemical biomass conversion processes. Part 1: reactions of pyrolysis. *Energy Sources, Part A*, *30*(7), 620-635. https://doi.org/10.1080/15567030600817258

Çağlar, A., & Demirbaş, A. (2002). Hydrogen rich gas mixture from olive husk via pyrolysis. *Energy Conversion and Management*, *43*(1), 109-117. https://doi.org/10.1016/S0196-8904(01)00012-7

Das, S. R., & Basak, N. (2021). Molecular biohydrogen production by dark and photo fermentation from wastes containing starch: recent advancement and future perspective. *Bioprocess and Biosystems Engineering*, *44*, 1-25.

Dębowski, M., Dudek, M., Zieliński, M., Nowicka, A., & Kazimierowicz, J. (2021). Microalgal hydrogen production in relation to other biomass-based technologies—A review. *Energies*, *14*(19), 6025. https://doi.org/10.3390/en14196025

Demirbaş, A. (2002). Gaseous products from biomass by pyrolysis and gasification: effects of catalyst on hydrogen yield. *Energy Conversion and Management*, *43*(7), 897-909. https://doi.org/10.1016/S0196-8904(01)00080-2

Demirbas, A. (2004). Characterization of products from two lignite samples by supercritical fluid extraction. *Energy Sources*, *26*(10), 933-939. https://doi.org/10.1080/00908310490473228

Demirbas, A. (2009a). Mechanisms of thermal degradation of wood in alkaline glycerol. *Energy Sources, Part A*, *31*(14), 1294-1299. https://doi.org/10.1080/15567030802089581

Demirbas, A. (2009b). Hydrogen-rich gases from biomass via pyrolysis and air-steam gasification. *Energy Sources, Part A*, *31*(19), 1728-1736. https://doi.org/10.1080/15567030802459693 3

Demirbas, A. (2009c). Diesel-like fuel from tallow by pyrolysis and supercritical water liquefaction. *Energy Sources, Part A*, *31*(10), 824-830. https://doi.org/10.1080/15567030701752776

Demirbas, M. F. (2006). Hydrogen from various biomass species via pyrolysis and steam gasification processes. *Energy Sources, Part A*, *28*(3), 245-252. https://doi.org/10.1080/009083190890003

Duman, G., & Yanik, J. (2017). Two-step steam pyrolysis of biomass for hydrogen production. *International Journal of Hydrogen Energy*, *42*(27), 17000-17008. https://doi.org/10.1016/j.ijhydene.2017.05.227

Eroğlu, E., Gündüz, U., Yücel, M., Türker, L., & Eroğlu, İ. (2004). Photobiological hydrogen production by using olive mill wastewater as a sole substrate source. *International Journal of hydrogen energy*, *29*(2), 163-171. https://doi.org/10.1016/S0360-3199(03)00110-1

Evans, R. L. (2007). *Fueling Our Future: An Introduction to Sustainable Energy*. Cambridge University Press.

Fang, H. H., & Liu, H. (2002). Effect of pH on hydrogen production from glucose by a mixed culture. *Bioresource Technology*, *82*(1), 87-93. https://doi.org/10.1016/S0960-8524(01)00110-9

Giang, T. T., Lunprom, S., Liao, Q., Reungsang, A., & Salakkam, A. (2019). Enhancing hydrogen production from Chlorella sp. biomass by pre-hydrolysis with simultaneous saccharification and fermentation (PSSF). *Energies*, *12*(5), 908. https://doi.org/10.3390/en12050908

Gokhale, A. A., Dumesic, J. A., & Mavrikakis, M. (2008). On the Mechanism of Low-Temperature Water Gas Shift Reaction on Copper. *Journal of the American Chemical Society, 130(4),* 1402–1414. https://doi.org/10.1021/ja0768237

Kapdan, I. K., & Kargi, F. (2006). Bio-hydrogen production from waste materials. *Enzyme and Microbial Technology*, *38*(5), 569-582. https://doi.org/10.1016/j.enzmictec.2005.09.015

Kareem, A., Al-Obaidi, S. A., & Mohammed, A. K. (2013). Bio production of hydrogen by water – gas shift reaction using packed bed reactor. *ResearchGate*. https://www.researchgate.net/publication/307593309_BIO_PRODUCTION_OF_HYDROGEN_BY_WATER_-_GAS_SHIFT_REACTION_USING_PACKED_BED_REACTOR

Kim, J. K., Nhat, L., Chun, Y. N., & Kim, S. W. (2008). Hydrogen production conditions from food waste by dark fermentation with Clostridium beijerinckii KCTC 1785. *Biotechnology and Bioprocess Engineering*, *13*, 499-504. https://doi.org/10.1007/s12257-008-0142-0

Kim, K. J., Lee, Y. L., Na, H. S., Ahn, S. Y., Shim, J. O., Jeon, B. H., & Roh, H. S. (2020). Efficient waste to energy conversion based on co-ceo2 catalyzed water-gas shift reaction. *Catalysts*, *10*(4), 420. https://doi.org/10.3390/catal10040420

Kim, M. S., Baek, J. S., & Lee, J. K. (2006). Comparison of H2 accumulation by Rhodobacter sphaeroides KD131 and its uptake hydrogenase and PHB synthase deficient

mutant. *International Journal of Hydrogen Energy*, *31*(1), 121-127. https://doi.org/10.1016/j.ijhydene.2004.10.023

Kim, M. S., Lee, T. J., Yoon, Y. S., Lee, I. G., & Moon, K. W. (2001). Hydrogen production from food processing wastewater and sewage sludge by anaerobic dark fermentation combined with photo-fermentation. In *Biohydrogen II* (pp. 263-272). Pergamon. https://doi.org/10.1016/B978-008043947-1/50020-X

Kisielewska, M., Dębowski, M., & Zieliński, M. (2015). Improvement of biohydrogen production using a reduced pressure fermentation. *Bioprocess and Biosystems Engineering*, *38*, 1925-1933. https://doi.org/10.1007/s00449-015-1434-3

Kumar, N., & Das, D. (2000). Enhancement of hydrogen production by Enterobacter cloacae IIT-BT 08. *Process Biochemistry*, *35*(6), 589-593. https://doi.org/10.1016/S0032-9592(99)00109-0

Lee, C. M., Chen, P. C., Wang, C. C., & Tung, Y. C. (2002). Photohydrogen production using purple nonsulfur bacteria with hydrogen fermentation reactor effluent. *International Journal of Hydrogen Energy*, *27*(11-12), 1309-1313. https://doi.org/10.1016/S0360-3199(02)00102-7

Lin, S., Harada, M., Suzuki, Y., & Hatano, H. (2005). Process analysis for hydrogen production by reaction integrated novel gasification (HyPr-RING). *Energy Conversion and Management*, *46*(6), 869-880. https://doi.org/10.1016/j.enconman.2004.06.008

Lovley, D. R. (2006). Microbial fuel cells: novel microbial physiologies and engineering approaches. *Current Opinion in Biotechnology*, *17*(3), 327-332. https://doi.org/10.1016/j.copbio.2006.04.006

Lu, Y. J., Jin, H., Guo, L. J., Zhang, X. M., Cao, C. Q., & Guo, X. (2008). Hydrogen production by biomass gasification in supercritical water with a fluidized bed reactor. *International Journal of Hydrogen Energy*, *33*(21), 6066-6075. https://doi.org/10.1016/j.ijhydene.2008.07.082Get rights and content

Lu, Y., Guo, L., Zhang, X., & Yan, Q. (2007). Thermodynamic modeling and analysis of biomass gasification for hydrogen production in supercritical water. *Chemical Engineering Journal*, *131*(1-3), 233-244. https://doi.org/10.1016/j.cej.2006.11.016

Lv, P., Chang, J., Wang, T., Fu, Y., Chen, Y., & Zhu, J. (2004). Hydrogen-rich gas production from biomass catalytic gasification. *Energy & Fuels*, *18*(1), 228-233. https://doi.org/10.1021/ef0301203

Marechal, F., Favrat, D., & Jochem, E. (2005). Energy in the perspective of the sustainable development: The 2000 W society challenge. *Resources, Conservation and recycling*, *44*(3), 245-262. https://doi.org/10.1016/j.resconrec.2005.01.008

Miyake, J., Matsunaga, T., & San Pietro, A. (2001). *Biohydrogen II*. Elsevier.

Nath, K., Kumar, A., & Das, D. (2005). Hydrogen production by Rhodobacter sphaeroides strain OU 001 using spent media of Enterobacter cloacae strain DM11. *Applied Microbiology and Biotechnology*, *68*, 533-541.

Ni, M., Leung, D. Y., Leung, M. K., & Sumathy, K. J. F. P. T. (2006). An overview of hydrogen production from biomass. *Fuel Processing Technology*, *87*(5), 461-472. https://doi.org/10.1016/j.fuproc.2005.11.003

Oh, Y. K., Seol, E. H., Kim, M. S., & Park, S. (2004). Photoproduction of hydrogen from acetate by a chemoheterotrophic bacterium Rhodopseudomonas palustris P4. *International Journal of Hydrogen Energy*, *29*(11), 1115-1121. https://doi.org/10.1016/j.ijhydene.2003.11.008

Song, Z. X., Dai, Y., Fan, Q. L., Li, X. H., Fan, Y. T., & Hou, H. W. (2012). Effects of pretreatment method of natural bacteria source on microbial community and bio-hydrogen production by dark fermentation. *International Journal of Hydrogen Energy*, *37*(7), 5631-5636. https://doi.org/10.1016/j.ijhydene.2012.01.010

Sun, K., Kohyama, M., Tanaka, S., & Takeda, S. (2017). Reaction mechanism of the low-temperature water–gas shift reaction on Au/TiO2 catalysts. *The Journal of Physical Chemistry C*, *121*(22), 12178-12187. https://doi.org/10.1021/acs.jpcc.7b02400

Tenca, A., Schievano, A., Perazzolo, F., Adani, F., & Oberti, R. (2011). Biohydrogen from thermophilic co-fermentation of swine manure with fruit and vegetable waste: maximizing stable production without pH control. *Bioresource technology*, *102*(18), 8582-8588. https://doi.org/10.1016/j.biortech.2011.03.102

Troshina, O., Serebryakova, L., Sheremetieva, M., & Lindblad, P. (2002). Production of H2 by the unicellular cyanobacterium Gloeocapsa alpicola CALU 743 during fermentation. *International Journal of Hydrogen Energy*, *27*(11-12), 1283-1289. https://doi.org/10.1016/S0360-3199(02)00103-9

Wolfrum, E., Manese, P. C., Watt, A., Vanzin, G., Huang, J., & Smolinski, S. (2003). Biological water gas shift, DOE Hydrogen. *Fuel Cell, and Infrastructure Technologies Program Review*.

Wu, X., Yao, W., & Zhu, J. (2010). Effect of pH on continuous biohydrogen production from liquid swine manure with glucose supplement using an anaerobic sequencing batch reactor. *International Journal of Hydrogen Energy*, *35*(13), 6592-6599

Xiao, B., & Liu, J. (2009). Biological hydrogen production from sterilized sewage sludge by anaerobic self-fermentation. *Journal of Hazardous Materials*, *168*(1), 163-167. https://doi.org/10.1016/j.jhazmat.2009.02.008

Zieliński, M., Korzeniewska, E., Filipkowska, Z., Dębowski, M., Harnisz, M., & Kwiatkowski, R. (2017). Biohydrogen production at low load of organic matter by psychrophilic bacteria. *Energy*, *134*, 1132-1139. https://doi.org/10.1016/j.energy.2017.05.119

https://doi.org/10.31674/book.2023pcbs010

Applications of Heteroisobenzofurans in Natural and Non-natural Product Synthesis

Biswajit Panda
Department of Chemistry, City College, Kolkata, West Bengal, India

Corresponding Author's Email: biswajitchem@gmail.com

ABSTRACT

The heteroanalogue of isobenzofurans, commonly known as heteroisobenzofurans, is a prevalent intermediate for the synthesis of various important heterocyclic compounds, and interest in heteroisobenzofuran chemistry has greatly increased recently. Heteroaromatic isobenzofurans are still in their infancy compared to isobenzofurans, and many potential molecules have yet to be produced. This problem can be solved by creating innovative heteroaromatic assemblies with biological importance and forming new heteroisobenzofurans. Natural products, both those obtained from nature and those produced synthetically, have gained enormous importance both as medications and as building blocks for intricate compounds. The application of various heteroisobenzofurans in the synthesis of biologically important natural and non-natural products will be discussed in this chapter, along with a brief overview of the synthesis and reactivity of this privileged reactive intermediate.

Keywords: Heteroisobenzofurans; Heterocycles; Natural Products; Organic Synthesis; Cycloaddition; Diels-Alder Reaction; Reactive intermediates

Introduction

Isobenzofurans are a kind of heterocyclic molecule that have a benzene ring fused to the 3,4-positions of a furan ring. They are also referred to as Benzo[c]furans and 2-Oxa-2H-isoindenes since they are isomers of benzofurans. They quickly polymerize and are very reactive. It is known that stable compounds with quite intricate structures and isobenzofuran moieties exist despite their instability. Similar to isoindole, the isobenzofuran nucleus has ten π-electrons. This chemical has a higher reactivity than isoindole. The isobenzofuran ring is highly reactive at the 1- and 3-positions and readily engages in a number of chemical reactions that allow the benzene ring to regenerate its aromaticity.

Nevertheless, the high reactivity of isobenzofurans comes at the expense of their poor stability. Since it is readily accessible and generally stable, 1,3-diphenylisobenzofuran is the most widely used isobenzofuran derivative. Isobenzofuran is approximately ten times more reactive but is very difficult to prepare and purify. As a result, it should be produced in situ and used in conjunction. Although the chemistry of isobenzofuran is well established, the chemistry of heteroisobenzofuran is still evolving, and several possible results are yet to be discovered.

Since the heteroisobenzofuran moiety already has a heterocyclic ring, it always produces new heterocyclic compounds after the reaction. It is well known that many heterocyclic frameworks can be classified as privilege compounds. In the rapidly developing area of heterocyclic chemistry, researchers continually discover new and intriguing applications for heterocyclic compounds. Heterocycles are essential in organic chemistry since they make over fifty percent of all known organic compounds. Heterocyclic moieties are often found in natural products, alternative fuels, herbicides and pesticides, drugs, and macromolecules (Panda, 2020). These molecules have been synthesized using a variety of methods (Panda, 2023), including click reactions, novel multicomponent domino processes (Panda *et al.,* 2010), and traditional condensation techniques. Moreover, green and sustainable chemists have a keen interest in developing novel methods for synthesising heterocycles (Panda *et al.,* 2011). By using heterocycles, it is possible to alter the solubility, lipophilicity, polarity, and hydrogen bonding capabilities of biologically active substances, which improves the ADME/Tox characteristics of medications or drug candidates. Drugs now include more heterocycles than ever before thanks to improvements in synthetic techniques like metal-catalyzed cross-coupling (Panda & Albano, 2021) and hetero-coupling processes (Panda & Sarkar, 2013), which provide easy access to a range of functionalized heterocycles. Contrarily, a large number of heterocyclic lead molecules were obtained from natural sources, and then their structures were amended by medicinal chemists. Hence, heterocycles are crucial for medicinal chemists, as they may be used to increase the accessible drug-like chemical space and support more successful drug development processes.

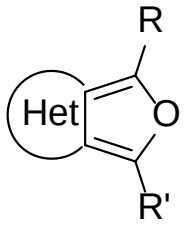

1

Figure 1: Heteroisobenzofuran

Literature Review

The synthesis of heteroisobenzofuran was well documented in a nice review by Basak and co-workers (Basak *et al.,* 2001). Heteroisobenzofuran can be synthesized through: (a) the thermolysis of 1,4-epoxide; (b) acid-catalyzed cyclization; (c) organometallic reagent-promoted cyclization; (d) the Rh-catalyzed Hamaguchi-Ibata reaction; (e) the Pummerer reaction of heteroaromatic ortho-keto sulfoxides; (f) the reaction of o-alkynyl carbonyl compounds with chromium carbene reagents; (g) base mediated elimination pathway. Various synthetic strategies for the preparation of heteroisobenzofuran are shown in figure 2.

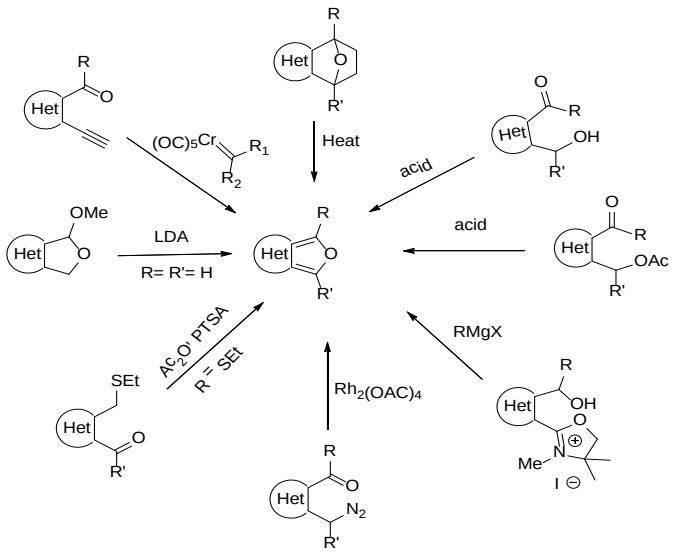

Figure 2: Synthesis of Heteroisobenzofuran

Heteroisobenzofuran is well documented in the literature due to its novel reactivity profile. The 10 π-electron system behaves as a suitable diene in a [4+2]-type cycloaddition reaction. Since in the Diels-Alder reaction, the nature of diene and dienophile plays a crucial role in the output and selectivity of the cycloaddition product, Like the [4+2] cycloaddition of other dienes and dienophiles, here also the HOMO and LUMO energy difference between the two polarophiles as well as the orbital-coefficient influence the selectivity of the addition product. Particularly in the case of heteroisobromzofuran, after the Diels-Alder reaction with dienophiles, the aromaticity-driven ring opening and elimination of water were also observed. In some cases, the reaction of heteroisombenzofuran with alkene, alkyne, and aryne was shown in Figure 3. The reactions of aryne and alkynes with heteroisobenzofuran provide the bridged addition product, which upon acid catalyzed rearrangement gave the phenolic compounds. On the other hand, reduction of the aforesaid bridged product with a reducing agent (e.g., $NaBH_4$) afforded the polynuclear hydrocarbon products.

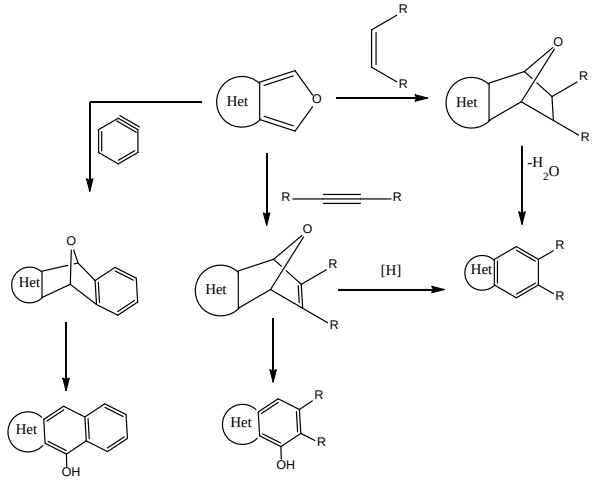

Figure 3: Reactivity Profile of Heteroisobenzofuran

Discussion

Natural product synthesis is a significant area of research, with benefits ranging from new scientific understanding to useful applications (Panda, 2019). Natural product synthesis is regarded by many as the pinnacle of organic synthesis and serves to establish the capabilities and limits of chemical synthesis at any specific period. It also contributes to the improvement of technology by striving to push the limits of molecular complexity, diversity, and efficiency. It is used to validate the structure, but it is also tested for novel synthetic techniques and occasionally used to help determine how the molecule is formed naturally. Although the application of isobenzofurans in the synthesis of natural products is quite high, in contrast to the use of hetero analogues, heteroisobenzofurans are comparatively less well documented in the literature. The application of heteroisobenzofurans as intermediates in the synthesis of natural and non-natural products is discussed below.

Synthesis of Ellipticine

The natural product ellipticine is a pyridocarbazole alkaloid that shows powerful anticancer properties. McKee and co-workers reported that Ellipticines have been shown to have fungicidal properties and have revealed promising results when tested against P. infestans growth (McKee *et al.,* 2020). The synthesis of ellipticine is one of the most intriguing uses of heteroisobenzofurans. Gribble and co-workers reported their first synthesis of ellipticine based on the cycloaddition reaction of 3,4-pyridyne and 1,3-dimethyl-4-(phenylsulfonyl)-4H-furo[3,4-b] indole (**2**) as the primary step (Figure 4) (Gribble *et al.,*1984). The [4+2] cycloaddition reaction provided the adduct as a 1:1 inseparable mixture of two regioisomers, 3 and 4, in a 38% overall yield. Reduction of the aforesaid mixture with $NaBH_4$ as a reducing agent in the presence of NaOH in a methanol solvent produced the desired natural product ellipticine 5 in a 23 % isolated yield along with the regioisomer isoellipticine 6 in a 29 % yield.

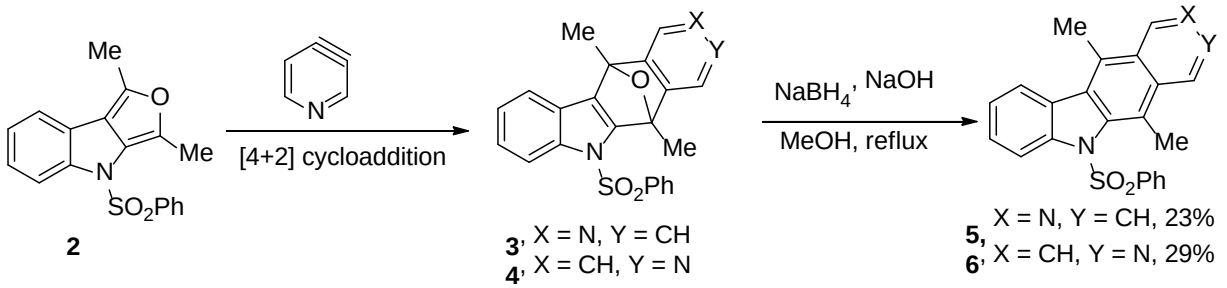

Figure 4: First Approach of Gribble's Synthesis of Ellipticine

In their second approach, Gribble *et al.* (1992) reported the trimethylsilyl trifluoromethanesulfonate-induced reaction between furoindole 2 and dihydropyridone 7 that produced lactam 8. The reaction is highly regioselective and produced lactam 8 in 89% yield (Figure 5). Reduction of lactam 8 with the strong reducing agent $LIAlH_4$ provides the cyclic amine, which is then dehydrogenated and debenzylated in the presence of a Pd/C catalyst to obtain the desired natural product ellipticine 5 in an 18% isolated yield.

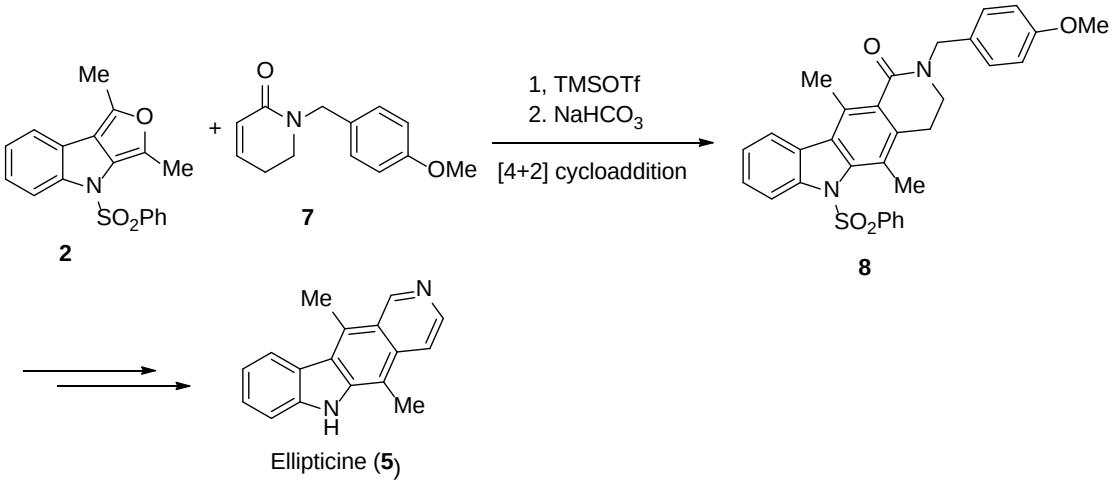

Figure 5: Second Approach of Gribble's Synthesis of Ellipticine

Diaz *et al.* (1998) described a polarity-controlled regioselective cycloaddition of 2-chloro 3, 4-pyridyne with heteroisobenzofuran and they used this reaction as a key step for the improved synthesis of ellipticine (Figure 6). This approach is a modified version of Gribble's method. The fluoride-promoted pyridine formation, followed by regiocontrol cycloaddition, provides the natural product ellipticine in a higher yield.

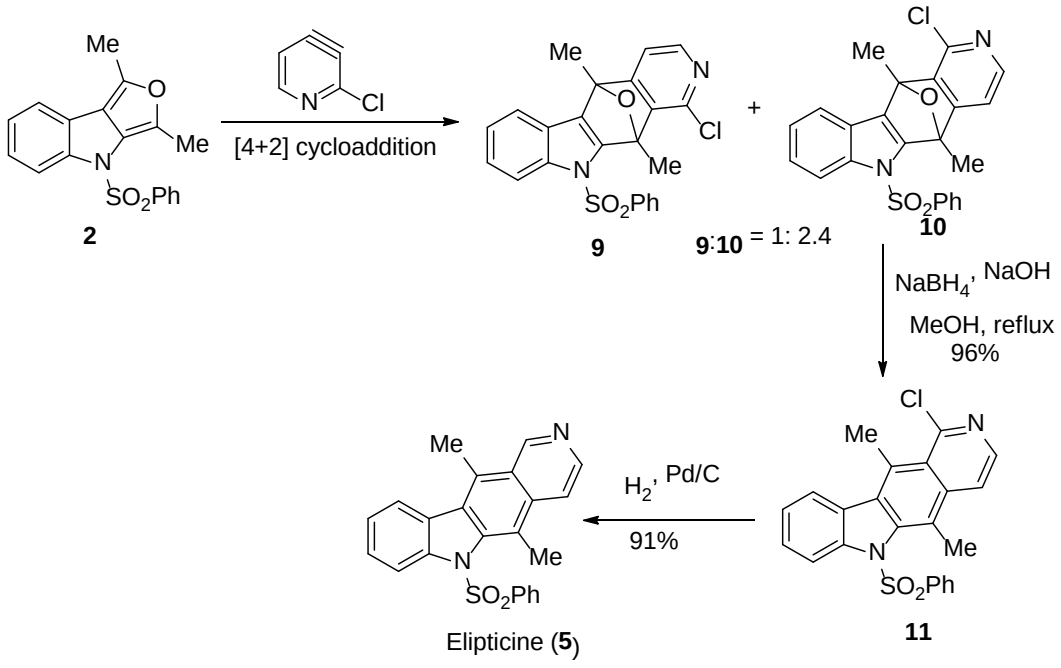

Figure 6: Guitian's Synthesis of Ellipticine

Synthesis of Murrayaquinone A

The natural product Murrayaquinone A is a carbazole alkaloid and it has been identified from the root bark of Murraya euchrestifolia Hayata. It shows cardiotonic activity on heart muscle.

Cagatay *et al.* (2021) was synthesize a series of Murrayaquinone A derivatives and found that these molecules have strong anti-cancer activity. Murrayaquinone A was synthesized by Miki and Hachiken in 1993 via a regioselective cycloaddition process between furo [3,4-blindole 14 and methyl acrylate 15 (Figure 7) (Miki & Hachiken, 1993). Their method entails the production of 4-benzyl-1-tert-butyldimethylsiloxy-4H-furo [3,4-blindole (14) by the deprotonation of lactone 13 by lithium bis (trimethylsilylamide, followed by o-silylation with tert-butyldimethylsilyl chloride (TBDMSCI), and regioselective trapping of this in-situ. After being treated with boron trifluoride etherate, the resulting adduct 16 produced methyl 9-
benzyl-4-hydroxycarbazole-3-carboxylate (17), which was then converted into murrayaquinone A 18.

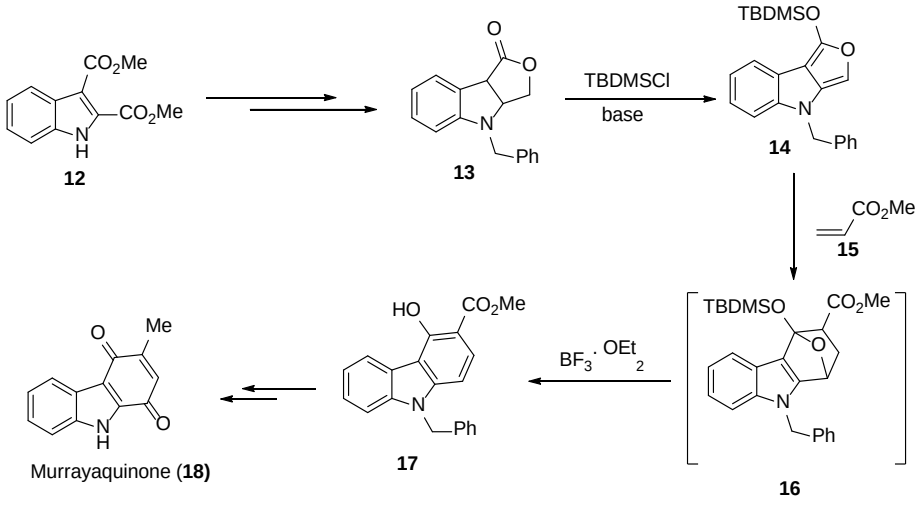

Figure 7: Synthesis of Murrayaquinone A

Synthesis of Heterolignans

In 1984, Masatomo and co-workers described a nice synthetic method for the synthesis of heterolignans, as shown in Figure 8 (Iwao, Inoue & Kuraishi, 1984). Sequential lithiation of pyridine-phthalide 19 with LDA followed by O-silylation with TBDMSCI results in the transitory intermediate 3-(silyloxy)pyrido [3,4-clfuran (20), which, when reacted with dimethyl fumarate, yields the stereoselective adducts 22 and 23 in lower yields. Para-toluenesulfonic acid-mediated reaction of the adduct 22 in benzene solvent under refluxing conditions provides the desired heterolignan 24 in good yield.

Moreover, Kuroda and co-workers have described the synthesis of heteroanalogues of 1-arylnaph-tulene lignans through the acid-catalyzed formation of a heteroisobenzofuran intermediate from an acetoxy-carbonyl molecule. Then this in-situ generated heteroisobenzofuran intermediate was reacted with dimethyl acetylenedicarboxylate through the [4+2] cycloaddition pathway to produce the heterolignan 28 (Figure 9) (Kuroda *et al.,* 1994). The thiolignan compound 28 exhibits potent antihyperlipidemic properties.

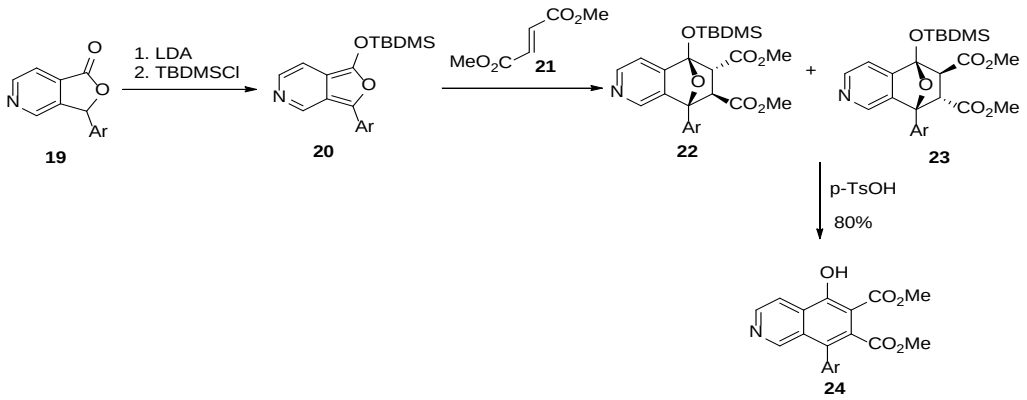

Figure 8: Synthesis of an Isoquinoline Lignan

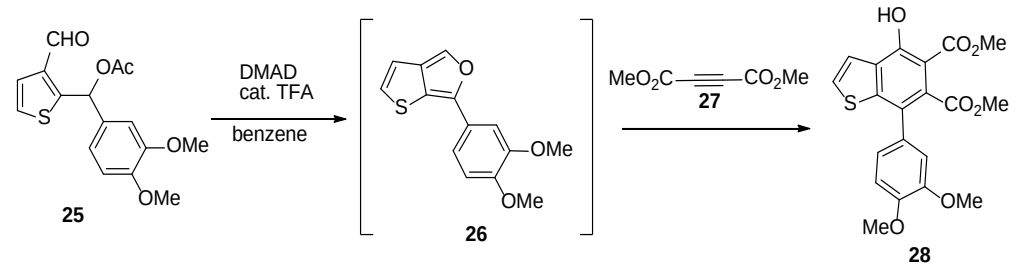

Figure 9: Synthesis of a Heterolignan

Synthesis of Conformationally Restricted Analogues of Nicotine and Anabasine

The chiral alkaloid nicotine is made up of two nitrogen-containing heterocycles, pyridine and N-methylpyrrolidine moieties, which are joined together by a single C-C bond. Since it is the most prevalent alkaloid that can be extracted from the dried leaves of the tobacco plants Nicotiana tabacum and Nicotiana rustica, nicotine is unquestionably one of the best-known naturally occurring N-heterocyclic compounds. Because of the possibility of pharmacological use in the treatment of Parkinson's disease, Alzheimer's disease, depression, and other disorders of the central nervous system, nicotine's clinical utility is restricted by its adverse effects on the heart, gastrointestinal tract, and neuromuscular systems, particularly its high potential for addiction.

There have been ongoing attempts at developing synthetic nicotine analogues that have been highly selective for particular nAChR subunits. Conformationally restricted derivatives, or changing the parent molecule in a way that severely restricts its original conformational mobility to one specific conformation, are of tremendous importance in this context (Panda & Albano, 2021). Because less entropy is lost when a ligand binds to a receptor, the ability to "freeze out" the conformational dynamics of a ligand might increase its affinity and specificity for that receptor. The pyridine and pyrrolidine moieties found in nicotine have been effectively linked with short chains comprised of simply carbon atoms or, in some circumstances, additionally including one or more heteroatoms to create a range of conformationally limited analogues of nicotine.

In the synthesis of conformationally constrained analogues of nicotine and anabasine, Sarkar and co-workers utilized the special benefit of intramolecular Diels-Alder chemistry of furo[3,4-c]-pyridines (Sarkar *et al.,* 2000). Due to their significance as neuronal acetylcholine receptors (nAChRs), nicotine and anabasine have gained interest in recent years. In their synthetic strategy, diazoacetic esters 29 and 30 are converted to the intermediate hetroisobenzofurans 31 and 32 through the $Rh_2(OAc)_4$-catalyzed reactions in benzene solvent under refluxing conditions for 1 hour. Finally, the ring opening reactions of compounds 33 and 34 perform successive proton transfer reactions to provide the biologically important molecules nicotine or anabasine in good yield (Figure 10).

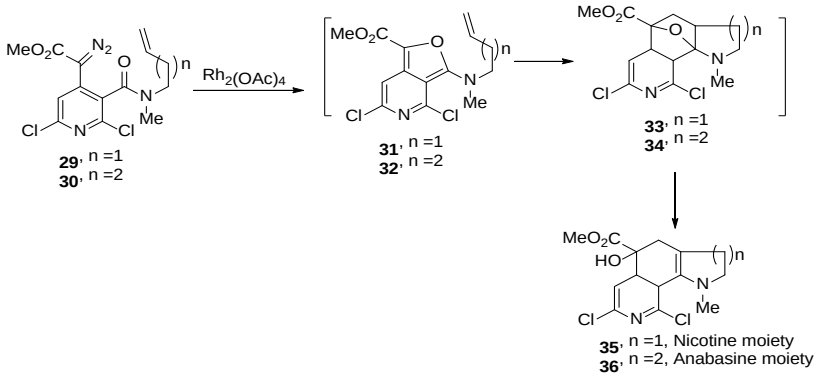

Figure 10: Synthesis of Conformationally Restricted Analogues of Nicotine and Anabasine

Synthesis of Aza-Homosteroid

In 2013, Roy and co-workers reported a novel method for the synthesis of aza-homosteroid moiety 40 via an intramolecular [4+2] cycloaddition reaction of aza-isobenzofuran 39 with a pendant alkene (Roy *et al.,* 2013) The intermediate aza-isobenzofuran 39 was generated by the reaction of γ, δ-unsaturated Fischer carbene complex with ortho-alkynyl heteroaryl carbonyl derivatives. The cycloaddition reaction in this case is highly regio- and stereoselective.

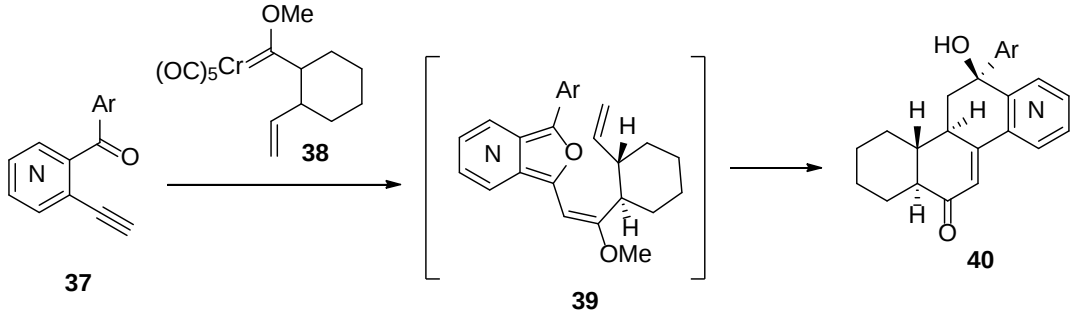

Figure 11: Synthesis of Aza-Homosteroid

Conclusion

In recent years, the chemistry of heteroisobenzofurans has seen a great surge of interest due to their potential for the synthesis of polycyclic heteroaromatics. In comparison to isobenzofurans, heteroaromatic isobenzofurans are still at an infant stage, and a lot of

possible compounds are yet to be developed. This challenge can be met by developing new heteroisobenzofurans and designing novel heteroaromatic assemblies with biological significance. Consequently, there has been an increase in research focused on this area. Natural products, such as those found in nature and those synthetically derived, have seen a huge rise in their importance, not only as pharmaceuticals but also as building blocks for complex molecules. As a result, the development of innovative synthetic strategies for generating heteroisobenzofuran natural products becomes highly desirable. In addition, efficient methods for the total synthesis of these compounds will have additional applications in drug discovery and medicinal chemistry. Thus, it is likely that this field of research will see advancements in both the number of novel compounds synthesized and the strategies employed for their synthesis in the upcoming years.

Acknowledgement

The author is grateful to City College, Kolkata, for their encouragement. He is also thankful to Dr. Bhaskar Paul, Dr. Totan Mondal, and Mr. Aranya Sarkar for their help and support.

References

Basak, S., Ghosh, S. K., & Sarkar, T. K. (2001). Progress in the chemistry of heteroisobenzofurans. *Journal of the Indian Institute of Science*, *81*(4), 431.

Cagatay, E., Akyildiz, V., Ergun, Y., & Kayali, H. A. (2021). Synthesis of Murrayaquinone-A Derivatives and Investigation of Potential Anticancer Properties. *Chemistry & Biodiversity*, *18*(11), e2100348. https://doi.org/10.1002/cbdv.202100348

Diaz, M. T., Cobas, A., Guitián, E., & Castedo, L. (1998). Polar control of the regioselectivity of hetaryne cycloadditions. Synthesis of ellipticine. *Synlett*, *1998*(02), 157-158. https://doi.org/10.1055/s-1998-1607

Gribble, G. W., Keavy, D. J., Davis, D. A., Saulnier, M. G., Pelcman, B., Barden, T. C., ... & BelBruno, J. J. (1992). Syntheses and Diels-Alder cycloaddition reactions of 4H-furo [3, 4-b] indoles. A regiospecific Diels-Alder synthesis of ellipticine. *The Journal of Organic Chemistry*, *57*(22), 5878-5891. https://doi.org/10.1021/jo00048a021

Gribble, G. W., Saulnier, M. G., Sibi, M. P., & Obaza-Nutaitis, J. A. (1984). Synthesis and Diels-Alder reactions of 1, 3-dimethyl-4-(phenylsulfonyl)-4H-furo [3, 4-b] indole. A new annulation strategy for the construction of ellipticine and isoellipticine. *The Journal of Organic Chemistry*, *49*(23), 4518-4523. https://doi.org/10.1021/jo00197a039

Iwao, M., Inoue, H., & Kuraishi, T. (1984). Generation and Diels–Alder Reaction of 1-Siloxy-3-Arylisobenzofurans from 3-Arylphthalides. *Chemistry Letters*, *13*(7), 1263-1266. https://doi. org/10.1246/cl.1984.1263

Kuroda, T., Takahashi, M., Ogiku, T., Ohmizu, H., Nishitani, T., Kondo, K., & Iwasaki, T. (1994). An Efficient Synthesis of Heterocyclic Analogs of 1-Arylnaphthalene Lignans. *The Journal of Organic Chemistry*, *59*(24), 7353-7357. https://doi.org/10.1021/jo00103a029

McKee, M. L., Zheng, L., O'Sullivan, E. C., Kehoe, R. A., Doyle Prestwich, B. M., Mackrill, J. J., & McCarthy, F. O. (2020). Synthesis and evaluation of novel ellipticines and derivatives as inhibitors of Phytophthora infestans. *Pathogens*, *9*(7), 558. https://doi.org/10.3390/pathogens9070558

Miki, Y., & Hachiken, H. (1993). Synthesis and Diels-Alder Reaction of 4-Benzyl-1-tert-butyldimethylsiloxy-4H-furo [3, 4-b] indole: Synthesis of Murrayaquinone-A. *Synlett*, *1993* (05), 333-334. https://doi.org/10.1002/chin.199408178

Panda, B. (2019). Total synthesis of xyloketals and related natural product alboatrin: strategies and tactics. *ChemistrySelect*, *4*(31), 9143-9164. https://doi.org/10.1002/slct.201900779

Panda, B. (2020). Towards the template synthesis of conjugated pyrrole based oligo-heteroaryls. *Journal of the Indian Chemical Society*, 97(11 A), 2287-2290. http://dx.doi.org/10.5281/zenodo.5653618.svg

Panda, B. (2023). Organocatalitic C-H Bond Functionalizations for the Synthesis of Heterocycles. *Current Organocatalysis*, http://dx.doi.org/10.2174/2213337210666230213120833

Panda, B., & Albano, G. (2021). Synthetic Methods for the Preparation of Conformationally Restricted Analogues of Nicotine, *Molecules* , *26*(24), 7544. https://doi.org/10.3390/molecules26247544

Panda, B., & Sarkar, T. K. (2013). Gold catalysis: regio-and stereoselective total synthesis of xyloketals D and G and the related natural product alboatrin. *The Journal of Organic Chemistry*, *78*(6), 2413-2421. https://doi.org/10.1021/jo302545n

Panda, B., Basak, S., Hazra, A., & Sarkar, T. K. (2010). A Domino Michael–Dieckmann-Peterson Approach to the Synthesis of Substituted Hydroxyquinolines and Hydroxyisoquinolines. *Journal of Chemical Research*, 34(2), 109-113. https://doi.org/10.3184/030823410x12659067482702

Panda, B., Bhadra, J., & Sarkar, T. K. (2011). An approach to highly functionalized quinolines and isoquinolines via a gold-catalyzed benzannulation. *Synlett*, 2011(05), 689-693. https://doi.org/10.1055/s-0030-1259555

Roy, P., Mitra, P., & Ghorai, B. K. (2013). Synthesis of azahomosteroid ring system through intramolecular [4+ 2] cycloaddition of in situ generated azaisobenzofuran intermediates. *Tetrahedron Letters*, *54*(11), 1440-1443. https://doi.org/10.1016/j.tetlet.2013.01.005

Sarkar, T. K., Basak, S., & Ghosh, S. K. (2000). A novel approach to conformationally restricted analogues of nicotine and anabasine by an intramolecular Hamaguchi–Ibata reaction. *Tetrahedron Letters*, *41*(5), 759-762. https://doi.org/10.1016/S0040-4039(99)02148-6

https://doi.org/10.31674/book.2023pcbs11

Profiling the Dynamics of a Stochastic Quantum System Modulated by Rapid Time-Periodic Stimulus

Anindita Shit
Department of Chemistry, Kandi Raj College, Kandi, Murshidabad, West Bengal, India

Corresponding Author's Email: anindita.pchem@gmail.com

ABSTRACT

The dynamics of a quantum dissipative system driven by a fast-oscillating high-frequency periodic field has been investigated here in the semi classical regime. As the system can no longer be considered to be in a conventional thermal equilibrium situation, the theoretical study of these non-adiabatically driven systems is cumbersome. Here, the frequency of external modulation is substantially higher as compared to all other pertinent system frequencies. Beginning with a quantum system-reservoir Hamiltonian with explicit time dependence, derive a time-independent effective c-number generalized Langevin equation (GLE) at leading order by exploiting a technique from the protocol of MSPT (multiple scale perturbation theory). Within the so obtained c-number GLE (which does not include explicit time-dependence), the original system dynamics can be evaluated by its slow part with the time-independent effective potential. Here the dynamics of the slow-part are explored perturbatively in terms of ω^{-1} (ω stands for the frequency of time-periodic oscillating force) up to the order ω^{-4}. Modulation of the parameters of the effective potential often provides a potential avenue to increase or abate the escape probability of the system from the region of attraction of the potential well.

Keywords: *Quantum Dissipative Systems; Dynamical Processes; Langevin Equation; Effective Potential; Multiple Scale Perturbation Analysis*

Introduction

The question of how a system responds to an external rapid periodic perturbation is one of the elementary problems in the field of chemical dynamics in condensed phases and has importance in classical as well as quantum mechanics (Bukov, D'Alessio & Polkovnikov, 2015; Hänggi, Luczka & Spiechowicz, 2020; Spiechowicz, Hänggi & Luczka, 2022). It plays primitive roles in many phenomenal applications, including escape from a metastable state (Kapitsa, 1951; Landau & Lifshitz, 2013; Paul, 1990). Classical or quantum time-dependent systems exhibit more difficult behaviour than corresponding time-independent systems. Here, it is claimed that for a clear insight (both qualitative and quantitative) into the dynamics of a rapidly modulated system, multiple scale perturbation theory (MSPT) may be used as an effective tool. Theoretical analysis of nonadiabatically driven systems is complicated, since one may no longer assume that the system is in thermal equilibrium. On the other hand, for equilibrium systems, the exponential part in the escape rate expression can be found as the height of the free energy barrier, but for nonequilibrium systems, the pre-factor case is even more complicated as there are no general relations from which it can be achieved.

Literature Review

There have been many attempts to resolve the nonadiabatic response problem in many contexts (Gammaitoni *et al.,* 1998; Jung, 1993; Denisov *et al.,* 2006; Denisov *et al.,* 2007; Denisov, Polyakov & Lyutyy, 2011; Kim *et al.,* 2010; Spiechowicz *et al.,* 2023). Thus, the development of an elaborate theory of the dynamics of the system under the impact of modulation is indispensable as well as useful. Here the dynamics of a quantum system has been presented which is driven by a rapid, time-periodic, space-dependent oscillating field, one of the most important classes of non-equilibrium systems. It is always hard to anticipate the qualitative properties of systems with periodic modulation as compared to the dynamics of structurally similar time independent systems, which are easy to perceive. Here, the dynamics of time-dependent modulated systems in which there exists a clear separation of time scales will be related to the dynamics of time-independent ones. Thus, by using the experience with the dynamics of time-independent systems, both qualitative and quantitative studies of the dynamics of time-dependent systems can be done. Here the Brownian dynamics is analysed in the quantum regime in terms of an effective time-independent Hamiltonian by invoking systematic expansion of the time-dependent system-bath Hamiltonian in (being the driving frequency) with a systematic time scale separation. It is found that the slow part of the motion may be interpreted by a time independent effective potential and modulation changes the activation barrier, which provides an effective control of the escape rate and a precise measurement of the system parameters (Floquet, 1883; Shirley, 1965; Chen *et al.,* 1973; Shit, Chattopadhyay & Ray Chaudhuri, 2012a; Shit, Chattopadhyay & Ray Chaudhuri, 2012b; Shit, Chattopadhyay & Ray Chaudhuri, 2012c; Shit, Chattopadhyay & Ray Chaudhuri, 2013). For rapidly oscillating field frequencies, where the driving becomes nonadiabatic, the expected major effect due to the field would "modulate" the system by changing its potential. Here the study such driven systems in a very general form for a wide range of driving frequencies, which goes far beyond the adiabatic limit. The description narrated below can be viewed as a generalization of the work of Kapitsa-Landau-Lifshitz (Kapitsa, 1951; Landau & Lifshitz, 2013) within the frame of system-bath model. This work may be implemented to explore the escape dynamics and the trapping mechanism for the Brownian particle moving in a space-dependent rapidly oscillating field (Shit, 2016).

Discussion

Consider the system to be a quantum particle of mass *m* associated with a bath consisting of harmonic oscillators with characteristic frequencies $\{\Omega_j\}$ and masses $\{m_j\}$. The system is evolving under the influence of an external periodic potential $\hat{V_1}(\hat{x}, \omega t)$ [where ω is the frequency of the external modulation]. Note that the average of the time-dependent periodic potential $\hat{V_1}(\hat{x}, \omega t)$ over a period $[\tau = (2\pi/\omega)]$ can be delineated as follows:

$$\hat{V}_1\big(\hat{x}, \omega(t+\tau)\big) = \hat{V_1}(\hat{x}, \omega t);$$

$$\frac{1}{\tau}\int_0^{\tau} \hat{V}_1(\hat{x}, \omega t) = 0$$

As expected, at t = 0 (when there is no external driving force), the harmonic bath is in thermal equilibrium with the system. Note that at t = 0+, $\hat{V}_1(\hat{x}, \omega t)$ is turned on and the

system starts moving in the external force. The total Hamiltonian (Weiss, 2012; Zwanzig, 1961; Zwanzig, 1973) can be constructed by a system part, a bath part and the system-bath interaction part:

$$\widehat{H} = \frac{\hat{p}^2}{2m} + \hat{V}_0(\hat{x}) + \hat{V}_1(\hat{x}, \omega t) + \sum_{j=1}^{N} \left\{ \frac{\hat{p}_j^2}{2m_j} + \frac{1}{2} m_j \Omega_j^2 \left(\hat{x}_j - \frac{c_j \hat{x}}{m_j \Omega_j^2} \right)^2 \right\} \quad (1)$$

Here $\hat{x}$ is the position operator, and $\hat{p}$ corresponds to the momentum operator of the system. $\{\hat{x}_j, \hat{p}_j\}$ stands for coordinate and momentum operators for the harmonic bath and obeys the relations $[\hat{x}_j, \hat{p}_j] = i\hbar\delta_{ij}$. The coupling between system and bath is linear in nature characterized by the coupling parameter c_j, $\hat{V}_0$ stands for the system potential in absence of coupling. Eq. (1) explicitly depicts that each of the harmonic bath oscillator is shifted relative to the system by an amount dependent on their correlative coupling that can be considered as a compensation of a renormalization of the system potential (Weis, 2012). In the present case, a revised bath Hamiltonian controls the proper distribution of initial states which is expressed as:

$$\widehat{H}_B = \sum_{j=1}^{N} \left[\frac{\hat{p}_j^2}{2} + \frac{1}{2} m_j \Omega_j^2 \left(\hat{x}_j - \frac{c_j \hat{x}}{m_j \Omega_j^2} \right)^2 \right], \text{ at } t = 0\,. \quad (2)$$

Exploiting Eq. (1), one can design Hamilton's equation of motion (EOM) for both the system variables as well as the bath degrees of freedom. These are two differential equations due to the mutual interplay between the system and the bath. The Langevin equation (which consists of both dissipation and fluctuation terms) can be obtained by solving the required expressions of the bath degrees of freedom and subsequently exploiting these equations into the corresponding equations of the system variables. The statistical properties of the system degrees of freedom are characterized by the distribution of the initial conditions of the bath degrees of freedom via the fluctuation-dissipation relation. Here, the microscopic structure of the dissipative term and the fluctuating force comprise the initial conditions of bath degrees of freedom. The operator Langevin equation to describe the evolution of the system can be expressed as:

$$\dot{\hat{x}} = \frac{\hat{p}}{m}$$

$$\dot{\hat{p}} = \hat{V}'_0(\hat{x}) - \hat{V}'_1(\hat{x}, \omega t) - \int_0^t dt' \gamma(t - t') \hat{p}(t') + \hat{\eta}(t) \quad (3)$$

In the present work, the expression for the damping kernel can be described as $\gamma(t - t') = \frac{1}{\pi} \int_{-\infty}^{+\infty} d\Omega [J(\Omega)/\Omega] \cos \Omega(t - t')$ where the term $J(\Omega)$ stands for the spectral density of the harmonic bath and the term $\hat{\eta}(t)$ describes the noise characterized by,

$$\hat{\eta}(t) = \sum_{j=1}^{N} \left[m_j c_j \Omega_j \left\{ \hat{x}_j(0) - c_j \hat{x}(0) \right\} \cos \Omega_j t + \frac{\hat{p}_j(0)}{m_j \Omega_j} \sin \Omega_j t \right]$$

In the Ohmic regime, $(\Omega) = m\gamma\Omega$, where γ denotes the friction coefficient. Note that $\hat{\eta}(t)$ considered here is a zero-mean Gaussian random noise. The statistical properties of $\hat{\eta}(t)$ can be constructed by exploiting appropriate canonical thermal distribution of bath degrees of freedom at initial stage, $t = 0$,

$$\langle\hat{\eta}(t)\hat{\eta}(t')+\hat{\eta}(t')\hat{\eta}(t)\rangle_{QS}=\hbar\int_{-\infty}^{+\infty}\frac{d\Omega}{\pi}J(\Omega)\coth\left(\frac{\hbar\Omega}{2k_BT}\right)\cos\Omega(t-t') \quad (4)$$

Note that the above equation, Eq.(4), is the famous fluctuation-dissipation theorem/relation (FDT/FDR) which is a very useful instrument in chemical physics for monitoring the counter intuitive behavioural aspect of systems that follows structure of detailed balance. Here k_BT (k_B stands for Boltzmann constant) delineates the equilibrium thermal energy. In the model, the average is computed over the initial bath-variables as

$$\langle\hat{O}\rangle_{QS}=\frac{Tr[\hat{O}exp(-\hat{H}_B/k_BT)]}{Tr[exp(-\hat{H}_B/k_BT)]} \quad (5)$$

where $\langle\dots\rangle_{QS}$ indicates a quantum statistical average over the bath-variables. As Eq. (3) is the generalized quantum mechanical operator form of Langevin equation (Shit, Chattopadhyay & Ray Chaudhuri, 2011b; Ghosh *et al.,* 2011), it is practically unmanageable and non-trivial task to obtain required solution. Therefore, it is practical to sketch Eq.(3) in an operator-free manner. Obeying the scheme suggested by Ray and co-workers (Barik & Ray, 2005), starting form a microscopic system-bath Hamiltonian, one gets the following *c*-number generalized quantum Langevin equation delineating the evolution of the expectation values position operators of the system under consideration:

$$m\dot{x}=p$$

$$\dot{p}=-U_0'(x)-U_1'(x,\omega t)-\gamma p+\eta(t) \quad (6)$$

Where

$$U_0'=V_0'\big(x(t)\big)-Q_V^0$$

$$U_1'=V_1'(x(t),\omega t)-Q_V^1 \quad (7)$$

Here

$$x(t)=\langle\hat{x}(t)\rangle_Q$$

$$p(t)=\langle\hat{p}(t)\rangle_Q$$

$$\eta(t)=\langle\hat{\eta}(t)\rangle_Q=\sum_j\left[m_jc_j\Omega_j^2\{\langle\hat{x}_j(0)\rangle_Q-c_j\langle\hat{x}(0)\rangle_Q\}\cos\Omega_jt+\frac{\langle\hat{p}_j(0)\rangle_Q}{m_j\Omega_j}\sin\Omega_jt\right] \quad (8)$$

$\langle\dots\rangle_Q$ describes quantum mechanical average estimate (Barik, Banerjee & Ray, 2009). Here, Q_V^0 and Q_V^1 symbolize the quantum mechanical correction terms, described by

$$Q_V^0=V_0'(x)-\langle V_0'(\hat{x})\rangle_Q$$

$$Q_V^1=V_1'(x,\omega t)-\langle V_1'(\hat{x},\omega t)\rangle_Q \quad (9)$$

The system parameters $\hat{x}$ and $\hat{p}$ can be described as

$$\hat{x}(t)=x(t)+\delta\hat{x}(t),\ \ \hat{p}(t)=p(t)+\delta\hat{p}(t), \quad (10)$$

Note that, in this model, the terms $x(=\langle\hat{x}\rangle_Q)$ and $p(=\langle\hat{p}\rangle_Q)$ can be considered as the quantum mechanical mean values. The operators $\delta\hat{x}$ and $\delta\hat{p}$ appear as quantum fluctuations around their respective average values and they obey:

$$\langle\delta\hat{x}(t)\rangle_Q=0=\langle\delta\hat{p}(t)\rangle_Q,\ \ [\delta\hat{x},\delta\hat{p}]=i\hbar \quad (11)$$

Exploiting Eq. (10) along with the Taylor series based expansion around x (Bhattacharya, Chattopadhyay & Ray Chaudhuri, 2009),

$$Q_V^0 = -\sum_{n\geq 2} \frac{1}{n!} V_0^{n+1}(x)\langle \delta\hat{x}^n(t)\rangle_Q$$

$$Q_V^1 = -\sum_{n\geq 2} \frac{1}{n!} V_1^{n+1}(x,\omega t)\langle \delta\hat{x}^n(t)\rangle_Q \quad (12)$$

Here the term $V^{n+1}(x)$ corresponds to the $(n+1)$th derivative of $V(x)$. Estimation of $Q_V^1(x,t), (i=0{,}1)$ relies on the quantum mechanical correction term $\langle \delta\hat{x}^n(t)\rangle_Q$ that can be computed exploiting the scheme mentioned in References (Shit, Chattopadhyay & Ray Chaudhuri, 2011b; Ghosh *et al.,* 2011). The following expression can be used to ascertain $\langle \hat{\eta}(t)\rangle_Q$ as a *c*-number noise:

$$\langle\langle \hat{\eta}(t)\rangle_Q\rangle_S = 0;$$

$$\langle\langle \hat{\eta}(t)\hat{\eta}(t')\rangle_Q\rangle_S = \frac{1}{2}\sum_{j=1}^{N} c_j^2\, \Omega_j^2 \hbar\Omega_j \coth\left(\frac{\hbar\Omega_j}{2k_B T}\right)\cos\Omega_j(t-t')\,; \quad (13)$$

Eq.(13) clearly advocates that the noise $\langle \hat{\eta}(t)\rangle_Q$ fulfils the quantum FDR, and is emerged if and only if the initial mean-values of parameters (momenta and coordinates) of the bath oscillators have canonical thermal Wigner distribution, P_j for the displaced harmonic oscillator:

$$\mathrm{P}_j = N\exp\left\{-\frac{\langle \hat{p}_j(0)\rangle_Q^2 + \Omega_j^2\left[\langle \hat{x}_j(0)\rangle_Q - c_j\langle \hat{q}(0)\rangle_Q\right]^2}{2\hbar\Omega_j\left(\bar{n}_j(\Omega_j)+\frac{1}{2}\right)}\right\} \quad (14)$$

Here, *N* appears as normalization constant. Note that positive definite function, P_j depends on the initial preparation of the system under study. Structural properties of P_j remains applicable as a pure state, non-singular distribution even at $T = 0$. In the above expression $\bar{n}_j$ can be characterized as average photon number at temperature T:

$$\bar{n}_j = \left[\exp\left(\frac{\hbar\Omega_j}{2k_B T}\right) - 1\right]^{-1} \quad (15)$$

In this model, the statistical average of any dynamical/observable O_j can be expressed as (quantum mechanical mean value)

$$\langle O_j(0)\rangle_S = \int O_j\, \mathrm{P}_j d\langle \hat{p}_j(0)\rangle d\left\{\langle \hat{x}_j(0)\rangle - \langle \hat{x}(0)\rangle\right\} \quad (16)$$

As expected, for the case that $\hbar\omega \ll k_B T$ (thermal limit), the form of the distribution of quantum mechanical mean values of the bath oscillators converts to the corresponding form of the Maxwell–Boltzmann distribution, the classical one. It is to be mentioned here that Eqs. (8), (14) and (16) can be exploited to reveal the characteristic features of the *c*-number noise. Eq. (6) can be viewed as the desired *c*-number quantum Langevin equation (QLE). In this model, the two quantum correction terms Q_V^0 and Q_V^1 emerge from the nonlinear nature of the potential used. Using a suitable physically motivated approximation (Shit, Chattopadhyay & Ray Chaudhuri, 2011b; Ghosh, Shit, Chattopadhyay & Ray Chaudhuri, 2011), Eq. (13) can be described as where,

$$\langle\langle \hat{\eta}(t)\hat{\eta}(t')\rangle_Q\rangle_S = 2D_q\delta(t-t')$$

$$D_q = \left(\frac{\gamma\hbar\Omega_0}{2}\right)\coth\left(\frac{\hbar\Omega_j}{2\mathrm{k}_B T}\right) \quad \textbf{(}17\text{)}$$

Here Ω_0 corresponds to a common linearized system frequency for all bath modes. In the present development, the usual quantum statistical average is described by $\langle\langle \ldots \rangle_Q\rangle_S$. It is to be noted here that although *c*-number noise $\eta(t)(=\langle\hat{\eta}(t)\rangle_Q)$ follows the FDR and furnishes the same anti-commutator just as operator noise term $\hat{\eta}(t)$, being a *c*-number term, the commutator form of the same vanishes. In that sense, the treatment present here is not fully quantum mechanical. Actually $\eta(t)$ is a classical-like noise in conjunction with quantum mechanical correction term. Thus, the present development can be considered as a semiclassical scheme. Basically, in the present work, the system is handled using a suitable quantum mechanical protocol, but the bath degrees of freedom have been managed semi-classically. It is worth mentioning that the complexity of treating the complicated operator quantum Langevin equation (OQLE) can be circumvented by exploiting the above mentioned semiclassical approach that attempts to handle the OQLE on the same footing as that of the classical LE while preserving the leading-order quantum effect. Note that in the high temperature quantum regime, $\frac{\hbar\Omega_0}{\mathrm{k}_B T} \ll 1$ (where the correction terms corresponding to the quantum effect emerge as a coupled infinite set of a hierarchy of equations) D_q can be approximated as $\gamma\mathrm{k}_B T$ and consequently, with this approximation, from Eq. (13), one can obtain the following form of the classical standard *δ*-correlated FDR, independent of the system frequency:

$$\langle\eta(t)\rangle_S = 0;$$
$$\langle\eta(t)\eta(t')\rangle_S = 2\gamma\mathrm{k}_B T\delta(t-t'), \quad (18)$$

Eq. (18) is the famous Einstein FDR in the Markovian limit. This scheme hence assists to get the classical form from the corresponding quantum mechanical relation.

Now, for the investigation of the dynamics of the present model, Eq. (6) with time dependent potential needs to be solved which is very tough to reach and generally can be achieved numerically by exploiting some physically motivated approx. scheme. In this model, the high frequency oscillating force exerts the force $\hat{F}(\hat{x},\omega t) = -\hat{V}_1'(\hat{x},\omega t)$. Here, the frequency ω is very large compared to all other pertinent system frequencies: $\omega\left(\omega > \frac{1}{\tau}\right)$. τ can be viewed as the order of magnitude of the period of motion of the system that it would perform in the field of $\hat{V}_0'(\hat{x})$. Therefore, the system does not have enough time to interact with the periodic force before the force alters sign. Under this condition, one can apply "Kapitsa-Landau time- window" in which the motion of the particle can be divided into a "slow" part as well as a "fast" one that comprises of a rapid motion around the "slow" part. It should be noted that the fast motion emerges in an effective potential for the "slow" motion. Therefore, focus on the following solution of Eq. (6):

$$x(t) = X(t) + \xi(X,\dot{X},\omega t) \quad (19)$$

Here, $X(t)$ describes the 'slow' part whereas ξ corresponds to the 'fast' part of the motion. In Ref. (Shit, Chattopadhyay & Ray Chaudhuri, 2012d), authors have demonstrated clearly that ξ will rely primarily on X and $\dot{X}$ rather on the higher order time derivatives. Here, ξ has been selected in such a fashion that Eq. (6) will yield a time-independent

equation for X. Although it is very difficult to achieve exact solution exploiting Eq. (6) but in the limit of high frequencies, one can obtain in orders of $\frac{1}{\omega}$. Here, the following fast time variable is suggested

$$\tau = \omega t$$

for which the time average of ξ over one period disappears:

$$\bar{\xi} = \frac{1}{2\pi}\int_0^{2\pi} d\tau \xi\left(X, \dot{X}, \tau\right) = 0 \tag{20}$$

It is to be clarified here that ξ is not periodic in t instead, it should be a periodic function of the τ. In the present work, both times, τ and *t* are handled as independent parameters. In terms of 'fast time' variable, τ,

$$\frac{d\xi}{dt} = \omega\frac{d\xi}{d\tau} + \frac{d\xi}{dX}\dot{X} + \frac{d\xi}{d\dot{X}}\ddot{X} \tag{21}$$

and

$$\frac{d^2\xi}{dt^2} = \omega^2\frac{\partial\xi}{\partial\tau^2} + 2\omega\left[\frac{\partial^2\xi}{\partial X\partial\tau}\dot{X} + \frac{\partial^2\xi}{\partial\dot{X}\partial\tau}\ddot{X}\right] + \frac{\partial\xi}{\partial X}\ddot{X} + \frac{\partial\xi}{\partial\dot{X}}\dddot{X}$$
$$+\frac{\partial^2\xi}{\partial X^2}\dot{X}^2 + 2\frac{\partial^2\xi}{\partial X\partial\dot{X}}X\ddot{\dot{X}} + \frac{\partial^2\xi}{\partial\dot{X}^2}\ddot{X}^2 \tag{22}$$

Exploiting Eqs. (21) and (22) along with Eq. (6) get the following form [for details, see reference (Shit, Chattopadhyay & Ray Chaudhuri, 2012a)]:

$$m\left\{\ddot{X} + \omega^2\frac{\partial\xi}{\partial\tau^2} + 2\omega\left(\frac{\partial^2\xi}{\partial X\partial\tau}\dot{X} + \frac{\partial^2\xi}{\partial\dot{X}\partial\tau}\ddot{X}\right) + \frac{\partial\xi}{\partial X}\ddot{X} + \frac{\partial\xi}{\partial\dot{X}}\dddot{X} + \frac{\partial^2\xi}{\partial X^2}\dot{X}^2 + 2\frac{\partial^2\xi}{\partial X\partial\dot{X}}\dot{X}\ddot{X} + \frac{\partial^2\xi}{\partial\dot{X}^2}\ddot{X}^2 \right\} + \gamma\dot{X} +$$
$$\gamma\left\{\frac{\partial\xi}{\partial X}\dot{X} + \frac{\partial\xi}{\partial\dot{X}}X + \ddot{\omega}\frac{\partial\xi}{\partial\tau}\right\} = -U_0'(X+\xi) - U_1'(X+\xi,\tau) + \eta(t) \tag{23}$$

Here the slow dynamics usually controls the overall dynamics of the particle. Note that the initial noise term entirely has its impact on the slow dynamics, and it has no effect on the fast dynamics. At the high frequencies, ξ becomes be very small (of the order of $\frac{1}{\omega^2}$). Thus, one can expand $U_0(X+\xi)$ and $U_1(X+\xi,\tau)$ in powers of; U_0 and U_1 are assumed to be smooth functions of the coordinate. Therefore, one can expand ξ in powers of $\frac{1}{\omega}$:

$$\xi = \sum_{n=1}^{\infty}\frac{1}{\omega^n}\xi_n \tag{24}$$

Here, selection of ξ_i should be in such a fashion that the equation of *x* which emerges from Eq. (23) does not rely on time variable, τ. From Eq. (24) so,

$$m\left\{\ddot{X} + \omega^2\frac{\partial^2}{\partial\tau^2}\sum_n\frac{1}{\omega^n}\xi_n + 2\omega\left(\dot{X}\frac{\partial^2}{\partial X\partial\tau}\sum_n\frac{1}{\omega^n}\xi_n + \ddot{X}\frac{\partial^2}{\partial\dot{X}\partial\tau}\sum_n\frac{1}{\omega^n}\xi_n\right) + \ddot{X}\frac{\partial}{\partial X}\sum_n\frac{1}{\omega^n}\xi_n + \right.$$
$$\dddot{X}\frac{\partial}{\partial\dot{X}}\sum_n\frac{1}{\omega^n}\xi_n + \dot{X}^2\frac{\partial^2}{\partial X^2}\sum_n\frac{1}{\omega^n}\xi_n + 2\dot{X}\ddot{X}\frac{\partial^2}{\partial X\partial\dot{X}}\sum_n\frac{1}{\omega^n}\xi_n + \ddot{X}^2\frac{\partial^2}{\partial\dot{X}^2}\sum_n\frac{1}{\omega^n}\xi_n \left.\right\} + \gamma\dot{X} +$$
$$\gamma\left\{\dot{X}\frac{\partial}{\partial X}\sum_n\frac{1}{\omega^n}\xi_n + \ddot{X}\frac{\partial}{\partial\dot{X}}\sum_n\frac{1}{\omega^n}\xi_n + \omega\frac{\partial}{\partial\tau}\sum_n\frac{1}{\omega^n}\xi_n\right\} = -\left[\{U_0'(X) + U_1'(X,\tau)\} + \right.$$
$$\{U_0''(X) + U_1''(X,\tau)\} \times \sum_{n=1}^{\infty}\frac{1}{\omega^n}\xi_n + \frac{1}{2!}\{U_0'''(X) + U_1'''(X,\tau)\}\sum_{n=1}^{\infty}\sum_{m=1}^{\infty}\frac{1}{\omega^n}\frac{1}{\omega^m}\xi_n\xi_m + \left.\cdots\right] + \eta(t)$$

(25)

To get the required equation, all the terms of the identical order are collected. From the very mode of discussion, it is evident that in the leading order of ω , the only contribution is

$$\frac{\partial^2 \xi}{\partial \tau^2} = 0. \tag{26}$$

Therefore, without sacrificing generality, one may adopt:

$$\xi_1 = 0 \tag{27}$$

For ω^0 so

$$m\left\{\ddot{X} + \frac{\partial^2 \xi_2}{\partial \tau^2}\right\} + \gamma \dot{X} = -U_0'(X) - U_1'(X,\tau) \tag{28}$$

To balance τ dependence, set

$$\frac{\partial^2 \xi_2}{\partial \tau^2} = \frac{1}{m} U_1'(X,\tau) \tag{29}$$

ξ_2 must be periodic in time variable, τ. To circumvent secular terms, the time integral needs to have a vanishing average over a period.

$$\xi_2 = -\frac{1}{m}\int_0^\tau d\tau \int_0^\tau d\tau\, U_1'(X,\tau) \tag{30}$$

Substituting ξ_2 in Eq. (28), get

$$m\ddot{X} = -U_0'(X) - \gamma \dot{X}. \tag{31}$$

In the next order (ω^{-1}) get

$$m\left(\frac{\partial^2 \xi_3}{\partial \tau^2} + 2\dot{X}\frac{\partial^2 \xi_2}{\partial X \partial \tau} + 2\ddot{X}\frac{\partial^2 \xi_2}{\partial \dot{X} \partial \tau}\right) + \gamma \frac{\partial \xi_2}{\partial \tau} = 0$$

From Eq. (30), it is evident that ξ_2 is not a function of $\dot{X}$ and hence the above equation reduces to

$$\frac{\partial^2 \xi_3}{\partial \tau^2} = -2\dot{X}\frac{\partial^2 \xi_2}{\partial X \partial \tau} - \gamma \frac{\partial \xi_2}{\partial \tau} \tag{32}$$

Now, using Eqs.(30) and (31), have the solution for ξ_3 as

$$\xi_3 = \frac{2}{m}\dot{X}\int_0^\tau d\tau \int_0^\tau d\tau \int_0^\tau d\tau\, U_1''(X,\tau) + \frac{\gamma}{m^2}\int_0^\tau d\tau \int_0^\tau d\tau \int_0^\tau d\tau\, U_1'(X,\tau) \tag{33}$$

Therefore, the terms of the order of ω^{-2} can be expressed as

$$m\left[\frac{\partial^2 \xi_4}{\partial \tau^2} + 2\left(\dot{X}\frac{\partial^2 \xi_3}{\partial X \partial \tau} + \ddot{X}\frac{\partial^2 \xi_3}{\partial \dot{X} \partial \tau}\right) + \ddot{X}\frac{\partial \xi_2}{\partial X} + \dot{X}^2\frac{\partial^2 \xi_2}{\partial X^2}\right] + \gamma\left[\dot{X}\frac{\partial \xi_2}{\partial X} + \frac{\partial \xi_3}{\partial \tau}\right] = -U_0''(X)\xi_2 - U_1''(X,\tau)\xi_2 \tag{34}$$

From Eq. (33), obtain the value of $\frac{\partial^2 \xi_4}{\partial \tau^2}$ as

$$\frac{\partial^2 \xi_4}{\partial \tau^2} = -\frac{U_0''(X)}{m^2}\int_0^\tau d\tau \int_0^\tau d\tau\, U_1'(X,\tau) + \frac{U_1''(X,\tau)}{m^2}\int_0^\tau d\tau \int_0^\tau d\tau\, U_1'(X,\tau) - \frac{3}{m}\dot{X}^2\int_0^\tau d\tau \int_0^\tau d\tau\, U_1'''(X,\tau) - \frac{3}{m}\ddot{X}\int_0^\tau d\tau \int_0^\tau d\tau\, U_1''(X,\tau) - \frac{3\gamma}{m^2}\dot{X}\int_0^\tau d\tau \int_0^\tau d\tau\, U_1''(X,\tau) - \frac{\gamma^2}{m^3}\int_0^\tau d\tau \int_0^\tau d\tau\, U_1'(X,\tau) \tag{35}$$

Let ξ_4 be periodic in τ. Now a function $f_1(X,\tau)$ is constructed as follows:

$$f_1(X,\tau) = \frac{1}{m^2} U_1''(X,\tau) \int_0^\tau d\tau \int_0^\tau d\tau\, U_1'(X,\tau) - \frac{1}{m^2} \overline{U_1''(X,\tau) \int_0^\tau d\tau \int_0^\tau d\tau\, U_1'(X,\tau)}, \tag{36}$$

so that $\bar{f}_1(X,\tau) = 0$.

Now choose ξ_4 as

$$\xi_4 = \frac{U_0''(X)}{m^2} \int_0^\tau d\tau \int_0^\tau d\tau \int_0^\tau d\tau \int_0^\tau d\tau\, U_1'(X,\tau) + \int_0^\tau d\tau \int_0^\tau d\tau\, f_1(X,\tau) -$$
$$\frac{3}{m}\dot{X}^2 \int_0^\tau d\tau \int_0^\tau d\tau \int_0^\tau d\tau \int_0^\tau d\tau\, U_1'''(X,\tau) - \frac{3}{m}\ddot{X} \int_0^\tau d\tau \int_0^\tau d\tau \int_0^\tau d\tau \int_0^\tau d\tau\, U_1''(X,\tau) -$$
$$\frac{3\gamma}{m^2}\dot{X} \int_0^\tau d\tau \int_0^\tau d\tau \int_0^\tau d\tau \int_0^\tau d\tau\, U_1''(X,\tau) - \frac{\gamma^2}{m^3} \int_0^\tau d\tau \int_0^\tau d\tau \int_0^\tau d\tau \int_0^\tau d\tau\, U_1'(X,\tau) \tag{37}$$

This solution equivalences all the τ-dependence of Eq.(35) and yields the following extra term,

$$\frac{1}{m^2} \overline{U_1''(X,\tau) \int_0^\tau d\tau \int_0^\tau d\tau\, U_1'(X,\tau)}$$

which for slow dynamics yields,

$$m\ddot{X} + \gamma\dot{X} = -U_0'(X) + \frac{1}{m\omega^2} \overline{U_1''(X,\tau) \int_0^\tau d\tau \int_0^\tau d\tau\, U_1'(X,\tau)} + O(\omega^{-3}) \tag{38}$$

The above equation can be considered as the leading order correction corresponding to the periodic potential U_1. The terms of the order of ω^{-3} of Eq. (25) provide:

$$m\left[\frac{\partial^2\xi_5}{\partial\tau^2} + 2\left(\dot{X}\frac{\partial^2\xi_4}{\partial X\partial\tau} + \ddot{X}\frac{\partial^2\xi_4}{\partial\dot{X}\partial\tau}\right) + \ddot{X}\frac{\partial\xi_3}{\partial X} + \dddot{X}\frac{\partial\xi_3}{\partial\dot{X}} + \dot{X}^2\frac{\partial^2\xi_3}{\partial X^2} + 2\dot{X}\ddot{X}\frac{\partial\xi_3}{\partial X\partial\dot{X}} + \dot{X}^2\frac{\partial^2\xi_3}{\partial\dot{X}^2}\right] +$$
$$\gamma\left[\dot{X}\frac{\partial\xi_3}{\partial X} + \ddot{X}\frac{\partial\xi_3}{\partial\dot{X}} + \frac{\partial\xi_4}{\partial\tau}\right] = -U_0''(X)\xi_3 - U_1''(X,\tau)\xi_3 \tag{39}$$

Now, ξ_5 will be chosen in a manner ensuring that it shall scarp all the periodic terms with vanishing average. Note that entire terms of LHS of Eq. (39) has a vanishing average. Consequently, only the terms of RHS of Eq. (39) shall contribute to the slow coordinate. This contribution will result only from $\overline{-U_0''\xi_3} - \overline{U_1''\xi_3}$ and, as the term $\overline{U_0''\xi_3}$ vanishes as per this model, one may easily obtain,

$$\overline{-U_1''\xi_3} = \frac{\gamma}{m^2} \overline{\int_0^\tau d\tau\, U_1''(X,\tau) \int_0^\tau d\tau \int_0^\tau d\tau\, U_1'(X,\tau)} \tag{40}$$

Incorporating the effect of this term [i.e., $O(\omega^{-3})$] into the slow dynamics, one will have (using integration by parts),

$$m\ddot{X} + \gamma\dot{X} = -U_0'(X) + \frac{1}{m\omega^2} \overline{\int_0^\tau d\tau\, U_1'(X,\tau) \int_0^\tau d\tau\, U_1''(X,\tau)} +$$
$$\frac{\gamma}{m^2\omega^3} \overline{\int_0^\tau d\tau\, U_1''(X,\tau) \int_0^\tau d\tau \int_0^\tau d\tau\, U_1'(X,\tau)} + O(\omega^{-4}) \tag{41}$$

the contribution of terms $O(\omega^{-4})$ to the equation of X is

$$\overline{-U_0''\xi_4} - \overline{U_1''\xi_4} - \frac{1}{2}\overline{U_0'''\xi_2^2} - \frac{1}{2}\overline{U_1'''\xi_2^2} \tag{42}$$

Although the averages of other terms have finite values, but the first term will vanish again. From Eqs.(30) and (37), one gets

$$\overline{-U_0''(X)\xi_4} - \overline{U_1''(X,\tau)\xi_4} - \frac{1}{2}\overline{U_0'''(X)\xi_2^2} - \frac{1}{2}\overline{U_1'''(X,\tau)\xi_2^2} = \frac{1}{2m^2}U_0'''(X)\overline{\left[\int_0^\tau d\tau \int_0^\tau d\tau\, U_1'(X,\tau)\right]^2} -$$
$$\frac{1}{2m^2}U_1'''(X,\tau)\overline{\left[\int_0^\tau d\tau \int_0^\tau d\tau\, U_1'(X,\tau)\right]^2} + \frac{U_0''(X)}{m^2}\overline{\int_0^\tau d\tau U_1''(X,\tau) \int_0^\tau d\tau \int_0^\tau d\tau \int_0^\tau d\tau\, U_1'(X,\tau)} +$$
$$\frac{1}{m^2}\overline{\int_0^\tau d\tau U_1''(X,\tau) \int_0^\tau d\tau \left[U_1'(X,\tau)\int_0^\tau d\tau \int_0^\tau d\tau\, U_1'(X,\tau)\right]} -$$
$$\frac{3}{m}\dot{X}^2\overline{\int_0^\tau d\tau U_1''(X,\tau) \int_0^\tau d\tau \int_0^\tau d\tau \int_0^\tau d\tau\, U_1'''(X,\tau)} -$$
$$\frac{3}{m}\ddot{X}\overline{\int_0^\tau d\tau U_1''(X,\tau) \int_0^\tau d\tau \int_0^\tau d\tau \int_0^\tau d\tau\, U_1''(X,\tau)} -$$
$$\frac{3\gamma}{m^2}\dot{X}\overline{\int_0^\tau d\tau U_1''(X,\tau) \int_0^\tau d\tau \int_0^\tau d\tau \int_0^\tau d\tau\, U_1''(X,\tau)} - \frac{\gamma^2}{m^3}\overline{\int_0^\tau d\tau\, U_1''(X,\tau) \int_0^\tau d\tau \int_0^\tau d\tau \int_0^\tau d\tau\, U_1'(X,\tau)}.$$

Including these terms $O(\omega^{-4})$ into the slow dynamic provide the EOM for slow variable as

$$m\ddot{X} + \gamma\dot{X} = -U_0'(X) - \frac{1}{m\omega^2}\overline{\int_0^\tau d\tau\, U_1'(X,\tau)\int_0^\tau d\tau\, U_1''(X,\tau)} +$$
$$\frac{\gamma}{m^2\omega^3}\overline{\int_0^\tau d\tau\, U_1''(X,\tau)\int_0^\tau d\tau \int_0^\tau d\tau\, U_1'(X,\tau)} - \frac{1}{2m^2\omega^4}U_0'''(X)\overline{\left[\int_0^\tau d\tau \int_0^\tau d\tau\, U_1'(X,\tau)\right]^2} -$$
$$\frac{1}{2m^2\omega^4}U_1'''(X,\tau)\overline{\left[\int_0^\tau d\tau \int_0^\tau d\tau\, U_1'(X,\tau)\right]^2} -$$
$$\frac{1}{m^2\omega^4}U_0''(X)\overline{\int_0^\tau d\tau \int_0^\tau d\tau\, U_1''(X,\tau) \int_0^\tau d\tau \int_0^\tau d\tau\, U_1'(X,\tau)} -$$
$$\frac{1}{m^2\omega^4}\overline{U_1''(X,\tau)\int_0^\tau d\tau \int_0^\tau d\tau\, U_1''(X,\tau)\int_0^\tau d\tau \int_0^\tau d\tau\, U_1'(X,\tau)} +$$
$$\frac{3}{m\omega^4}\dot{X}^2\overline{\int_0^\tau d\tau \int_0^\tau d\tau U_1''(X,\tau) \int_0^\tau d\tau \int_0^\tau d\tau\, U_1'''(X,\tau)} + \frac{3}{m\omega^4}\ddot{X}\overline{\left[\int_0^\tau d\tau \int_0^\tau d\tau\, U_1''(X,\tau)\right]^2} +$$
$$\frac{3\gamma}{m^2\omega^4}\dot{X}\overline{\left[\int_0^\tau d\tau \int_0^\tau d\tau\, U_1''(X,\tau)\right]^2} + \frac{\gamma^2}{m^3\omega^4}\overline{\int_0^\tau d\tau \int_0^\tau d\tau\, U_1''(X,\tau) \int_0^\tau d\tau \int_0^\tau d\tau\, U_1'(X,\tau)} + O(\omega^{-4}) +$$
$$\eta(t) \qquad (43)$$

Substitution of $\ddot{X}$ by $-\frac{V_0'}{m} - \frac{\gamma}{m}\dot{X}$, incorporates a very insignificant error of the order of $\omega^{-4}[O(\omega^{-4})]$ in Eq. (43). Performing suitable manipulation of algebra, finally get the following the EOM for the slow part (corrected up to the order ω^{-4})

$$m\ddot{X} + \gamma\dot{X} = -U_{eff}'(X) + \frac{3}{m\omega^4}\dot{X}^2\overline{\int_0^\tau d\tau \int_0^\tau d\tau U_1''(X,\tau) \int_0^\tau d\tau \int_0^\tau d\tau\, U_1'''(X,\tau)} +$$
$$\frac{3U_0'}{m^2\omega^4}\overline{\left[\int_0^\tau d\tau \int_0^\tau d\tau\, U_1''(X,\tau)\right]^2} + \frac{\gamma}{m^2\omega^3}\overline{\int_0^\tau d\tau\, U_1''(X,\tau)\int_0^\tau d\tau \int_0^\tau d\tau\, U_1'(X,\tau)} +$$
$$\frac{\gamma^2}{m^3\omega^4}\overline{\int_0^\tau d\tau \int_0^\tau d\tau\, U_1''(X,\tau) \int_0^\tau d\tau \int_0^\tau d\tau\, U_1'(X,\tau)} + \eta(t) \qquad (44)$$

where $U_{eff}(X)$ can be considered as the effective potential and can described as,

$$U_{eff}(X) = U_0(X) - \frac{1}{2m\omega^2}\overline{\left[\int_0^\tau d\tau\, U_1'(X,\tau)\right]^2} + \frac{1}{2m^2\omega^4}\overline{U_1''(X,\tau)\left[\int_0^\tau d\tau \int_0^\tau d\tau\, U_1'(X,\tau)\right]^2} +$$
$$\frac{1}{2m^2\omega^4}\overline{U_0''(X)\left[\int_0^\tau d\tau \int_0^\tau d\tau\, U_1'(X,\tau)\right]^2} \qquad (45)$$

It is to be noted here that the noise term only arises in the EOM of the slow variable, and the γ-containing terms are explicitly dropped from arising in the equation of U_{eff}, rather, two other terms of EOM contain it owing to the dissipative surrounding. If there is no interaction of the system with surrounding, the γ-containing terms do not arise in the dynamical equation. Here quantum effect is manifested in Eq. (44) in U_0 and U_1 through the correction terms Q_V^0 and Q_V^1 . If one had used the classical calculation only, there would be no contribution of Q_V^0 and Q_V^1. Then, the contribution of U_0 and U_1 would have been

replaced by V_0 and V_1. In the classical limit ($\hbar \to 0$), on incorporation of terms O (ω^{-3}), Eq.(44) converts to the following form

$$m\ddot{X} + \gamma\dot{X} = -U_0'(X) + \frac{1}{m\omega^2}\overline{\int_0^\tau d\tau U_1'(X,\tau) \int_0^\tau d\tau\, U_1''(X,\tau)} + \frac{\gamma}{m^2\omega^3}\overline{\int_0^\tau d\tau\, U_1''(X,\tau) \int_0^\tau d\tau \int_0^\tau d\tau\, U_1'(X,\tau)} + \eta(t)$$

which is identical with equation (28) of Ray Chaudhury and co-workers (Shit, Chattopadhyay & Ray Chaudhuri, 2012a). At this point, it is important to note that in the previous works (Shit, Chattopadhyay & Ray Chaudhuri, 2012, Shit, Chattopadhyay & Ray Chaudhuri, 2011a), pure quantum mechanical model upto the order ω^{-2} has been published. From the expression of effective time independent Langevin equation [Eq. (44)] of this description, different dynamical studies may be performed. By defining a particular model system potential, Eq. (44) may be numerically simulated (Shit, 2016) to investigate the escape rate of the perturbed/dressed particle and the influence of the external modulation on the resulting rate along with the thermal noise may also be studied. The effective potential described and characterized above has the capability to confine the particle. It is very crucial to note that a bound rapidly oscillating potential confines systems even if its time average disappears. This work may also have some applications. For instance, depending on the nature of spatial variation of the applied forces, the effective potential defined above often have more than one local minimum even if the initial (unmodified) potential has only single local minima. Under such situations, a collection of Brownian particles would tend to segregate in two separate collections.

Conclusion:

Reaction and feedback of a dynamical system to a rapidly oscillating periodic driving force are two of the most challenging and fundamental issues in the realm of chemical dynamics in condensed phases. Time dependent rapidly driven quantum dissipative systems exhibit an intricate interplay of linearity, SB coupling, and nonequilibrium behaviour as a result of the time dependent driving. In this work, beginning from a quantum mechanical system-bath Hamiltonian with explicit time-dependence, using multiple scale perturbation theory, an effective time-independent *c*-number generalized Langevin equation at leading order is derived with an effective time independent potential which permits one to survey the dynamics of the system under the influence of rapidly oscillating fields, in the architecture of methodologies that were designed for systems in the presence of time-independent potentials. Calculations for the dynamics of the slow part have been done perturbatively in powers of the frequency (ω) of the external driving force used to the order of $1/\omega^4$. The described work may contribute to the microscopic understanding of barrier crossing phenomena under the impact of a rapidly oscillating field in condensed phases, and in particular non-adiabatic effects and may help to understand and interpret many experimental results.

Acknowledgement

The author expresses her gratitude to Professor Sudip Kumar Chattopadhyay and Professor Jyotipratim Ray Chaudhuri, and is thankful to Kandi Raj College, Kandi, Murshidabad, West Bengal, India.

References

Barik, D., & Ray, D. S. (2005). Quantum state-dependent diffusion and multiplicative noise: a microscopic approach. *Journal of Statistical Physics*, *120*, 339-365. https://doi.org/10.1007/s10955-005-5251-y

Barik, D., Banerjee, D., & Ray, D. S. (2009). *Quantum Brownian motion in C-numbers: Theory and applications*. Nova Science Publishers.

Bhattacharya, S., Chattopadhyay, S., & Ray Chaudhuri, J. (2009). Investigation of Noise-Induced Escape Rate: A Quantum Mechanical Approach. *Journal of Statistical Physics*, *136*, 733-750. https://doi.org/10.1007/s10955-009-9802-5

Bukov, M., D'Alessio, L., & Polkovnikov, A. (2015). Universal high-frequency behavior of periodically driven systems: from dynamical stabilization to Floquet engineering. *Advances in Physics*, *64*(2), 139-226. https://doi.org/10.1080/00018732.2015.1055918

Chen, J. C., Hambro, L., Sinfailam, A. L., & Chung, K. T. (1973). Multiple-Scattering Expansions for Nonrelativistic Three-Body Collision Problems. VIII. Eikonal Approximation for the Faddeev-Watson Multiple-Scattering Expansion. *Physical Review A*, *7*(6), 2003. https://doi.org/10.1103/PhysRevA.7.2003

Denisov, S. I., Polyakov, A. Y., & Lyutyy, T. V. (2011). Resonant suppression of thermal stability of the nanoparticle magnetization by a rotating magnetic field. *Physical Review B*, *84*(17), 174410. https://doi.org/10.1103/PhysRevB.84.174410

Denisov, S. I., Sakmann, K., Talkner, P., & Hänggi, P. (2006). Mean first-passage times for an ac-driven magnetic moment of a nanoparticle. *Europhysics Letters*, *76*(6), 1001. https://doi.org/10.1209/epl/i2006-10403-3

Denisov, S. I., Sakmann, K., Talkner, P., & Hänggi, P. (2007). Rapidly driven nanoparticles: Mean first-passage times and relaxation of the magnetic moment. *Physical Review B*, *75*(18), 184432. https://doi.org/10.1103/PhysRevB.75.184432

Floquet, G. (1883). Sur les équations différentielles linéaires à coefficients périodiques. In *Annales Scientifiques de l'École Normale Supérieure, 12*, 47-88. https://doi.org/10.24033/asens.220m

Ghosh, P., Shit, A., Chattopadhyay, S., & Chaudhuri, J. R. (2011). A semiclassical approach to explore the bistable kinetics of a Brownian particle in a nonequilibrium environment. *Journal of Statistical Mechanics: Theory and Experiment*, *2011*(02), P02026. https://doi.org/10.1088/1742-5468/2011/02/P02026

Hänggi, P. (2002). Stochastic resonance in biology how noise can enhance detection of weak signals and help improve biological information processing. *ChemPhysChem*, *3*(3), 285-290. https://doi.org/10.1103/RevModPhys.70.223

Hänggi, P., Łuczka, J., & Spiechowicz, J. (2020). Many faces of nonequilibrium: anomalous transport phenomena in driven periodic systems. *arXiv preprint arXiv:2002.11690*. https://doi.org/10.5506/APhysPolB.51.1131

Jung, P. (1993). Periodically driven stochastic systems. *Physics Reports*, *234*(4-5), 175-295. https://doi.org/10.1016/0370-1573(93)90022-6

Kapitsa, P. L. (1951). THERMAL CONDUCTANCE AND DIFFUSTION IN LIQUID MEDIUM IN THE CASE OF PERIODIC FLOW. I. DETERMINATION OF COEFFICIENT OF WAVE TRANSFER IN A PIPE, SLIT, AND CHANNEL. *Zhur. Eksptl'i Teoret. Fiz.*, *21*.

Kim, C., Talkner, P., Lee, E. K., & Hänggi, P. (2010). Rate description of Fokker–Planck processes with time-periodic parameters. *Chemical Physics*, *370*(1-3), 277-289. https://doi.org/10.1016/j.chemphys.2009.10.027

Landau, L. D., & Lifshitz, E. M. (2013). *Quantum Mechanics: Non-Relativistic Theory* (Vol. 3). Elsevier.

Paul, W. (1990). Electromagnetic traps for charged and neutral particles. *Reviews of Modern Physics*, *62*(3), 531. https://doi.org/10.1103/RevModPhys.62.531

Shirley, J. H. (1965). Solution of the Schrödinger equation with a Hamiltonian periodic in time. *Physical Review*, *138*(4B), B979. https://doi.org/10.1103/PhysRev.138.B979

Shit, A. (2016). High-frequency behavior of periodically modulated stochastic quantum system: activated escape. *Journal of Statistical Mechanics: Theory and Experiment*, *2016*(5), 053204. https://doi.org/10.1088/1742-5468/2016/05/053204

Shit, A., Chattopadhyay, S., & Chaudhuri, J. R. (2011a). Effective quantum Brownian dynamics in presence of a rapidly oscillating space-dependent time-periodic field. *Physical Review E*, *83*(6), 060101. https://doi.org/10.1103/PhysRevE.83.060101

Shit, A., Chattopadhyay, S., & Chaudhuri, J. R. (2011b). Towards an understanding of escape rate and state dependent diffusion for a quantum dissipative system. *Chemical Physics*, *386*(1-3), 56-72. https://doi.org/10.1016/j.chemphys.2011.06.002

Shit, A., Chattopadhyay, S., & Chaudhuri, J. R. (2012a). Controlling activated processes of nonadiabatically, periodically driven dynamical systems: A multiple scale perturbation approach. *The Journal of Chemical Physics*, *136*(23), 234506. https://doi.org/10.1063/1.4729848

Shit, A., Chattopadhyay, S., & Chaudhuri, J. R. (2012b). Escape rate for a quantum particle moving in a time-periodic rapidly oscillating potential: A time-independent approach. *Physical Review E*, *85*(5), 051102. https://doi.org/10.1103/PhysRevE.85.051102

Shit, A., Chattopadhyay, S., & Chaudhuri, J. R. (2012c). Quantum escape in the presence of a time-periodic oscillating force. *Europhysics Letters*, *97*(4), 40006. https://doi.org/10.1209/0295-5075/97/40006

Shit, A., Chattopadhyay, S., & Chaudhuri, J. R. (2013). Kapitza-Landau time window for a periodically driven system with friction: a system-bath Hamiltonian approach. *The European Physical Journal B*, *86*, 1-9. https://doi.org/10.1140/epjb/e2012-30852-0

Shit, A., Chattopadhyay, S., & Ray Chaudhuri, J. (2012d). Time-independent description of rapidly driven systems in the presence of friction: Multiple scale perturbation

approach. *Chaos: An Interdisciplinary Journal of Nonlinear Science*, *22*(1), 013131. https://doi.org/10.1063/1.3692970

Spiechowicz, J., Hänggi, P., & Łuczka, J. (2022). Velocity multistability vs. ergodicity breaking in a biased periodic potential. *Entropy*, *24*(1), 98. https://doi.org/10.3390/e24010098

Spiechowicz, J., Marchenko, I. G., Hänggi, P., & Łuczka, J. (2023). Diffusion coefficient of a Brownian particle in equilibrium and nonequilibrium: Einstein model and beyond. *Entropy*, *25*(1), 42. https://doi.org/10.3390/e25010042

Weiss, U. (2012). *Quantum dissipative systems*.

Zwanzig, R. (1961). Lectures in Theoretical Physics vol 3 ed WE Brittin. *BW Downs and J Downs (New York: Interscience)*.

Zwanzig, R. (1973). Nonlinear generalized Langevin equations. *Journal of Statistical Physics*, *9*(3), 215-220. https://doi.org/10.1007/BF01008729

https://doi.org/10.31674/book.2023pcbs012

A Review Article on Cryopreservation of Human Embryo - Methods, Timing, and Other Considerations for Optimizing Embryo Cryopreservation Program

Somdeb Bhattacharya, Rajosree Seth, Debolina Das, Shanaz Parveen, Chaitali Barman*

Department of Zoology, Surendranath College, University of Calcutta, West Bengal, India

*Corresponding Author's Email: chaitalibarman@gmail.com

ABSTRACT

The contribution of embryo cryopreservation to the birth rate per in vitro fertilization cycle has escalated from a rare subsidy to a vital tool that is called upon to augment the cycle outcome. Embryology laboratories must identify the embryo stage, quality criteria and methodology that will optimize their ability to preserve each embryo's reproductive potential. This chapter reviews the principles of cryopreservation, outcomes based on embryo stage and cryopreservation method and benchmarks that may be employed by the laboratory to measure the performance of their embryo cryopreservation program. Cryopreservation of human embryos from the 2-cell stage up to the morula stage is a safe procedure that has been carried out for the last 25 years. Experience with blastocyst cryopreservation is still limited and pregnancy rates after the use of frozen or thawed blastocysts vary greatly. Vitrification has improved the success of embryo cryopreservation. However, this technique cannot yet be considered a routine procedure. Despite all of the advantages for infertile couples, cryopreservation of human embryos creates severe ethical problems because of the surplus frozen embryos that either have to be destroyed or perhaps used for research. Embryo adoption may provide a solution to imminent medical, ethical and social problems. Cryopreservation of embryos is increasing worldwide. As more data becomes available, scientists are now able to report on outcomes. With better outcomes for women and pregnancies as a result of frozen embryo transfer, they need to consider the implications of using it in routine practice, especially in preference to the current strategy of fresh embryo transfer.

Keywords**:** *Cryopreservation; Pregnancy; Blastocyst; Frozen Embryo; Fresh Embryo Transfer; Vitrification; Pronuclear Stage; Slow Freezing; IVF*

Introduction

In 1972, two research groups independently reported the successful cryopreservation of mouse embryos. The following year, the first calf was born from frozen embryos (Wilmut,1973). In the same year, the first human pregnancy was successfully induced from frozen embryos; however, the pregnancy was terminated in the second trimester due to spontaneous abortion. Subsequently, cryopreservation of sperm and embryos (CP) became routine procedures in Human Assisted Reproduction (AR), and Oocyte Cryopreservation (EC) became increasingly popular in clinical practice. In addition, embryo CP has reduced

the number of new embryo transfers and increased the efficiency of IVF cycles. Embryo CP is also a critical tool in canceling embryo transfers (ETs) due to the risk of Ovarian Hyperstimulation, Endometrial Bleeding, Elevated Serum Progesterone Levels on the day of trigger, and other unforeseen events. However, there is still a lot of debate on the optimal stage, protocols and procedures, and Cryoprotective Additives (CPA's) to be used. On average, a Frozen Stored Embryo has a potential of 4% to become a living child, and Cryopreserved Embryos do not exceed 8% to 10% of the total number of BIRs born from AR (de Jong *et al.,* 2002). However, it cannot be denied that the success of zygote/embryo CP has significantly increased the clinical benefit and cumulative conception rate for couples after a single cycle of ovulatory stimulation and IVF in almost 70% of frozen cycles. Patients ranged in age from 31 to 40 years, with 7.5% >41 years. The 'age effect' is evident in the Frozen Embryo Survival Rate (FESR), which has slowly but steadily declined over the past decade as the age of patients increased by an average of 4 years without any alteration in the freezing process. (89% versus 81%; $P < 0.0001$). Frozen cycles are much less likely to be successful over the age of 30, and there's a big difference in success rates over the age of 35 compared to those under 30. The success rate depends on a few things, like how well the freezing process works, which carriers are used (open vs. closed), how often embryos and oocytes are frozen in assisted reproductive programs, how you pick them, and how successful the fresh embryo transfers are. The success rate can be expressed in terms of survival rates, but that's not enough - it's also important to make sure the cells keep working properly.

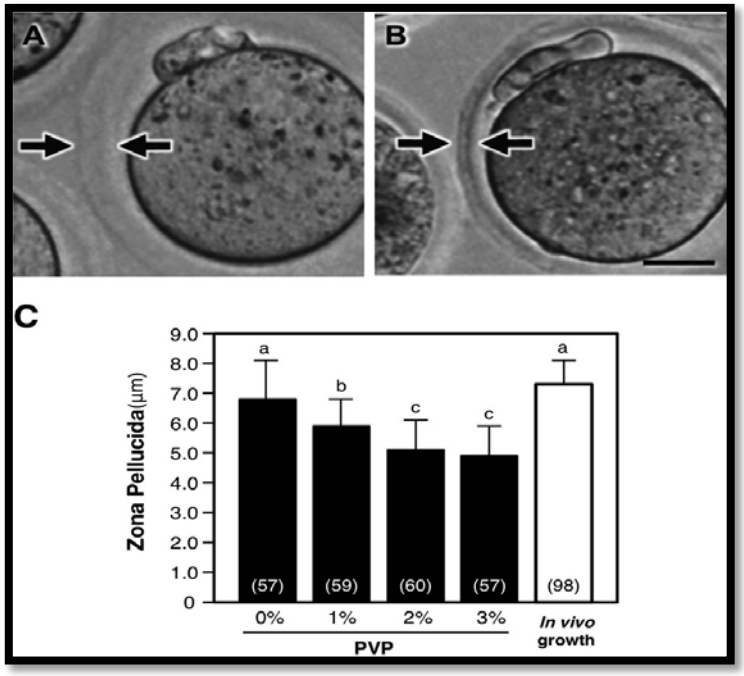

Source:https://www.researchgate.net/publication/323206028/figure/fig5/AS:618288744771590@1524422932053/Comparison-of-zona-pellucida-thickness-after-growth-in-culture-medium-supplemented-with.png

***Figure 1: Comparison of Zona Pellucida Thickness after Growth in Culture Medium Supplemented with Various Concentrations of PVP*.**

Methodology

Principles of Cryopreservation

Cryopreservation is basically trying to slow down embryos by cooling them down from room temperature (20°C) to 196 °C. This means that during changes in temperature and phase, the embryos are exposed to an environment where they can't survive without help, which puts them at risk for different types of harm, or "cryoinjury". Cryopreservation has previously been extensively discussed in reproductive medicine (Leibo & Pool, 2011). There are four different temperature ranges for the damage that happens during cooling (Nagy *et al.,* 2009).

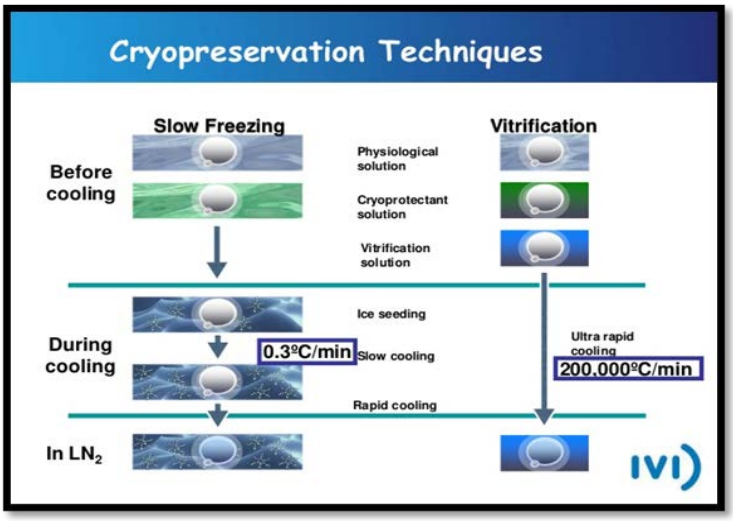

Source:https://image.slidesharecdn.com/humanembryotransfer11-141015070029-conversion-gate01/95/human-embryo-transfer11-19-638.jpg?cb=1413356445

Figure 2: Techniques of Embryo Cryopreservation

+15 to -5°C

Chilling injury refers to permanent damage that occurs prior to the cells' exposure to freezing temperatures. The lipid bilayer of a cell membrane is fluid and permeable. Phospholipids transition from a liquid to a gel phase as the embryos cool down to -5°C (Ghetler *et al.,* 2005) . When you're cryopreserving embryos from certain mammals that have high levels of lipids, this kind of irreversible harm is a big problem. Oocyte meiotic spindles, microtubules, and cytoplasmic lipid droplets can all be harmed by a chilling injury (Bianchi *et al.,* 2005) . Cryopreservation procedures need to be adapted to the embryonic stage because the ability of mammalian embryos to withstand chilling injuries changes over time (Pedro *et al.,* 2005).

-5 to -80°C

When temperatures go from -5°C to -80°C, ice crystals form on both the inside and outside of cells. These ice crystals can cause damage to the cells, either physically or chemically. Scientists first came up with the idea of a "two-stage hypothesis" for cell damage at these temperatures back in 1972 (Mazur, 1963; Mazur, Leibo & Chu, 1972). Slow cooling causes

extracellular ice to form. When cells cool slowly, the gases in the embryo's environment become hypertonic, reducing the amount of intracellular ice. The hypertonic solution pulls water out of the cell. The "solution effect" destabilizes proteins and damages the cell membrane. However, cells can be damaged when exposed to high levels of electrolytes for long periods of time. Rapid cooling, which prevents water from leaving the cell quickly enough to form lethal intracellular ice, may be equally harmful (Kleinhans & Mazur, 2007).

-50 to -150°C

Solutions can break at temperatures between 50 and 150°C. If the solution is too broken, it can damage big cells or groups of cells, like oocytes or embryos, and it can also damage the cytoplasm or zonal pellucida. The frequency of solution fracture damage has not been published, and this is still a speculative concern (Rall & Meyer, 1989).

-150 to -196°C

Embryos are stored in nitrogen vapours (-190°C) or, in general, in deterrent nitrogen (-196°C). Patients in perpetuity provoke requests like its endless storage leads to subordinate ecchymosis. As of now, there is no proof that anything was harmed while being stored for a period comparable to a human lifetime. Accidental warming is a common cause of cryoinjury, but if storage temperatures are kept stable, chemical reactions stop at -120°C and storage at -196°C prevents thermally driven reactions, so the embryos are essentially suspended in time (Gao & Critser, 2000). Although background ionizing radiation had been raised as a potential danger, the accumulation of direct harm would take centuries (Rall, 2001). Since liquid nitrogen is not sterile and most microorganisms can survive its storage, there is a chance that infectious agents could be transmitted during storage (Bielanski, 2012). Virus from cryopreserved human embryos was transmitted twice, and bovine viral diarrhea virus was transmitted twice after cryopreserved embryo transfer (Drew *et al.,* 2002). Although these diseases cannot be directly linked to embryo cryopreservation and storage, it was demonstrated under experimental conditions that the concern about disease transmission is valid and should be considered when selecting cryopreservation and storage equipment (Bielanski *et al.*, 2000).

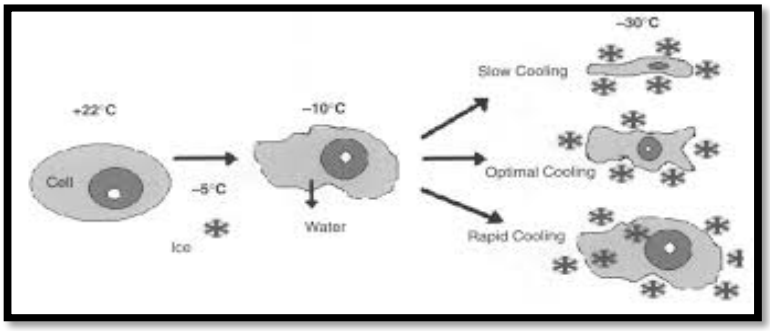

Source:https://www.google.com/url?sa=i&url=https%3A%2F%2Fwww.semanticscholar.org%2Fpaper%2FMechanisms-of-cryoinjury-in-living-cells.-Gao

Figure 3: Mechanisms of Cryoinjury in Living Cells

Warming from -190 to +20°C

The risk of injury during warm-up is the same as during cool-down. Warming has different effects depending on whether intracellular ice builds up or the cells are dehydrated during freezing once intracellular ice develops. Rapid thawing can protect cells by preventing small intracellular ice crystals from recrystallizing into larger, more dangerous ice crystals. In addition to preserving the plasma membrane surrounding the cytoplasm in an apparently viable form, cryopreservation techniques should protect embryos from damage that may not be visible on morphological examination, such as damage to intracellular organelles, the cytoskeleton and cell junctions (Vincent & Johnson, 1992). Despite all these risks to embryo health and survival, they have a remarkable ability to repair or avoid damage using recognized cryopreservation techniques and cryoprotectants, and after thawing, they continue to grow (Van den Abbeel *et al.,* 1997).

Cryoprotectants

Karow defines a cryoprotectant as "any additive that can be introduced into cells prior to freezing and that results in a higher post-thaw survival rate than can be achieved without its addition" and is useful for cryopreservation of cells (Karow, 1974). He has two categories of cryoprotectants (CPAs). Osmotic agents, including small compounds that permeate cell membranes, displace intracellular water, and balance intracellular solutes, and impermeable macromolecular agents like CPA, help maintain the external osmotic gradient and contribute to cellular dehydration. Permeable CPAs include substances such as 1,2-propanedial (PROH), dimethylsulfoxide (DMSO), ethylene glycol (EG), and glycerol. Low molecular weight disaccharides such as sucrose and trehalose are popular choices for sugars used as impermeable CPAs. Impermeable CPA, which is lost after thawing, creates an osmotic gradient that controls the passage of water across cell membranes and helps avoid osmotic shock. For cells to survive cryopreservation, water and invading CPA must be able to cross the cell membrane. The osmotic gradient pushes the highly permeable intracellular water out of the cell, causing the cell to contract, and when the embryo is immersed in a solution containing CPA at hyperosmolarity, the permeable CPA gradually diffuses into the cell. allows you to The ratio of water volume to cell membrane surface area, permeability to water at each stage, and the fact that oocytes and early-stage embryos are less permeable to CPA than morulae and blastocysts Maximize water and CPA exchange (Kasai *et al.*, 1990).The two strategies through which water and entering CPAs invade the cell film are basic dissemination over the lipid bilayer, which is exceptionally temperature-dependent, and through temperature-independent, hydrophilic channels made by proteins called aquaporins. A later ponder found that the kind and amount of aquaporins communicated alter with each formative organization and may influence the layer porousness of CPAs that's interesting to each level (Xiong *et al.,* 2013). A realistic appearance of channel sorts, layer porousness, and alteration in cell measure with each embryonic stage was included within the records of the Alpha agreement assembly on cryopreservation.

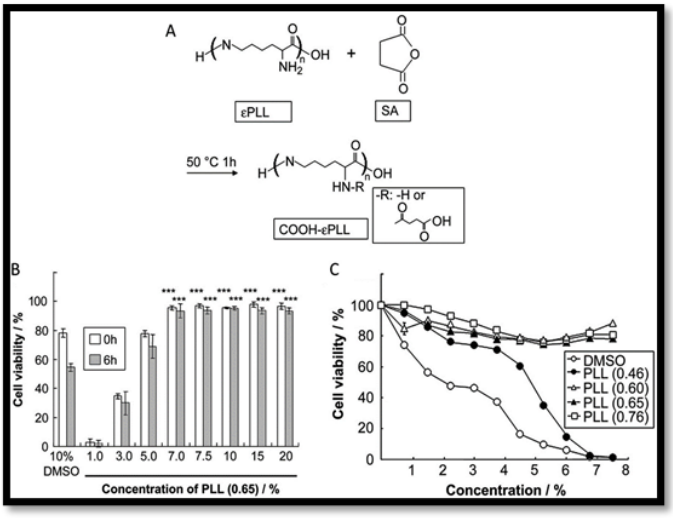

Source:https://media.springernature.com/original/springerstatic/image/chp%3A10.1007%2F978-981-13-1244-1_18/MediaObjects/435189_1_En_18_Fig1_HTML.png

Figure 4: Development and Application of Cryoprotectants

Results and Discussion

Embryos are frequently vitrified by either slow freezing or quick freezing during cryopreservation. Permeating and nonpermeating CPAs are utilized in both approaches and are eventually reduced to allow for controlled embryonic rehydration during heat. The main differences among the techniques are the duration of CPA exposure, CPA concentration, chilling rate, and warming rate.

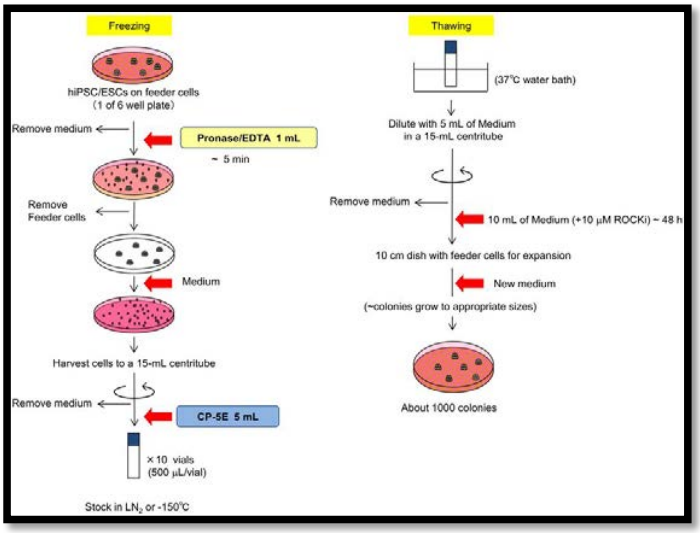

Source:https://www.researchgate.net/profile/TeruoAkuta/publication/260214091/figure/fig3/AS:214337806442502@1428113523669/Schema-shows-the-protocol-for-the-slow-freezing-procedure-with-the-combined-use-of.png

Figure 5: Scheme Shows the Protocol for the Slow-Freezing Procedure with the Combined use of Pronase/EDTA and Cryopreservation Medium CP-5E (Left) And Rapid Thawing (Right).

Slow Freezing

Moderate hardening, additionally popularly known as unity hardening, addresses intracellular glaze composition and osmotic harm by promoting yell or cautious dosages of CPAs. In 1989, Testart and companions Earlier to hardening, embryos are equilibrated in a hyperosmotic composition holding 1 to 2 M recording CPA (glycerol for blastocysts, PROH or DMSO for pronuclear and gap systematized embryos), accompanying the CPA either in a distinct step over the course of 10 to 20 records or in a step-intelligent habit. Cell decrease is guarded as the water firmly leaves the container and is replaced with each coming CPA. Once balance has been achieved, the container book is rebuilt. The embryos are moved to a mass killing of an ethnic group holding an alliance of 1 to 2 M filtering and 0.2 to 0.3 M nonpermeating CPAs before being introduced into 0.25 mL straws or cryovials and established in a reserved-rate icebox. The embryos are cooled just before 6 to 8 strengths Celsius—just over the point at which something melts from the solution—at a pace of 1 to 2 points per minute. Since the concentrations second-hand for liberal chilling are incompetent to completely prevent intracellular glaze establishment, the aggregation of CPA is raised, all the while abating the process by advancing hailstone composition. Extracellular hail is manually fashioned (plant) by accompanying pre-discouraged grippers by touching the container or hay as certainly from the embryos as it stands proficient. When water freezes, extracellular CPAs and different solutes abridge, forming a new osmotic slope that pulls more water away from the fetus while allowing more CPA in. The hotness of the regulated-rate room is claimed to be loyal for an additional 10 notes to present the embryos with an opportunity to readjust before being very evenly (0.3°C/brief time period) reduced to beneath 30°C. The container is a desire for liquid nitrogen, which is enough intracellular CPA to limit further intracellular hailstone results. The appropriate thawing rate is predetermined to establish the temperature at which chilling stops. Embryos that have undergone cooling at a temperature of 30 to 40°C would have a higher water content and require a higher rate of toasting (200 to 350°C / brief time period) compared to those that have undergone abating at 80°C, and would require a more consistent rehydration rate (25°C for a short time period). In order to control rehydration, the embryos are introduced to an aggregation of nonpermeating CPA (frequently sweet substance), that is to say, two occasions above the aggregation of the definitive cryopreservation resolution. By lowering the standard of osmotic inequality across the container sheath, harsh CPAs have more opportunity to wordy consume the container, and well-absorbed water enters the container at a slower rate (Leibo, 1983).

Vitrification

The term "vitrification" is used to refer to the process of transforming a material into glass; however, it is also used interchangeably to refer to the techniques employed to achieve this transformation. By allowing CPAs to permeate the cell membrane, cell dehydration is accomplished similarly to slow freezing but in a different way. In slow chilling, there is no attempt to assert evenness on either side of the container sheath, the moment of truth for aridity is brief, the aggregation of CPAs is greater, and the rate of chilling is particularly fast.

What keeps cells alive? By drastically increasing viscosity and reducing the amount of time the sample is exposed to temperatures that might lead to chilling damage and the production of ice crystals, vitrification aims to transform liquid into glass. Vitrification is the name given to the process of turning a material into a bottle, but it's more often used to describe the techniques used to manage this change..

Source:https://encryptedtbn0.gstatic.com/images?q=tbn:ANd9GcTj1cy6V0JdauDKrRtvsNaVAtjEGcSUdFb0cKrZmIswopbmNz6PhE8Fg_lxF7L4Gu6KZJ0&usqp=CAU

Figure 6: Embryo Vitrification

Cell dehydration is accomplished similarly to slow freezing by allowing CPAs to permeate the cell membrane, but unlike slow chilling, there is no attempt to uphold balance on either side of the container sheet, the moment of truth for aridity is short, the aggregation of CPAs is larger, and the rate of abating is considerably faster. How do cells remain alive? The goal of vitrification is to turn liquid into glass by dramatically increasing viscosity while minimizing the amount of time the sample is exposed to temperatures that might cause chilling damage and ice crystal formation (Fahy *et al.,* 1984). Compared to slow freezing, embryo vitrification procedures are far simpler to use and do not require controlled-rate freezers or other expensive equipment. To make penetrating CPAs, it is usual to join EG and hydrogen with PROH, glycerol, or DMSO. Embryos are exposed to these CPAs in two stages: In order to let intracellular water out of the container and to allow CPA transportation to achieve evenness, initially they are not subjected to a 50% aggregate of the decisive CPA aggregation over 5 to 15 meeting notes. Then, they are only unprotected from the 30 to 40% resolution of CPAs because they should be (about 60 in 2007) (Ghetler *et al.,* 2005). For example, the fetus is cooled at a temperature set per person who carries or carries something, and the sample and liquid nitrogen capacity and resolution arrangement are cooled at 2.5*30*103 °C/short time. The fetus is quickly cooled by taking it out of liquid nitrogen at a temperature of -196°C and filling it with a warmed solution that has reached the ideal temperature. The harsh CPAs must be remote as instantly as likely to humiliate the amount momentary the embryos are unprotected to the poisonous answer. The filtering CPA spreads out slightly from the container, but the toasting answers contain a super-

aggressive aggregation of a non-permeable CPA (usually about 1.0 M of hydrogen) to show osmotic protection and slow down the rate at which the water comes back in. This is the same as thawing later on in steady, chilly weather. The relatively simple vitrification processes used today are the result of years of research into how to cool and bake at fast speeds while still keeping the embryos safe from heat and contamination in liquid nitrogen. After the first human pregnancies and births were reported in the early 1980s, slow refrigeration quickly became the standard for cryopreservation of human embryos. At that time, vitrification wasn't considered possible because of the dangerous CPA concentrations needed to cool large amounts of solution in straws and bottles used for slow freezing. In order to correctly lacquer rodent embryos, Rall and Fahy set a 45-liter blend of CPAs (DMSO, acetamide, propylene glycol, and EG) into a standard 0.25 cc cryostraw before soaking it in liquid nitrogen in 1985. Recognizing the need to lower the detrimental results of singular CPA, this was accomplished (Fahy *et al., 1984*). Despite claims that pups were innate from transplanted embryos that had sustained vitrification, the use of likely perilous DMSO and the temperate toxin acetamide dissuaded investigators from investigating this further vitrification of human embryos. Efforts to replicate this method with cleavage-stage human embryos only resulted in 1/11 surviving (9%). This was thought to be due to the toxic levels of cells "swelling and bursting" after the CPAs were heat-depleting step by step. This was because there wasn't any nonpermeable CPA, but it was probably more likely due to Osmotic Shock in Vitrification Solution, 0.25-0.5 M Nonpermeating Sucrose + 2 M Highly Permeable DMMO) increased embryo survival to 9/11 (82%), but no pregnancies were observed after transfers to six individuals (Kola *et al.,* 1988).

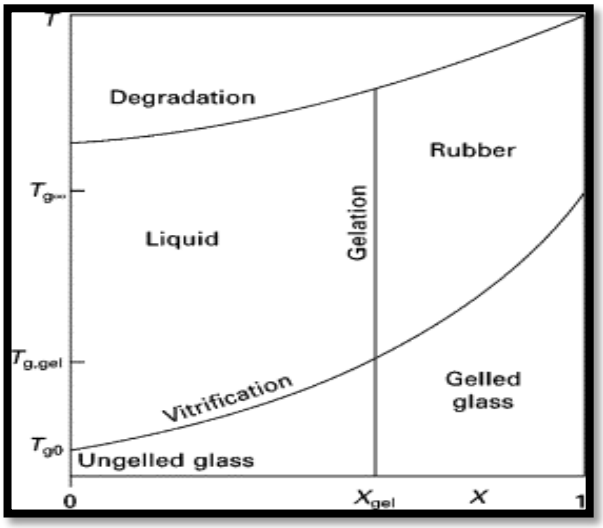

Source: https://ars.els-cdn.com/content/image/3-s2.0-B9780857090867500018-f01-04-9780857090867.gif

Figure 7: Vitrification – An Overview

The development of vitrification solutions containing various ratios of piercing and nonpenetrating CPAs was the focus of study over the following ten years, and reports of births after vitrification of animal oocytes and embryos were made (Kasai *et al.,* 1990).

Researchers looking for strategies to cryopreserve oocytes and, due to enhanced culture systems, blastocyst-stage embryos have rekindled interest in vitrification for clinical IVF procedures (Kuleshova *et al.,* 1999).It became very obvious that they needed to make some more changes to speed up cooling and heating to make sure to get consistently high survival rates since both types of cells seem to be really sensitive to cold damage. The most effective way to speed up this process was to reduce the temperature of the sample and the size of the device we were using to contain the embryo (Arav *et al.* 1996). They showed that by cooling and rewarming oocytes and embryos in a range of 0.07 L, or "minimum droplet size," they were able to vitrify these cells at about 50% less CPA concentration than we would need for large-volume vitrification (Arav, 1992). Almost a decade ago, more than 20 devices were created to hold embryos by cooling and heating microvolumes of vitrification solutions, as early papers described the efficient vitrification of embryos in small volumes (Vajta & Nagy, 2006). Clinical IVF facilities are using different vitrification methods to preserve human embryos now that there's more and more proof that embryos survive, develop, and even give birth to healthy babies after vitrification. Different stages of embryos go through different CPAs, but cooling can be done by either directly touching the open system or by touching the closed system with liquid nitrogen. These variables must be considered when selecting and developing a method for use in clinical settings (Valbuena *et al*., 2012).

Finally, the percentage of thawed embryos that result in healthy babies is used to measure the effectiveness of cryopreservation technology. Embryo quality and stage before and after cryopreservation should be considered when comparing the results of cryopreserved embryo transfer with those of non-frozen controls. Since embryo quality criteria may be stricter in cryopreserved embryo transfer than in fresh embryo transfer or embryo stage, the transition time may vary from treatment group to treatment group (Surrey *et al.,* 2010). Because of the virtually infinite combinations of embryo stage, selection criteria, caspase-paired plasma (CPA) type and concentration, device type, cooling and heating rate, and other factors, a comprehensive comparative analysis of reported results in the field of Human Embryo Cryopreservation has been largely unsuccessful. Not many RCTs have been conducted to evaluate the clinical effectiveness of various embryo cryo-reservation methods or to identify the stage of development that maximizes the rate of cumulative zygotic and neonatal growth for a collection cycle (AbdelHafez *et al.,* 2010). Reviewing research that contrasts fresh and frozen embryo transfers is important in determining the impact of cryopreservation on embryos, especially if enough information is provided to establish the number of children per zygote for the oocyte extraction (Ali & Shelton*,* 1993).

Conclusion

Embryo cryopreservation has become an integral part of the IVF process, playing a significant role in the cumulative, one-off increase in live births from conception to egg retrieval following the birth of the initial frozen cut-stage embryo. There has been much debate among IVF doctors about the idea of abandoning all new transfers, as evidence shows that after frozen embryo transfer, live births and newborns are better for singleton

pregnancies than with fresh transfers. A significant change in clinical practice would require large-scale RCTs, as such an approach has many social, clinical, and economic implications. The purpose of this review was to examine the results of different cryopreservation techniques at each stage of development. The best stage and quality of cryopreserved embryos must be determined by programs that are not limited by legal restrictions. The laboratory must be able to evaluate its performance against competitors using key performance indicators provided by the Alpha Society. 47 After gradual freezing and vitrification, pronuclear-stage embryos exhibit comparable results, according to this review. In general, vitrification promotes better blastocyst and cleavage-stage embryo survival rates. Some facilities have tailored their slow-freezing procedure to provide similarly high implantation and survival rates per thawed embryo at both phases. The observation of decreased metabolism in embryos at the cleavage stage following gradual freezing suggests that vitrification could be a preferable option. 119 If the survival and implantation rates for both procedures are the same for blastocyst-stage embryos, the choice boils down to staffing, equipment, and the cryopreservation device. Slow freezing takes significantly longer than vitrification, but when large numbers of embryos are ready for cryopreservation, vitrification can take longer. Even though vitrification only takes a tiny amount of liquid nitrogen and only takes about an hour to get from the fridge to storing the embryos, slow freezing takes a lot of expensive equipment to keep up and makes it harder to get rid of the embryos. Plus, it needs to be kept cold. And since glazing can be contaminated, it has to be done in a closed environment kept cold because of the possibility of contamination, glazing must be done in closed equipment. By using HSV straws produced excellent results despite slower cooling and warming rates. Other sealed glass devices are available, but the results of these devices were not included in the discussion because the formulas for the glass solutions were not disclosed. Validation studies and training programs must be created before any new method is used in the lab to guarantee that performance will meet standards. These metrics will offer performance evaluations in a timely manner.

Acknowledgement

The authors express their sincere thanks to the Principal, Surendranath College for his support and encouragement in implementing this review project at the undergraduate level. The authors are also grateful to all the teachers of the Department of Zoology, Surendranath College for their able guidance and support. The authors expressed a special thanks to Dr. Harishankar Biswas, Department of Chemistry, of the same college, for his continuous support in completing the article within the stipulated time. The authors are also very thankful to their families, friends, and all well-wishers who have helped and supported them a lot in the completion of this review article.

References

AbdelHafez, F. F., Desai, N., Abou-Setta, A. M., Falcone, T., & Goldfarb, J. (2010). Slow freezing, vitrification and ultra-rapid freezing of human embryos: a systematic review and meta-analysis. *Reproductive Biomedicine Online*, *20*(2), 209-222. https://doi.org/10.1016/j. rbmo.2009.11.013

Ali, J., & Shelton, J. N. (1993). Design of vitrification solutions for the cryopreservation of embryos. *Reproduction*, *99*(2), 471-477.

Arav, A. (1992). Vitrification of oocyte and embryos. In 'New Trends in Embryo Transfer'.(Eds A. Lauria and F. Gandolfi.) pp. 255–264.

Arav, A., Zeron, Y., Leslie, S. B., Behboodi, E., Anderson, G. B., & Crowe, J. H. (1996). Phase transition temperature and chilling sensitivity of bovine oocytes. *Cryobiology*, *33*(6), 589-599. https://doi.org/10.1006/cryo.1996.0062

Bianchi, V., Coticchio, G., Fava, L., Flamigni, C., & Borini, A. (2005). Meiotic spindle imaging in human oocytes frozen with a slow freezing procedure involving high sucrose concentration. *Human Reproduction*, *20*(4), 1078-1083. https://doi.org/10.1093/humrep/deh736

Bielanski, A. (2012). A review of the risk of contamination of semen and embryos during cryopreservation and measures to limit cross-contamination during banking to prevent disease transmission in ET practices. *Theriogenology*, *77*(3), 467-482. https://doi.org/10.1016/j.theriogenology.2011.07.043

Bielanski, A., Nadin-Davis, S., Sapp, T., & Lutze-Wallace, C. (2000). Viral contamination of embryos cryopreserved in liquid nitrogen. *Cryobiology*, *40*(2), 110-116. https://doi.org/10.1006/cryo.1999.2227

de Jong, D., Eijkemans, M. J. C., Beckers, N. G. M., Pruijsten, R. V., Fauser, B. C. J. M., & Macklon, N. S. (2002). The added value of embryo cryopreservation to cumulative ongoing pregnancy rates per IVF treatment: is cryopreservation worth the effort?. *Journal of Assisted Reproduction and Genetics*, *19*, 561-568. https://doi.org/10.1023/A:1021211115337

Drew, T. W., Sandvik, T., Wakeley, P., Jones, T., & Howard, P. (2002). BVD virus genotype 2 detected in British cattle. *The Veterinary Record*, *151*(18), 551.

Fahy, G. M., MacFarlane, D. R., Angell, C. A., & Meryman, H. T. (1984). Vitrification as an approach to cryopreservation. *Cryobiology*, *21*(4), 407-426. https://doi.org/10.1016/0011-2240(84)90079-8

Gao, D., & Critser, J. K. (2000). Mechanisms of cryoinjury in living cells. *ILAR Journal*, *41*(4), 187-196. https://doi.org/10.1093/ilar.41.4.187

Ghetler, Y., Yavin, S., Shalgi, R., & Arav, A. (2005). The effect of chilling on membrane lipid phase transition in human oocytes and zygotes. *Human Reproduction*, *20*(12), 3385-3389. https://doi.org/10.1093/humrep/dei236

Karow Jr, A. M. (1974). Cryopreservation: pharmacological considerations. Organ preservation for transplantation, 86-107.

Kasai, M., Komi, J. H., Takakamo, A., Tsudera, H., Sakurai, T., & Machida, T. (1990). A simple method for mouse embryo cryopreservation in a low toxicity vitrification solution, without appreciable loss of viability. *Reproduction*, *89*(1), 91-97.

Kleinhans, F. W., & Mazur, P. (2007). Comparison of actual vs. synthesized ternary phase diagrams for solutes of cryobiological interest. *Cryobiology*, *54*(2), 212-222. https://doi.org/10.1016/j.cryobiol.2007.01.007

Kola, I., Kirby, C., Shaw, J., Davey, A., & Trounson, A. (1988). Vitrification of mouse oocytes results in aneuploid zygotes and malformed fetuses. *Teratology*, *38*(5), 467-474. https://doi.org/10.1002/tera.1420380510

Kuleshova, L., Gianaroli, L., Magli, C., Ferraretti, A., & Trounson, A. (1999). Birth following vitrification of a small number of human oocytes: case report. *Human Reproduction*, *14*(12), 3077-3079. https://doi.org/10.1093/humrep/14.12.3077

Leibo, S. P. (1983). A one-step in situ dilution method for frozen thawed bovine embryos. *Cryo-letters*, *4*, 387-400.

Leibo, S. P., & Pool, T. B. (2011). The principal variables of cryopreservation: solutions, temperatures, and rate changes. *Fertility and Sterility*, *96*(2), 269-276. https://doi.org/ 10.1016/j.fertnstert.2011.06.065

Mazur, P. (1963). Kinetics of water loss from cells at subzero temperatures and the likelihood of intracellular freezing. *The Journal of General Physiology*, *47*(2), 347-369. https://doi.org/10.1085/jgp.47.2.347

Mazur, P., Leibo, S. P., & Chu, E. H. Y. (1972). A two-factor hypothesis of freezing injury: evidence from Chinese hamster tissue-culture cells. *Experimental Cell Research*, *71*(2), 345-355. https://doi.org/10.1016/0014-4827(72)90303-5

Nagy, Z. P., Vajta, G., Chang, C., Kort, H. (2009). The human embryo: vitrification. In: Gardner, D.K., Weissman, A., Howles, C.M., Shoham, Z., eds. Textbook of Assisted Reproductive Technologies, Laboratory and Clinical Perspectives, 3rd ed. London, UK: Informa, 289.

Pedro, P. B., Yokoyama, E., Zhu, S. E., Yoshida, N., Valdez Jr, D. M., Tanaka, M., ... & Kasai, M. (2005). Permeability of mouse oocytes and embryos at various developmental stages to five cryoprotectants. *Journal of Reproduction and Development*, *51*(2), 235-246. https://doi.org/10.1262/jrd.16079

Rall, W. F. (2001). Cryopreservation of mammalian embryos, gametes, and ovarian tissues: current issues and progress. *Assisted Fertilization and Nuclear Transfer in Mammals*, 173-187.

Rall, W. F., & Meyer, T. K. (1989). Zona fracture damage and its avoidance during the cryopreservation of mammalian embryos. *Theriogenology*, *31*(3), 683-692. https:// doi.org/ 10.1016/0093-691X(89)90251-3

Surrey, E., Keller, J., Stevens, J., Gustofson, R., Minjarez, D., & Schoolcraft, W. (2010). Freeze-all: enhanced outcomes with cryopreservation at the blastocyst stage versus pronuclear stage using slow-freeze techniques. *Reproductive Biomedicine Online*, *21*(3), 411-417. https://doi.org/10.1016/j.rbmo.2010.04.008

Testart, J., Forman, R., Belaisch-Allart, J., Volante, M., Hazout, A., Strubb, N., & Frydman, R. (1989). Embryo quality and uterine receptivity in in-vitro fertilization cycles with or without agonists of gonadotrophin-releasing hormone. *Human Reproduction*, *4*(2), 198-201. https://doi.org/10.1093/oxfordjournals.humrep.a136871

Vajta, G., & Nagy, Z. P. (2006). Are programmable freezers still needed in the embryo laboratory? Review on vitrification. *Reproductive Biomedicine Online*, *12*(6), 779-796. https://doi.org/10.1016/S1472-6483(10)61091-7

Valbuena, D., Póo, M. E., Aguilar-Gallardo, C., Martinez, S., Cobo, A. C., Pellicer, A., & Simón, C. (2012). Comparison of Cryotip vs. Cryotop for mouse and human blastomere vitrification. *Fertility and Sterility*, *97*(1), 209-217. https://doi.org/10.1016/j.fertnstert.2011.10.008

Van den Abbeel, E., Camus, M., Van Waesberghe, L., Devroey, P., & Van Steirteghem, A. C. (1997). Viability of partially damaged human embryos after cryopreservation. *Human Reproduction (Oxford, England)*, *12*(9), 2006-2010. https://doi.org/10.1093/humrep/12.9.2006

Vincent, C., & Johnson, M. H. (1992). Cooling, cryoprotectants, and the cytoskeleton of the mammalian oocyte. *Oxford Reviews of Reproductive Biology*, *14*, 73-100.

Wilmut, I. U. (1973). Experiments on the low temperature preservation of cow eggs. *Vet. Rec.*, *92*, 686-690.

Xiong, Y., Tan, Y. J., Xiong, Y. M., Huang, Y. T., Hu, X. L., Lu, Y. C., ... & Sheng, J. Z. (2013). Expression of aquaporins in human embryos and potential role of AQP3 and AQP7 in preimplantation mouse embryo development. *Cellular Physiology and Biochemistry*, *31*(4-5), 649-658.

https://doi.org/10.31674/book.2023pcbs013

X-ray Diffraction and Photophysical Studies of Pyromellitic Dianhydride-Anthracene Molecular Charge Transfer Complex at 298K

Sugata Samanta
Department of Chemistry, The Bhawanipur Education Society College, Kolkata, West Bengal, India

Corresponding Author's E-mail: sugata.samanta@thebges.edu.in

ABSTRACT

A molecular charge transfer (CT) complex was characterized by crystal structure analysis, and photophysical studies, followed by theoretical calculations, utilizing anthracene as a donor and pyromellitic dianhydride (PMDA) as an acceptor. A (π-π) stacking interconnection is observed in the 1:1 PMDA-Anthracene charge transfer complex. The optimized geometry structures obtained from the density functional theory (DFT) calculation in the gas phase support the observed result. In pure and mixed solvents, an unusual decrease in wavelength was observed in steady state absorption and emission spectra with increasing solvent polarity. The binding constant for the PMDA-Anthracene charge transfer (CT) complex is determined to be in the order of 10^3.

Keywords: *Charge Transfer Complex; Crystal Structure; Stacking Interconnection; Binding Constant*

Introduction

Donor-acceptor charge transfer (CT) complexes possessing low-energy electronic states serve as valuable systems for studying the influence of molecular interactions on electron hole delocalization as well as transfer rates. Molecular donor-acceptor cocrystals indeed represent ideal systems for investigating charge transfer phenomena due to their chemical simplicity and well-defined structures.

Various chemical reactions like addition, substitution, and condensation are known to involve the participation of charge transfer complexes (Datta *et al.,* 2000). Non-linear optical materials and electrical conductivities have received significant attention due to their involvement in these complexes (Yakuphanoglu *et al.,* 2005). The electron donor-acceptor (EDA) interaction plays a crucial role not only in the drug-receptor binding mechanism but also in interface chemistry, solar energy storage, and various biological fields (Andrade *et al.,* 2000). In pharmaceutical analysis, the EDA interactions of specific π-acceptors have been utilized, highlighting their significance in this field (Hamed *et al.,* 2000).

Methodology

Pyromellitic dianhydride (PMDA) (Figure 1A), anthracene (Figure. 1B), acetonitrile (ACN), dichloromethane (DCM), and potassium bromide (KBr) used in the study were all reagent grade chemicals purchased from Sigma-Aldrich. Unless otherwise mentioned, these chemicals were used without purification. ACN and DCM were purified by distillation while anthracene was purified by sublimation.

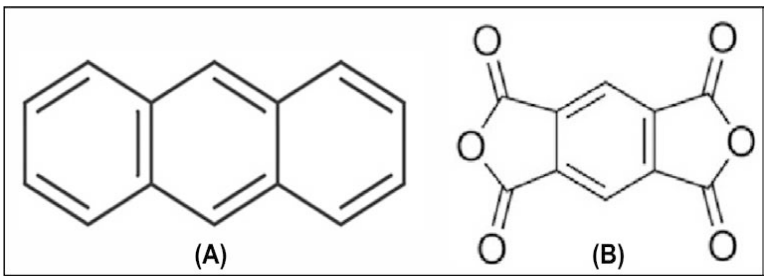

Figure 1: Structures of (A) PMDA (Pyromellitic dianhydride) and (B) Anthracene

Synthesis of the complex

The single crystal of the CT complex was grown by allowing a 1:1 solution of the donor and the acceptor in dichloromethane (DCM) to slowly evaporate at room temperature. The solution was transferred into a glass tube, which was then covered by parafilm with a tiny orifice. The tube was placed inside a desiccator and left undisturbed for a period of two months. PMDA-Anthracene CT complex was found in red color. To prepare a powder sample, a little quantity (5%) of the crystal was combined with potassium bromide (KBr). The mixture was then ground together and a transparent pellet of the CT complex was prepared for photophysical studies.

Instrumentations

Crystallography study

The convenient crystal of the PMDA-Anthracene CT complex (red block) was arranged on glass fiber. The intensity data of the crystal was determined at a temperature of 298 K. During the data collection no crystal decay was observed. Absorption corrections based on multi-scans were applied in all cases using the SADABS software. The structure was solved using the direct method (Sheldrick *et al.,* 1990), which involved all available data and aimed to minimize the residuals. For structural solutions and refinements, SHELXL-97 software (Sheldrick, 1996) was employed. In the study, Table 1 provides the crystallographic data and refinement details. Anisotropic refinement was performed for all non-hydrogen atoms in the study. In the final refinement, the hydrogen atoms were fixed isotropically with a C-H bond length in the order of 0.95 Å. Data collection was performed using the SMART software package, while data reduction was carried out using the SAINT software package.

Absorption, and steady state emission studies

The UV-Vis absorption spectra were recorded using a Hitachi U-4010 spectrophotometer Model at room temperature. The steady state emission measurements were conducted using a Hitachi F-7000 Spectrofluorimeter Model equipped with a Xenon lamp (150W). A quartz cell with a path length of 1 cm and solid-state accessories were employed for the measurements.

Density Functional Theory (DFT) and Time-Dependent Density Functional Theory (TDDFT) calculations:

The results reported here were performed using the "Gaussian 03 program package" with the support of Gauss View. The geometry structures of the PMDA-anthracene charge transfer (CT) complex in the gas phase have been developed at 6-31 G and 6-31(d) G (Hehre *et al.,* 1972) levels. The optimizations were carried out using the BELYP functional for the ground state. Optimized geometry structures in the excited state were also obtained using the CIS method with the same basis sets.

Results and Discussion:

Descriptions of Crystal Structure:

A single crystal of PMDA-Anthracene CT complex, which is convenient for solid state structural investigation has been obtained and is depicted in Figure 2. Figure 2A displays a view of the subunit with a (1:1) stoichiometry, showcasing the atom labeling. In the triclinic P-1 space group, the donor and acceptor subunits of PMDA-Anthracene are crystallized, with one molecular mass unit accommodated per unit cell. A closer examination of the packing arrangement in the subunit reveals that the cocrystal is primarily composed of alternating π-acceptor/π-donor stacks (Figure 2B). The planes of the acceptor and donor components are nearly parallel to each other. Figure 2C illustrates the distance between the two planes in the stack, which measures 3.25Å.

Table 1: The Crystallographic Data for the PMDA-Anthracene Charge Transfer (CT) Complex

Parameters	PMDA-Anthracene
Composition	$C_{24}H_{12}O6$
Formula wt.	396.35
Crystal System	Triclinic
Space group	P-1
Stoichiometry	1:1
Data collection temperature	298 K
a, Å	7.2308(7)
b, Å	7.3652(6)
c, Å	9.5532(8)
α, deg	69.516(4)
β, deg	87.440(5)
γ, deg	68.744(5)
V, Å^3	442.202
ρ_{calc}, Mg.m^{-3}	1.462
λ(Mo K$_\alpha$), [Å]	0.71073
Z	9
F (000) / μ mm^{-1}	848 / 0.101
$2\theta_{max}$ [^{o}]	55
Reflections Collected/Unique	4108 / 3882
R_{int}/ GOF on F^2	0.0212 / 0.837
No. of parameters	289
$R1^a(F_0)$, $wR2^b(F_0)$	0.0349, 0.1017
Largest difference peak, Deepest hole, eÅ^{-3}	0.228, -0.254

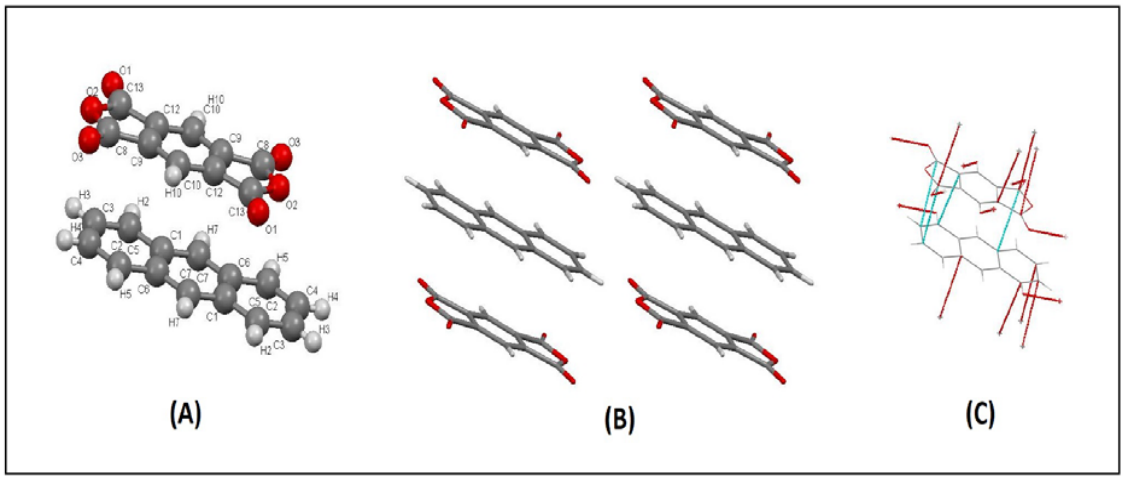

Source: Primary Source

Figure 2: The Single Crystal Structure of the PMDA-Anthracene Charge Transfer Complex Demonstrating (A) Repeating Donor and Acceptor Unit with Labeling, (B) The Packing Arrangement (Hydrogen Atoms Omitted) Showing the Extended Stacks of the Alternate Units, (C) Short Contacts Observed within the CT Complex.

Absorption Studies in Pure and Mixed Solvents at 298K:

Figure 3 and Table 2 display the absorption spectra of the CT complex recorded at 298K in various solvents, including acetonitrile (ACN), dichloromethane (DCM), and mixed solvents containing both ACN and DCM.

For the determination of the binding constant of the PMDA-Anthracene charge transfer (CT) complex, the increase of the charge transfer band in the absorption spectra was monitored by gradually adding the acceptor to a constant concentration of the donor. The binding constant was calculated using the Benesi Hilderbrand equation (Benesi *et al.,* 1949) represented by Equation 1.

$$\frac{1}{\Delta A} = \frac{1}{b\Delta\epsilon[C]_0[H]_0K_a} + \frac{1}{b\Delta\epsilon[H]_0} \qquad \text{.....(1)}$$

Where:

ΔA represents the enhancement in the CT absorbance, H_0 is the total concentration of the donor, C_0 is the concentration of the acceptor, K_a is the binding constant, and ε is the molar absorptivity of the charge transfer complex.

Binding constant (K_a) of PMDA-Anthracene charge transfer (CT) complex was determined by plotting 1/ΔA against $[C]_0^{-1}$ according to the Benesi-Hilderbrand equation. Figure 4 illustrates the Benesi Hilderbrand plot of the CT complex. Slope of this linear plot corresponds to the binding constant (Ka). In this case, the calculated binding constant is found to be 4.0×10^3.

Table 2: Absorption and Emission Spectral Data of PMDA-Anthracene Charge Transfer (CT) Complex in Pure Solvents and Mixed Solvents At 298K.

Solvent	$\lambda_{max}^{(A)}$ (nm)	$\bar{\nu}_A$ (cm^{-1})	$\lambda_{max}^{(F)}$ (nm)	$\bar{\nu}_F$(cm^{-1})
Pure DCM	502	1.9920×10^4	605	1.6528×10^4
DCM:MeCN(4:1)	488	2.0491×10^4	590	1.6949×10^4
DCM:MeCN(3:2)	484	2.0661×10^4	585	1.7094×10^4
DCM:MeCN(1:1)	482	2.0746×10^4	582	1.7182×10^4
DCM:MeCN(2:3)	480	2.0833×10^4	580	1.7241×10^4
DCM:MeCN(1:4)	478	2.0920×10^4	578	1.7301×10^4
Pure MeCN	476	2.1008×10^4	576	1.7361×10^4

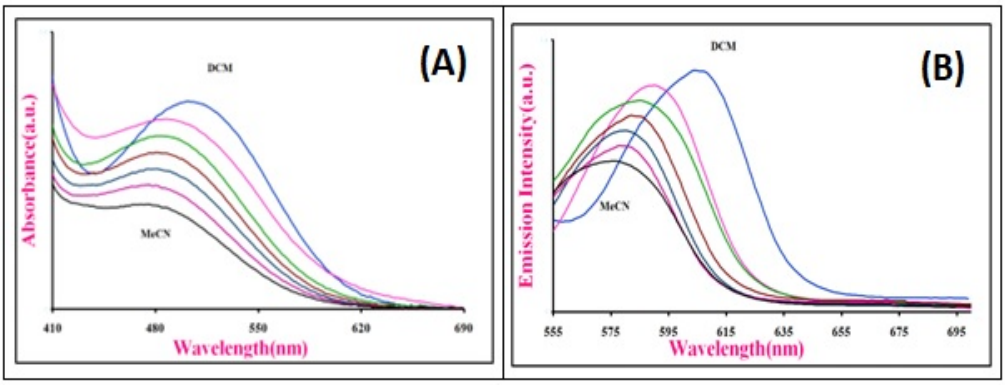

Source: Primary Source

Figure 3: The (A) Absorption and (B) Steady State Emission Spectra of PMDA-Anthracene Charge Transfer (CT) Complex at 298K in the Following Solvents: 1. Dichloromethane (DCM) 2. DCM : ACN (4:1) 3. DCM : ACN (3:2) 4. DCM : ACN (1:1) 5. DCM : ACN (2:3) 6. DCM : ACN (1:4) 7. Acetonitrile (ACN)

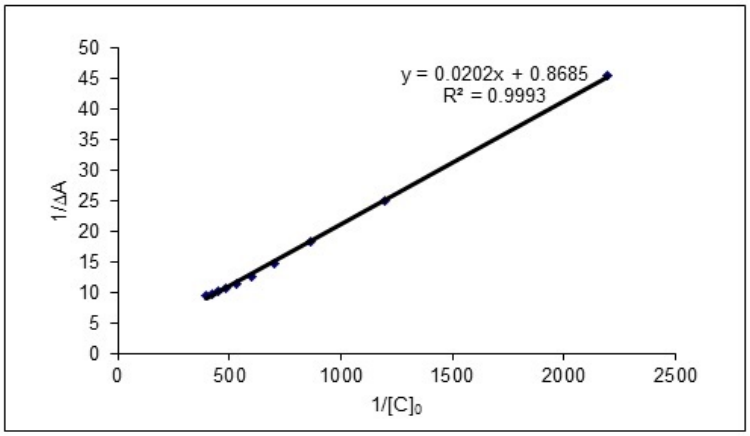

Source: Primary Source

Figure 4: The Benesi Hildebrand Plot for the PMDA-Anthracene CT Complex

Steady State Emission Spectra Studies at 298K:

Figure 3 (Table 2) displays the steady state emission spectra of the PMDA-Anthracene charge transfer (CT) complex in various solvents, including acetonitrile (ACN), dichloromethane (DCM), and mixed solvents. The stacking structure of the PMDA-Anthracene complex exhibits an interesting phenomenon of blue shift as the polarity of the solvent increases, in two pure solvents and mixed solvents. In acetonitrile (ACN), the PMDA-Anthracene complex shows a blue shift of 3647 cm^{-1}, while in dichloromethane (DCM), the blue shift is observed to be 3392 cm^{-1}. Figure 5 presents the steady state emission spectra of PMDA-Anthracene charge transfer (CT) complex in solid state. The emission peak of the charge transfer complex is observed at 618 nm. The PMDA-Anthracene charge transfer (CT) complex in the solid state demonstrates a red shift in the absorption and emission spectra compared to that observed in the solution (Table 2).

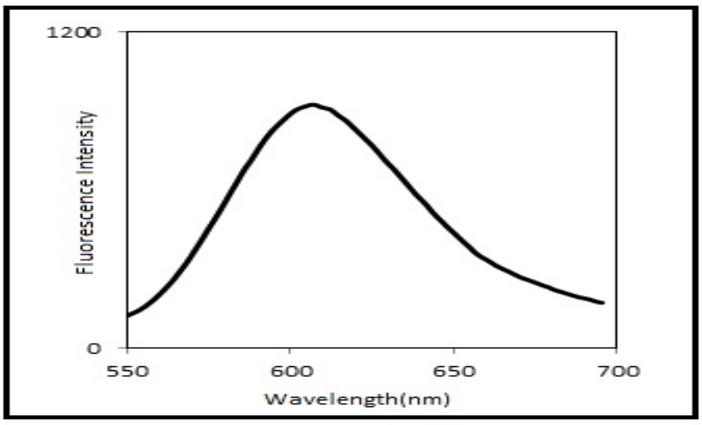

Source: Primary source

Figure 5: Emission Spectra of PMDA-Anthracene Charge Transfer (CT) Complex in Solid State at 298K

Density Functional Theory (DFT) and Time-Dependent Density Functional Theory (TDDFT) calculations:

All the bond distances of the PMDA-Anthracene charge transfer (CT) complex in the gas phase, as obtained from the optimized structure, closely resemble those determined from the X-ray diffraction studies. Table 3 provides the ionization potential values and presents the dipole moment values for both the ground state and excited state of PMDA-Anthracene charge transfer (CT) complex. Additionally, it highlights the presence of a (π-π) stacking interconnection in the complex. Figure 6 illustrates the geometry-optimized structures of the PMDA-Anthracene CT complex in both ground and excited states. The distance between the acceptor and donor plane is determined to be 3.3Å. Figure 7 displays the distribution of formal charges on different atoms within the PMDA-Anthracene charge transfer (CT) complex. The calculated values obtained from the DFT-TDDFT studies exhibit a good agreement with the experimental data. This indicates that the theoretical calculations accurately capture the properties and behavior of the PMDA-Anthracene charge transfer (CT) complex, providing reliable insights and supporting the experimental findings.

Table 3: Excitation Properties of PMDA-Anthracene CT Complex from Theoretical Calculation

Complex	λ_{ab}(nm)	E_{CT}(theo) (eV)	ν_0(eV)	IP_1 (eV)	IP_2 (eV)	IP_{av} (eV)	μ_{ground}(D)	$\mu_{excited}$(D
PMDA-Anthracene	502	2.4594	2.4701	6.5068	6.829	6.6679	0.1433	0.3841

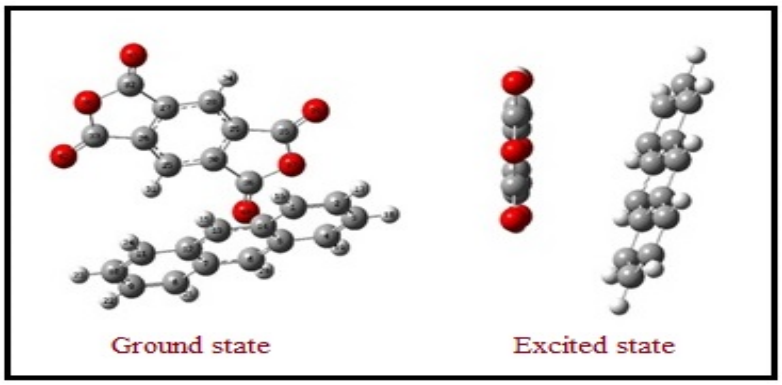

Source: Primary source

Figure 6: Geometry Optimized Structure of PMDA-Anthracene CT Complex

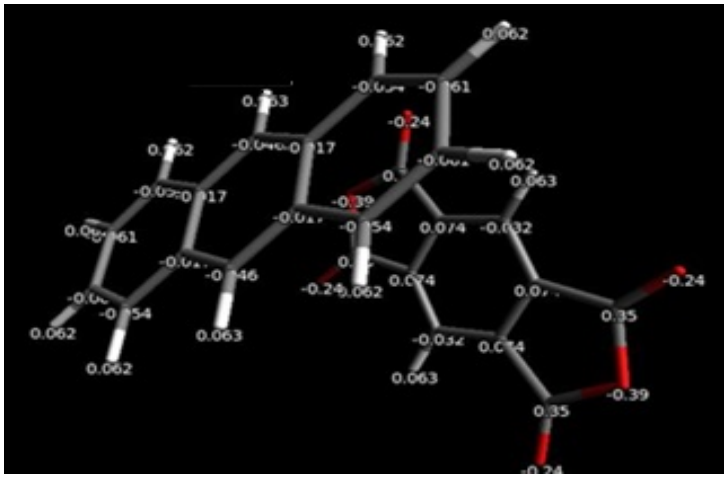

Source: Primary source

Figure 7: Distribution of Formal Charges on Different Atoms of PMDA-Anthracene CT Complex

Conclusion:

The crystal structure of PMDA with anthracene demonstrates a (π-π) stacking interaction between the acceptor and donor molecules. The electronic spectra of the PMDA-Anthracene charge transfer (CT) complex have been extensively characterized in two pure solvents, various mixed solvents, and solid state. The observed unusual blue shift in the electronic spectra of the PMDA-Anthracene charge transfer (CT) complex with increasing solvent polarity can be attributed to the specific interactions of the acceptor molecule with the solvent. The stacking structure of the PMDA-Anthracene charge transfer (CT) complex, as determined by X-ray crystallography, exhibits a close

agreement with the structure obtained from theoretical calculations. The features of the stacked PMDA-Anthracene charge transfer (CT) complex described in this study have implications beyond the specific system investigated. The observed stacking interaction provides valuable insights into the intermolecular interactions in supramolecular assemblies, biomolecules, and their complexes with other molecules.

Acknowledgement:

Acknowledgement is bestowed with warmest thanks to the supervisor Dr. Sanjib Ghosh and also special thanks should be given to Dr. Manoranjan Maity for crystal structure analysis, Ms. Sagarika Sanyal for DFT-TDDFT calculations, and Dr. Pinki Saha Sardar for providing solid state accessories in F-7000 Spectrofluorimeter.

References:

Andrade, S. M., Costa, S. M., & Pansu, R. (2000). Structural changes in W/O Triton X-100/cyclohexane-hexanol/water microemulsions probed by a fluorescent drug Piroxicam. *Journal of Colloid and Interface Science*, *226*(2), 260-268. https://doi.org/10.1006/jcis.2000.6821

Benesi, H. A., & Hildebrand, J. H. J. (1949). A spectrophotometric investigation of the interaction of iodine with aromatic hydrocarbons. *Journal of the American Chemical Society*, *71*(8), 2703-2707. https://doi.org/10.1021/ja01176a030

Datta, K., Banerjee, M., Seal, B. K., & Mukherjee, A. K. (2000). Ground state EDA complex formation between [60] fullerene and a series of polynuclear aromatic hydrocarbons. *Journal of the Chemical Society, Perkin Transactions 2*, (3), 531-534. https://doi.org/10.1039/a907219e

Hamed, M. M. A., Abdel-Hamid, M. I., & Mahmoud, M. R. (1998). Molecular complexes of some N-aryldithiocarbamates with π-electron acceptors. *Monatshefte für Chemie, 129*(2), 121-127. https://doi.org/10.1007/PL00010148

Hehre, W. J., Ditchfield, R., & Pople, J. A. (1972). Self—consistent molecular orbital methods. XII. Further extensions of Gaussian—type basis sets for use in molecular orbital studies of organic molecules. *The Journal of Chemical Physics*, *56*(5), 2257-2261. https://doi.org/10.1063/1.1677527

Sheldrick, G. M. (1990). Phase annealing in SHELX-90: direct methods for larger structures. *Acta Crystallographica Section A: Foundations of Crystallography*, *46*(6), 467-473. https://doi.org/10.1107/S0108767390000277

Sheldrick, G. M. (1996). shelxl-97: fortran program for the refinement of crystal structures from diffraction data, Göttingen University, Göttingen, Germany, 1997. Molecular graphics were done using the commercial package shelxtl-plus, Release 5.05/V, Siemens Analytical X-ray Instruments. *Inc., Madison, I*. https://doi.org/10.1107/S0021889800007184

Yakuphanoglu, F., Arslan, M., Küçükislamoğlu, M., & Zengin, M. (2005). Temperature dependence of the optical band gap and refractive index of poly (ethylene terepthalate) oligomer–DDQ complex thin film. *Solar Energy*, *79*(1), 96-100. https://doi.org/10.1016/j.solener.2004.09.017

https://doi.org/10.31674/book.2023pcbs014

Benefits of Green Tea: A Review

Nilofer Khatoon
Department of Botany, Surendranath College, University of Calcutta, West Bengal, India

Corresponding Author's Email: niloferk.botanysnc@gmail.com

ABSTRACT

Green tea is considered one of the most beneficial beverages, not only by traditional Chinese medicine but also worldwide. Green tea is not only a hydrating beverage, but its chemical composition consists of catechins and other polyphenols, which make it responsible for having a health-promoting effect. Green tea also contains certain vitamins and minerals that increase its antioxidant potential. Recent reviews and different studies have shown its health benefits in different diseases like cardiovascular, few forms of cancer, obesity, weight control, skin effects and diabetic control. They also contribute to the betterment of oral health and other physiological functions like anti-hypertensive effects, anti-fibrotic properties, neuroprotective properties, antibacterial and antivirasic activity. Considering the vast beneficial effect of green tea, it has been included in the group of beverages with important functional properties. The health benefits and adverse effects of green tea have been reviewed time and again. This review paper is intended to highlight the positive effects of drinking green tea.

Keywords: *Green Tea; Polyphenol; Catechin; Antioxidant*

Introduction:

Camellia sinensis (L.) Kuntze. (Gardner, Ruxton & Leeds, 2007), is the most popular beverage after water consumed worldwide. Green, black and Oolong teas are consumed depending on their fermentation process and antioxidant level (Graham, 1992, Yamamoto *et al.,* 1997). The most significant health effects of different polyphenolic compounds (flavandiols, flavonols, flavonoids, and phenolic acids) found in green tea have been thoroughly investigated and may constitute about 20% of the dry weight (Dulloo *et al.,* 1999). Approximately 3 million tons of different tea leaves are produced per year worldwide, of which 20% are green tea (Cabrera, Artacho & Giménez, 2006). Green tea was first exported from India to Japan in the 17th century. A tea ceremony is held in Japanese society to celebrate the culture of drinking tea. There are two varieties of green tea very popular among the Japanese population: Matcha and Sencha, both derived from the same tea plant but differing mostly in flavour and texture (Wilson, 2018). During the winters in Japan, the farmers covered the tea leaves to protect them from freezing, which led to the harvesting of Matcha tea leaves. The Matcha variety is cultivated after keeping it in shade for a month or two before harvesting. The cultivation method of Matcha tea leaves increases its chlorophyll content along with its amino acid content giving its distinct bright, vibrant green colour and umami flavour. The complete tea leaves are consumed in Matcha providing more health benefits. In the case of Sencha tea leaves, only the leaves are consumed, which are harvested by sun drying throughout the year and then steamed immediately to maintain the colour and nutrient content (Jakubczyk *et al*., 2020; Horie, Ema & Sumikawa, 2017). History shows that the Western world preferred black tea,

whereas the Asian world consumed more green tea. Recently, green tea has gained global attention due to the presence of naturally preserved potential biochemical contents like polyphenols, catechins and others that have huge health benefits like neurodegenerative diseases, anti-anxiety, cardiovascular disease, anti-inflammatory, cancer, regulating aging, cholesterol, anti-arthritic, and anti-angiogenic impacts (Chacko *et al*., 2010; Sumpio *et al*., 2006).

The green tea polyphenols are mostly represented by the flavonols, especially catechins. Amongst all the sources, like chocolate, red grapes, wine, and apples, the predominant source of catechins is green tea (Cabrera, Artacho & Giménez, 2006; Wierzejska, 2014). The main composition of black tea is tannin, and that of green tea is catechins. The caffeine in tea leaves varies depending on the age of the leaf, where younger leaves will have a higher concentration (Dufresne & Farnworth, 2001). Green tea contains 126 mg/100 ml of catechins, according to the European Food Safety Authority (EFSA), whereas, according to the Food and Drug Administration (FDA), green tea contains 71 mg/100 ml of epigallocatechin gallate (Rietveld & Wiseman, 2003). Green tea also contains proteins (15–20% dry weight), minerals and trace elements (5% dry weight), carbohydrates (5-7% dry weight), and trace amounts of vitamins (B, C, E), xanthic bases and lipids (linoleic and linolenic acid), pigments (chlorophyll, carotenoids), and volatile compounds (alcohols, lactones, aldehydes, esters and hydrocarbons). Different minerals like calcium, manganese, selenium, magnesium, fluoride, and zinc are present in different concentrations depending on the age and size of tea leaves (Cabrera, Artacho & Giménez, 2006). The chemical content of fresh tea leaves is 3%–4% methylxanthine alkaloids, which include theobromine, caffeine, theophylline, and phenolic acids (Gulcin, 2006).

Table 1: Composition of Green tea, black tea and its infusion (Cabrera, Artacho & Giménez, 2006)

Compound	Green tea*(%)	Black tea*(%)	Infusion†(%)
Proteins	15	15	trace
Amino acids	4	4	3.5
Fibre	26	26	0
other carbohydrates	7	7	4
Lipids	7	7	trace
Pigments	2	2	trace
Minerals	5	5	4.5
Phenolic compound	30	5	4.5
Oxidised phenolic compounds	0	25	4.5

* Data referred to dry weight

† Black tea, infusion time: 3 min

Literature Review

In Asian folk medicine and traditional Chinese medicine, green tea is used as an effective medicine for treating different diseases (Wierzejska, 2014; Eberhardt, Lee & Liu, 2000). Since green tea can provide many physiological benefits, it is considered a functional food as well. Studies have shown that green tea is also known for its positive effect on blood pressure and heart disease. It possesses high levels of antioxidants and is used for anti-

aging and neuroprotective effects (Afzal, Safer & Menon, 2015). The fresh leaves are heated at high temperatures after harvesting to inactivate the polyphenol oxidizing enzymes, which helps to protect the vitamin content of tea (Yamamoto *et al.,* 1997).

Several reports using animal models show that green tea catechins can provide protection against degenerative diseases (Crespy & Williamson, 2004; Roomi *et al*., 2005). Studies also suggest that green tea has antiproliferative activity on hepatoma cells and hypolipidemic activity on treated hepatoma rats and can act as a preventive agent in mammary cancer post-initiation. Green tea extract and its isolated components were found to be effective as antitumorigenic agents and as immune modulators in immune dysfunction, which can be caused by either carcinogen treatment or transplanted tumours (Babu, Sabitha & Shyamaladevi, 2006; Unno *et al*., 2007). They were also found to be effective in controlling neurological problems and oxidative stress. Different findings have shown that green tea possesses antimutagenic, antioxidant, and anticarcinogenic properties that are applied in the prevention of different types of cancer (Koo & Cho, 2004; Yamamoto *et al.,* 1997). The most common cancer among women is malignant breast cancer. The preventive and therapeutic activities of green tea components have shown anticarcinogenic effects against breast cancer in several experimental studies (Zhang *et al*., 2007). Several reports show that green tea catechins inhibit neuraminidase activity and viral replication by controlling the cellular oxidation reduction process, suggesting that the natural polyphenols, especially the flavonols, can antagonize the proliferation of SARS-Cov-2 (Elmezayen *et al*., 2021; Aanouz *et al*., 2021; Enmozhi *et al*., 2021). The polyphenols were found to be less toxic than any other drugs, and even when consumed at high concentrations, they showed no cytotoxic effect, making them a potential antiviral drug. Green tea has had an inhibitory effect against *Helicobacter pylori*, influenza virus and *Herpes simplex* virus showing its efficiency in treating diarrhea and typhoid since ancient times. They are also effective against adenovirus in in vitro condition. The effectiveness of green tea catechins as antifungal activity against *Candida albicans* in humans has also been studied by Hirasawa and Takada (2004). Studies show that the polyphenol content of green tea has shown activity against a wide range of microorganisms. They slow down the growth of both Gram positive and Gram-negative bacterial species with moderate potency (Yam, Shah & Hamilton-Miller, 1997; Taylor, Hamilton-Miller & Stapleton, 2005).

The catechin called epigallocatechin-3-gallate (EGCG), which is one of the important compounds in green tea with antioxidant properties, helps to prevent the formation of free radicals in the body by stopping cell damage and therefore strengthening the immune system. Research has shown EGCG's ability to help treat various diseases. A significant quantity of essential oils is present in green tea (Ganesan, Kumar & Rao, 2011). The benefits are huge if used properly and under proper guidance (Vuong, 2014). Green tea has a huge role to play in oral hygiene maintenance due to its antibacterial and antioxidant properties (Page & Kornman, 1997; Priya *et al*., 2015). Several reports have shown that green tea intake can reduce the risk of fatty liver diseases, liver cirrhosis, hepatitis, and chronic diseases (Yin *et al*., 2015; Fisher *et al*., 1997). Diabetes, obesity and overweight are growing rapidly throughout the world and are becoming threats to human health, affecting a large number of populations. This threat can be controlled and prevented with

the help of long-term consumption of tea catechins that reduces high fat diet induced obesity and coronary diseases. The photoprotective activity of green tea polyphenols helps in the prevention of solar UVB light induced skin disorders like photoaging, melanoma and others. Several studies suggest that green tea has an anti-wrinkle effect as well (Katiyar, 2003). Green tea shows good ROS scavenging activity, which makes it a potential applicant in antiphotoaging therapy. In a recent study, the polyphenol extract of green tea was fed to mice affected by photoaging. The polyphenols seem to increase the collagen level and elastin fibers, which enhanced the skin quality of the mice, thereby showing an antiwrinkle effect (Lee, Kim & Kim, 2014).

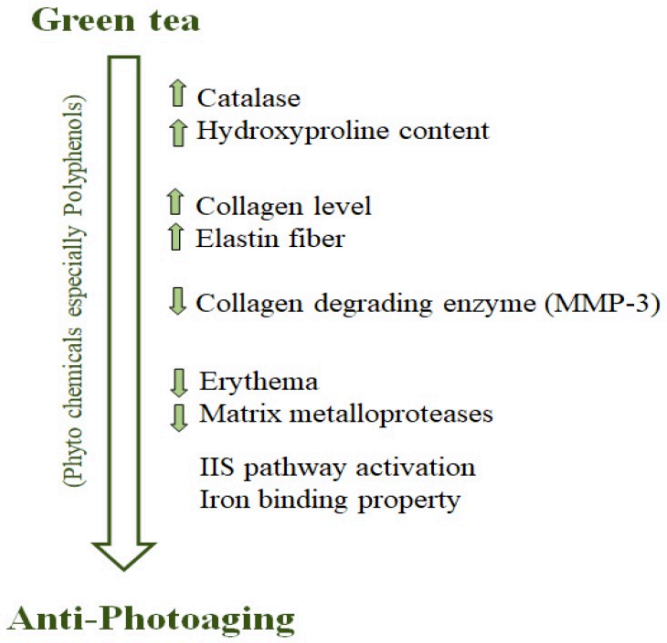

Figure 1: Antiphotoaging property of green tea phytochemicals. (Cabrera, Artacho & Giménez, 2006).

Conclusion

Green tea's beneficial health effect is immense, and people are advised to regularly consume this popular and potentially beneficial beverage. Herbs like green tea can be effectively used for different health-related problems, such as the prevention of diabetes, cancer, high blood pressure, obesity, skin diseases, liver cirrhosis, and obesity. This beverage is a natural source for the prevention of the above-mentioned health related issues and is also cost-effective. Several studies are still in progress for the development of more specific methods with more models, along with the development of the best predictive biomarkers, so that a better understanding of the whole interaction of green tea with the endogenous system and exogenous factors can be known. It not only shows beneficial effects but is also rich in antioxidants. Specific research is being carried out all over the world for better future implementation of the health benefits of green tea.

Acknowledgement

The author is grateful to her Principal Sir Dr. Indranil Kar and Department of Botany, for their support and encouragement.

References

Aanouz, I., Belhassan, A., El-Khatabi, K., Lakhlifi, T., El-Ldrissi, M., & Bouachrine, M. (2021). Moroccan Medicinal plants as inhibitors against SARS-CoV-2 main protease: Computational investigations. *Journal of Biomolecular Structure and Dynamics*, *39*(8), 2971-2979. https://doi.org/10.1080/07391102.2020.1758790

Afzal, M., Safer, A. M., & Menon, M. (2015). Green tea polyphenols and their potential role in health and disease. *Inflammopharmacology*, *23*, 151-161. https://doi.org/10.1007/s10787-015-0236-1

Babu, P. V. A., Sabitha, K. E., & Shyamaladevi, C. S. (2006). Therapeutic effect of green tea extract on oxidative stress in aorta and heart of streptozotocin diabetic rats. *Chemico-biological Interactions*, *162*(2), 114-120. https://doi.org/10.1016/j.cbi.2006.04.009

Cabrera, C., Artacho, R., & Giménez, R. (2006). Beneficial effects of green tea—a review. *Journal of the American College of Nutrition*, *25*(2), 79-99. https://doi.org/10.1080/07315724. 2006.10719518

Chacko, S. M., Thambi, P. T., Kuttan, R., & Nishigaki, I. (2010). Beneficial effects of green tea: a literature review. *Chinese Medicine*, *5*(1), 1-9.

Crespy, V., & Williamson, G. (2004). A review of the health effects of green tea catechins in in vivo animal models. *The Journal of Nutrition*, *134*(12), 3431S-3440S. https://doi.org/10.1093/jn/134.12.3431S

Dufresne, C. J., & Farnworth, E. R. (2001). A review of latest research findings on the health promotion properties of tea. *The Journal of Nutritional Biochemistry*, *12*(7), 404-421. https://doi.org/10.1016/S0955-2863(01)00155-3

Dulloo, A. G., Duret, C., Rohrer, D., Girardier, L., Mensi, N., Fathi, M., ... & Vandermander, J. (1999). Efficacy of a green tea extract rich in catechin polyphenols and caffeine in increasing 24-h energy expenditure and fat oxidation in humans. *The American Journal of Clinical Nutrition*, *70*(6), 1040-1045. https://doi.org/10.1093/ajcn/70.6.1040

Eberhardt, M. V., Lee, C. Y., & Liu, R. H. (2000). Antioxidant activity of fresh apples. *Nature*, *405*(6789), 903-904. https://doi.org/10.1038/35016151

Elmezayen, A. D., Al-Obaidi, A., Şahin, A. T., & Yelekçi, K. (2021). Drug repurposing for coronavirus (COVID-19): in silico screening of known drugs against coronavirus 3CL hydrolase and protease enzymes. *Journal of Biomolecular Structure and Dynamics*, *39*(8), 2980-2992. https://doi.org/10.1080/07391102.2020.1758791

Enmozhi, S. K., Raja, K., Sebastine, I., & Joseph, J. (2021). Andrographolide as a potential inhibitor of SARS-CoV-2 main protease: an in silico approach. *Journal of Biomolecular Structure and Dynamics*, *39*(9), 3092-3098. https://doi.org/10.1080/07391102.2020.1760136

Fisher, G. J., Wang, Z., Datta, S. C., Varani, J., Kang, S., & Voorhees, J. J. (1997). Pathophysiology of premature skin aging induced by ultraviolet light. *New England Journal of Medicine*, *337*(20), 1419-1429. https://doi.org/10.1056/NEJM199711133372003

Ganesan, K., Kumar, K. S., & Rao, P. S. (2011). Comparative assessment of antioxidant activity in three edible species of green seaweed, Enteromorpha from Okha, Northwest coast of India. *Innovative Food Science & Emerging Technologies*, *12*(1), 73-78. https:// doi.org/10.1016/j.ifset.2010.11.005

Gardner, E. J., Ruxton, C. H. S., & Leeds, A. R. (2007). Black tea–helpful or harmful? A review of the evidence. *European Journal of Clinical Nutrition*, *61*(1), 3-18. https://doi.org/10.1038/sj.ejcn.1602489

Graham, H. N. (1992). Green tea composition, consumption, and polyphenol chemistry. *Preventive medicine*, *21*(3), 334-350.https://doi.org/10.1016/0091-7435(92) 90041-F

Gülçin, I. (2006). Antioxidant and antiradical activities of L-carnitine. *Life sciences*, *78*(8), 803-811. https://doi.org/10.1016/j.lfs.2005.05.103

Hirasawa, M., & Takada, K. (2004). Multiple effects of green tea catechin on the antifungal activity of antimycotics against Candida albicans. *Journal of Antimicrobial Chemotherapy*, *53*(2), 225-229. https://doi.org/10.1093/jac/dkh046

Horie, H., Ema, K., & Sumikawa, O. (2017). Chemical components of Matcha and powdered green tea. *J. Cook. Sci. Jpn*, *50*, 182-188.

Jakubczyk, K., Kochman, J., Kwiatkowska, A., Kałduńska, J., Dec, K., Kawczuga, D., & Janda, K. (2020). Antioxidant properties and nutritional composition of matcha green tea. *Foods*, *9*(4), 483. https://doi.org/10.3390/foods9040483

Katiyar, S. K. (2003). Skin photoprotection by green tea: antioxidant and immunomodulatory effects. *Current Drug Targets-Immune, Endocrine & Metabolic Disorders*, *3*(3), 234-242. https://doi.org/10.2174/1568008033340171

Koo, M. W., & Cho, C. H. (2004). Pharmacological effects of green tea on the gastrointestinal system. *European Journal of Pharmacology*, *500*(1-3), 177-185. https://doi.org/10.1016/j.ejphar.2004.07.023

Lee, K. O., Kim, S. N., & Kim, Y. C. (2014). Anti-wrinkle effects of water extracts of teas in hairless mouse. *Toxicological Research*, *30*, 283-289.https://doi.org/10.5487/TR.2014. 30.4.283

Page, R. C., & Kornman, K. S. (1997). The pathogenesis of human periodontitis: an introduction. *Periodontology 2000*, *14*(1), 9-11. https://doi.org/10.1111/j.1600-0757.1997. tb00189.x

Priya, B. M., Anitha, V., Shanmugam, M., Ashwath, B., Sylva, S. D., & Vigneshwari, S. K. (2015). Efficacy of chlorhexidine and green tea mouthwashes in the management of dental plaque-induced gingivitis: A comparative clinical study. *Contemporary Clinical Dentistry*, *6*(4), 505. https://doi.org/10.4103/0976-237X.169845

Rietveld, A., & Wiseman, S. (2003). Antioxidant effects of tea: evidence from human clinical trials. *The Journal of Nutrition*, *133*(10), 3285S-3292S. https://doi.org/10.1093/jn/133.10.3285S

Roomi, M. W., Ivanov, V., Kalinovsky, T., Niedzwiecki, A., & Rath, M. (2005). In vitro and in vivo antitumorigenic activity of a mixture of lysine, proline, ascorbic acid, and green tea extract on human breast cancer lines MDA-MB-231 and MCF-7. *Medical Oncology*, *22*, 129-138. https://doi.org/10.1385/MO:22:2:129

Sumpio, B. E., Cordova, A. C., Berke-Schlessel, D. W., Qin, F., & Chen, Q. H. (2006). Green tea, the "Asian paradox," and cardiovascular disease. *Journal of the American College of Surgeons*, *202*(5), 813-825. https://doi.org/10.1016/j.jamcollsurg.2006.01.018

Taylor, P. W., Hamilton-Miller, J. M., & Stapleton, P. D. (2005). Antimicrobial properties of green tea catechins. *Food science and technology bulletin*, *2*, 71. https://doi.org/10.1616%2F1476-2137.14184

Unno, K., Takabayashi, F., Yoshida, H., Choba, D., Fukutomi, R., Kikunaga, N., ... & Hoshino, M. (2007). Daily consumption of green tea catechin delays memory regression in aged mice. *Biogerontology*, *8*, 89-95. https://doi.org/10.1007/s10522-006-9036-8

Vuong, Q. V. (2014). Epidemiological evidence linking tea consumption to human health: a review. *Critical Reviews in Food Science and Nutrition*, *54*(4), 523-536. https://doi.org/10.1080/10408398.2011.594184

Wierzejska, R. (2014). Tea and health—A review of the current state of knowledge. *Przegl Epidemiol*, *68*(3), 501-6.

Wilson, D. (2018). The Japanese tea ceremony and pancultural definitions of art. *The Journal of Aesthetics and Art Criticism*, *76*(1), 33-44.

Yam, T. S., Shah, S., & Hamilton-Miller, J. M. T. (1997). Microbiological activity of whole and fractionated crude extracts of tea (Camellia sinensis), and of tea components. *FEMS Microbiology letters*, *152*(1), 169-174. https://doi.org/10.1111/j.1574-6968. 1997.tb10424.x

Yamamoto T., Juneja L.R., Chu D., & Kim M. (1997). *Chemistry and Applications of Green Tea.* CRC Press, Boca Raton, FL, USA: pp. 6–34.

Yin, X., Yang, J., Li, T., Song, L., Han, T., Yang, M., ... & Zhong, X. (2015). The effect of green tea intake on risk of liver disease: a meta analysis. *International Journal of Clinical and Experimental Medicine*, *8*(6), 8339.

Zhang, M., Holman, C. D. A. J., Huang, J. P., & Xie, X. (2007). Green tea and the prevention of breast cancer: a case–control study in Southeast China. *Carcinogenesis*, *28*(5), 1074-1078. https://doi.org/10.1093/carcin/bgl252

Subject Index

ISBN 978-967-2819-22-6

e ISBN 978-967-2819-23-3

Published by:

Lincoln University College, Malaysia

www.lucp.net